Applying Shock Damping

to the Problem of Transmission Line Cascades

by

Alan Bowe Peabody

March 2004

Department of Civil Engineering and Applied Mechanics

McGill University

Montreal, Canada

A Thesis submitted to McGill University in partial fulfillment of the requirements for the degree of Doctor of Philosophy

Your file Votre référence
ISBN: 0-612-98345-5
Our file Notre référence
ISBN: 0-612-98345-5

Abstract

Early in the 20th Century, the design and construction of high-voltage overhead electric power lines began. In the nearly 100 years since those first lines were built, the progressive collapse of large numbers of structures has been a continuing problem. These large progressive collapses are known today as cascades.

While not all structural failures result in cascades, longitudinal cascades begin with a failure in the structural system that maintains tension in the overhead wires. These failures are represented most simply by a broken wire. Broken wires cause dynamic loads on the towers much higher than the intact wire tensions.

This research tests the hypothesis that adding supplemental springs and mechanical dampers to electric transmission towers can help control the dynamic forces on towers that lead to cascades. Two new methods of incorporating springs and dampers into towers were invented: the "post spring-damper" and the "rotating crossarm spring-damper." A case study modeling a typical 230 kV line using the finite element dynamics program ADINA (ADINA 2003) was used to test these two new methods.

Both the post spring-damper and the rotating crossarm spring-damper proved to be effective. They substantially reduce the peak dynamic loads while dissipating a large fraction of the total energy released by broken wires.

Sommaire

La conception et la construction des lignes aériennes de transport d'électricité à haute tension ont débuté dans la première décennie du 20e siècle, soit il y a presque 100 ans. En dépit de cette longue expérience, le problème d'effondrement en série de grands nombres de pylônes perdure. Ces effondrements sont aujourd'hui désignés comme des cascades de pylônes.

Bien que tous les effondrements de pylônes ne dégénèrent pas en cascades, les cascades longitudinales de pylônes sont initiées par une rupture dans le système structural qui maintient la traction mécanique dans les câbles. Ce type de rupture est représenté, dans le cas le plus simple, par un bris de câble. Les bris de câbles causent des surcharges dynamiques beaucoup plus élevées que les tractions des câbles intacts sur les pylônes adjacents.

Cette recherche teste l'hypothèse que l'ajout de ressorts et amortisseurs mécaniques dans les pylônes peut aider à contrôler les forces dynamiques qui provoquent des cascades. L'auteur a inventé deux nouvelles méthodes pour incorporer des ressorts et amortisseurs aux pylônes: le ressort-amortisseur sur membrure rigide (*post spring-damper*) et la console pivotante avec resssort-amortisseur (*rotating crossarm spring-damper*). Ces deux nouvelles méthodes ont été évaluées en utilisant des modèles numériques d'analyse dynamique par éléments finis (logiciel ADINA - ADINA 2003) pour un cas type d'une ligne à 230 kV.

L'auteur a démontré que les deux méthodes proposées sont efficaces. Elles permettent de réduire substantiellement les forces dynamiques de pointe en dissipant une grande partie de l'énergie libérée par les bris de câbles.

Originality and Contributions to Knowledge

To the best of the author's knowledge, this research includes the following original contributions:

- Invention of the "Post Spring-Damper System" and the "Rotating Crossarm Spring-Damper System" using viscous dampers to reduce the shock loads on towers due to broken wires and other longitudinal disturbances.
- Dynamic finite element analysis of the two spring-damper systems for broken wires.
- Dynamic finite element analysis of rotating crossarms with both vertical and inclined axes for broken wires.
- Application of aerodynamic damping to broken wire analyses.
- Application of digital filtering to the results of dynamic finite element analyses of broken wire problems.
- Invention of longitudinal V-string insulator assemblies using composite post insulators.

Acknowledgements

My advisor, Dr. Ghyslaine McClure of McGill University, for encouraging me to pursue this research and for the many lively discussions we have had about transmission design.

The Natural Sciences and Engineering Research Council of Canada, Hydro Quebec and TransEnergie, the Emil Nenniger family, the Joseph S. Stauffer Foundation and the Friends of McGill for their financial support.

Dr. William Cook for all his help with my computer problems, great and small.

Robert Kluge of American Transmission Co. for lending me the film of the EPRI Wisconsin tests and our discussions about the tests.

Brian and Pat White for their company and encouragement in a new country and new city.

Most of all, my wife Sharon, the light of my life, without whom I never would have continued my formal education.

Table of Contents

List of Figures

List of Tables

Nomenclature

A	=	total cross sectional area of the cable, m^2
A_p	=	projected area, m^2
A_w	=	wave amplitude, m
A_R	=	reflected wave amplitude, m
A_T	=	transmitted wave amplitude, m
C	=	torsional damping constant, kN m s/rad
C_d	=	drag coefficient, dimensionless
E	=	modulus of elasticity of the cable, Pa
F_d	=	damping force, N
H	=	horizontal component of wire tension, N
IFI	=	impact factor on the intact tension, dimensionless
IFR	=	impact factor on the residual static tension, dimensionless
J	=	torsional moment of inertia, kg m^2
K	=	torsional spring constant, kN m/rad
L	=	moment arm, m
N	=	number of steps
P	=	applied force, N
Re	=	Reynolds number, dimensionless
R_x	=	reaction along the X axis (longitudinal), N
R_z	=	reaction along the Z axis (vertical), N
S	=	actual (stressed) length of the cable, m
S_0	=	unstressed length of the cable, m

T = tension at any point in the cable, N

T_i = intact tension, N

T_e = effective or average tension in the cable, N

V_L = longitudinal wave speed, m/s

V_r = relative velocity, m/s

V_T = transverse wave speed, m/s

W = work or energy, J

ΔW = change in work or energy, J

Z_i = wave impedance, kg/s

Z_L = longitudinal wave impedance, kg/s

Z_T = transverse wave impedance, kg/s

a = span, m

b = elevation difference between supports, m

c = straight-line distance between supports, m

c_h = Haro's empirical constant

c_v = viscous damping constant, kg/s

c_{cr} = critical viscous damping constant, kg/s

c_t = torsional damping constant, kg m^2/s

d = sag, m

d_w = wire diameter, m

f = frequency, Hz

g = gravitational constant, 9.80665 m/s^2

k_g = global stiffness matrix, N/m

k_i	=	stiffness matrix of member i, N/m
k_t	=	torsional stiffness, kN m/rad
m	=	unit mass of wire, kg/m
m_g	=	gobal mass matrix, kg
m_i	=	mass matrix of member i, kg
m_L	=	lumped translational mass for movement in the longitudinal direction, kg
m_t	=	lumped rotational mass for rotation about the vertical axis, kg m^2
m_v	=	lumped rotational mass for rotation about the longitudinal axis, kg m^2
x	=	horizontal distance from low point of sag to a point on the catenary, m
x_1, x_2	=	horizontal distance from low point of sag to conductor attachment point, m
Δx_i	=	movement in x direction during step i, m
y	=	elevation difference from low point of sag to a point on the catenary, m
y_1, y_2	=	elevation difference from low point of sag to conductor attachment point, m
t	=	time, s
w	=	unit weight of wire: mg, N/m
z	=	a dimensionless parameter: aw/2H
α	=	a parameter, see Equation A-5
δ	=	deflection, m
ε	=	strain, a dimensionless ratio
μ	=	viscosity, Pa s
ζ	=	damping ratio, a dimensionless constant: c_v/c_{cr}
ρ	=	density, kg/m^3

ω_n, ω_i = natural frequency, radian/s

λ = a parameter used in the transcendental equation for symmetric modes

Chapter 1
Introduction

The research described in this thesis was undertaken to investigate the feasibility of adding structural dampers to high voltage electric transmission towers. The purpose of these structural dampers is to reduce the dynamic forces on the towers when the wires the towers support experience a sudden loss of tension. This loss of tension may be due to breaks in the wires themselves or other failures in the structural systems that maintain tension in the wires.

1.1 Background

Transmission lines can experience large scale progressive collapses called cascades. Cascades are typically defined as the progressive collapse of more than two (or three) structures in either direction from an initial failure. Cascades have been a problem for designers and operators of transmission lines since the first high voltage lines were constructed early in the last century. They remain a problem today. In 1916, R. D. Coombs referred to lines "falling longitudinally like a 'house of cards'" (Coombs 1916, p. 128). More recently, there have been a number of major cascades in the U.S. and Canada including 18 steel tower cascades and 37 wood structure cascades in Quebec alone during the great ice storm of January 1998 (Peyrot 1999). Cascades can be devastating in their extent. In 1991, Iowa Power lost 108 km of line, including 269 structures, in one cascade (Pohlman and Kaup 1991); in the 1998 ice storm, 256 structures on Hydro-Québec's Yamaska to Saint Cesaire line were lost in cascades (Commission - 1998 Ice Storm 1999d, Table 9, p. 181).

Conceptually, the simplest event to trigger a cascade is the tension failure of a cable. Tension failures have been caused by ice overloads, aircraft strikes and damage due to gunshots, aeolian vibration, galloping and electrical arcing during short circuits.

Figure 1-1 shows schematically a short section of an H-frame line annotated to show the conductors, shield wire, a suspension insulator assembly, a dead-end insulator assembly and tangent and dead-end structures.

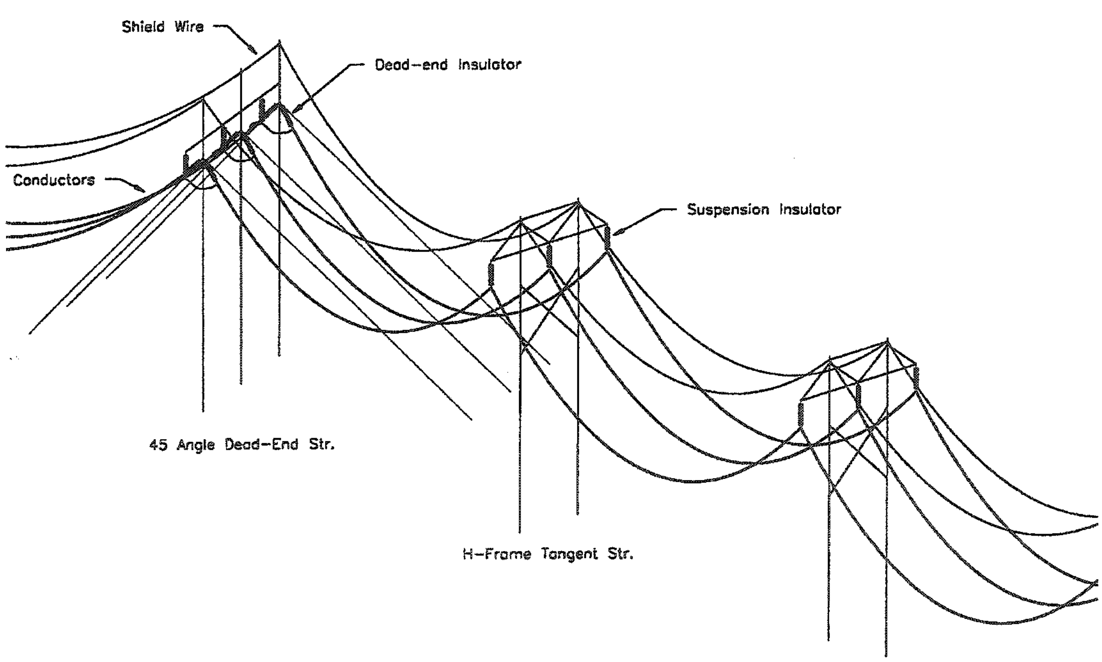

Figure 1-1
Transmission Line Elements

Suspension insulator assemblies on tangent structures are perpendicular to the wires and do not support the tension in the wires. At small angles in the line, they will carry the component of wire tension due to the change in direction of the wires. Dead-end insulator assemblies are in-line with the wires and must carry the full wire tension. Most of the structures in a line will be basic tangent structures. The other structures are used only at the ends of the line and when needed due to changes in the direction of the line or uneven terrain. The problem of preventing cascades centers on the design of the basic tangent structure for longitudinal loads. With intact wires, the tangent structures may see some longitudinal load during construction or when some spans are loaded with ice and other spans are bare. These loads are generally much smaller than those that can occur when a wire breaks.

Figure 1-2 shows a graph of the tension in an insulator string during a full scale broken wire test performed by the Electric Power Research Institute (Peyrot et al. 1978).

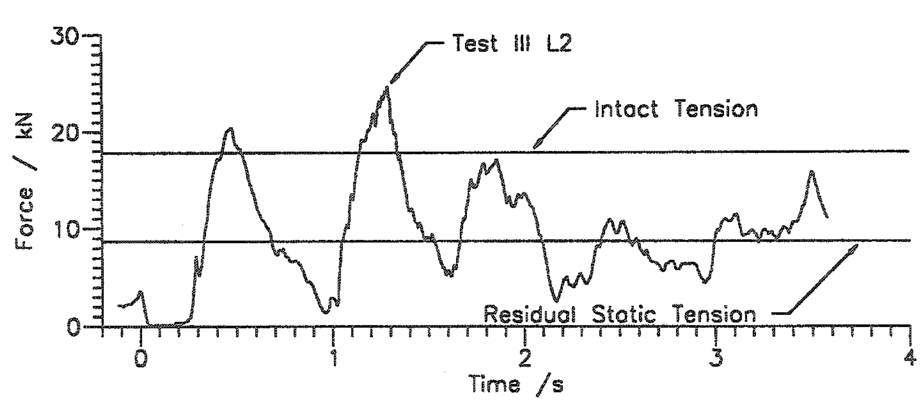

Figure 1-2
Broken Wire Time History of Force in Suspension Insulator Assembly (Peyrot et al. 1978)

Before time 0.00 s, the insulator tension equals the weight of wire supported by the insulator. At time 0.00 s the wire was severed on one side of the insulator and the insulator began to swing to the side. At this point the tension has fallen to near 0 kN. As the insulator comes in line with the wire, the tension in the insulator reaches the first peak at about 0.40 s. The wire has now pulled the insulator in line, but the wire in the middle of the span is still falling. When the wire bottoms out, the second peak is reached at about 1.2 s. After the dynamic effects have damped out, the conductor reaches its "residual static tension," which is the reduced tension in the wire based on adding the length of the insulator assembly to the wire in the span and including the effect of the deflections of the structures. In this test the peak longitudinal load on the tower was greater than the intact tension in the wire. As can be seen from the test data, a tower, which normally is subjected to very small longitudinal loads, can experience very high dynamic longitudinal loads after a failure in the wire tensioning system.

1.2 Problem Definition

Transmission line cascades are caused by the large unbalanced longitudinal loads on tangent suspension towers that occur when the tension in the wires is released due to failures in the structural system that maintains that tension. The peak impact loads can be substantially higher than the tension in the wires at the time of the failure. The problem addressed in this research is how to minimize the impact loads on the towers during these failures.

1.3 Research Objectives

The research described here has two objectives:

- To determine the technical feasibility of incorporating longitudinal shock damping in high voltage transmission line towers.
- To demonstrate the application of longitudinal shock damping to a typical high voltage transmission line.

1.4 Thesis Organization

Chapter 2 is a review of the literature related to cascades, broken wire tests and analytical modeling of broken wire loads. A brief review of the literature relating to the use of dampers in building structures for seismic loading and some references related to the design of dampers are also included. In separate publications, the evolution of the philosophy of design in the transmission industry for longitudinal loads (Peabody 2001), and a history of mechanical devices intended to limit the effects of broken wire loads on towers (Peabody and McClure 2002b) have been described.

Chapter 3 discusses the research methodology in more detail. An analytical computer model is used to determine the effects of adding damping to the towers. In Chapter 4, the analytical model is developed in reference to modeling full scale broken wire tests that were performed in the late 1970's. Chapter 5 discusses the results of applying shock damping on a typical 230 kV transmission line. Chapter 6 draws conclusions about the feasibility of using shock damping in transmission structures and makes suggestions for future research.

Chapter 2
Literature Review

This research is motivated by a desire to find methods of reducing the number and severity of transmission line cascades. Experience with cascades led to full-scale and model tests to try and understand the forces involved. This experience also led to static analyses of the residual static conditions after a conductor break, and then to the first primitive dynamic analyses which in turn led to the more sophisticated dynamic analyses that can be done today. During this evolution in testing and analytic methods, there have been many attempts to develop mechanical means of limiting the forces on structures which start cascades. In this chapter, the literature documenting cascades will be reviewed first. Secondly we will look at the testing that has been done and the evolution of the techniques of static and dynamic analysis. Thirdly, the mechanical devices that have been invented to cope with the forces will be discussed, and finally, a brief introduction to dampers will be given.

In the following discussion, many references will be made to impact factors. Two definitions have traditionally been used (e.g. Thomas 1981). The first, given in Equation 2-1 relates the peak tension in the wire to the tension in the intact wire before the break or other disturbance.

$$IFI = \frac{Peak\ Tension}{Intact\ Wire\ Tension} \qquad \text{Equation 2-1}$$

Equation 2-2 relates the peak tension in the wire to the tension in the first intact span after the system has come to rest. The load on the first intact tower is the residual static load.

$$IFR = \frac{Peak\ Tension}{Residual\ Static\ Wire\ Tension} \qquad \text{Equation 2-2}$$

2.1 Cascades

Cascades have been a problem since the earliest days of transmission line operation and they continue to be a problem today. Surprisingly, the literature describing cascades is remarkably sparse and uninformative about the causes of the initial failures and the details of the construction of the failed lines. For only a few cascades is more information than the date, length of line and tower type available in the open literature.

Coombs (1916), in a discussion of the advantages and disadvantages of flexible structures describes the failure of lines constructed of flexible structures as "…falling longitudinally like a house of cards" – a clear reference to a cascade. He illustrates the point with the example of a planar A-frame line which lost 56 of its 86 structures in a storm in December 1914.

Frandsen and Juul (1976) report that a Danish 150 kV line lost 167 towers in a cascade in 1966. The cascade started with the collapse of a 30° angle tower near one end of the line. The cascade halted where a tower fell into a gorge. Apparently the roughness of the ground provided enough restraint to the conductors to prevent failure of the next tower. Based on records of relays (circuit breakers) operating on lines crossed by the cascading line, the authors estimated that the 50 km of line took ten minutes to collapse with a tower failing every 3 to 4 seconds. The collapse front traveled at 300 to 400 km/hr. As far as the author can determine, this is the only documented evidence of the speed at which a cascade propagates.

On January 11, 1975, cascades destroyed one line and severely damaged a second line in Southeast Wisconsin. Madison Gas and Electric's North Madison–South Fond du Lac 345 kV line lost 103 km (64 mi) of line including 262 structures (Wisconsin PSC 1975). Wisconsin Power and Light's South Fond du Lac–Fitzgerald 345 kV line lost 11.7 km (7¼ mi) of line including 31 structures (Wisconsin PSC 1976). The North Madison-South Fond du Lac 345 kV line, which cost US$ 4,100,000 to build in 1971 was essentially a total loss. These cascades led to funding by the Electric Power Research Institute of two projects to better define longitudinal loads, (Mozer 1978; Peyrot et al. 1978). Three of the full-scale tests described in Peyrot, Kluge and Lee (1978) were used to test the finite element modeling used in this research.

Iowa Power & Light's 345 kV system suffered devastating cascades in 1990 and 1991 (Anjam 1991; Gupta 1991; Gupta et al. 1993; Kaup et al. 1990; Pohlman and Kaup 1991). The Sycamore to Lehigh line cascaded in both 1990 and 1991, losing 31 km (19 mi) and 69 structures in the first cascade, and 47 km (29 mi) and 116 structures in the second. The Roan to Sycamore line cascaded in the same storm in 1991, losing 108 km (67 mi) of line including 269 structures. The 1990 cascade started when a cast malleable iron fitting broke. The fitting was part of the suspension insulator string on a tower at a small angle in the line. These cascades and others led to the establishment of the EPRI

"Longitudinal Load and Cascading Risk Assessment (CASE)" project (Ostendorp 1997a; b; c; d).

In January 1998, a large freezing rainstorm struck southeastern Ontario, southern Quebec and the northern parts of New York, Vermont, New Hampshire and Maine. This storm, which caused extensive damage to transmission and distribution lines, was the most costly natural disaster in Canada's history with damages estimated at C$ 4 billion (approximately 3 billion US$). Hydro-Quebec's transmission system in the Montreal area had 18 major cascades of steel tower lines and 37 major cascades of wood H-frame lines (Peyrot 1999). In Maine, a wood H-frame line belonging to Bangor Hydro also had a cascade (Jones and Mulherin 1998). A provincial commission headed by Roger Nicolet investigated the effects of this storm. The Commission produced a four-volume report in French (Commission - 1998 Ice Storm 1999b; c; d; e) and a one-volume summary report available in both French and English (Commission - 1998 Ice Storm 1999a). In many ways, these reports document the reliance of modern society on a reliable electric transmission system and the consequences of its failure. Some examples of problems during the ice storm include the difficulty of buying groceries when electronic cash registers and payment systems are not working, and the near loss of water pressure to fight fires in Montreal when power to water pumping stations was lost.

Cascades and other failures during the 1998 ice storm are tabulated in Commission – 1998 Ice Storm (1999d). Table 2-1 lists the other North American cascades found in the literature. It must be emphasized that descriptions of most cascades are not published.

Table 2-1 Historic North American Cascades

Date Completed or Energized	Date of Cascade	Vol-tage kV	Type of Structure	Miles Lost	Strs Lost	Reference
	Dec 1914		A-Frame		56	(Coombs 1916)
1914	28 Dec 1921				69	(Oliver 1925)
	28 Dec 1921		A-Frame		78	(Oliver 1925)
	1924				94	(Oliver 1925)
1910	1940's				100	(Ralston 1979)
	1966-74	500			4	(Lummis and Pohlman 1974)
	1966-74	230			28	(Lummis and Pohlman 1974)
	1966-74	500			8	(Lummis and Pohlman 1974)
	1966-74	735			37	(Lummis and Pohlman 1974)
	1966-74	735			32	(Lummis and Pohlman 1974)
	1966-74	500			7	(Lummis and Pohlman 1974)
	1966-74	500			6	(Lummis and Pohlman 1974)
	1966-74	500			9	(Lummis and Pohlman 1974)
	1966-74	500			10	(Lummis and Pohlman 1974)
	1966-74	500			6	(Lummis and Pohlman 1974)
	13 Nov 1969	735	Lattice Steel Towers		6	(Electrical World 1969)
	13 Nov 1969	735	Lattice Steel Towers		24	(Electrical World 1969)

Table 2-1 Historic North American Cascades (continued)

Date Completed or Energized	Date of Cascade	Voltage kV	Type of Structure	Miles Lost	Strs Lost	Reference
28 Dec 1971	23 Oct 1972	345	Lattice Aluminum H-Frames	7	32	(Wisconsin PSC 1976)
Dec 1974	18 Apr1975		LatticeAluminum H-Frames	12		(Electrical Week 1975)
28 Dec 1971	11 Jan 1975	345	LatticeAluminum H-Frames	7	31	(Wisconsin PSC 1976)
Aug 1972	11 Jan 1975	345	LatticeAluminum H-Frames	64	262	(Wisconsin PSC 1975)
	12 Oct 1975	345	Wood H-Frames	64		(Ostendorp 1998b)
	12 Oct 1975	345	Lattice H-frames	70		(Ostendorp 1998b)
	15 July 1980	345	Wood K-frames		53	(Ostendorp 1998b)
	1980	?	?		227	(Ostendorp 1998b)
	1980	500	Rectangular Lattice Steel		84	(Ostendorp 1998a)
	1980	500	Rectangular Lattice Steel		60	(Ostendorp 1998a)
	14 June 1981	345	Wood K-frames		229	(Ostendorp 1998b)
	23 June 1981	345	Wood K-frames		43	(Ostendorp 1998b)
	1982	?	?		84	(Ostendorp 1998b)
	1983	115	Wood H-Frames		40	(Grand Forks Herald 1983)
	1987	345	Lattice H-frames	60		(Ostendorp 1998b)
	3 Feb 1988	345	Lattice H-frames	30	41	(Ostendorp 1998b)
1970's	7 Mar 1990	345	Tubular Steel H-frames	19	69	(Gupta et al. 1993)

Table 2-1 Historic North American Cascades (continued)

Date Completed or Energized	Date of Cascade	Vol-tage kV	Type of Structure	Miles Lost	Strs Lost	Reference
	31 Oct 1990	345	Steel H-frames	96	386	(Ostendorp 1998b)
1970's	1 Nov 1991	345	Tubular Steel H-frames	29	116	(Pohlman and Kaup 1991)
1970's	1 Nov 1991	345	Tubular Steel H-frames	67	269	(Pohlman and Kaup 1991)
	1 Nov 1991	345	Wood K-frames		114	(Ostendorp 1998b)
	26 Dec 1991	345	Multiple lines in System			(Ostendorp 1998b)
	July 1993	345	Wood H-Frames	64	406	(Ostendorp 1998b)
	Oct 1993	345	Lattice Towers	5	17	(Ostendorp 1998b)
	24 Oct 1995	69	Wood H-Frames	3	24	(Ostendorp 1998b)
	13 Dec 1995	500	Lattice H-frames	5	32	(Ostendorp 1998b)
	29 Jun 1996	345	Wood K-frames		12	(Ostendorp 1998b)
	1 July 1997	345	Wood K-frames		96	(Ostendorp 1998b)
	1 July 1997	345	Wood H-Frames	42	240	(Ostendorp 1998b)
	8 July 1997	?	Wood H-Frames	8	47	(Ostendorp 1998b)

2.2 Full-scale and Model Tests

Tests are one of the best methods for investigating structural performance. Table 2-2 lists the full-scale tests reviewed here and Table 2-3 the model tests. Full-scale tests of mechanical devices to reduce the loads are covered later.

Table 2-2
Full-scale Tests

Year	Tower Type	Volt-age kV	Reference
1926	Single Circuit Lattice	220	(Healy and Wright 1926)
1956	Internally Guyed Lattice Steel Frm Internally Guyed Lattice Steel Frm Wood Portal Frame w/ Steel Xarms Guyed Lattice Steel Portal Frame	50 ± 110 110 220	(Haro et al. 1956)
1961	Double Circuit Lattice Steel	138	(Stefoff et al. 1961)
1970	Not Available	150	(Govers 1969; 1970)
1976	Tubular Steel Monopole	115	(Richardson 1976; 1977)
1978	Double Circuit Lattice Steel	138	(Peyrot et al. 1978)
1997	Tubular Steel Monopole	138 345	(Ostendorp 1997d)
1997	Wood H-Frame	138 345	(Ostendorp 1997c)

Table 2-3
Model Tests

Year	Scale	Wire Type	Reference
1960	1/30	Small steel chain	(Paris 1960)
1968	not avail	not available	(Borges et al. 1968)
1970	not avail	not available	(Govers 1970)
1976	1/50	Steel beaded chain	(Richardson 1976)
1977	1/25	Steel beaded chain	(Richardson 1977)
1978	1/30	Steel beaded chain Weighted copper wire	(Mozer 1978)
1984	1/30	Weighted copper wire	(ANCO 1984)
1997	1/23.3	Steel beaded chain Weighted stainless steel cable	(Kempner 1997)

In addition to the tests listed in Tables 2-1 and 2-2, Bonar (1968) and Alt et al. (1984) discuss methods of simulating broken wire loads during proof testing of towers. Alt et al. include a comparison between field and proof tests; however, there is not enough detail to provide a meaningful comparison with the tests listed in Tables 2-1 and 2-2. Frandsen and Juul (1976) refer to unpublished reports of full-scale tests of a lattice steel 60 kV line and a 60 kV line with wood portal structures.

One of the earliest full-scale tests of broken wire loads was performed by Pennsylvania Power and Light Co. during the construction of their Wallenpaupack-Sigfried 220 kV line (Healy and Wright 1926). The line had a 335 m (1100 ft) ruling span and insulator strings with an effective length of 2.74 m (9 ft). The conductor was a 795 kcmil ACSR (aluminum area of 408.2 mm^2, stranding not provided). Calculations were made to determine the effect of unbalanced tensions based on level 335 m spans. Two sets of tests were performed for comparison with the calculations. The first set simulated unbalanced ice loads on the intact conductor system. The second set, which is of interest here, simulated broken conductors under various conditions. This is the oldest report of broken wire tests the author has found.

The test section included 6 spans and 7 towers with the conductors anchored to the ground at the end of each section. The test section was on fairly rough terrain. The spans ranged from 270 to 426 m (885 to 1398 ft) with substantial elevation differences between towers. The line was built with suspension clamps intended to slip under a longitudinal load of about 22.2 kN (5000 lb). Bare conductor broken wire tests were performed with the clamps fully tightened and with the clamps purposely not fully tightened so they would slip. A test was also done using sand bags hung from the wire every 6.1 m (20 ft) to give a load equivalent to 25.4 mm (1 in) radial ice with a 383 Pa (8 psf) wind, an additional load of 46.3 N/m (3.17 lb/ft). In this test the clamps were set to slip. Table 2-4 summarizes the broken wire tests. The peak load in the insulator string was measured using both a spring dynamometer with a follower needle and a special impact dynamometer connected in series. Healy and Wright were of the opinion that the impact dynamometer was more reliable than the spring dynamometer.

Table 2-4
Broken Wire Tests (Healy and Wright 1926)

Test No.	Clamp status	Added Load kg/m	Temp °C	Wind m/s	Initial Tension kN	Residual Static Tension kN	Maximum Insulator Tension	
							Impact Dyno. kN	Spring Dyno. kN
1	Tight	0	5.0	2.1	20.2	11.9	31.2	30.5
2	Tight	0	7.2	-	20.2	-	28.9	-
3	Tight	0	7.2	-	20.2	-	27.1	25.8
4	Tight	0	7.2	4.1	20.2	-	30.7	35.6
5	Set to slip	0	0.0	-	20.0	-	28.0	-
6	Tight	0	1.7	-	66.7	24.6	68.7	95.6
7	Set to slip	4.72	1.0	-	64.5	-	38.9	44.5

The second three tests are repeats of the first test. The average peak tension in the insulator string for the first four tests is 29.2 kN and the coefficient of variation is 5.5%. The ratio of the mean peak tension to the initial tension is 1.45 and to the residual static tension is 2.45. It appears that the clamps did not slip in test 5 even though they were intended to slip at 22.2 kN. It is clear, however, that the clamps slipped in test 7. In test 7, with the simulated ice and wind load, the ratio of peak insulator tension to initial tension is 0.60. Fig. 8 of the paper indicates that the conductor slipped substantially at three structures. Most of the conductor in the first span was lying on the ground. Part of the conductor in the next two spans was also in contact with the ground.

The sliding clamps were very effective in this test, which demonstrated the effectiveness of load limiting devices. The sliding clamps both limited the load and absorbed energy equal to the product of the frictional force and amount of slip. With this demonstrated effectiveness, why are sliding clamps rarely used? It is difficult to calibrate the release load of sliding clamps because the friction between the conductor and clamp is dependent on both the ice and wind load and the weight span. Steffof et al. (1961) report that properly operating sliding clamps can release when ice drops off one span before the ice drops off in the adjacent span. In addition the coefficient of friction will change as the conductor ages. Aged clamps may not slide when needed and if the sliding force is too much larger than intended, tower failures may still occur. When the wires are covered with ice, the clamps cannot slide without crushing or splitting the ice coating; this will increase the sliding force compared with bare conditions and introduce still further variability in the force applied to the tower.

Haro et al. (1956) report on a series of full-scale broken wire tests performed in Finland. The tests were conducted with bare conductor. Tests were made using three existing lines, two 110 kV lines and one 220 kV line with spans next to the break of 225, 208 and 290 m respectively. Three insulator string lengths were used: 643, 1150 and 1785 mm. Four copper conductors with areas from 66 mm^2 to 147 mm^2 were tested with the intact stress varying from 73 to 206 MPa.

They describe the action of the wires after a break in the following terms:

> "After conductor breakage the tension in the conductor immediately decreases by the test tower down to 5 to 10% of the initial tension. The tension remains at this value of some tenths of a second a time that diminishes with shortening insulator chain and increasing initial tension.
>
> The tension then rises linearly and reaches its first peak. The rate of the rise depends both on the initial tension and the length of the chain as shown in figure 6. Then peaks and downs follow in turn, the steady state value being reached after 1 to 2 min.
>
> Reflections from the second support cause considerable tension peaks on the first support after 2 to 4 s (in figure 5 the peak caused by the reflections appears after appr. 3.5 s). For a given span length this time varies with the initial tension and the length of the insulator chain.
>
> At low initial tensions the highest peak often occurs at the above mentioned reflection, whereas at high initial tensions the highest peak will be found at the beginning of the curve."

For one set of tests using the 93 mm^2 conductor (Haro et al. Figure 8), there is enough information to calculate *IFR*. This data is shown in Figure 2-1.

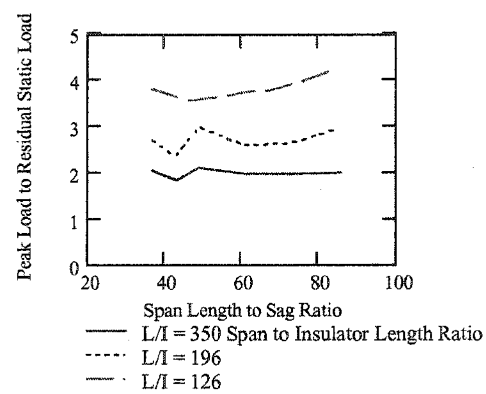

Figure 2-1
Data from Haro et al. (1956)

Paris (1960) performed a series of model tests. He describes in detail the process of determining the model length scale of around 1/30 and the choice of a model conductor – a small steel chain, and the instrumentation. Data traces with very good agreement in the shape of curves comparing a single span model test with a full-scale test are included. Paris comments that the effects of wave reflections in the full-scale test are not well reproduced in the model test. A comparison is also shown for a model and a full-scale test performed in Finland by Haro et al. (1956) including five intact spans. He presents an empirical formula for the peak load, discusses bundled conductor, methods of performing dynamic tests on a test stand and testing scale model lattice towers. Some of the variables in his formula and in the headings of the tables are not defined in the paper making it difficult to interpret. The results are not discussed in the paper, making it primarily of interest to researchers planning model tests.

Stefoff, Swart and Zobel (1961) report on tests that were made to test the hypothesis that the impact load from a broken wire would be absorbed by the crossarm and that the tower body would experience less load. A tower was designed using this assumption. The shield wire peaks were designed for a longitudinal load of 32.9 kN (7400 lb). The tower crossarms where the phase conductors attach were designed for a longitudinal load of 30 kN (6750 lb). The tower body was designed for a longitudinal load of 13.3 kN (3000 lb) applied at either the shield wire attachment point or any one phase attachment point. Four tests were performed during construction of the transmission line, one on the top left phase, two on the middle left phase and one on the bottom left phase. Load cells were installed in the insulator string and one strain gauge was installed on each of 14 of the tower members. The main focus of the tests was to determine the dynamic distribution of forces in the tower due to a conductor break. The tower members with strain gauges were all single angle members. This type of member is typically connected by one leg of the angle leading to substantial eccentricity in the loads applied to individual angles. This caused major problems in relating the strain gauge readings to the forces in the members, leading the authors to conclude that the numerical results could only be used in a qualitative sense. They were, however, able to answer the question posed by their hypothesis - concluding that the crossarms did not provide any impact absorption. Peak impact loads for the four tests were reported to be between 9.8 and 11.3 kN (2200 to 2550 lb) and the residual static tensions between 5.6 and 6.7 kN (1250 to 1500 lb). The data provided from these tests is not sufficient to compare with other tests or to provide a basis for analytic modeling.

Govers (1970) summarizes the results of both full-scale and model tests. Practically no details about the tests themselves are provided. From the annotations on the graphs, we can conclude that tests were performed for both a copper conductor and an ACSR conductor. Experiments were also performed to look at the effect of the length of the span, the number of spans to a dead-end and the length of the insulator strings. Govers concluded that the conductor type and the number of spans have little effect on the impact ratio, but the insulator length and conductor tension have a large effect. He was the first to express the impact factors, *IFI* and *IFR* (Equations 2-1 and 2-2), as a function of two other dimensionless ratios: span to sag and span to insulator length. Figure 2-2 shows Govers' Figure 10 with impact factor *IFR*.

The author has been unable to obtain a copy of the tests by Borges et.al. (1968), however some information is included by Thomas (1981). Borges includes Equation 2-3 for *IFI* (Equation 2-1) where w is the unit weight of the wire, a is the span length and T_i is the intact tension before the break. The constant c_h was calculated to be 3.5 for Borges' single span cases, 3.8 for the two span cases and 3.0 for the data of Haro et al. (1956).

$$IFI = c_h \sqrt{\frac{wa}{T_i}} \qquad \text{Equation 2-3}$$

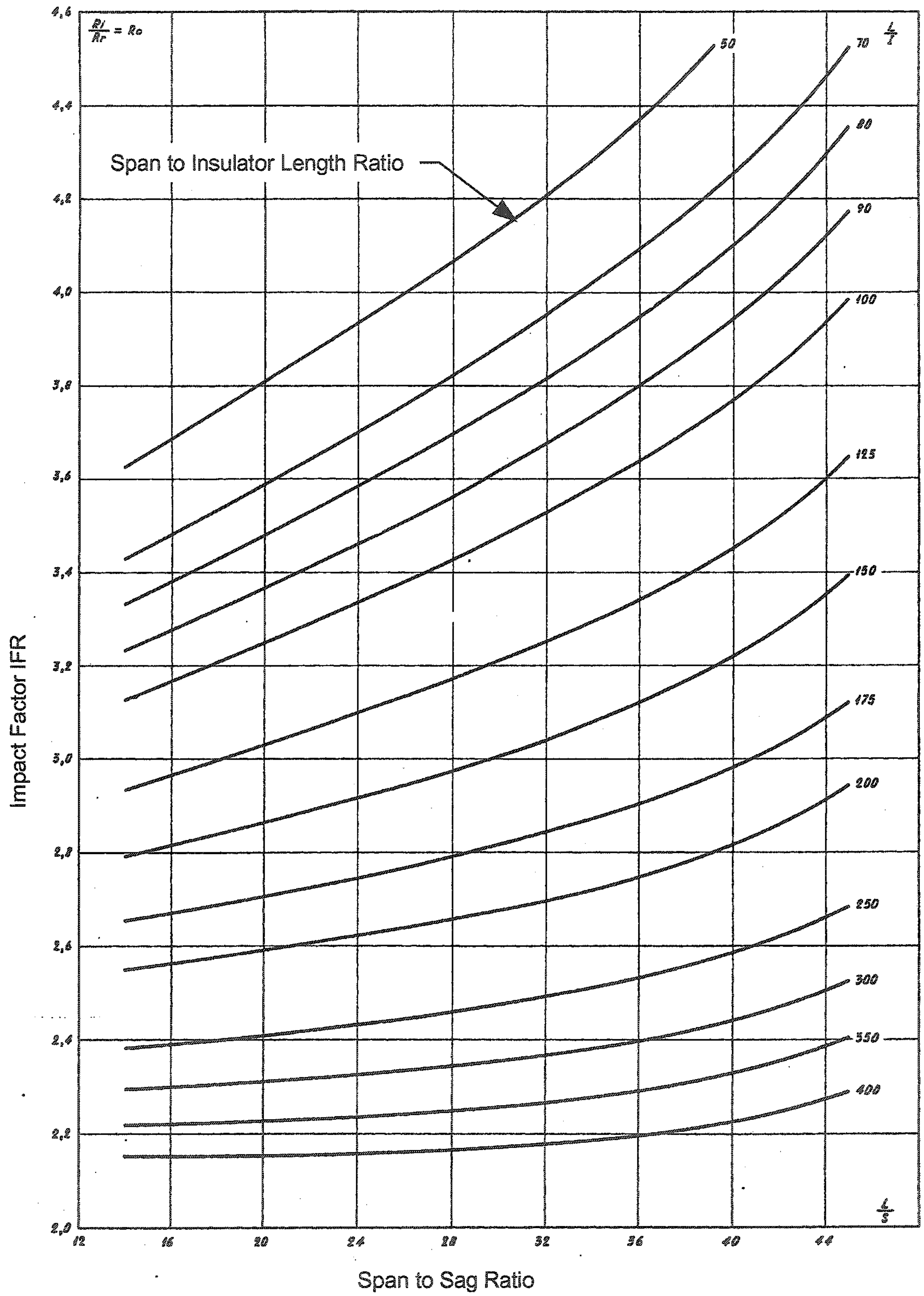

Figure 2-2 Govers (1970) Figure 10

Comellini and Manuzio (1968) include a discussion of the effect of tower flexibility on the peak dynamic loads due to broken bundled conductors. The results shown in Figure 2-3 (their Figure 19) are apparently from model tests using beaded chain and model towers formed of rods or tubes. The ratio T_d to T_o is *IFI,* the ratio of the peak dynamic tension to the everyday tension in the wire before the break, the ratio M_d to M_o is the ratio of the peak bending moment in the structure to the static bending moment due to a force T_o applied at the insulator attachment point on the tower and γ is the tower flexibility measured at the insulator attachment point.

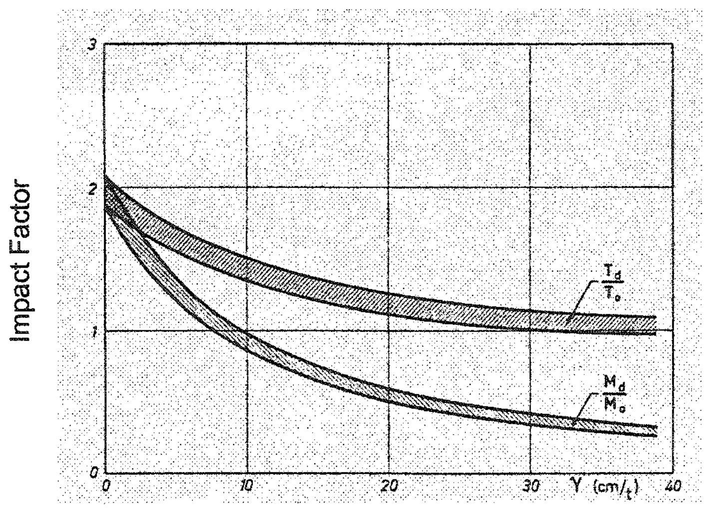

Figure 2-3 Results from Comellini and Manuzio (1968)

Commelini and Manuzio concluded:

> "An increase in tower-flexibility reduces the dynamic peak of longitudinal force and especially the bending moment at the tower base, as long as the period of free oscillation of the tower is smaller than the propagation time of traveling waves in the span. This fact is due to the effect of traveling waves on the intact phases and earth wires; these waves become greater as the flexibility of the tower increases and tend to equilibrate the wave acting on the broken bundle, which on the contrary decreases as the flexibility increases."

Commelini and Manuzio recognize the importance of wave phenomena to understanding the forces due to broken wires, however, no data supporting the potential increase in peak loads when the period of the tower coincides with the propagation time of the traveling wave is presented.

Richardson (1976; 1977; 1987) made both model and limited full-scale tests for a section of a 115 kV single circuit transmission line that was being built near Billerica, Massachusetts by New England Electric Company. The single pole tubular steel structures have all three tubular steel davit arms on the same side (typical construction along streets and roads) with the single shield wire mounted directly to a vang at the top of the pole. The conductor is Condor 795 kcmil 54/7 ACSR and the shield wire is 7 No. 9 alumoweld. Table 2-5 lists the spans and structure types. The angle towers with suspension insulators have a horizontal strut insulator to hold them plumb.

Table 2-5
Line Section Modeled in Richardson's Tests

Str. No.	Type	Line Angle deg	Back Span m	Pole Height m	Back Span ft	Pole Height ft
22	Dead-end			24.4		80
23	Suspension		145.7	25.9	478	85
24	Suspension		145.7	25.9	478	85
25	Suspension w/ Strut	7.5	145.7	27.4	478	90
26	Suspension		111.6	25.9	366	85
27	Suspension		115.8	25.9	380	85
28	Suspension w/ Strut	9.5	114.0	29.0	374	95
29	Suspension		112.5	33.5	369	110
30	Suspension w/ Strut	7.5	109.7	30.5	360	100
31	Suspension		126.5	29.0	415	95
32	Dead-end	45	127.1	30.5	417	100
33	Dead-end		79.9	16.2	262	53

All measurements, both model and full-scale, were made near the base of the structure. The results are shown as an equivalent pole top load, which is convenient for comparing with the capacity of the poles installed on the line, but which makes comparisons with other tests difficult. Deflections were not measured. Most of the tests were performed at a scale of 1/50. For comparison with full-scale tests of the broken shield wire, Richardson used more sophisticated 1/25 scale models. Richardson shows a reasonably good comparison between his 1/25 scale model tests and the full-scale tests of broken shield wires. Two lengths of insulator were modeled in the 1/50 scale tests: 1.37 m (4.5 ft) and 2.13m (7 ft).

The 1/50 scale broken wire tests were made by cutting the wire midway between structures 24 and 25. The wires were modeled as having the equivalent of 12.5 mm (1/2 in) radial ice with a 191.5 Pa (4 psf) wind pressure. Table 2-6 shows the impact factors, IFR (Equation 2-2) for the 1/50 scale broken wire tests.

Table 2-6
Impact Factors *IFR* from Richardson's Tests

Wire	Str. No.	Insulator Length	
		1.37 m (4.5 ft)	2.13 m (7 ft)
Conductor	24	2.99	4.58
Conductor	25	3.02	5.51
Shield Wire	24	1.57	1.67
Shield Wire	25	1.54	1.63

Both full-scale and 1/25 scale model tests were performed for bare shield wires cut on either side of structure 23. Table 2-7 shows the impact factors for structure 23.

Table 2-7
Comparison of Impact Factors *IFR* for Richardson's Full-scale and Model Shield Wire Tests

Cut Location	Str. No.	Test	
		Full-scale	Model
Back	23	1.88	1.75
Ahead	23	1.92	2.07

Peyrot, et al. (1978) report tests performed on a 138 kV double circuit line slated for replacement by a new 345 kV line. This report is the most thorough and complete report of broken wire tests the author has found. The tests are used to test the finite element model developed for this research. They are described in detail in Chapter 4.

Mozer (1978) reports a series of broken wire tests based on a 1/30 scale model of a double circuit 345 kV line with 1590 kcmil ACSR 45/7 Lapwing conductor (Mozer 2003). The results were used to verify the accuracy of the computer program, BRODI, which calculates the residual static tension in the wires after a break, and for comparison with the energy formula for arm impact factors proposed in Peyrot et al. (1978). Structure response factors were also developed.

A single tubular steel pole with the shield wire attachment on the pole and the upper two steel davit arms was modeled. The lower two davit arms on either side were not modeled, on the assumption that the suspension insulators would sufficiently decouple the bottom two phases of each circuit so that the results would not be significantly affected. This reduced the complexity of the model. The model had 3 spans of 9.75 m

(32 ft) at model scale, 292.6 m (960 ft) at full-scale. With the conductor break in the first span, the dynamic effects were due to the action of only the two remaining spans.

The comparison with BRODI was done using steel beaded chain to compare the static deflections and forces after the broken wire comes to rest. After further tests, the researchers came to the conclusion that the beaded chain was not suitable for dynamic modeling because it introduced too much damping. They report only the 52 broken conductor tests and 4 broken shield wire tests that were performed using copper wires with weights crimped and glued on to give the correct unit weight. A broken suspension insulator test was also performed.

Tests were performed with three lengths of insulator 76, 114 and 178 mm (3, 4.5 and 7 in) corresponding to full-scale lengths of 2.29, 3.43 and 5.33 m (7.5, 11.25 and 17.5 ft). Three structure stiffnesses were modeled, 1391, 4271 and 12,877 N/m (7.94, 24.39, and 73.33 lb/in), which at full-scale correspond to 42, 128 and 386 kN/m (2.9, 8.8 and 26.5 kip/ft). For the most flexible structure, an additional mass was added for some tests. This gave structures having 4 different natural frequencies. Tests were made with and without the shield wire installed. When the shield wire was installed it was rigidly attached to the structure, with the exception of one case where a 12.7 mm (½ in) link was used. The effect of shield wire stiffness is added to the structure stiffness in the reported results. The paper does not convert the model scale to full-scale results. The stiffness of the conductor uses a parameter λ which is the ratio of the full-scale to model modulus of elasticity. The ratio used for the conductor is based on stress strain tests of the model wire. The actual model wire was 0.87 mm in diameter, somewhat smaller than the 18 gauge wire reported (Mozer 2003).

Impact factors *IFR* (Equation 2-2) for each test were calculated. These are shown in Figure 2-4 for the stiffest structure which is most similar to lattice steel towers. Figure 2-5 shows the comparable impact factors calculated using the energy formula of Peyrot et al. (1978). Note the poor agreement between the model test results and the energy formula applied at full-scale.

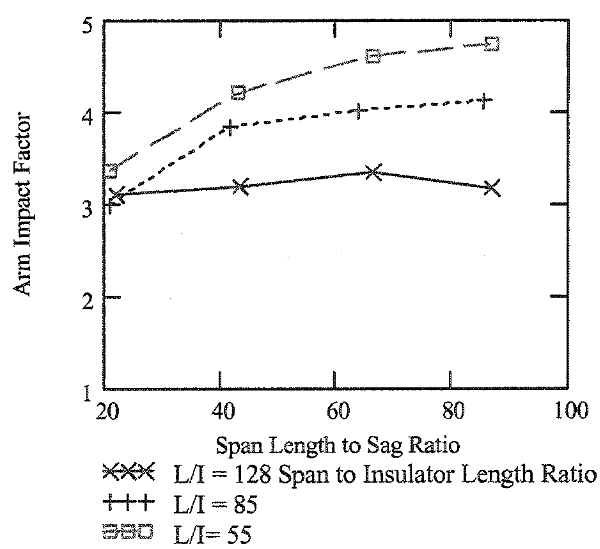

Figure 2-4
Impact Factors from Model Tests (Mozer 1978)

Kempner (1997) performed a series of 1/23.33 scale model tests to assess whether Bonneville Power Administration's failure containment (cascade prevention) criteria were reasonable. He ran a series of broken wire model tests that included simulating structure failures, to see the effects of the failures on the loads on the next intact structures.

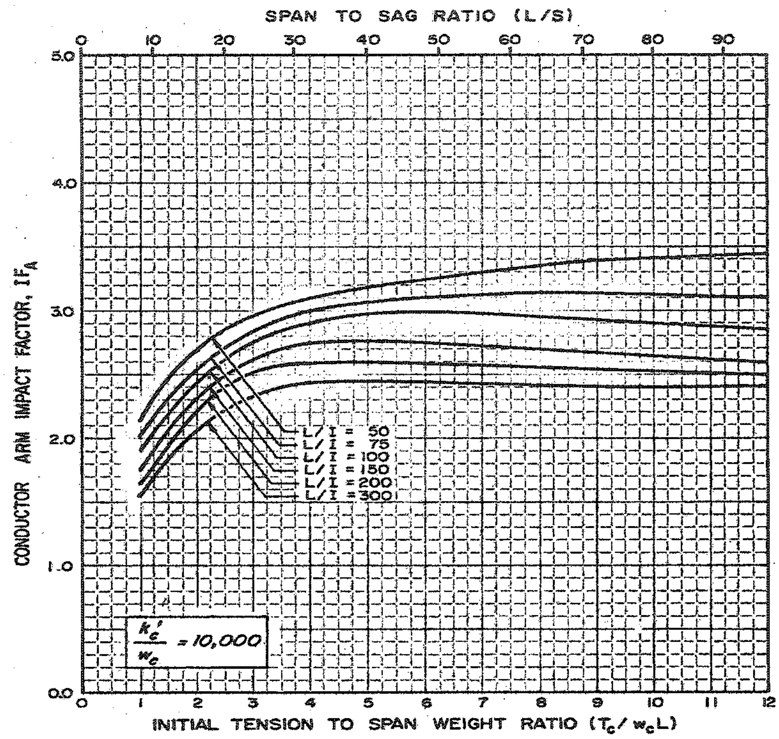

Figure 2-5
Impact Factors Based on Energy Formula (Mozer 1978, Fig. 5-4g)

The suspension towers were modeled using aluminum tubing pinned at the bottom and attached near the top to a rigid support using a spring. Mass could be added to the tubing. By changing the spring and added mass, different tower natural frequencies could be modeled. A mechanical fuse was placed between the spring and the support that simulated a tower failure by allowing the whole model tower to fall to the ground while rotating about its pinned base.

Of particular interest for comparing analytic results with the test results is the filtering used in the data acquisition system. An analog low pass filter with 50 Hz cutoff was used. At full-scale this corresponds to a 10.4 Hz cutoff frequency.

The line section modeled consisted of five 274.3 m (900 ft) intact spans with an additional span in which the break took place. The break was assumed to occur at mid span. Two cases were reported that included the residual static tensions (D120B2 & B3, tests no. 1773 and 1774). *IFR* (Equation 2-2) for both cases was 3.2. The span to sag ratio was 50 and the span to insulator length ratio was 100 for both cases.

Kempner's simulation of tower failures showed that the impact load on the first intact tower is progressively reduced as the number of failed towers increases. He concluded that to limit the number of failed towers to four on each side of a break, the longitudinal design load should be 82.2 % of the initial tension for lattice steel towers and 71.3 % for single pole structures and H-frames.

Ostendorp (1997c) reports the results of 19 full-scale tests (which include 3 broken suspension insulator tests) on a four span 345 kV wood H-frame line, performed as part of the Electric Power Research Institute's Cascading Failure Risk Assessment project (EPRI CASE Project). In a second set of tests (Ostendorp 1997d), 16 tests were performed on a single circuit tubular steel pole line. Both lines consisted of four 304.8 m (1000 ft) spans between dead-ends with three suspension structures. Also, both sets of tests used two lengths of insulator assembly 1.52 and 3.05 m (5 and 10 ft).

In both sets of tests, load cells were installed in the conductor and shield wire 3.1 m (10 ft) ahead and back of the first suspension structure, and 3.1 m (10 ft) ahead of the other two structures. Load cells were also installed in the suspension insulator strings of the three suspension structures. For each test, the reports include the average value for the entire period, the average value before the break, the average value after the break, the maximum and minimum values, the median value, the standard deviation and coefficient of variation. In many cases the maximum value reported is exactly equal to the average value before the break, leaving one to guess whether the value has any meaning in relationship to the time history. The reports imply that the average value after the break represents the residual static load; however, 30 seconds is not long enough for the wire to come completely to rest. Although the time histories for each test were recorded, none of them are included in the report to allow the values that are reported to be interpreted. The information included in these reports is insufficient for an independent comparison with other researchers' results.

2.3 Static Analyses

The earliest analyses of broken wires focused on determining the position of the wires after they had come to rest. Nevertheless, the severity of broken wire loads was recognized very early. Wilkinson (1910) said "From the mechanical point of view the worst stresses for which a transmission line must be designed are those due to the breakage of wires, accompanied at the same time by ice deposit and a high velocity wind blowing at right angles to the line." He goes on to describe the apparent advantages of flexible towers (since proven by experience to be doubtful) and gives an example of determining the approximate tower deflection with a broken wire. Brown (1913) describes in detail a method for calculating the static force on a tower with a broken wire and determining the sag in the span adjacent to the break. The desire to maintain clearances over roads and railroads after a wire had broken led Den Hartog (1928) and Bissiri and Landau (1947) to develop iterative methods for determining the static sags and tensions that included the effect of the swing of the suspension insulators.

Poskitt (1964) developed a system of simultaneous equations describing a line section that could be solved iteratively using the Newton-Raphson method. He considered only the suspension insulators and the wire and did not include the tower stiffness. The effect of combinations of ice loads, wind loads and the residual static position after a broken wire, could be analyzed using the computer program he developed. Campbell (1970) compares two iterative methods for performing static analyses of transmission lines composed of flexible tubular steel structures using the direct stiffness method. The tower stiffness is included, but P-Delta effects were not addressed.

Frandsen and Juul (1976) include equations and a graph to determine the residual static load.

Kansog (1973) describes the use of a computer program to automate the iterative procedures needed to determine the residual static sags and tensions after a wire has broken. Kansog's program considered the equilibrium of two spans at a time iterating repeatedly through the line section being considered. The program was able to calculate the sags and tensions due to broken wires and unbalanced ice loads.

Peyrot and Goulois (1978) describe the theoretical basis for a catenary cable finite element and its application to the static analysis of transmission lines. The catenary cable element requires iterative calculations intended for placement in a subroutine that calculates the tangent stiffness of the element for use in the main finite element program. The routine can account for the effect of portions of the cable lying on the ground. For static analyses, this element allows a span of wire to be represented by only one element.

Lindsey (1978a) describes a computer program for static analysis of transmission lines under longitudinal loads based on a relaxation process similar to that used in the method of moment distribution (Cross 1932). While he considers an elasto-plastic model of the foundations of tubular steel structures, he does not address the P-Delta effects of the vertical loads when there are large longitudinal deflections.

Fleming et al. (1978) describe the computer program BRODI1 for static analyses of unbalanced snow loads and the residual static forces after broken wire loads. BRODI1 included the tower flexibility in the calculations, but as with Campbell's approach, did not account for P-Delta effects that are particularly important for flexible structures. BRODI1 was limited to straight line sections, with all supports for each individual wire at the same elevation. The tower flexibility matrix was a user input. BRODI2 (Mozer 1983) expanded the capabilities of BRODI1 to allow longer line sections and variations in elevation. It included a separate program BROFLEX which could be used to calculate the flexibility matrices of the structures. P-Delta effects were recognized, but accounted for by using a modified flexibility matrix. Arm impact factors using the energy formula proposed by Peyrot (1978, Appendix A) were incorporated in the program.

The determination of the residual loads is still of interest because some current design guides base their recommendations for broken wire loads on the residual static tension in the span adjacent to the break (ASCE 1991; 2001). Some modern transmission line design tools now include provision for analyzing the residual static sag and tension (SAGSEC 1998).

2.4 Dynamic Analyses

Four analytic approaches have been taken to determine the dynamic impact on transmission structures due to broken wires. These include the use of an analog computer, deriving formulas for the impact factor based on simplified dynamic theory, writing computer software designed specifically for this problem, and using commercially available structural dynamics software for general problems.

Both Borges et al. (1968) and Peyrot (1978) have derived formulas for impact factors. Borges' formula is based on model tests discussed above (see Equation 2-3). Equation 2-4 is Peyrot's formula after Mozer (1978).

$$IFR = 1 + \omega\sqrt{\frac{2|W|}{wag}} \qquad \text{Equation 2-4}$$

Where: IFR is defined by Equation 2-2 as the ratio of the peak tension to the residual static tension, ω = the natural frequency of the first span after the break at its residual static tension taking into account the support stiffnesses, w = unit weight of wire, a = span length, W = the sum of the changes in gravitational potential energy and strain energy in the first span after the break, and g = the acceleration due to gravity.

Elgerd (1963) used an analog computer to calculate the forces due to a broken wire. The analog computer used electrical components analogous to the mechanical components of a transmission line. Elgerd did not consider the stiffness due to the catenary shape of the wire to be of importance, saying "Indeed, the elastic forces are so predominant that the gravity forces will have a very insignificant effect upon the crossarm force." This gross simplification reduced the non-linearity of the problem making it solvable. At best, his solution would have given the first tension peak due to the elastic contraction of the wire.

Siddiqui (1981) wrote "BROKE," one of the first finite element dynamic computer programs to specifically analyze broken wire loads. The structures were modeled with multiple elements; however, each suspension insulator and each span of wire was modeled as a single non-linear finite element with only longitudinal degrees of freedom.

Thomas (1981) also developed a computer program to analyze broken wire loads. Here the structures and intact conductors were modeled as an elastic spring with a "spring constant equivalent to the combined stiffness of the tower and the remaining attached, unbroken conductors and shield wires." Only straight sections of line were modeled; however, support elevation differences could be modeled. The insulator string and conductors were modeled as catenary cable elements with the mass lumped at the ends. The conductor was modeled with varying numbers of cable elements. The forces in the conductor elements were calculated using the catenary properties in a subroutine developed by Peyrot and Goulois (1978). The number of cable elements used in a span was varied and the simulations compared with experimental data from broken wire tests.

In preliminary studies, Thomas experimented with up to 20 elements in the first span and up to five spans. She settled on a three span model with ten elements for the first span, four elements for the second span and two elements for the third span.

The magnitudes of Thomas's analytic peak loads on the tower next to the break correlated relatively well with the experimental data, but the timing of the peaks and details of the time history were not well reproduced. Thomas attributed this to the build-up of round off error in the calculations; however, these problems may have been due to the large amount of damping used.

After trying axial damping of 10%, 15% and 20% of the critical damping for a rod, Thomas settled on 20%. This high value was justified by reference to the work of Wen (1968); however, Wen's use of 20% of critical damping was based on the aerodynamic damping on a conductor in a high wind, a situation which is not analogous to a broken conductor in still air. The high level of damping may have been needed to suppress spurious vibrations induced by the choice of finite element mesh. Using a small number of longer elements lowers the frequency of the spurious vibrations, and changing the length of elements in the mesh causes internal wave reflections that do not occur in nature (Bazant 1978; Holmes and Belytschko 1976).

Thomas went on to perform a parametric study using her program to investigate the influence of variations in span length, tower stiffness, initial conductor tensions and insulator length on the peak loads on the first tower. She concluded:

> "The most significant changes in peak tension are due to changes in the initial line tension and the span. Although the tower stiffness, insulator length, and additional line weight have less effect, they cannot be eliminated from consideration..."

Anjam (1991) and Gupta (1991) studied the 1990 failure of Iowa Power and Light's Sycamore to Lehigh 345 kV line. Anjam modeled individual conductors using a modified and updated version of the program CABLE 7 developed by Thomas (Thomas 1981). The update included allowing the conductor to slide along the ground surface using the techniques described in Peyrot and Goulois (1978). Towers were still modeled as a simple spring-mass system. His results were compatible with the hypothesis that the cascade started with the failure of a malleable iron socket Y-clevis on a running angle structure. Anjam does not give the number of catenary cable elements used or the internal damping assumed. His results were used to guide Gupta's static analysis of a section of line and his attempt to model the time history of the cascade. The software used in the analysis was the Electric Power Research Institute's (EPRI) ETADS (EPRI 1990). A static analysis of the assumed pre-cascade conditions was successful. A dynamic analysis was attempted but failed due to numeric instabilities. Six spans with five structures were modeled using a total of 245 nodes and elements. Each span of wire (30 in all) was modeled with one catenary cable element. The length of the time steps used in the analysis appears to have been 0.05 s which is substantially longer than the time steps used in similar analyses. For example, in his successful analysis using ADINA, Lapointe (2003) used a substantially smaller time step of 0.0015 s.

Lilien and Dal Maso (1990) refer briefly to the use of the computer program SAMCEF Cable, now Mecano Cable (*Mecano Cable* 2003) for simulating broken conductors and show good results when compared with one of the tests reported by Mozer (1978).

Kempner compared his model results reviewed above with computer simulations performed using an in-house computer program ESMCABLE, developed by Bonneville Power Administration. It is based on CABLE10 which was developed at the University of Wisconsin Madison, a successor to CABLE7 used by Thomas (1981). It appears that each span in the simulation was modeled with one catenary cable element (few details of the analytic model were provided). Kempner concluded that the sensitivity of the peak impact load magnitude was directly related to the selection of the analytic damping. He attributed this to load spikes due to the discrete distribution of element masses in the model. In his results, these spikes are manually edited from the data. The analytic models that simulated the tests of multiple tower failures had stability problems and could only run for 0.8 seconds of the desired 3.07 seconds. The analytic and scale model time histories did not match well because the model conductor hit the ground and the analytic model was not capable of simulating ground contact.

Nafie (1997) developed a computer program DYNTRN to perform dynamic analysis of broken wire, galloping and broken insulator loads on transmission lines which uses two node tension only truss members to represent the cable. He developed a method of condensing the cable degrees of freedom in the dynamic analysis to reduce the number of elements in the global finite element analysis. Nafie noted that a time step of 0.001 s was used in his analysis of a broken conductor problem with a smaller time step of 0.0001 s used during the parts of the analysis when the cable was slack. The magnitude of the forces in Nafie's model was also highly dependent on the amount of damping included in the model.

The use of a generalized commercial finite element dynamics program (ADINA 1984) for modeling transmission lines was pioneered by McClure (McClure 1989; McClure and Tinawi 1987; 1989a; b). Her work includes an extensive review of the literature concerning dynamic modeling of lattice and cable structures (McClure 1986).

Using ADINA, McClure modeled, with good results, several of the reduced scale tests performed by Mozer (1978). The model time histories agreed well with the experimental time histories, always within 20%. Using ADINA allowed different solution methods to be tried without the burden of writing a program for each different method. McClure and Tinawi (1987) report some of these results.

McClure was also the first researcher to model numerically a complete transmission line section including all three phases, the two shield wires, dead-end towers and suspension towers. Due to limitations in the capacity of computers at the time, the lattice suspension towers were modeled as transverse planar structures with the correct longitudinal distribution of mass and stiffness. The lines modeled were based on Hydro Quebec's James Bay 735 kV lines. The three dimensional model was compared to two dimensional models. She concluded that the three dimensional model is superior because of the influence of the shield wires on the stiffness of the conductor attachment points, the influence of the higher modes of tower vibration (note that 735 kV tower are very tall ≈ 45 m) and for the outside phases, the importance of the torsional characteristics of the towers.

Both Jamaleddine and Roshan Fekr (Jamaleddine et al. 1993; Roshan Fekr 1995) successfully used the finite element dynamics program ADINA (latest version ADINA 2003) for modeling conductor motion after ice dropped from intact spans of wire.

Lapointe (2003) analyzed the failure of a double circuit 120 kV transmission line during an ice storm in 1997 (See also McClure and Lapointe 2003). Two towers collapsed after two conductors broke while loaded with an estimated 20 to 25 mm of radial ice.

Lapointe made three types of models, all using the finite element dynamics program ADINA (ADINA 2001). The first modeled only the conductor and suspension insulators as two node isoparametric truss elements with the insulators pin connected to a rigid support. The second suspended the insulators from elasto-plastic beams, and the third modeled the line section in three dimensions including all cables and suspension insulators and their structures. In the third model, the suspension towers were modeled in three dimensions using a combination of beam elements and truss elements and the dead-ends were modeled as rigid supports for the conductors. The towers modeled are very narrow base lattice towers that are more akin to today's tubular steel structures in longitudinal stiffness but can be expected to be more torsionally flexible. The tower's longitudinal and torsional stiffness and natural frequencies are not given. Lapointe concludes that the 3D model better represents reality than the 2D model, although that model did not include any consideration of the tower mass and stiffness. His 3D analysis showed that the failure mode of the towers modeled could be explained through the dynamic analysis. Lapointe extended McClure's (1989) modeling of a complete transmission line with planar structures to fully modeling complete structures in three dimensions using a generally available commercial finite element dynamics program.

Table 2-8 shows impact factors *IFR* (Equation 2-2) for Lapointe's 2D model. Lapointe's time histories of the insulator string tensions showed load spikes similar to those mentioned by Kempner (1997). Lapointe suggests they are due to a divergence in the equilibrium iterations and were caused by the properties assumed for the insulator strings.

Table 2-8
Impact Factors *IFR* for Lapointe's (2003) 2D Models

Span Length (m)	Description	Radial Ice (mm)	Initial Tension (kN)	Residual Static Tension (kN)	Maximum Tension (kN)	Span to Sag Ratio	Span to Insulator Length ratio	Impact Factor
195	Cond_sp4	0	19.3	13.4	45	37.9	195	3.4
	Cond_sp4	20	44.1	32.3	95	31.2	195	2.9
	Cond_sp4	25	52.6	39.1	110	29.9	195	2.8
208	Cond_sp5	0	19.3	11.1	38	35.6	208	3.4
	Cond_sp5	20	44.1	28.2	80	29.3	208	2.8
	Cond_sp5	25	52.6	34.5	105	28.1	208	3.0

2.5 Longitudinal Load Limiting Devices

Using special mechanical devices to limit the longitudinal loads due to broken wires and other longitudinal disturbances dates back to the earliest days of the transmission line construction. Sliding clamps to limit longitudinal loads were being tried as early as 1910 (Wilkinson 1910). Recent reviews of load limiters include those of CIGRE Working Group 22.06 (2000) and the author (Peabody and McClure 2002b). Only a few devices have been tested (see Table 2-9).

The tests by Healy and Wright (1926) are described in Section 2.2. The sliding clamps successfully reduced the peak loads on the tower due to the break of a simulated iced conductor.

Table 2-9
Full-scale Tests of Load Limiters

Year	Description	Reference
1926	Sliding Clamp	(Healy and Wright 1926)
1928	Rotating Arm	(ENR 1928)
1948	Bendable Arm	(Chappée and Mauzin 1948)
1978	Porcelain Post Insulator Support	(Lindsey 1978b)
1989	Extending Insulator Support	(ANCO 1989)

An article in Engineering News Record (ENR 1928) describes tests of a tower with rotating crossarms designed by engineers at the Riter-Conley Co. in Pittsburg, PA. The hinge for the crossarm was inclined outward at the top end to provide a restoring force due to the weight of the wire (see Figure 2-6). The rotation of the crossarms after breaking a wire was reported as 90, 80, 60, 30, and 10 degrees at the 1st, 2nd, 3rd, 4th, and 5th towers, respectively, from the break.

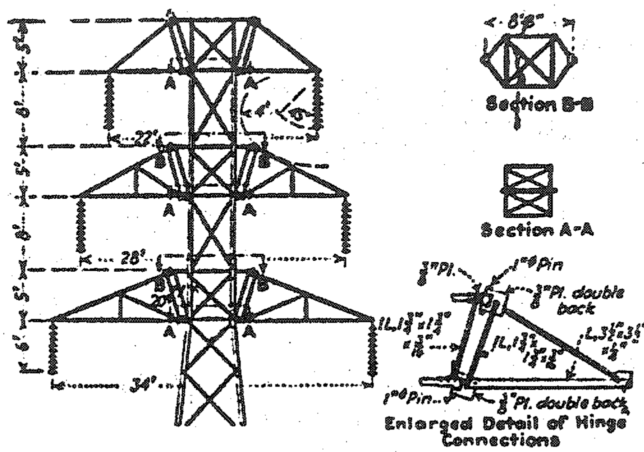

Figure 2-6
Rotating Crossarm by Riter-Conley (ENR 1928)

Cook (1959) discusses the use of crossarms on British Columbia Hydro's system that were made purposefully weaker than the rest of the tower to force failures to occur in the crossarms. Chappée and Mauzin (1948) report tests by the French National Railway of a deformable crossarm used to limit tower loads due to broken wires. The crossarms, rather than being hinged, used a bendable link between the crossarm and the tower body. The towers were tested by breaking a wire with and without the bendable links. The mast failed without the links and survived with them.

Lindsey developed a deformable base for porcelain post insulators (Lindsey 1970; Lindsey and Sammons 1967) to address the problem of insulator cascades. Both drop weight and full-scale broken wire tests were performed (Lindsey 1978b) showing the effectiveness of the deformable bases in limiting impact loads. These devices are currently listed in the Lindsey Manufacturing Company catalog.

In the early 1980's ANCO engineers received a contract from the U.S. Department of Energy under the Small Business Innovation Research Program to develop a load limiting device for high voltage transmission lines. Several different materials and methods for making load limiters were examined before settling on a particular device which was patented (Ibanez and Merz 1988). The device consists of two flat steel discs cut so that they will unwind under load into a spiral. Figure 2-7 shows excerpts from the patent drawings. Models of the new device were tested (ANCO 1984), and later full-scale tests were performed at the Electric Power Research Institute's Transmission Line Mechanical Research Center in Haslet, Texas (ANCO 1989; Sverdrup and EPRI 1986). Figure 2-8 shows the results of full-scale tests with and without the device (Ibanez and Stoessel 1996). These tests are of interest because they show the potential effectiveness of mechanical devices to reduce the impact loads on structures. Despite the successful tests, the ANCO load limiter is not a commercial success.

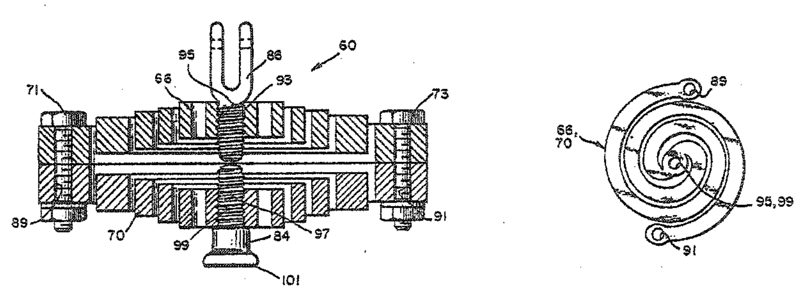

Figure 2-7
ANCO Load Limiter (Ibanez and Merz 1988)

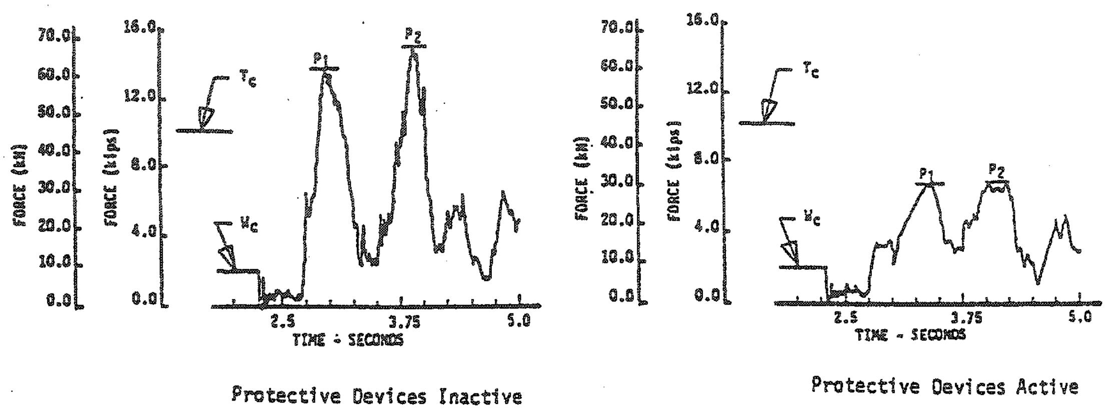

Figure 2-8
Test Results for ANCO Load Limiter (Ibanez and Stoessel 1996)

Interest in adding damping to the tower-insulator system can also be found in the literature about cable galloping. Galloping occurs when ice accretes unevenly on a cable forming an airfoil that can develop lift (Gilbert/Commonwealth 1979). The motion of the conductor has low frequencies, typically in the first three fundamental vertical modes, and high amplitudes – 5 to 500 conductor diameters – i.e., as much as 10 to 15 m. Richardson et al. (1965) propose using a longitudinal V-string attached to a rotational friction damper to damp the longitudinal motion of the insulator caused by galloping (see Figure 2-9).

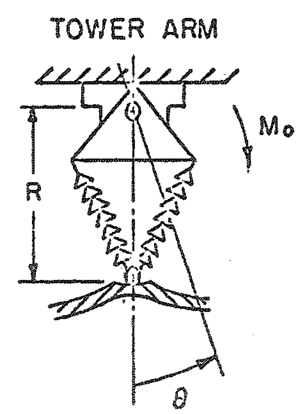

Figure 2-9
Anti-Galloping Friction Damper
(Richardson et al. 1965)

The author has observed this type of longitudinal motion being driven by galloping. As the span on one side of the tower was rising, the span on the other side was falling and the end of the insulator moved back and forth in time with the motion. A rotary viscous damper attached between a reaction beam at the end of the insulator assembly and the wire was tested by Ontario Hydro (Edwards et al. 1972). This system was effective in damping conductor galloping in the higher vibration modes but was unable to effectively damp the fundamental symmetric mode.

2.6 Structural Dampers

Webster's New Collegiate Dictionary defines a damper as "a device designed to bring a mechanism to rest with minimum oscillation." Use of dampers in buildings to control the motion of the building frame is relatively recent. In 1969, renowned structural engineer Leslie E. Roberston used approximately 10,000 viscoelastic dampers in the twin towers of the World Trade Center to control wind induced vibrations (Mahmoodi et al. 1987). This was the first application of dampers in a civilian building. Methods of adding damping to buildings have developed rapidly since that pioneering application, especially in the area of seismic design. Soong and Dargush (1997) provide an excellent overview of this development and detailed information on many different methods. Hydraulic and friction dampers are of interest for this research. Avtar Pall, while a graduate student at Concordia University in Montreal, invented a friction damper based on automotive brake materials for use in buildings (Pall 1979; Pall and Marsh 1982). Concordia's new library, completed in 1991, uses Pall dampers furnished by Pall Dynamics as part of its seismic force resisting system (Pall et al. 1987). In 1993, San Bernardino County's new

Arrowhead Regional Medical Center in Colton, California incorporated telescopic hydraulic dampers designed and built by Taylor Devices, a longtime manufacturer of dampers for military applications (Taylor 2003). To date, Pall Dynamics has furnished dampers for over 70 structures and Taylor Devices for more than 110.

Although use of dampers in buildings is a relatively recent development, mechanical engineers have been using dampers to control motion and reduce transient forces for over 100 years. Taylor (2003) describes the development of dampers for artillery pieces beginning in the 1860's. Development of dampers for automotive use progressed hand in hand with the automobile. Dixon's books include concise histories of this development (Dixon 1996; 1999).

Three of the many types of damper are of particular interest here, the rotary viscous damper, the rotary vane damper and the telescopic damper. The rotary viscous damper (see Figure 2-10) uses the shearing of a viscous fluid between rotating and stationary surfaces. They can rotate continuously and are often used to control the descent of loaded cables (Efdyn 1993).

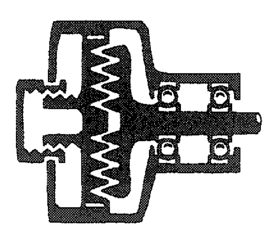

Figure 2-10
Rotary Viscous Damper
(Kinetrol 1996)

Houdaille (1909) patented the first rotary vane damper. Figure 2-11 is an excerpt from his patent drawings. Figure 2-12 shows a conceptually similar damper with a single vane that allows greater total rotation (Nash 1995). Morris and Dowling (1987) patented a spring-damper system combining a torsion bar with a rotary vane damper for use in the bogey wheel suspensions of tracked vehicles where they are commonly used (Els and Holman 1999). Rotary vane dampers are cataloged by several manufacturers for a variety of uses; see, for example, the Efdyn catalog (Efdyn 1993).

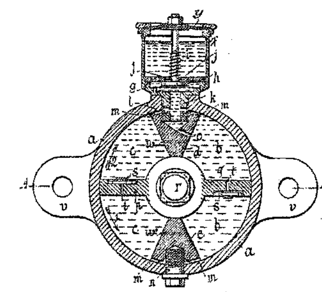

Figure 2-11
Rotary Vane Damper
(Houdaille 1909)

Modern automobiles use telescopic dampers almost exclusively. Telescopic dampers are also furnished as seismic dampers for civil engineering structures. Figure 2-13 from Dixon (1999) shows typical telescopic dampers.

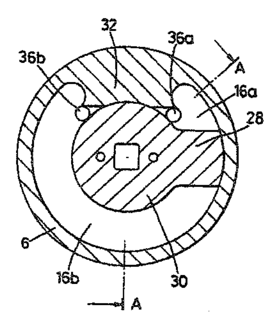

Figure 2-12
Rotary Vane Damper
(Nash 1995)

Dixon (1999) describes the theory of shock absorber design. Both rotary vane dampers and telescopic dampers rely on the turbulent flow of the damping fluid through orifices in the vane or piston. The flow is caused by the pressure differential due to their movement.

Turbulent flow through an orifice in a thin plate, by itself, gives a resisting force proportional to velocity squared. Valves are used to vary the flow based on the pressure differential between the fluid chambers to give a resisting force proportional to velocity. Figure 2-14 from Dixon (1999) shows three common valves. Using the spool valve as an example, as the pressure increases, the spool valve opens. The damping characteristics are controlled by area of the slots in the sides of spool which can be tailored to the pressure. Damper designers are able to achieve damping that is close to pure viscous damping, i.e. the damping force is proportional to velocity. Figure 2-15 shows a damping curve for an automotive damper from Bastow and Howard (1993).

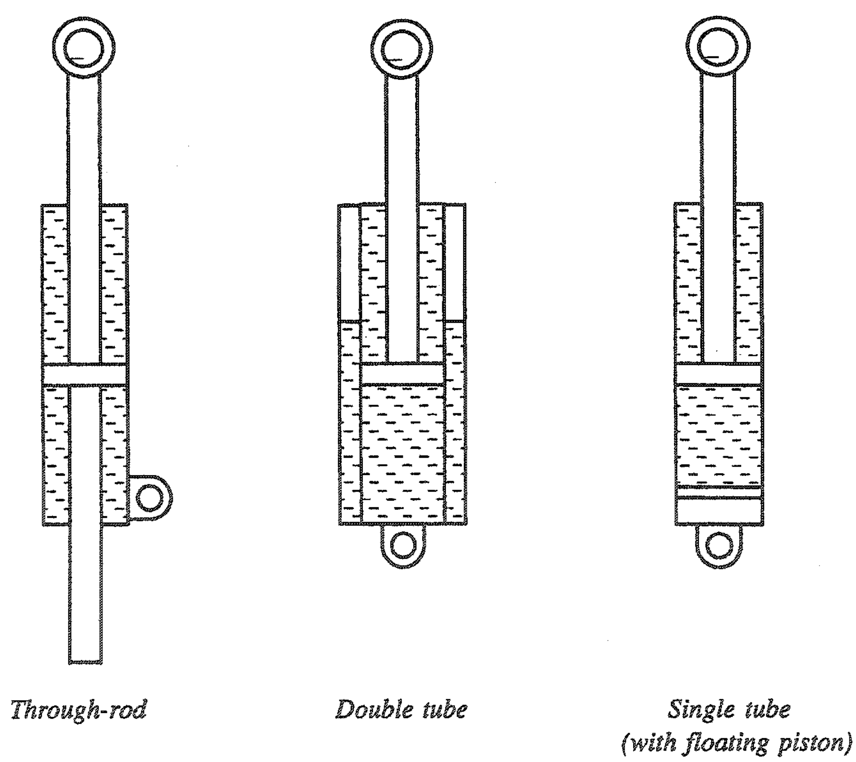

Figure 2-13
Telescopic Dampers after Dixon (1999) Fig. 1.3.5

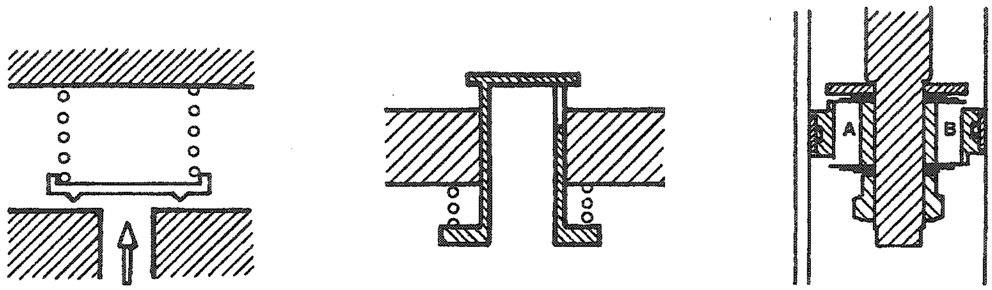

Coil-spring loaded disc. *Coil-spring loaded spool valve.* *Shim disc valves (double acting).*

Figure 2-14
Damper Valves after Dixon (1999) Fig. 6.2.1

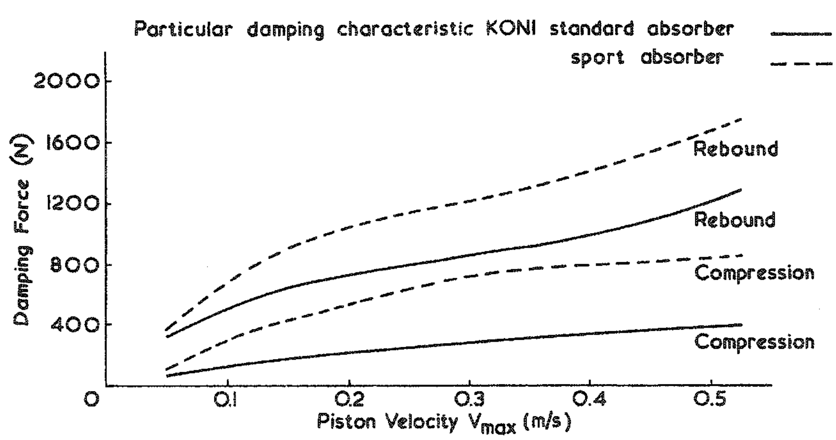

Figure 2-15
Damping Curve from Bastow and Howard (1993)

2.7 Comments on Modeling

There are still some questions to be answered in the area of modeling transmission line conductors. Most of the analytic studies have had load spikes in the conductor and insulator tensions that have either been suppressed using axial damping or manually edited out of the time histories. It is well accepted that the finite element mesh introduces some spurious forces into the time history due to both the discrete mass representation of a continuous system and due to wave reflections at changes in impedance. One avenue of investigation to reduce these problems is to determine whether the mesh size and time step length can be chosen to separate the frequencies of these spurious forces from the frequencies of interest to the structural behavior. If this can be achieved, the spurious frequencies can be suppressed using a digital filter. This is analogous to the use of analog filters in full-scale and model tests to eliminate noise outside the frequency band of interest.

Both the physical model tests and the analytic modeling that have been performed to date have looked at the effect of span length and number of spans independently. A new approach would be to hold the total length of wire and the total initial strain constant and vary the number of spans making up the total length. For example, 3500 m can be divided into equal spans of 125, 140, 250, 350, 500 and 750 m. The initial strain energy can then be held constant. A similar study that holds the total change in energy from initial to residual static conditions could also be tested by holding the total length constant, with the initial tension adjusted for each span length to give a constant total change in energy. This type of study could give some insight into the source and magnitudes of the classic two-peak time history of forces. Varying the span length within a given total length also more realistically models a real transmission line which, once the route has been set, has a fixed length. The designer then has some freedom within this length to tailor the spans to the type of structure used.

2.8 Summary

Transmission line cascades have been occurring for almost a century. The catastrophic series of cascades during the January 1998 ice storm shows that the design, construction and operation of transmission lines still needs to be improved. The many tests and analytic studies reviewed show the impact loads on the intact structures from longitudinal disturbances to the wire tensioning system can be as much as four times the residual static loads. The tests by Healy and Wright (1926) showed very early that substantial reductions in the impact forces can be achieved. This was confirmed more recently by full-scale tests of the ANCO Load Limiter (ANCO 1989). Although these devices are not commercially successful, they show that methods of controlling the energy released by broken wires have the potential to greatly reduce the impact loads on the towers.

Since the first use of dampers to control wind vibrations in buildings in 1969, great strides have been made in the application of both friction and viscous dampers to buildings and bridges to control wind and seismic motion. Investigating the application of supplemental mechanical dampers to the problem of controlling broken wire forces is a natural extension of these concepts. In parallel with the advances in application of dampers have been advances in the speed and memory of personal computers and the capabilities of the analysis software. It is now feasible to test the application of dampers to transmission lines using commercial finite element dynamics programs like ADINA (ADINA 2003)

Chapter 3
Research Approach

The focus of this research is to find a way to reduce the peak loads on the towers due to broken wires and other disturbances to the wire tensioning system. Figure 3-1 shows a typical 230 kV porcelain suspension insulator assembly attached to a tower crossarm. Figure 3-2 shows a typical shield wire assembly. Two methods of modifying the tower-insulator system are proposed to reduce the impact loads, the "post spring-damper" and the "rotating crossarm spring-damper." These are the subjects of this research.

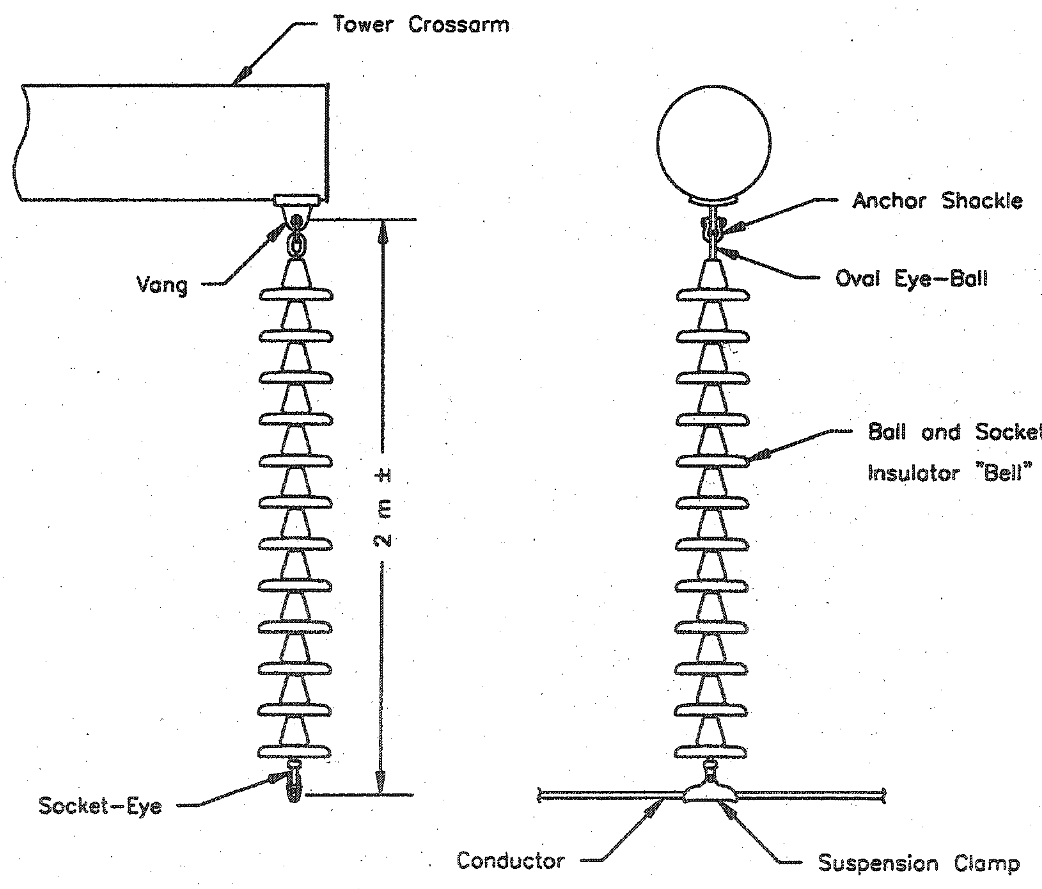

Figure 3-1
230 kV I-String Insulator Assembly

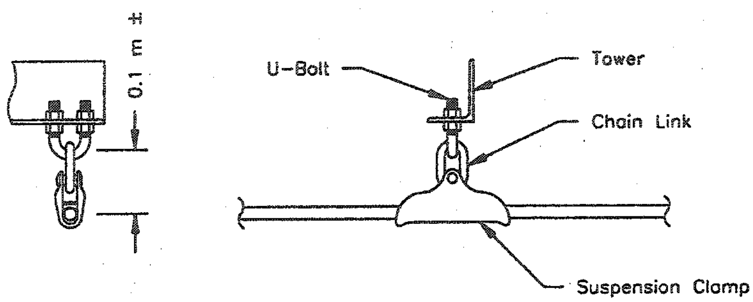

Figure 3-2
Shield Wire Suspension Assembly

3.1 Research Subjects

The Post Spring-Damper: For the conductor, this system uses a composite post insulator (an insulator designed for cantilever loads) connected to the tower through a rotational spring-damper system as shown in Figure 3-3. The same system using a composite post in place of the post insulator was investigated for attaching the shield wire to the structure. When there is a sudden longitudinal imbalance in the wire tension, the wire moves longitudinally, causing the post to rotate. The rotation of the post is resisted by the torsional spring. As the base of the post rotates, the damper absorbs part of the kinetic energy.

The Rotating Crossarm Spring-Damper: The rotating crossarm spring-damper is shown in Figure 3-4. A standard suspension insulator attaches the wire to the crossarm. The crossarm is attached to the tower using a vertical axle. A torsional spring and a torsional damper are attached between the rotating arm and the tower. When tension is lost on one side of the insulator, the suspension insulator swings in line with the conductor pulling longitudinally on the end of the crossarm. This causes the crossarm to rotate about its vertical axle at the tower body. This motion is resisted by the spring, with the damper absorbing part of the rotational kinetic energy.

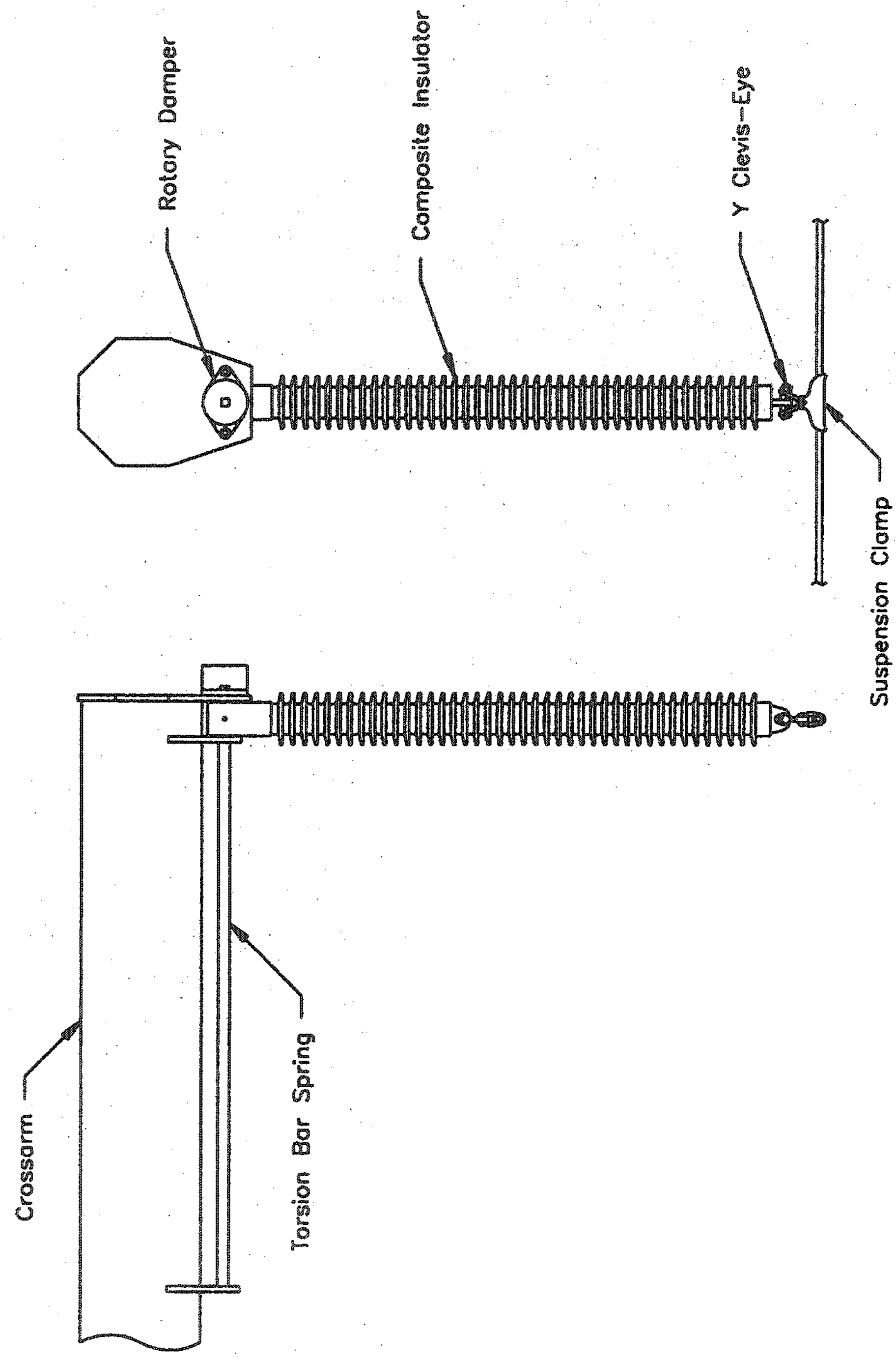

Figure 3-3
Post Spring-Damper System

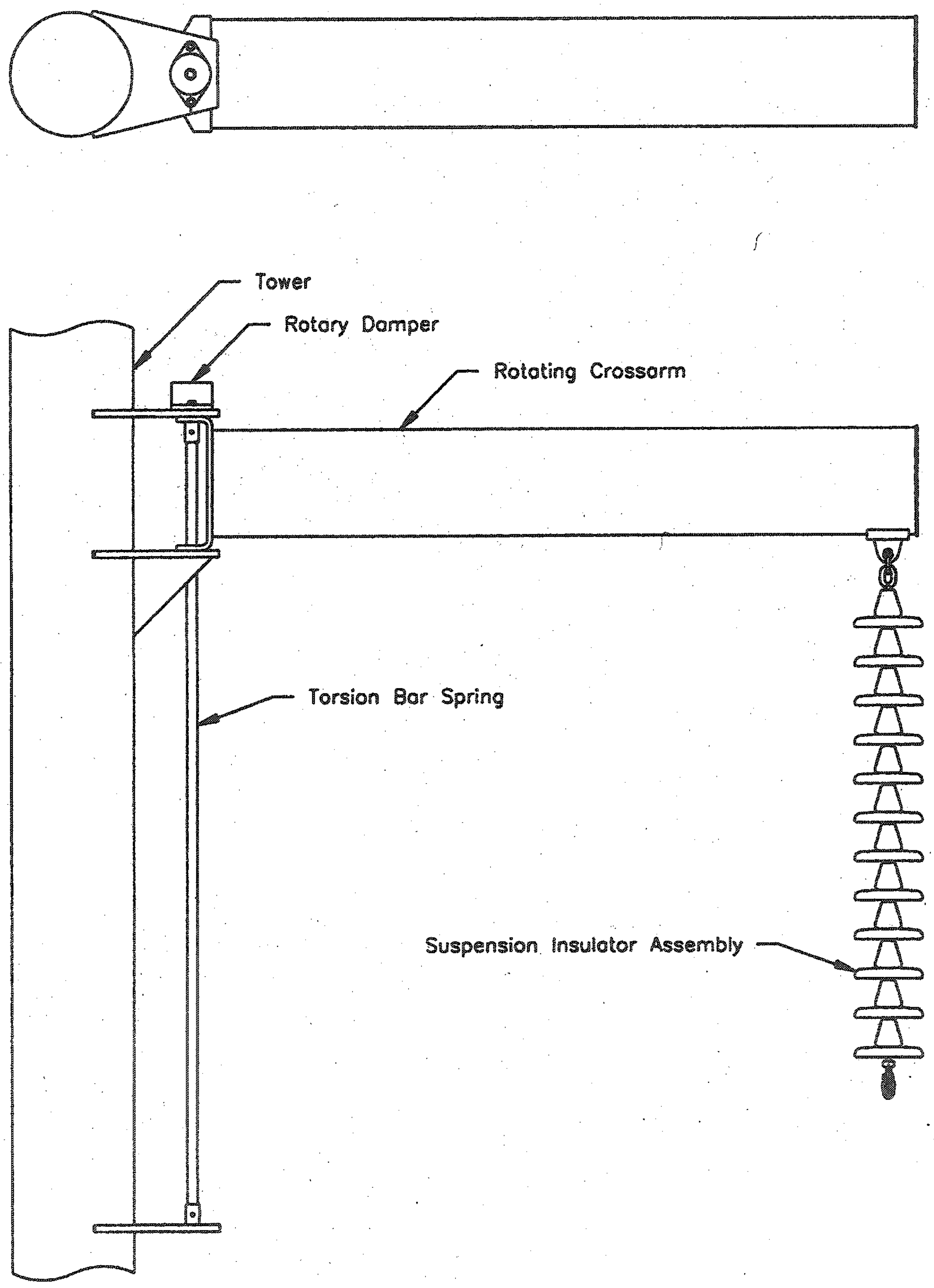

Figure 3-4
Rotating Crossarm Spring-Damper

3.1.1 Telescopic Springs and Dampers

In Figures 3-3 and 3-4, the springs are torsion bars. The damping is provided by rotary dampers. Figure 3-5 shows how telescopic dampers can be substituted for the rotary dampers. A coil spring (not shown) can be installed around the telescopic damper to replace the torsion bars.

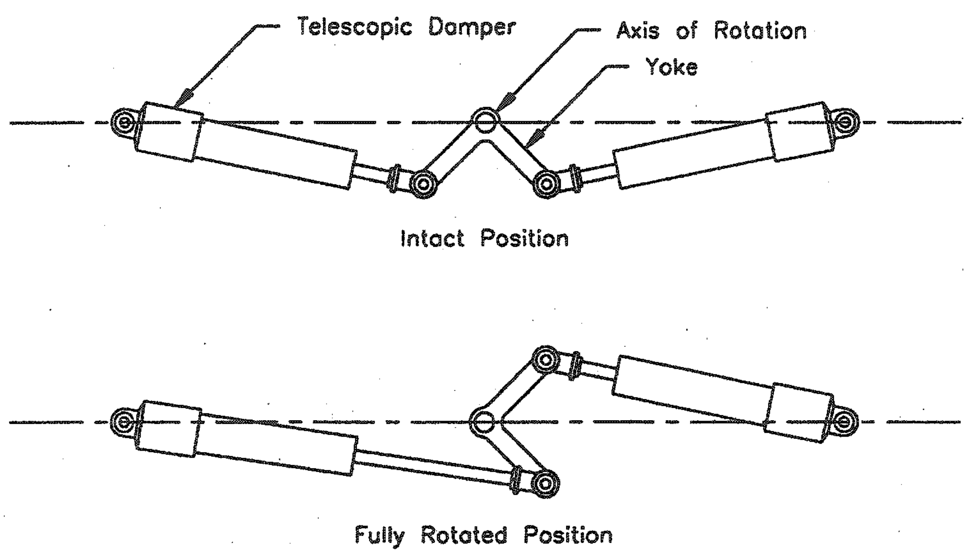

Figure 3-5
Application of Telescopic Dampers

3.2 Research Approach

There are four approaches for investigating whether the post or rotating crossarm spring-dampers reduce the impact loads on towers when there is a sudden loss of tension in the wire:

- Theory
- Model tests
- Full scale tests
- Finite Element Dynamic Models

To date, there is no theoretical solution for predicting the tower loads due to broken wires. Two semi-empirical formulas have been proposed, see Equations 2-3 and 2-4 (Borges et al. 1968; Peyrot et al. 1978). The constant in Borges' formula is based on test data and Peyrot's formula gives different results when applied at model scale and full scale. Entering Figures 2-4 and 2-5 for a span to sag ratio of 60 and a span to insulator length ratio of 50 to 55 gives impact ratios of 4.5 and 3.4 respectively. The impact ratios in Figure 2-4 are based on model tests; Peyrot's formula was used to construct Figure 2-5 (Mozer 1978). A theoretical approach was, therefore, rejected.

Model tests (see Table 2-3) have used scale factors ranging from 1/50 to 1/23.3. Even at these small scales, a large building can accommodate only a few spans. A 350 m span at 1/30 scale requires approximately 12 m per span. For this reason, the tests performed by Mozer (1978) included only 2 intact spans, and those of Kempner (1997) 5 intact spans. Richardson's 1/50 scale tests included 10 intact spans, but they were performed outside on the roof of a large building. Most of the model tests performed to date have had unrealistically short sections of line due to the space limitations. With no theoretical guidance for an appropriate range of spring stiffnesses and damping constants, model testing would require many different setups to find the proper area of investigation. Due to the need for a large space and the lack of a starting place for the values of spring constant and damping coefficient, model testing was not considered.

Full scale tests have the same problems as model tests with the additional problem of great cost and the need for a very large site. The tests performed by Healy and Wright

(1926) and Stefoff et al. (1961) were performed in conjunction with construction of new lines. The construction of the test sections could be done on the new line's right-of-way in conjunction with the larger project, thereby minimizing the cost. The EPRI-Wisconsin Power and Light tests (Peyrot et al. 1978) were performed on an existing line that was going to be dismantled. There was no construction cost, and if the towers were damaged or destroyed during the tests, only material that would have been scrapped anyway would be damaged. The lines used in Ostendorp's tests (1997c; 1997d) are among the few lines built expressly for that purpose. The author's last design project before beginning this research was a single circuit 230 kV line in Alaska. It cost approximately C$400,000 per km for construction exclusive of the right-of-way. The cost of constructing a ten span test line (3.5 km) would run in excess C$1,000,000. Securing financing for full scale tests is very difficult unless they can be performed in conjunction with constructing a new line or rebuilding an existing line. For these reasons, full scale tests were not considered.

Dynamic finite element modeling was chosen for this study because it has been successfully used for similar analyses of cable problems in the past (Jamaleddine et al. 1993; Lapointe 2003; McClure 1989; Roshan Fekr 1995; Thomas 1981). It also avoids the cost and space problems inherent in both model and full scale tests. Perhaps more importantly, modeling can provide a good indication of whether the methods work well enough to warrant testing. If tests are performed, the modeling can provide reasonable values for the spring stiffness and damping constants around which the tests can be planned.

3.3 Research Tools

The Microsoft Windows version of ADINA from ADINA R&D (ADINA 2001; ADINA 2003) was used for this study. There is other software that has similar capabilities, DYNA3D for example. ADINA was chosen because it has been successfully used for wire dynamics problems in the past, McGill University already had a license to use ADINA, and it has the finite elements needed for modeling these problems. Most of the modeling was performed on personal computers with 2 GHz Intel Pentium CPUs, although some modeling was done on slower computers.

3.4 Research Plan

Transmission lines are constructed from a wide variety of materials and types of structures (for more detail see Appendix C). Table 3-1 shows a partial list of transmission line variables and the range of values commonly encountered.

Table 3-1
Transmission Line Variables

Variable	Typical Low Value	Typical High Value
Span length (m)	80	550
Spans between dead-ends (number)	1	125
Wire diameter (mm)	12.8	47.8
Wire modulus of elasticity (GPa)	54	184
Bare wire catenary constant 0° C (m)	600	3000
Design ice thickness (mm)	0	66
Insulator assembly length (m)	0.75	5.80
Longitudinal tower natural frequency (Hz)	1	4

Note that even with these broad ranges, there are lines that have values outside the range. For example, spans typically range from about 80 m to 550 m, but there are lines with individual spans over 2500 m.

This study was planned as if it were an experimental study. The "experiments," which are performed with a computer and software, determine the effects of two new variables or treatments, the spring stiffness and the damping constant, on the peak dynamic load. A factorial design (Clarke and Kempson 1997; Lye 2002) looks at the interaction of all the variables. The number of experiments necessary is the product of the number of values of each variable being considered (permutations of the treatment levels). For example, we could consider only the variables Thomas (1981) concluded were significant; these five variables are: the initial line tension (represented in Table 3-1 by the catenary constant), the span, the tower stiffness, the insulator length and the additional line weight (the weight of ice). If we add the spring stiffness and damping constant for the "post spring-damper" and look at only two levels of each variable we need $2^7 = 128$ experiments. We may, however, need more levels of damping constant and spring stiffness to find the optimal values, say five of each, requiring $5 \times 5 \times 2^5 = 800$ experiments. This quickly becomes unwieldy even using a computer instead of physical models. Based on these considerations, a case study was chosen to allow the effects of changes in spring stiffness and damping constant to be thoroughly evaluated.

Before beginning the case study, three of the EPRI-Wisconsin Power and Light tests (Peyrot et al. 1978) were modeled. The modeling is described in detail in Chapter 4. This modeling was done to verify the suitability of ADINA for this study, to become familiar with dynamic modeling and to become familiar with the capabilities of ADINA. The test line was originally built in 1931. Both conductors used in the test are small by today's standards. Instead of using the test line as a basis for the study, a new prototype line was developed.

The case study is based on a 230 kV single circuit lattice steel tower line with 350 m spans, Cardinal conductor and 7/16 EHS shield wire. These choices are explained in more detail in Appendix C. Sag tension data and more detailed information on the tower are included in Appendix D. Table 3-2 shows the tower properties. The wire properties are shown in Table 3-3. Figure 3-6 shows bare and iced profiles of the prototype line.

Table 3-2
Tower Properties

Property	Value
Stiffness (kN/m)	377
Equivalent mass (kg)	933
Frequency (Hz)	3.2
Damping % Critical	5.0

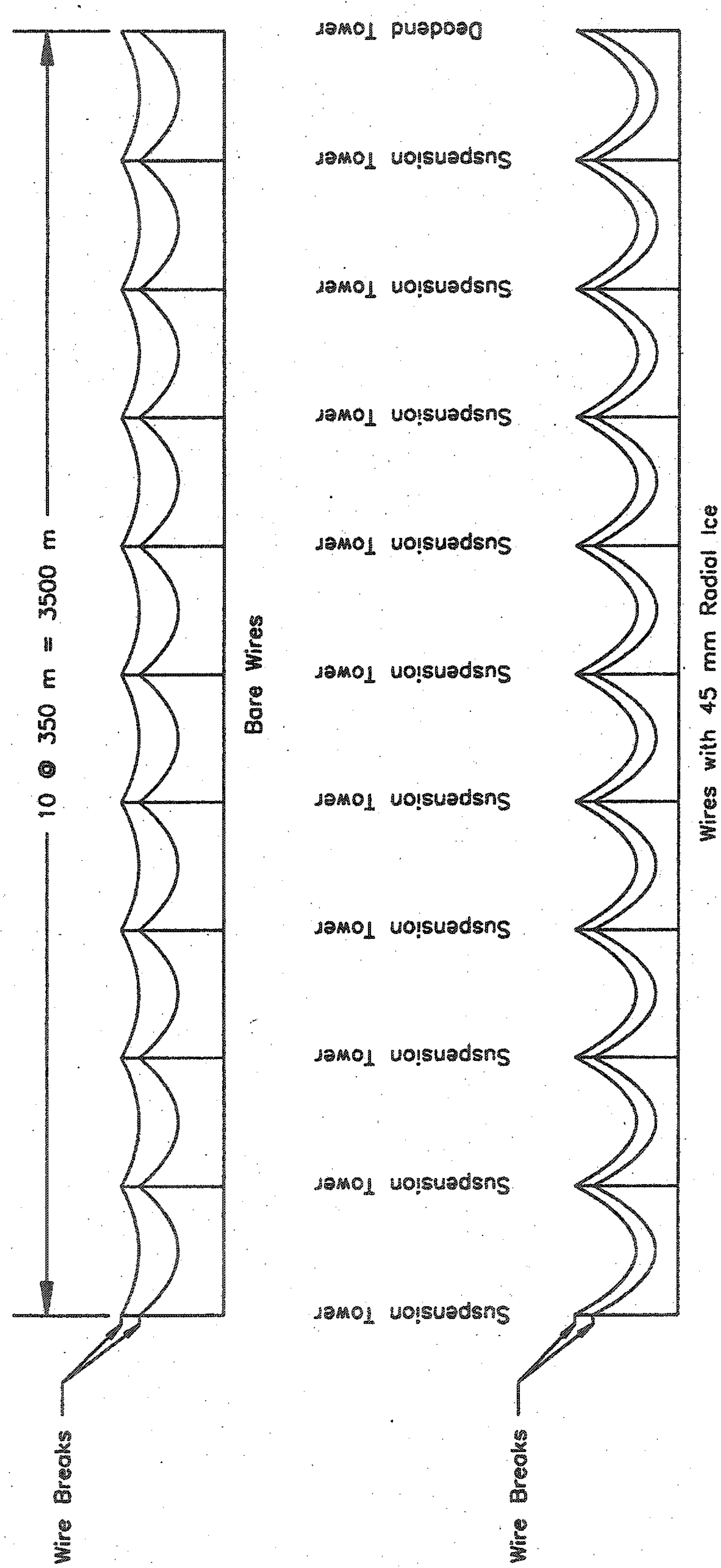

Figure 3-6 Profiles of Prototype Line

Table 3-3
Conductor and Shield Wire Properties

Description	**Cardinal**	**7/16 EHS**
Size (kcmil)	954.0	-
Stranding (Alum/Steel)	54/7	0/7
Percent Steel by Weight	26.75	100.00
Steel Area (mm^2)	63	74.6
Aluminum Area (mm^2)	483	-
Total Area (mm^2)	546	74.6
Diameter (mm)	30.4	11.0
Unit mass (kg/m)	1.8290	0.5938
Average Density (kg/m^3)	3350	7962
Rated Tensile Strgth (kN)	150	93
Rated Tensile Stress (kPa)	275	1241
Final Modulus of Elasticity (GPa)	65.8	184.1
Alcoa Sag-Tension Chart No.	1-838	1-1246

Table 3-4 shows the insulator and crossarm properties.

Table 3-4
Insulator and Rotating Crossarm Properties

Property	Conductor Post Insulator	Shield Wire Post	Rotating Arm	Suspension Insulator
Length (m)	2.0	0.5	2.0	2.0
Outside diameter (mm)	75.0	75.0	400.0	16.0
Inside diameter (mm)	0.0	0.0	391.0	0.0
Density (kg/m^3)	2000	2000	7820	2000
Elastic Modulus (GPa)	37	37	200	37

3.5 Finite Element Models

The finite element models are based on the model described in Chapter 4. For the "post spring-damper" the model was simplified by eliminating the arm and its associated torsional degrees of freedom. This allowed these models to be run as 2D models instead of 3D models, which substantially reduces the computation time. For all of the models, the tower node was fixed vertically rather than incorporating a spring representing the vertical stiffness of the tower. Figure 3-7a shows the finite element model of the tower for a bare conductor. The conductor model is the same one used to model the EPRI-Wisconsin Power and Light tests, see Figure 4-11.

As can be seen in Figure 3-2, shield wires have a very short link between the suspension clamp and the tower. Because the link length is so short, longitudinal loads for the shield wire attachments are typically calculated based on the shield wire being attached directly, a zero length link. The post spring-damper for the shield wire was given a length of 0.5 m to provide torque to operate the spring and damper (Figure 3-7a). For comparison, a model with no link was also made (Figure 3-7b).

Based on the impact factors in the literature, it appeared that the longitudinal impact loads for the iced conductor would be beyond the cantilever load capacity of a single post insulator. The iced conductor was modeled with a longitudinal V-string insulator assembly as shown in Figure 3-8. This type of insulator would have to be mounted outboard of the end of the crossarm.

The finite element model of the rotating crossarm spring-damper is shown in Figure 3-9a & b. In addition to modeling the rotating crossarm with a vertical axis of rotation, an axis inclined at 20° to the vertical was analyzed with no spring-damper installed, see Figure 3-9c. The axis was inclined as shown for the Riter-Conley test tower in Figure 2-6 (ENR 1928).

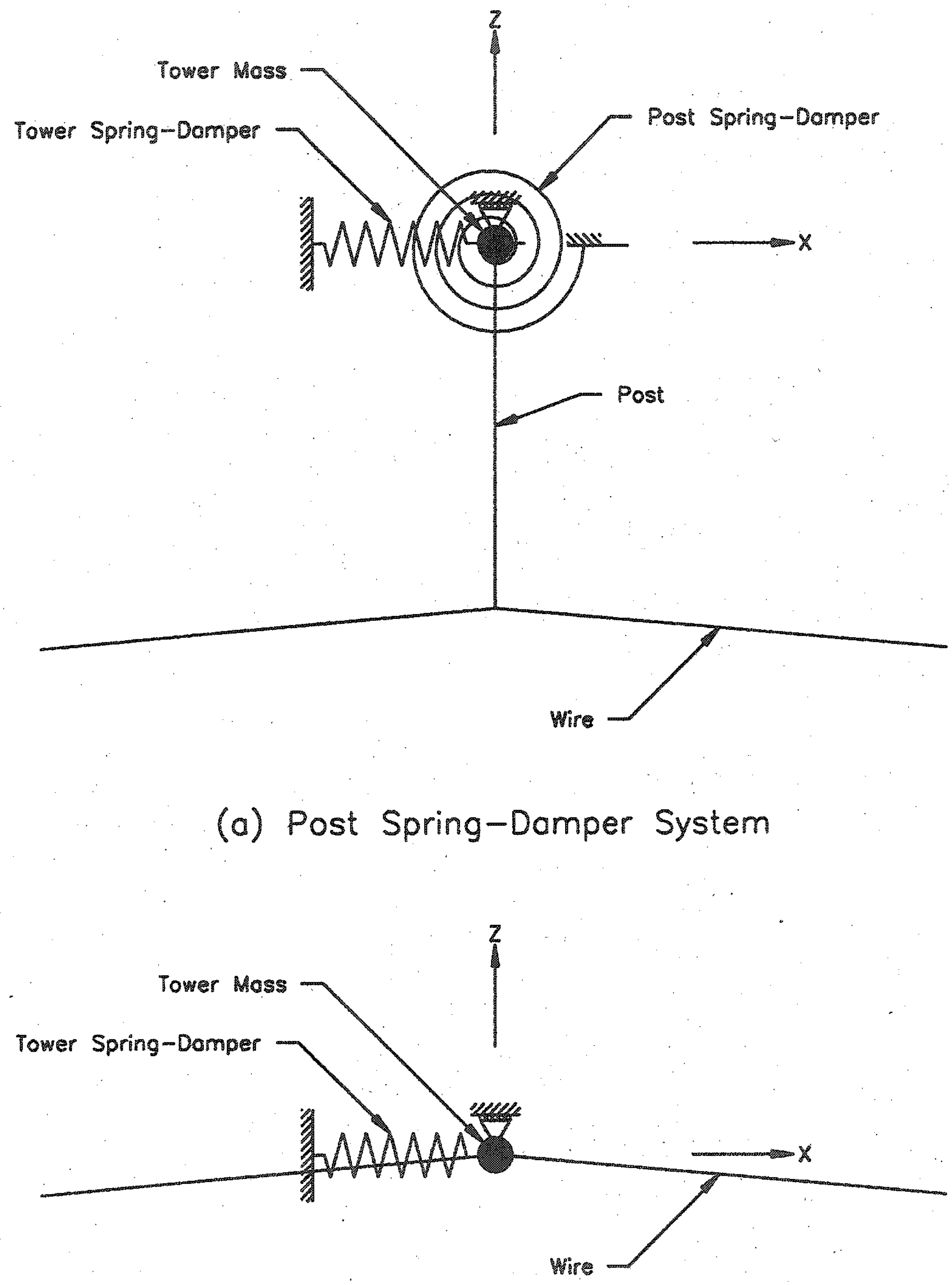

(b) Shield Wire without Post Spring-Damper

Longitudinal Elevations

Figure 3-7
Finite Element Tower Models

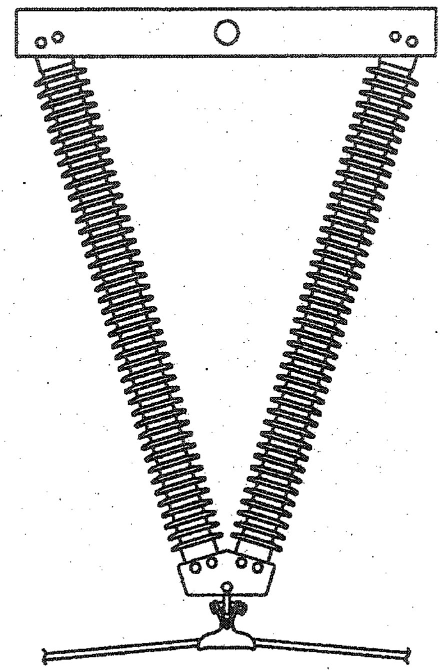

Prototype

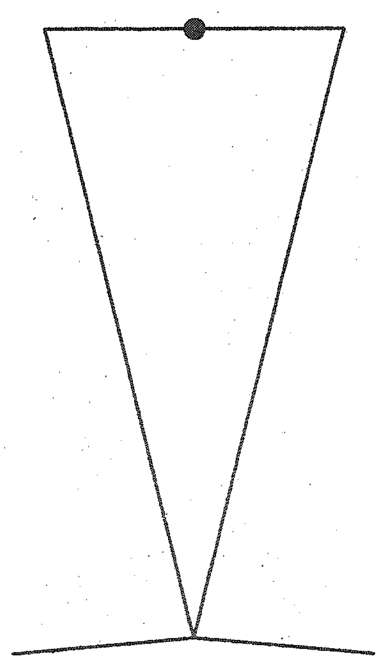

Model

Figure 3-8
Longitudinal V-String

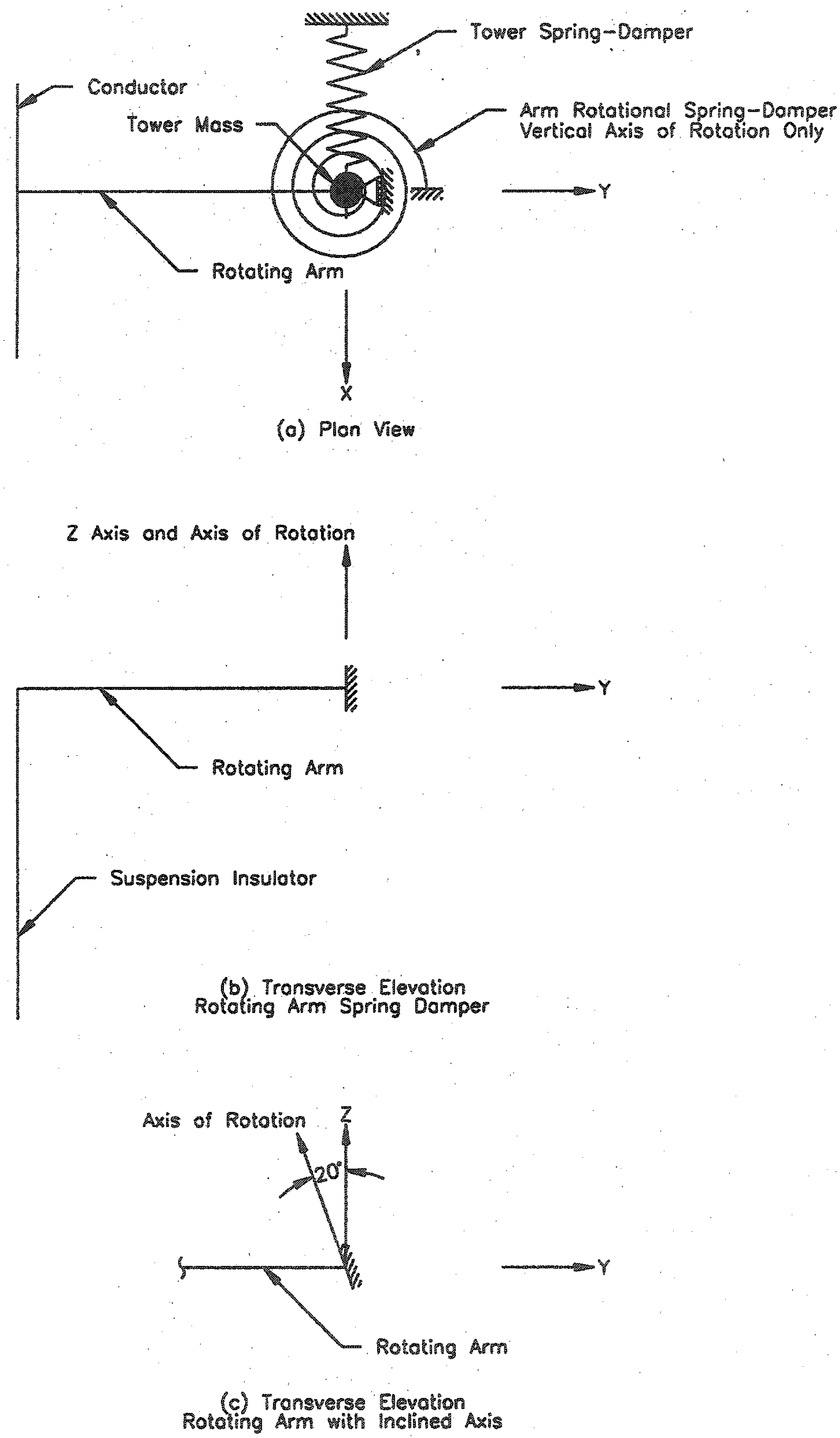

Figure 3-9
ADINA Models of Rotating Crossarms

For all the finite element models, the wire and suspension insulators are modeled as 2 node truss elements. The composite post insulators and crossarms are modeled as hermitian beam elements. The springs are modeled as linear springs. The dampers are modeled as viscous dampers.

Two types of finite element analysis were performed. First, the residual static tension and an appropriate range of spring stiffnesses were determined. Second, dynamic time history analyses were performed. In both analyses the first step is to get the wire installed at the correct tension and sag. This is done by calculating the coordinates of each wire node based on its catenary shape. The following discussion of catenary calculations is based on Ehrenburg's classic paper (Ehrenburg 1935). The line geometry variables are shown in Figure 3-10 where a is the span, b is the elevation difference between supports and c is the slope distance between supports. For spans with different attachment elevations, the low point of sag is first calculated using Equation 3-1, where *H* is the horizontal tension and *w* is the unit weight of the wire and *z* is a parameter defined in Equation 3-2. Note that when the elevation difference between supports is large, the low point may lie outside the span.

$$x_1 = \frac{H}{w}\left[arcsinh\left(\frac{bz}{a\ sinh(z)} \right) + z \right] \qquad \text{Equation 3-1}$$

$$z = \frac{aw}{2H} \qquad \text{Equation 3-2}$$

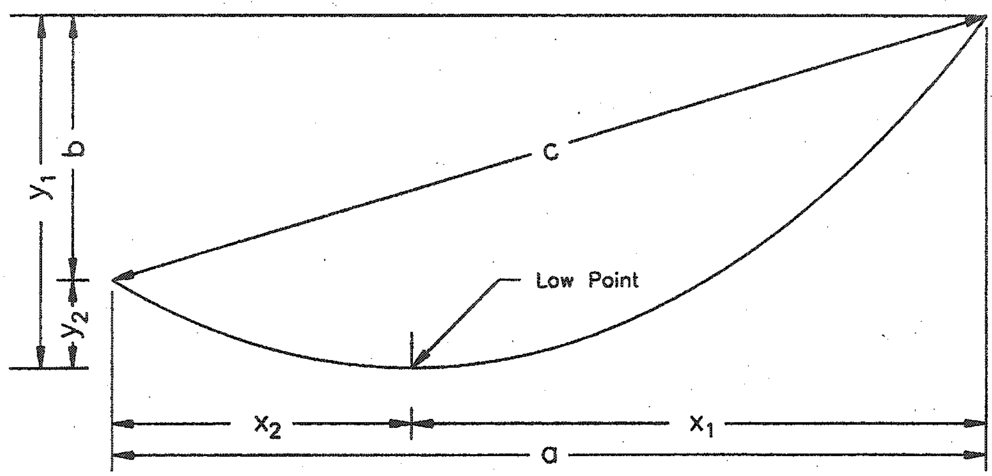

Figure 3-10
Line Geometry Variables

With the low point of sag known, the coordinates of the catenary using the low point of sag as the origin are calculated using Equation 3-3, with y the elevation above the low point of sag.

$$y = \frac{H}{w}\left[cosh\left(\frac{xw}{H}\right) - 1\right] \qquad \text{Equation 3-3}$$

The tension in the conductor varies continuously between the horizontal component of the tension at the low point to the tension at the supports. The support tension is the resultant of the horizontal tension and the weight of wire between the low point and the support. The effective tension is that tension, which if applied uniformly over the total unstressed length of wire in the span, would stretch the wire the same amount as it is stretched by hanging from the supports. The effective tension in the wire T_e is calculated with good approximation using Equation 3-4 where S is the stressed length of the wire given in Equation 3-5.

$$T_e = \frac{wS}{4z}\left\{\left(\frac{S^2+b^2}{S^2}\right)z\,coth(z)+\frac{a^2}{S^2}\right\} \cong \frac{wS}{2z}+\frac{wSb^2z}{6c^2} \qquad \text{Equation 3-4}$$

$$S = \sqrt{a^2\left(\frac{sinh(z)}{z}\right)^2+b^2} \qquad \text{Equation 3-5}$$

The initial strain in the wire, ε can then be calculated using Equation 3-6.

$$\varepsilon = \frac{T_e}{AE} \qquad \text{Equation 3-6}$$

The first step in the finite element analysis (both for residual static loads and time histories) is to apply a gravity load to the wire prestressed by using the initial strain from Equation 3-6. This was done in one step for all cases. During this step, the tensions in the cable adjust from all having the same tension at the start of the step to varying from the low point to the supports at the end of the step. This step was performed using the "Full Newton" analysis.

3.5.1 Residual Static Analysis

The residual static state of the wire is the final at-rest position after all the dynamic effects due to a break in the wire or other longitudinal disturbance have damped out. The wire elements are defined as tension only members by setting the modulus of elasticity in compression to zero. Referring to Figure 3-11, which represents the leftmost tower in Figure 3-6, the finite element analysis is done in a series of steps. At each step, the position of node 100 is moved a fixed distance along the x axis. The total distance covered by this series of small steps is set large enough that the force in element 7-1 reaches zero before the end of the series. With the density of the material for element 7-1 set to 0, when the steps are complete, it exerts no force on the rest of the wire elements.

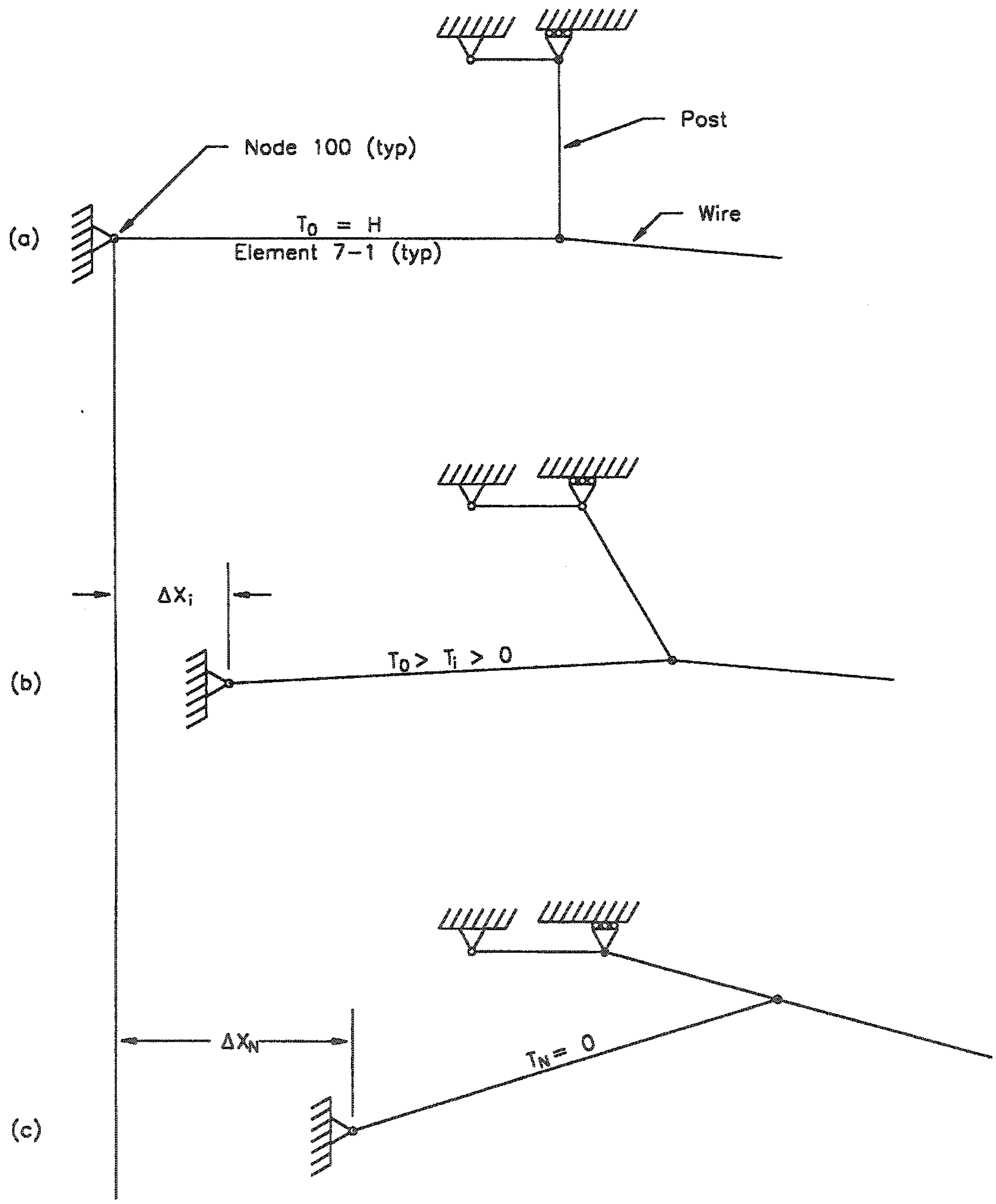

Figure 3-11
Residual Static Analysis

When a wire breaks, both strain energy and gravitational potential energy are released. The total change in energy can be calculated from the results of the residual static analysis using Equation 3-7, where ΔW is the energy or work done by the wire, Δx is the x displacement and R_x the x reaction at step i with the intact static position of the wire taken as step 0 and N is the number of steps.

$$\Delta W = \sum_{i=1}^{N} \left(\Delta x_i - \Delta x_{i-1}\right)\frac{\left(R_{x_i} + R_{x_{i-1}}\right)}{2} \qquad \text{Equation 3-7}$$

3.5.2 Determination of Spring Stiffnesses

In order to determine reasonable values of the spring stiffness, a residual static analysis of a single span identical to the first span of the 10 span model was performed. The reaction forces at Node 100 were used in the one span model to calculate the spring force needed to hold the wire in position at each step, assuming that the post was infinitely rigid. Figure 3-12 shows the force relationships. Equation 3-8 was used to calculate the spring stiffness. Figure 3-13 shows the results for the conductor and 3-14 for the shield wire. Spring stiffnesses were chosen to give post rotations of approximately 20, 40 and 60°.

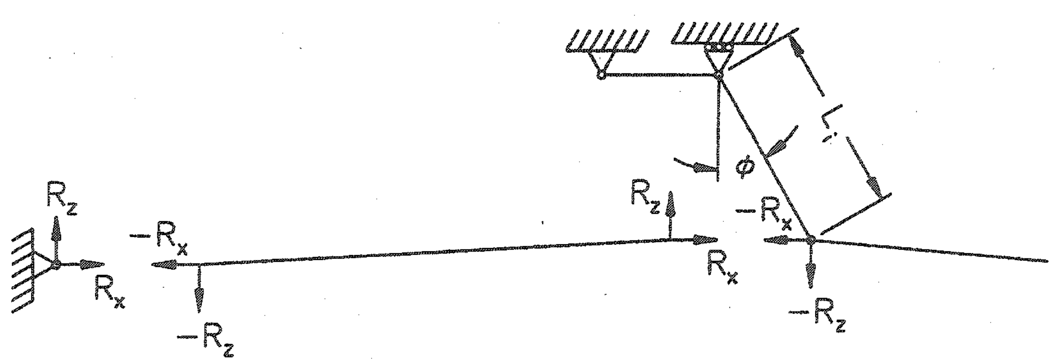

Figure 3-12
Spring Constant Force Diagram

$$k_t = \frac{-(R_z \sin\phi + R_x \cos\phi)L_i}{\phi}$$ Equation 3-8

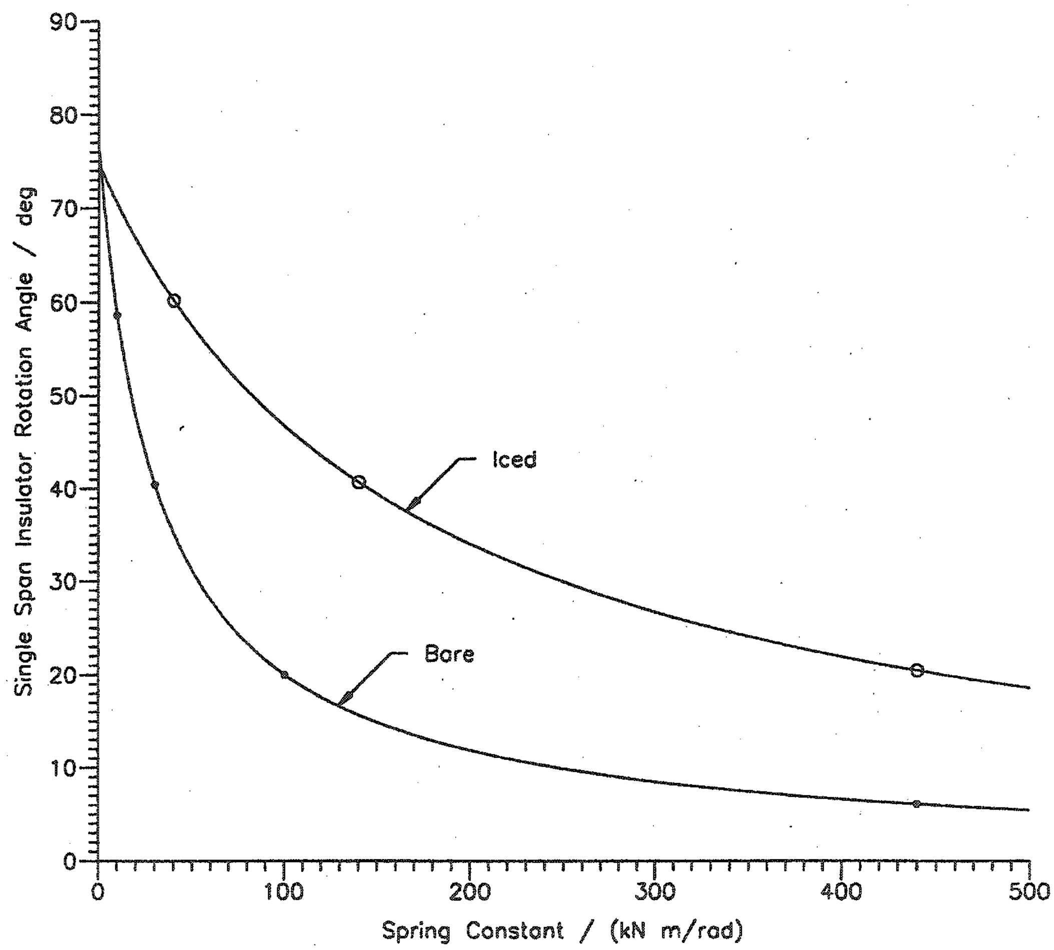

Figure 3-13
Post Spring-Damper
Conductor Spring Constants

This simple approach was not suitable for the rotating crossarm. For the rotating crossarm, the residual static position was calculated for a series of spring stiffnesses. The results are shown in Figures 3-15 and 3-16.

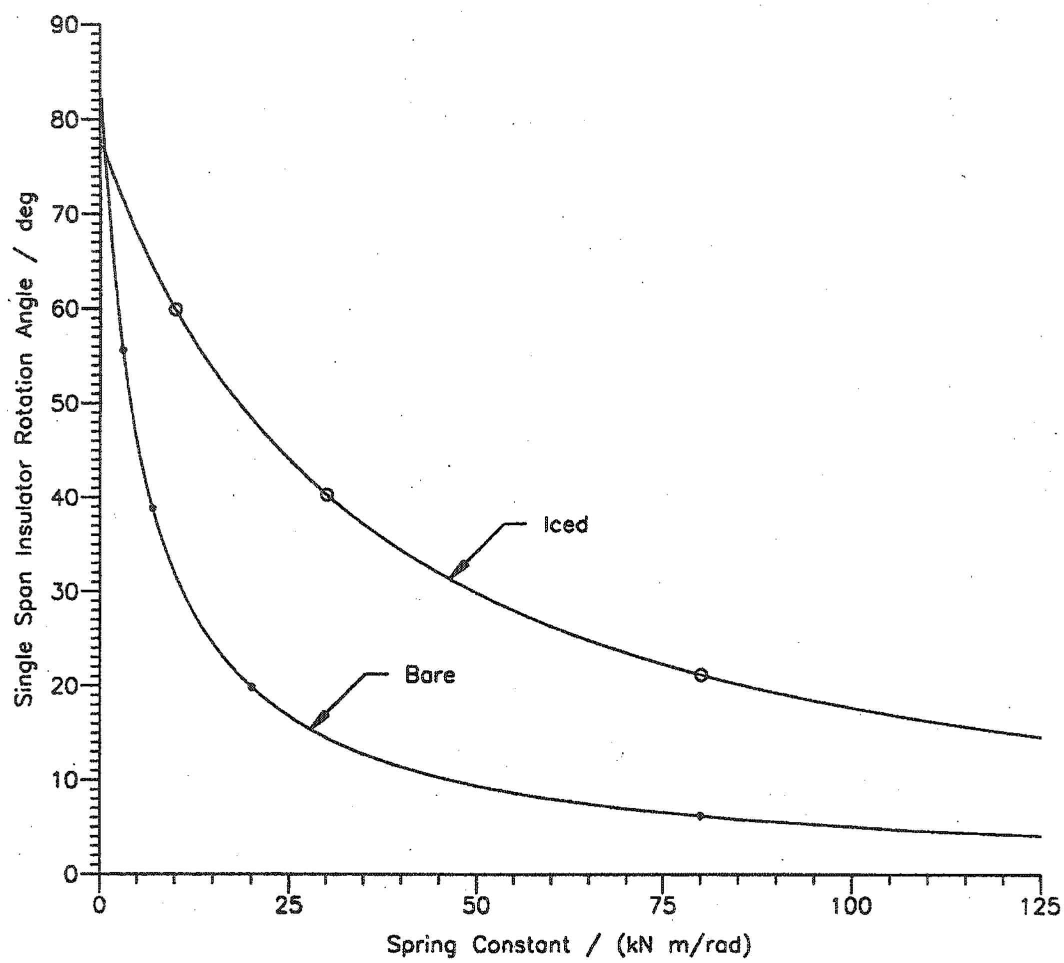

Figure 3-14
Post Spring Damper, Shield Wire Spring Constants

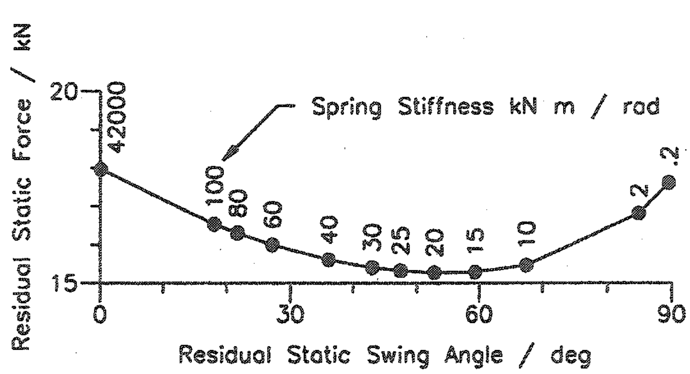

Figure 3-15
Rotating Crossarm Spring-Damper
Bare Conductor Spring Constants

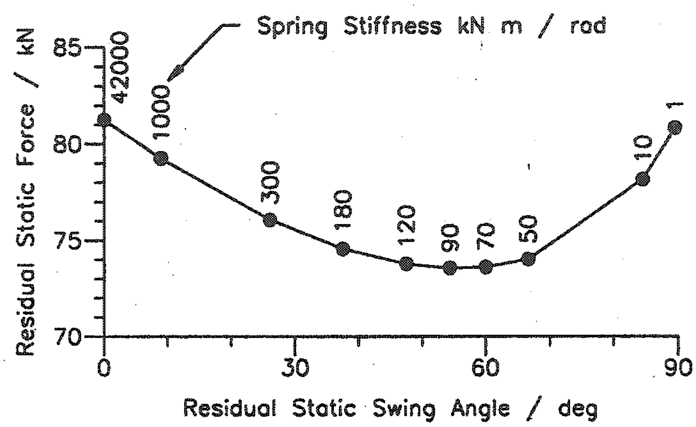

Figure 3-16
Rotating Crossarm Spring-Damper
Iced Conductor Spring Constants

3.5.3 Determination of Damping Constants

Some preliminary analyses showed that the reduction in the peak load for each increment in damping went down as the damping increased. A relatively small value of damping constant was chosen for the first non-zero value; this value was then doubled, and doubled again in geometric progression. In some cases, additional values were added for analysis.

3.5.4 Dynamic Time History Analyses

With the spring stiffnesses and damping constants determined as described above, time history analyses were performed for the combinations of values shown in Figure 3-17. For the post spring-damper, analyses for bare and iced shield wire attached directly to the tower to simulate a zero length link were performed. Time history analyses were also performed for both iced and bare conductor installed on a rotating arm with inclined axis.

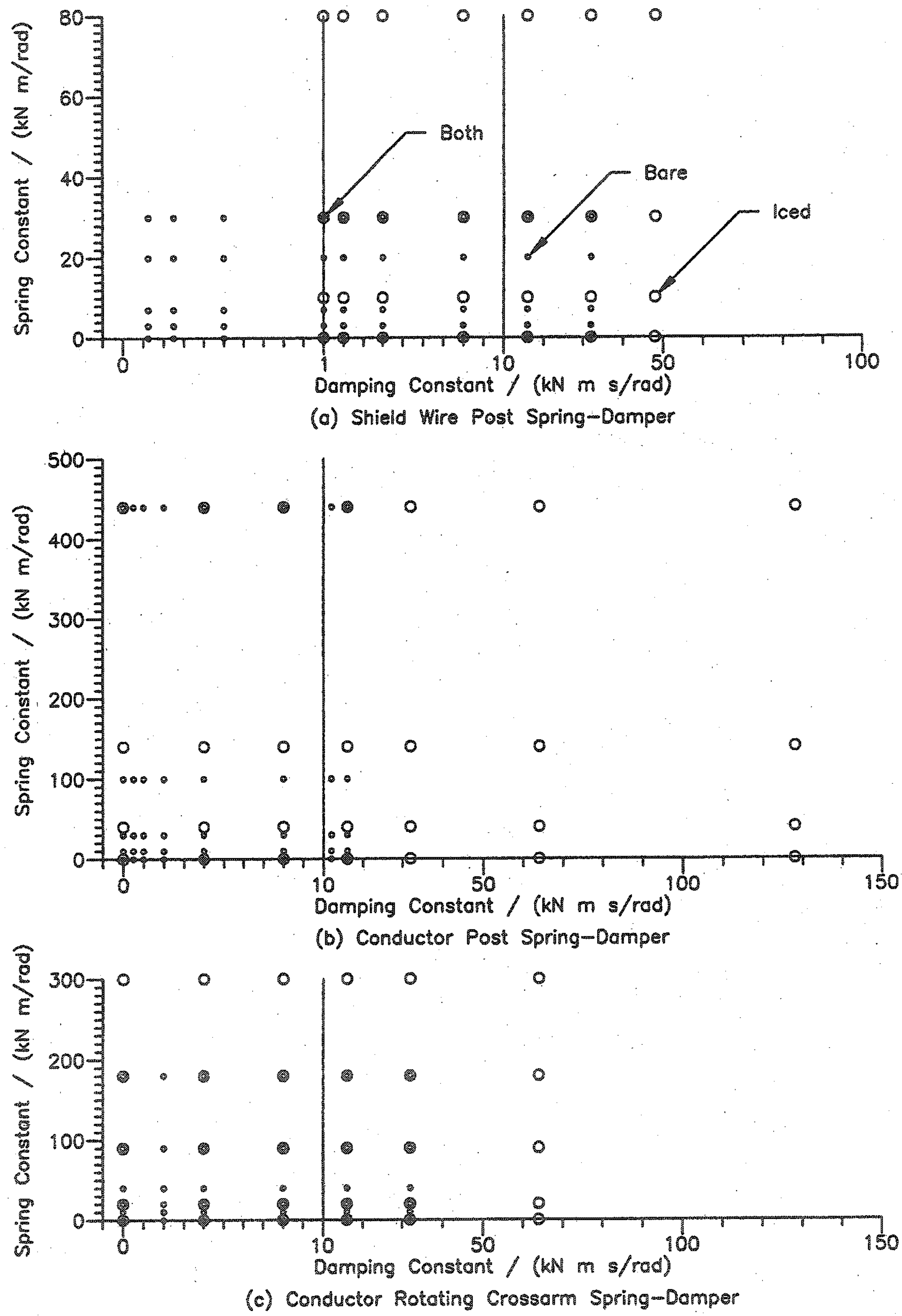

Figure 3-17
Spring-Damper Combinations

Performing a dynamic analysis requires two sets of iterative calculations. The best description of this process the author has found is in Nathan Newmark's ground breaking paper describing the method of analysis now named after him (Newmark 1959).

The first set of iterative calculations determines the position, velocity and acceleration of the masses in the model. ADINA has two choices, the Newmark method (Newmark 1959) and the Wilson-Theta method (Wilson et al. 1973). The Wilson Theta method with theta of 1.4 was used for the dynamic analyses. This method introduces some numerical damping and is also more stable than Newmark's method.

The second set of iterative calculations finds the forces in the members consistent with those positions, velocities and accelerations. ADINA has three choices, Full Newton, Modified Newton, and BFGS Matrix Update. The BFGS method was used for the dynamic analyses and the Full Newton for the static analyses (initial tensioning of the conductor and the residual static analyses). The BFGS method is a general method of finding maxima and minima in large sets of simultaneous equations. In structural applications, the total strain energy is minimized. This method was independently described in the same year by Broyden (1970), Fletcher (1970), Goldfarb (1970), and Shanno (1970). The results of the calculations are discussed in Chapter 5.

Chapter 4
Modeling the EPRI-Wisconsin Power and Light Tests

4.1 Introduction

Peyrot et al. (1978) reported on full-scale tests performed on a double circuit 138-kV line owned by Wisconsin Power and Light. Robert Kluge of American Transmission Co. kindly lent the author a film made about the tests (EPRI 1978). The line was slated for replacement with a new 345-kV line, making it available for destructive tests. The line was built in 1931 using lattice steel towers with square bases. The line had two 7 No. 8 Copperweld shield wires. The left circuit was strung with a 397 kcmil ACSR 26/7 conductor and the right circuit with a 471A Anaconda cable with 7 hard drawn copper wires over a 3 wire calsun bronze core. The test section had 7 towers as shown in Figure 4-1 (Peyrot et al. 1978, Fig. 3.1). All of the wires were anchored to the ground at the ends of the test section. The outline of the towers is shown in Figure 4-2.

4.2 Description of Tests

Tests were performed to determine the natural frequency of the towers, the effect of a broken suspension insulator and the effect of broken conductors. Only the tests of natural frequency and broken wires are of interest here.

4.2.1 Tower Natural Frequency

Two tests to determine the natural frequency of the tower were performed, one with all of the wires attached to the tower with their normal suspension hardware and one with the shield wires detached

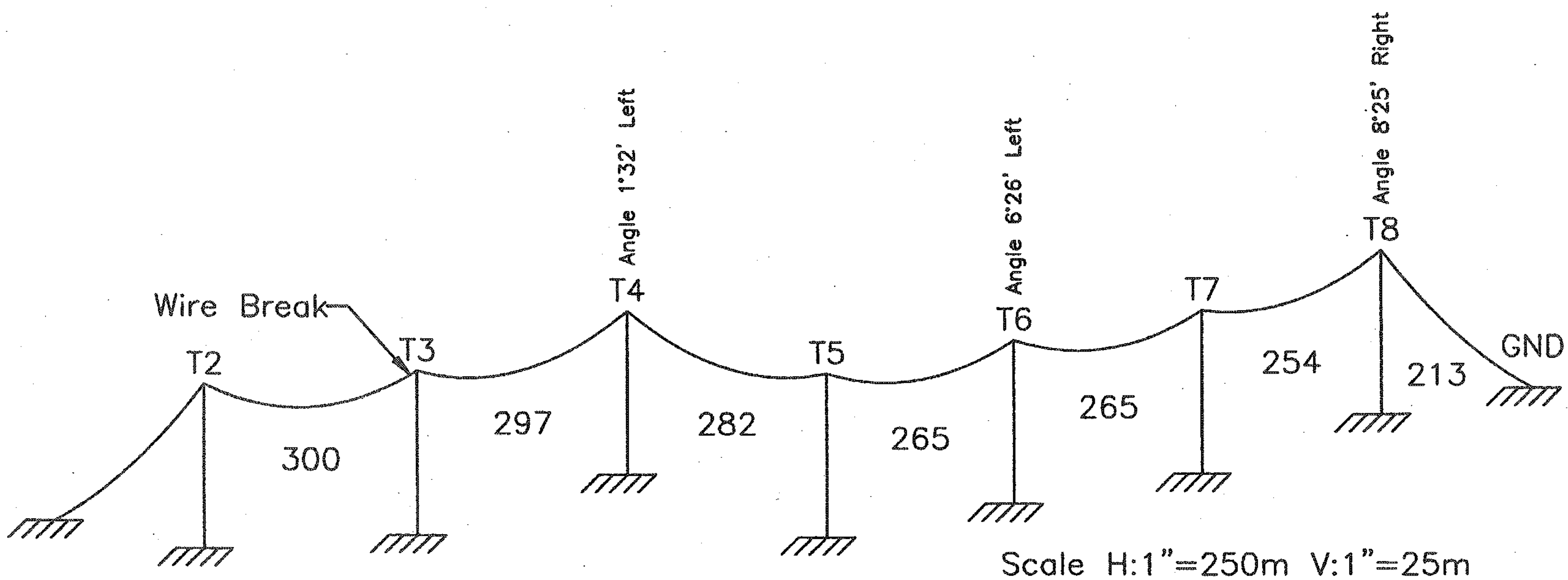

Figure 4-1 EPRI Wisconsin Test Line Profile

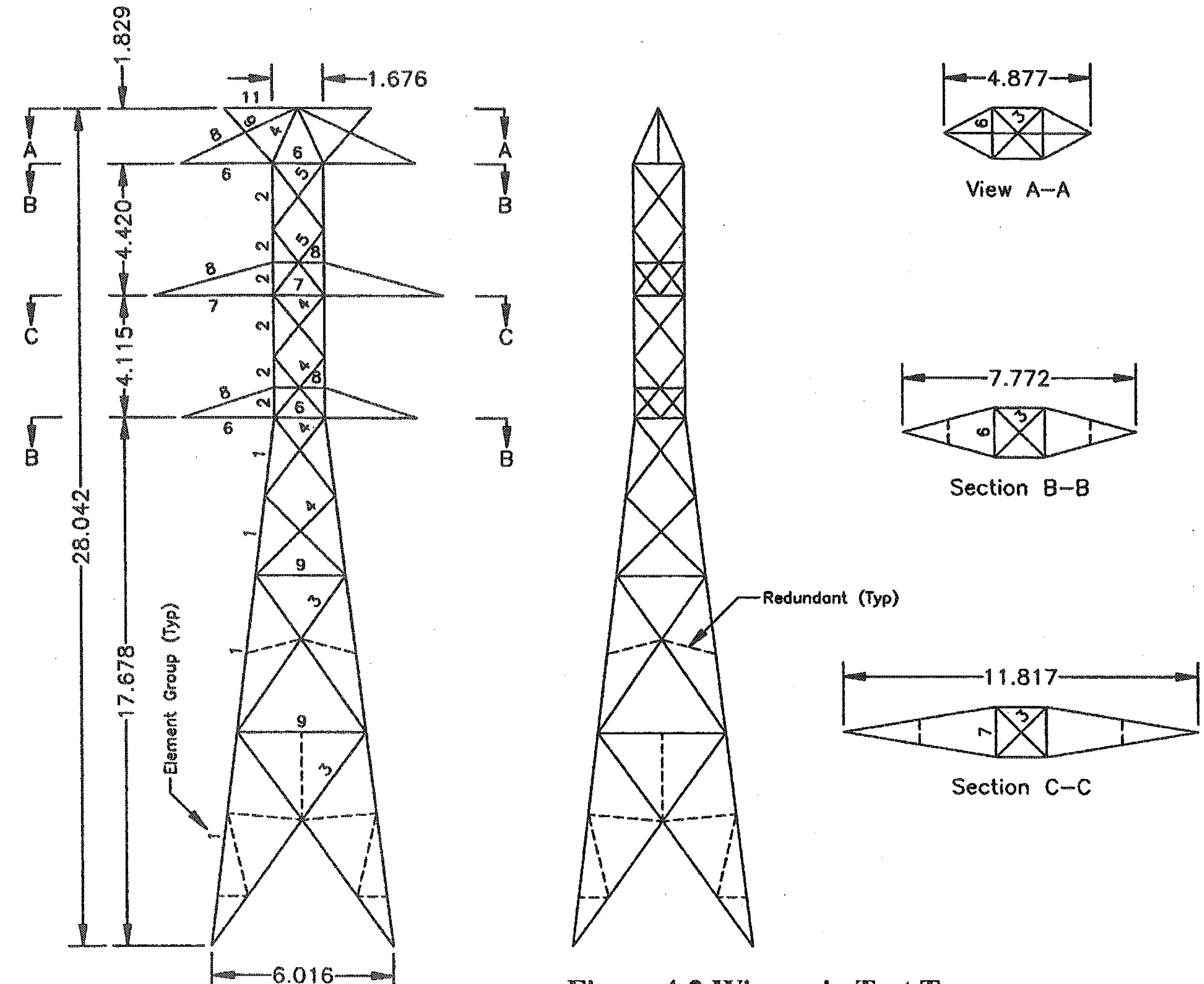

Element Group	Member Size
1	L5x5x5/16
2	L3½x3½x¼
3	L1½x1½x3/16
4	L2½x2½x3/16
5	L2½x2x3/16
6	L3½x3½x3/16
7	L4x3x¼
8	L2x2x3/16
9	L3x3x3/16
10	Dummy
11	2L3x2½x3/16

Notes:
Angles are U.S. sizes in inches
Tower Dimensions are in meters

Figure 4-2 Wisconsin Test Towers

The tower was excited by tensioning a cable attached to the top of tower to approximately 9.8 kN (1000 kgf) and suddenly releasing it. The static deflection was measured as 2 to 3 cm. The movement of the tower top was measured using an accelerometer. The period of the first mode of the tower with the shield wires detached is reported to be 0.25 s (4 Hz) with a damping ratio of 4%. With the shield wires attached, the period was reported to be 0.24 s (4.2 Hz) with a damping ratio of 7%.

4.2.2 Broken Conductor Tests

Twelve broken conductor tests were performed as shown in Table 4-1. The tests of most interest are the tests of the ACSR conductor. Today, copper conductor is rarely used in the construction of new transmission lines. The majority of the existing high voltage and extra high voltage transmission systems use all aluminum, aluminum alloy or ACSR conductor.

4.2.3 Inconsistencies in the Test Data

The test report and film of the tests (EPRI 1978; Peyrot et al. 1978) have inconsistencies in the length reported for the span between Towers T3 and T4 (the span next to the breaks) and the length of the insulator strings. The first span was assumed to be 297 m. The insulator string was assumed to be 2.08 m long.

4.3 Analysis of the Broken Conductor Test Data

For comparison with the finite element model being developed for this research project, the data from three of the EPRI Wisconsin tests were analyzed. The tests were performed at the top, center and lower left crossarms with three different conductor tensions – tests

IIIL1, IIIL2, and IIIL3 (see Table 4-1). All of the tests were performed using a 397 kcmil ACSR 26/7 conductor. This conductor matches standard Ibis ACSR which consists of a 7 strand steel cable overlayed with 26 strands of aluminum wire in two layers, see Figure 4-3. Table 4-2 (next page) shows the conductor properties reported by Peyrot et al. (1978) and published conductor properties for Ibis conductor (Alcoa 1974; Farr 1980).

Table 4-1
EPRI-Wisconsin Power & Light
Broken Conductor Tests

Test No.	Conductor	Effective I-String Length (m)	Starting Tension (kN)	Residual Static Tension (kN)
IIIR1	Copper/Bronze	2.2	18.66	11.00
IIIR2	Copper/Bronze	2.2	19.10	11.01
IIIR3	Copper/Bronze	2.2	Broken Arm	
IIIL1	ACSR	2.2	12.43	6.96
IIIL2	ACSR	2.2	17.77	8.69
IIIL3	ACSR	2.2	21.32	9.33
VR1	Copper/Bronze	4.3	15.99	7.55
VR2	Copper/Bronze	4.3	18.21	7.95
VR3	Copper/Bronze	4.3	Broken Arm	
VL1	ACSR	4.3	14.22	5.11
VL2	ACSR	4.3	No Load Cell Data	
VL3	ACSR	3.7	23.55	7.24

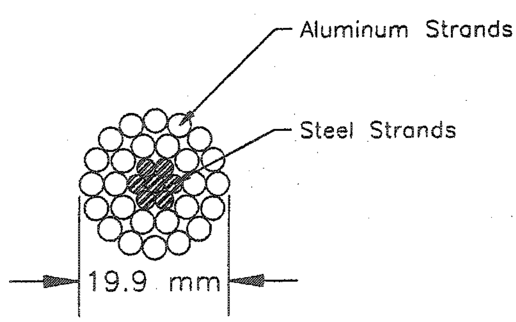

Figure 4-3
Ibis Conductor

Table 4-2
Conductor Properties

Description	Peyrot et al.	Published Values	
Stranding	26 / 7	26 / 7	
Name	-	Ibis	Ibis
Steel Area	-	32.8 mm^2	0.0508 in^2
Aluminum Area	-	201.2 mm^2	0.3119 in^2
Total Area	234.0 mm^2	234.0 mm^2	0.3627 in^2
Diameter	-	19.9 mm	0.783 in
Unit mass	0.814 kg/m	0.813 kg/m	0.5466 lbm/ft
Average Density	-	3476 kg/m^3	217 lbm/ft^3
Rated Tensile Strength	68.5 kN	72.5 kN	16.3 kips
Final Modulus of Elasticity	69.6 GPa	74.2 GPa	10,760 ksi
Sag-Tension Chart No.	-	1-782 (No. 8)	

The time histories for tests IIIL1, 2 and 3 shown in Figure 6-4 of the report were digitized, resampled to have a uniform time step and scaled in Newtons. Figure 4-4 shows the time histories. Test IIIL 1 had a gap in the time history for the 2^{nd} peak. The timing and magnitude of the 2^{nd} peak was taken from Table 6-2 of the report. Fourier analyses of the two complete time histories are shown in Figure 4-5. Both have a definite peak at a frequency of 1.35 Hz with a period of 0.75 s. The time history of test IIIL1 shows a bifurcated first peak. This may be due to incipient buckling of the crossarm noted by Kluge (2002).

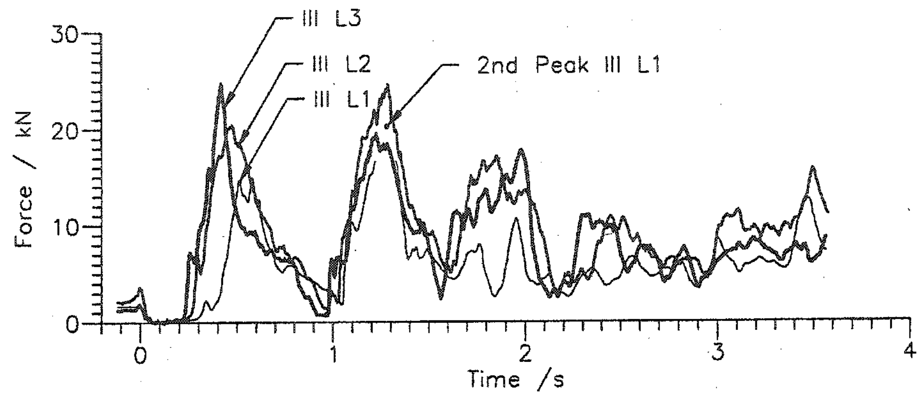

Figure 4-4
Insulator Tension at Tower T3, Tests IIIL 1, 2 & 3

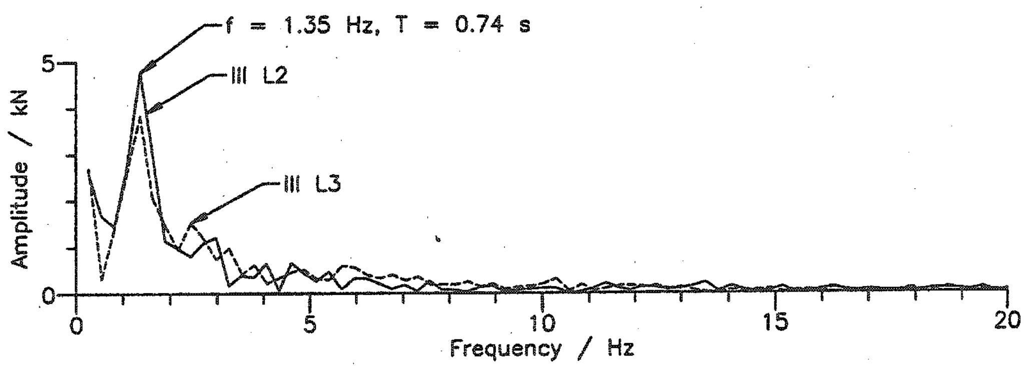

Figure 4-5
Fourier Spectra, Wisconsin Tests IIIL 2 & 3

4.4 Tower Finite Element Model

The tower was modeled as a pin-connected truss using ADINA (ADINA 2001). A static analysis was performed for comparison with the tower deflections included in Table 3-1 of Peyrot (1978). The reported deflections appear to be based on an analysis assuming that all the members of the tower are tension-compression members. The X-braces in the lowest two panels of the tower are obviously intended to carry tension only. They are L1½x1½x3/16 (38.1 mm x 38.1 mm x 4.76 mm) angles with horizontal compression members bounding them. Table 4-3 compares the reactions for a 9807 N (1000 kgf) load at the center of the top of the tower with the reactions for an analysis assuming these x-braces are tension-compression members and with an analysis assuming they are tension-only members. These analyses did not include the dead load of the tower. The tension-only members were modeled by using a modulus of elasticity in compression of 1/1000 the modulus in tension. Note that the longitudinal reactions are equal at all four legs for the tension-compression analysis but that more longitudinal load is carried by the back supports in the tension-only analysis.

Table 4-3
Reaction Comparison

Location	Dir.	Reported (kN)	Adina T-C (kN)	Adina T-only (kN)
Ahead Left	L	-2.46	-2.45	-2.10
Adina Node 1	T	-3.95	-3.93	-2.81
Peyrot et al. B2	V	23.2	22.9	22.9
Back Left	L	-2.46	-2.45	-2.80
Adina Node 3	T	3.95	3.93	3.91
Peyrot et al. B1	V	-23.2	-22.9	-22.9
Back Right	L	-2.46	-2.45	-2.80
Adina Node 5	T	-3.95	-3.93	-3.91
Peyrot et al. B3	V	-23.2	-22.9	-22.9
Ahead Right	L	-2.46	-2.45	-2.10
Adina Node 7	T	3.95	3.93	2.81
Peyrot et al. B4	V	23.2	22.9	22.9

The deflections at key points are compared in Table 4-4.

Table 4-4
Deflection Comparison

Location	Longitudinal Deflection due to 9.807 kN Longitudinal Load applied at Location		
	Reported (cm)	Adina T-C (cm)	Adina T-only (cm)
Center of Tower Top	1.90	1.85	1.90
Shield Wire Attachment Point	2.51	2.38	2.60
Upper Phase Attachment Point	2.88	2.64	3.08
Middle Phase Attachment Point	2.10	1.97	2.59
Lower Phase Attachment Point	0.97	0.89	1.33

In order to be able to reduce the number of nodes and members in the transmission line model, a dynamically similar model for the tower attachment point was constructed. A two-degree of freedom spring mass system is needed in the horizontal direction to model the combined longitudinal and torsional vibration characteristics of the tower and a single degree of freedom spring mass system is needed to model the vertical vibration characteristics. The horizontal and vertical spring stiffnesses should match the stiffnesses at the tower attachment point and the spring mass systems should have the same natural frequencies as the tower.

The static analyses also included load cases to determine the attachment stiffness in the vertical and longitudinal directions. The dead load of the tower was included in all load cases. The first load case was a longitudinal load of 9.807 kN (1000 kfg) applied at the top left phase attachment point to determine the overall deflection of the attachment point. The second case was two longitudinal loads of 4.9035 kN (500 kgf) applied at the two upper phase attachments. This case gives the longitudinal deflection at the phase attachments without the torsional component of the deflection. In a separate load case, a 9.807 kN vertical load was applied to the attachment point to measure the vertical stiffness. These results are summarized in Table 4-5.

Table 4-5
Wisconsin Test Tower Deflections and Stiffnesses

	Applied Longitudinal Load				
	Upper Left Phase (N)	Upper Right Phase (N)	Total (N)	Deflection (cm)	Stiffness (kN/m)
Total Deflection	9807.0	-	9807.0	3.138	313
Balanced Deflection	4903.5	4903.5	9807.0	1.437	682
Torsional Deflection	9807.0	-	9807.0	1.700	577

Analysis of the natural frequencies and mode shapes of the tower was also performed. The analysis was done for two cases, the first assuming that the tension-only cross bracing acted as tension-compression bracing and in the second, the modulus of elasticity of the tension-only members was assumed to be one-half the modulus of elasticity of steel. This simulated the stiffness of a tension-only system by giving the total stiffness of these members equal to the stiffness of one of them. Changing the modulus rather than the area keeps the same mass in the model. Table 4-6 compares the two.

Table 4-6
Wisconsin Test Tower Frequencies

		Frequency (Hz)	
Mode No.	Description	Tension-Compression Bracing	Tension Only Bracing
1	1^{st} Transverse Mode	4.74	4.67
2	1^{st} Longitudinal Mode	4.79	4.72
3	1^{st} Torsional Mode	9.67	7.79

Note that there is very little difference in the 1st transverse and longitudinal modes. There is a significant difference in the frequency of the 1st torsional mode because the bracing is the main contributor to the torsional stiffness. Peyrot et al. (1978) reported a natural frequency by analysis of approximately 5 Hz, which is consistent with the frequencies reported in Table 4-6.

The natural frequencies of the ADINA Model were also explored by plucking the tower with a 20 kN force released in 0.005 s. This was applied in three directions, longitudinally with a 10° downdrop angle (x and -z), transversely (y) and vertically (-z). Figure 4-6 shows the Fourier analysis of the plucking loads (5 s duration of record). Table 4-7 compares the frequency analysis with the plucking analysis.

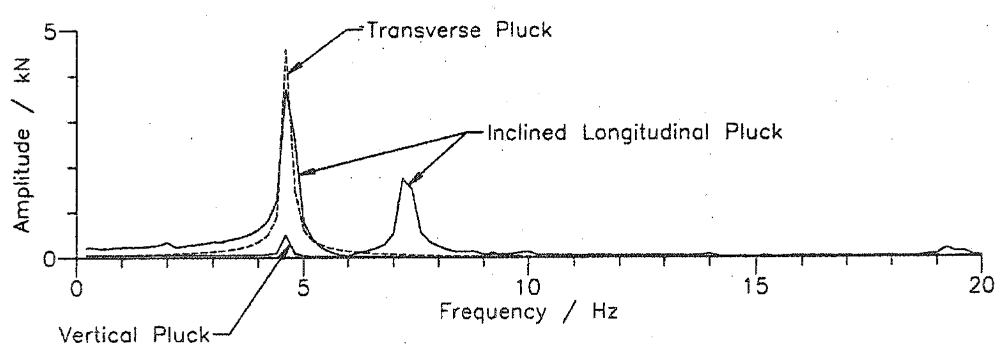

Figure 4-6
Fourier Spectra of Space Truss Tower Model

Plucking the arm vertically excites the tower in the first transverse mode with a frequency of 4.6 Hz.

Table 4-7
Comparison of Frequency Analysis and Plucking Analysis

Mode No.	Description	Frequency (Hz)	
		Frequency Analysis	Plucking Analysis
1	1st Transverse Mode	4.67	4.60
2	1st Longitudinal Mode	4.72	4.60
3	1st Torsional Mode	7.79	7.2-7.4

The longitudinal motion of the tower at the end of the crossarm is made up of a balanced longitudinal component and a torsional component requiring a two-degree of freedom system of springs and masses to represent the longitudinal motion of the tower. With its small relative amplitude, the vertical motion of the tower can be represented by a single degree of freedom spring-mass system decoupled from the longitudinal spring mass system. Figure 4-7 shows the first model considered. The global stiffness matrix for the longitudinal direction alone (decoupled from the vertical) is shown in Equation 4-1 and the mass matrix in Equation 4-2.

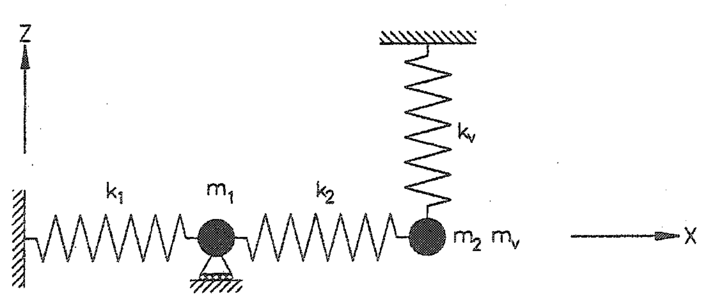

Figure 4-7
Linear 2 DOF Spring-Mass System

$$k_g = \begin{bmatrix} k_1 + k_2 & -k_2 \\ -k_2 & k_2 \end{bmatrix} \qquad \text{Equation 4-1}$$

$$m_g = \begin{bmatrix} m_1 & 0 \\ 0 & m_2 \end{bmatrix}$$ Equation 4-2

The natural frequencies are determined by solving the eigenproblem in Equation 4-3.

$$\left| k_g - \omega_n^2 m_g \right| = 0$$ Equation 4-3

In this case, the natural frequencies and the stiffnesses are known and the associated masses are needed. Solving Equation 4-3 for the mass m_2 in terms of mass m_1 gives Equation 4-4.

$$m_2 = \frac{k_2 \omega_n{}^2 m_1 - k_1 k_2}{m_1 \omega_n{}^4 - (k_1 + k_2)\omega_n{}^2}$$ Equation 4-4

Using equation 4-4 but assuming two natural frequencies, ω_1 and ω_2, gives Equation 4-5 which can be solved for m_1 in terms of the spring stiffnesses and natural frequencies giving Equation 4-6.

$$m_2 = \frac{k_2 \omega_1^2 m_1 - k_1 k_2}{m_1 \omega_1^4 - (k_1 + k_2)\omega_1^2} = \frac{k_2 \omega_2^2 m_1 - k_1 k_2}{m_1 \omega_2^4 - (k_1 + k_2)\omega_2^2}$$ Equation 4-5

$$m_1^2 \left\lfloor k_2 \omega_1^2 \omega_2^2 \left(\omega_2^2 - \omega_1^2\right)\right\rfloor + m_1 \left\lfloor k_1 k_2 \left(\omega_1^4 - \omega_2^4\right)\right\rfloor + k_1 k_2 (k_1 + k_2)\left(\omega_2^2 - \omega_1^2\right) = 0$$ Eq. 4-6

Equation 4-6 is a quadratic equation in m_1. For the solution to have physical sense, the mass must be positive and real. There may be no real positive root, one root or two roots. For the Wisconsin tower, Equation 4-6 has imaginary roots making the model shown in Figure 4-7 unsuitable for use in modeling the test line.

The tower can, however, be modeled with a different set of springs and masses. The balanced longitudinal mode of vibration is modeled as a linear translational spring-mass system. The torsional mode is modeled as a torsional spring with a rotational inertial mass. Both linear and torsional springs are connected to a rigid massless arm with length L equal to the horizontal distance from the center of the tower to the conductor attachment point as shown in Figure 4-8. The vertical motion of the tower is also modeled using a torsional spring with a rotational inertial mass as shown in Figure 4-8. The mass associated with the linear longitudinal spring was calculated using Equation 4-7.

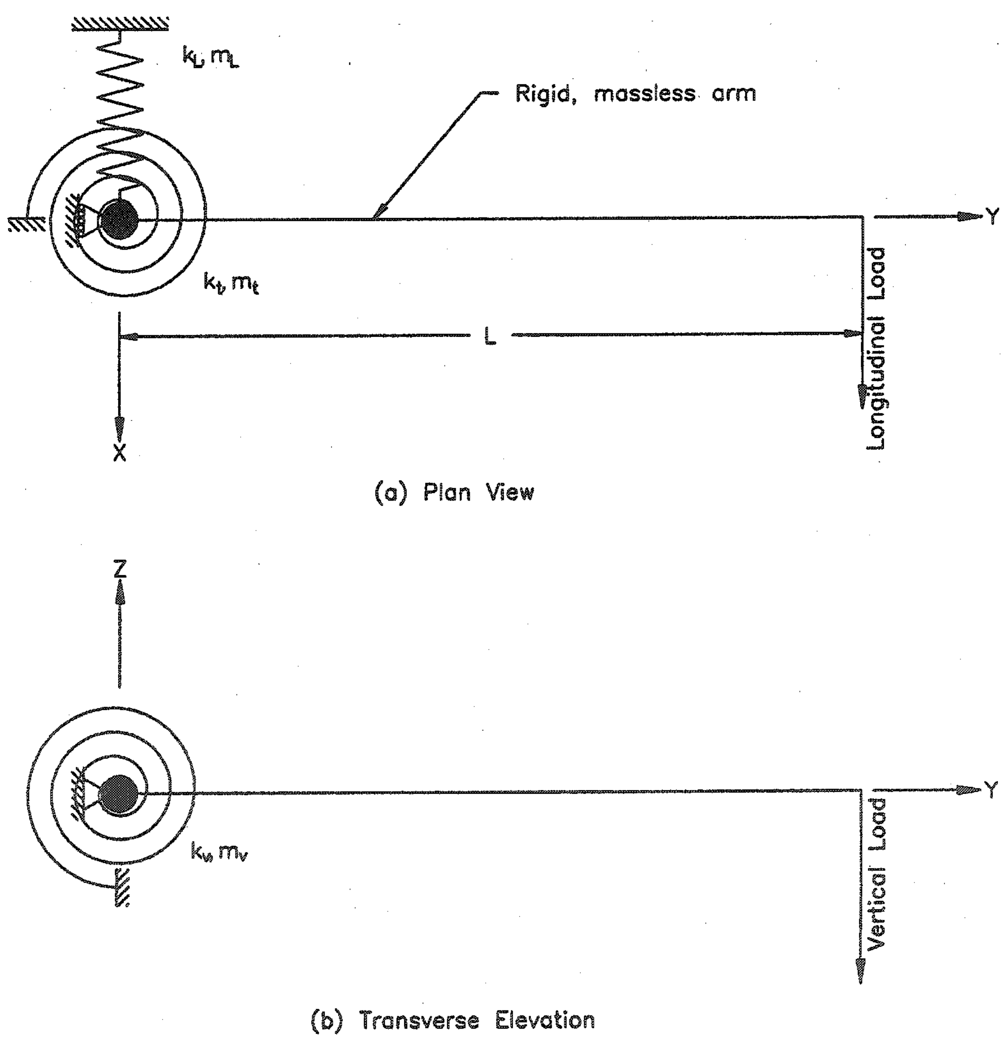

Figure 4-8
Wisconsin Tests–Reduced Tower Model

$$m_L = \frac{k}{\omega_n^{\ 2}}$$ Equation 4-7

The torsional spring constants and rotational moments of inertia were calculated using Equations 4-8 and 4-9 where P is the applied load and δ is the resulting longitudinal deflection. The results are summarized in Table 4-8.

$$k_t = \frac{PL}{\arcsin\left(\frac{\delta}{L}\right)}$$ Equation 4-8

$$J = \frac{k_t}{\omega_n^2}$$ Equation 4-9

Damping for the linear and torsional spring-mass systems is calculated using Equations 4-10 and 4-11, respectively.

$$c_v = 2\zeta\, m\omega_n$$ Equation 4-10

$$c_t = 2\zeta\, J\,\omega_n$$ Equation 4-11

Table 4-8 shows the properties of the equivalent spring-mass systems.

Table 4-8
Equivalent Mass, Stiffness and Damping

	Frequency (Hz)	Natural Frequency (rad/s)	Stiffness (kN/m)	Associated Mass/ Rotational Inertial Mass (kg)	Damping 5% Critical (kg/s)
Longitudinal	4.60	28.9	682	817	2360
	(Hz)	(rad/s)	(kN-m/rad)	(kg-m^2)	(kg-m^2/s)
Torsional	7.20	45.2	8708	4255	19000
Vertical	4.60	28.9	17620	21100	61000

Figure 4-9 compares the time histories of the longitudinal displacements of the full tower model and the reduced tower model described above under a longitudinal plucking load that is inclined downwards at a 10° angle from horizontal. Figure 4-10 shows the Fourier spectra for the full and reduced tower models. The natural frequencies of the reduced tower model match very well with those of the full tower model.

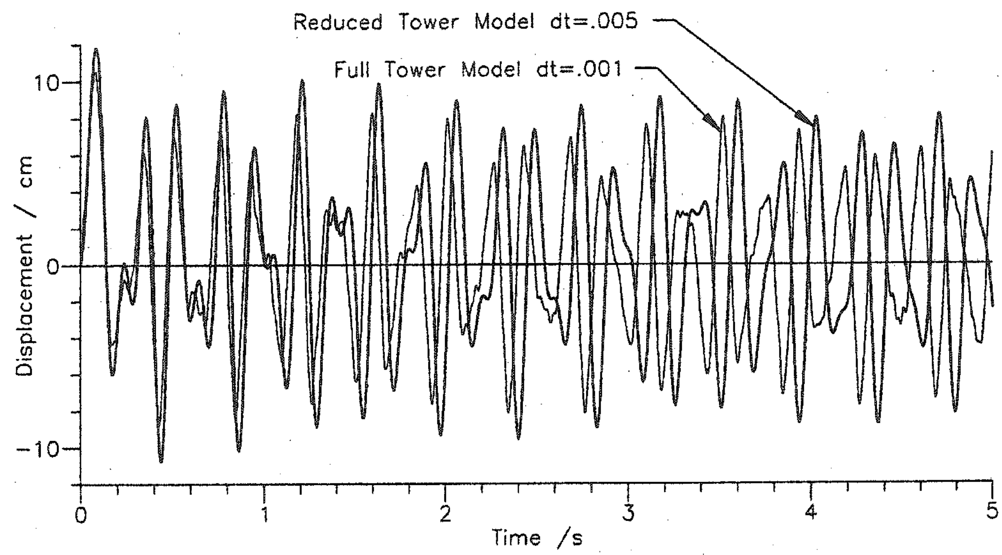

Figure 4-9
Longitudinal Deflection at Upper Left Phase
Comparison of Full and Reduced Tower Models

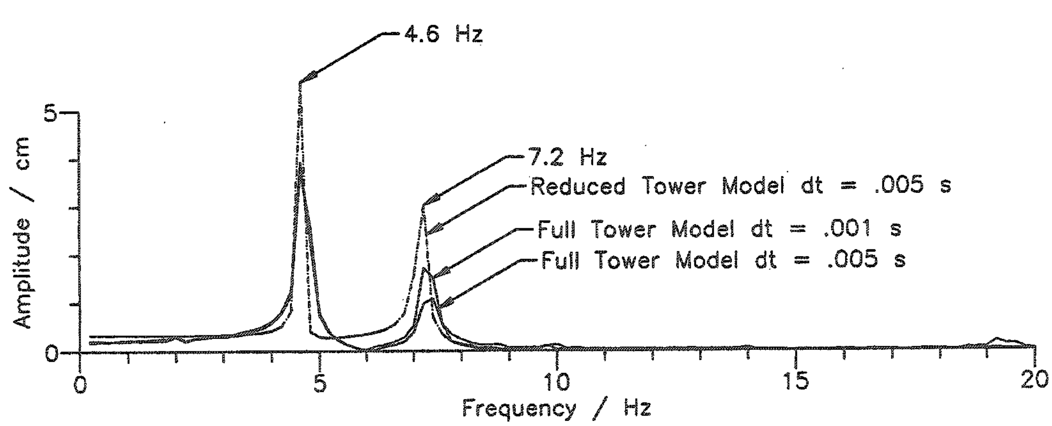

Figure 4-10
Fourier Spectra–Tower Model Comparison

4.5 Modeling the Conductor

4.5.1 Introduction

When a conductor breaks next to a suspension insulator and the insulator swings into the span, there are several aspects to the conductor response (Haro et al. 1956; Peyrot et al. 1978). These include a reduction in the static tension (the tension at rest after dynamic effects have damped out), an axial release wave which travels along the conductor, a transverse wave which is excited by the upward motion of the insulator string as it swings into the span and excitation of the natural vibration modes of the span by the fall of the wire.

4.5.1.1 Axial Release Waves

The release wave travels down the conductor axis due to the sudden loss of tension. In the conductor, which is a taut string, this wave travels at approximately the speed of sound in the material as given in Equation 4-12 (Main 1978, p171) where E is the modulus of elasticity and ρ is the mass density of the material.

$$V_L = \sqrt{\frac{E}{\rho}} \qquad \text{Equation 4-12}$$

The Ibis conductor used in the tests consists of a straight galvanized steel core wire with six galvanized steel wires wrapped around it in helixes (see Figure 4-3). Over this seven strand steel cable, two layers of aluminum wires are also wound in helixes. The diameter of the helixes is larger in the outer layers. The release wave must travel slightly farther in each layer than in the layer below. Each layer, however, is bound to the adjacent layers by the friction between the strands which depends on the tension in the wire and whether the individual wires were preformed before stranding.

Rods with area A have a characteristic impedance Z_L to longitudinal waves as given in Equation 4-13 (Main 1978, p172) which has the same units as viscous damping, kg/s.

$$Z_L = A\sqrt{E\rho} \qquad \text{Equation 4-13}$$

Table 4-9 compares the speed of sound in aluminum and galvanized steel rods [properties from Thrash et al. (1994, Table 1-1)] and in the completed conductor based on its composite density and modulus of elasticity (Alcoa 1974; Farr 1980). Also included for comparison is a 38.1 mm (1.5 in) diameter steel rod typical of a 100 kN (22,500 lb) canister load cell. The longitudinal wave velocities of the steel and aluminum rods are practically the same. It is reasonable to model the conductor as a solid bar with the final modulus of elasticity given in Table 4-9 (Farr 1980).

Table 4-9
Longitudinal Material Properties

			Modulus	Longitudinal	
Description	Area (mm^2)	Density (kg/m^3)	Of Elasticity (GPa)	Velocity (m/s)	Impedance (kg/s)
Aluminum Rod	7.74	2705	69.0	5051	106
Galvanized Steel Rod	4.68	7780	200.0	5070	185
Ibis Conductor	234.00	3476	74.2	4620	3758
100 kN Load Cell	1140.00	7820	200.0	5057	45100

4.5.1.2 Transverse Waves

The suspension insulator swings upward even while the conductor starts to fall. A portion of the motion of the conductor will be perpendicular to the conductor axis generating a transverse wave that travels at the velocity given in Equation 4-14 (Main 1978, p139).

$$V_T = \sqrt{\frac{T_e}{m}} \qquad \text{Equation 4-14}$$

The characteristic impedance to transverse waves is given in Equation 4-15 (Main 1978, p146). As with the longitudinal impedance, the units are those of viscous damping, kg/s.

$$Z_T = \sqrt{T\,m} \qquad \text{Equation 4-15}$$

4.5.1.3 Changes in Impedance

At changes in the impedance, part of the wave is reflected and part transmitted. The amplitudes of the transmitted A_T and reflected waves A_R for a wave with amplitude A_w traveling in a conductor with impedance Z_1 and encountering a change of impedance to Z_2 are given in Equations 4-16, (Main 1978, p149-151). These equations apply to both transverse and longitudinal waves.

$$A_R = A_w\left(\frac{Z_1 - Z_2}{Z_1 + Z_2}\right) \qquad A_T = A_w\left(\frac{2\,Z_1}{Z_1 + Z_2}\right) \qquad \text{Equations 4-16}$$

There is a large change in the transverse impedance at a suspension string, particularly for a downward wave where the entire mass of the insulator string and part of the tower must be accelerated. Most of the wave will be reflected; Buchanan (1934) reports reflected amplitudes of 92 to 98 percent of the incident amplitudes. This property is taken advantage of in sagging transmission and distribution lines by the "return wave method" (RUS 1998). Similarly, one could expect reflections of longitudinal waves at the interface between the conductor and a load cell or the conductor and dead-end.

4.5.2 Natural Frequencies and Mode Shapes of Conductors

Methods of calculating the natural frequencies of single spans of wire are described in Appendix A. One measure of the goodness of the finite element model of a structure is how well the natural frequencies calculated for the finite element model conform to the theory. A second measure is how the frequencies converge as the length of the elements is reduced. Table A-1 compares theoretical calculations of the natural frequencies of a typical 300 m span with the results of ADINA analyses for different numbers of elements in the span. There is little change in the natural frequencies for the higher modes when at least 60 elements 5 m long are used and practically no difference between 120 elements 2.5 m long and 300 elements 1 m long. Based on the results in Table A-1, the length of the wire elements was chosen to be approximately 2.5 m. Each span was broken into the number of equal length elements closest to 2.5 m.

4.5.3 Conductor Damping

Damping of transmission conductors can be separated into internal damping and aerodynamic damping. The internal damping is a combination of hysteretic damping within the individual cable strands and damping due to the sliding friction between strands as they move past one another during cable movement. Aerodynamic damping arises from the motion of the cable through the air.

Much of the literature related to the damping of transmission conductors is focused on the energy dissipated by the cable when excited by vortex shedding in smooth laminar winds. This motion is known as aeolian vibration. The results of tests of the self-damping capabilities of the conductor are usually stated in terms of the energy dissipated per unit length as a function of the vibration frequency. The peak to peak amplitude of vibration is very small, typically less than the conductor diameter (Gilbert/Commonwealth 1979, p 3). These measurements often do not distinguish between the internal damping and the aerodynamic damping, in some cases describing the vortex excitation as negative aerodynamic damping. The internal damping due to friction between the strands is reduced as the tension in the wire increases, and increases as the amplitude of vibration increases. Diana et al. (2000) indicate that the damping coefficient for ACSR conductor is in the range of 0.1 to 0.01 percent of critical for the frequencies and amplitudes of interest for aeolian vibration. Carne (Carne 1980) in discussing guys for vertical axis wind turbines reports damping of less than 0.2 percent of critical. In Bachmann et al. (1995, p 96) a value of 0.05 percent of critical is suggested.

4.5.3.1 Internal Damping

The internal damping can be divided into two parts, axial damping that takes place due to changes in the conductor tension, and lateral damping due to bending of the conductor. The critical axial viscous damping for a rod is given in Equation 4-17.

$$c_{cr} = 2\sqrt{A E m} \qquad \text{Equation 4-17}$$

Note that the critical damping constant is independent of the length of the rod. Table 4-10 shows some values of axial damping used in previous time history analyses of conductor motion. McClure and Tinawi (1989a; 1989b) did not use explicit damping; however, some of the time history analysis algorithms they investigated introduce some numerical damping.

Little information seems to be available on the lateral damping of ACSR conductor; however, Yu (1952) presents results of some tests performed on slack steel cables similar to those used for shield wires and the steel core of ACSR. These tests indicate there may be substantial lateral damping.

Table 4-10
Axial Damping Ratios

Reference	Description	Axial Damping Ratios % Critical
Thomas (1981)	Broken Wire Analysis	5 to 20%
McClure & Tinawi (1989a; 1989b)	Broken Wire Analysis	0% (see text)
Roshan-Fekr (1995)	Ice Shedding Analysis Bare Conductor Iced Conductor	 2% 10%
McClure & Lapointe (2003)	Broken Wire Analysis Bare Conductor Iced Conductor	 2% 10%

Axial damping of 0.5% of critical was used in this study.

4.5.3.2 Aerodynamic Damping

ADINA has the capability of modeling the aerodynamic damping directly. Aerodynamic damping is due to the motion of the conductor relative to the air. In still air the aerodynamic damping force is given by Equation 4-18 (Dyrbye and Hansen 1996, p. 76).

$$F_d = \frac{1}{2}\rho V_r^2 C_d A_p \qquad \text{Equation 4-18}$$

Where F_d is the damping force, ρ is the air density and V_r is the velocity relative to the air, C_d is the drag coefficient and A_p is the projected area. C_d depends on the Reynolds number (Equation 4-19) where d_w is the conductor diameter and μ is the viscosity of air.

$$Re = \frac{\rho V_r d_w}{\mu}$$ Equation 4-19

For smooth circular cylinders, C_d is between approximately 0.9 and 1.2 for Reynolds numbers between 200 and 100,000 (Binder 1973; Eisner 1931), which correspond to relative velocities for Ibis conductor of 0.15 m/s and 73 m/s, respectively. As the relative velocity is reduced below a Reynolds number of 200, C_d steadily increases to over 50 at a Reynolds number of 0.1. A C_d of 1.25 was used.

4.5.3.3 ADINA Conductor Model

Figure 4-11 shows the basic conductor model used in ADINA with both axial and aerodynamic damping. Although the aerodynamic damping should be applied normal to the direction of movement, this would be more difficult to model in ADINA. Instead, the aerodynamic damping was applied to the vertical motion of the conductor using the initial horizontal projected area.

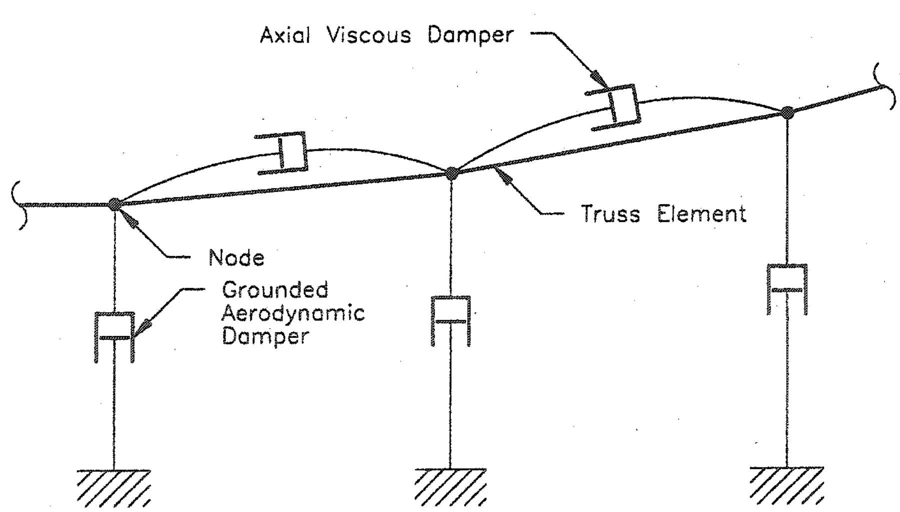

Figure 4-11
Conductor Model

4.6 Modeling of the Insulator Assemblies

Figure 4-12 shows a complete insulator assembly and the three insulator models used in the analysis. In the instrumented insulator string at tower T3, the porcelain insulators were replaced with a section of wire rope and a Dillon 10,000 lb (44.5 kN) load cell. At tower T4, a load cell was also included; however, the film (EPRI 1978) shows four porcelain insulator bells left in the string. The remaining towers are assumed to have the original insulator strings. No information is included in the test report on the connections, dimensions and properties of the load cells and wire rope.

The wire rope is assumed to be 16 mm (5/8 in) improved plow steel with 6x19 fiber core stranding. The area is 103 mm^2 (0.16 in^2); after prestressing, the modulus of elasticity is 82.7 GPa (12,000 psi) for loads between 21% and 65% of the rated tensile strength of 149 kN (16.7 U.S. tons) (Wire Rope Technical Board 1993).

Based on information in the current Dillon Catalog (Dillon 1998), the load cells are estimated to be constructed of steel with a diameter of 34.9 mm (1.375 in). The length used in the model includes an allowance for hardware to connect the load cells to the conductor clamp and the wire rope.

The swinging brackets and insulators are modeled as 15.875 mm (0.625 in) steel rods. Lumped masses are added at nodes in the model to get the same total mass and approximately the same mass distribution as the test components.

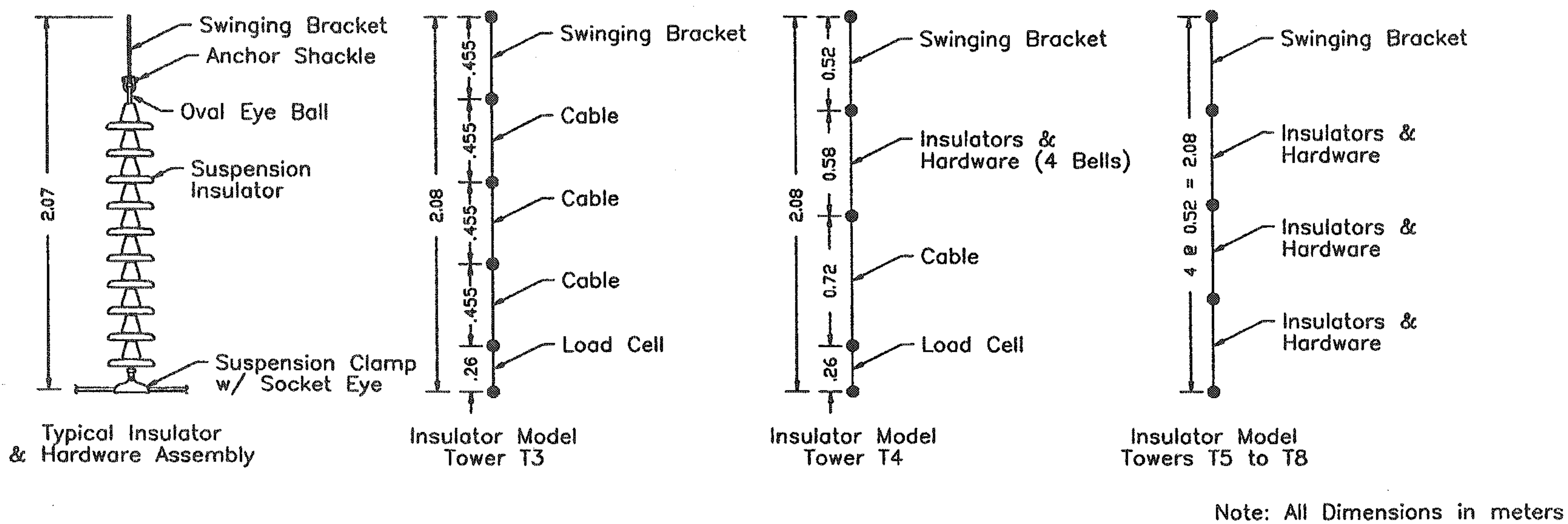

Figure 4-12 Insulator and Hardware Assembly Models

4.7 Time History Analysis Results

Figure 4-13 shows the load cell tension at tower T3 from a time history analysis of test III L3 performed with ADINA (ADINA 2001). A summary of the parameters used in the ADINA model is given in Appendix B. Also shown in Figure 4-13 is the load cell tension from Peyrot et al. (1978).

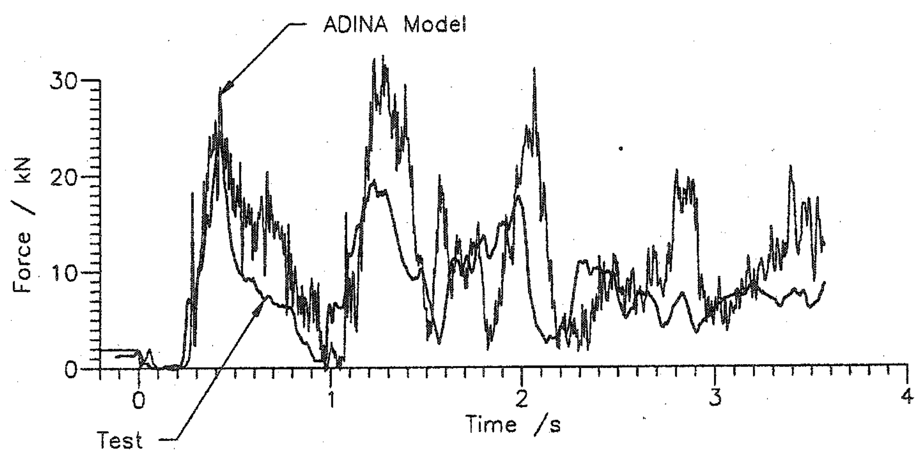

Figure 4-13
Insulator Tension at Tower T3--Test IIIL3 vs ADINA Model

Figures 4-14 & 4-15 show the Fourier transforms of both the ADINA time history and the test record for test IIIL3. The amplitudes of frequencies above 8 to 10 Hz in the test record are very small in comparison to the amplitudes from the ADINA Model. An inverse Fourier transform of only the frequencies below 10 Hz in the test record could not be distinguished from the original, while higher frequencies are obviously represented in the ADINA time history.

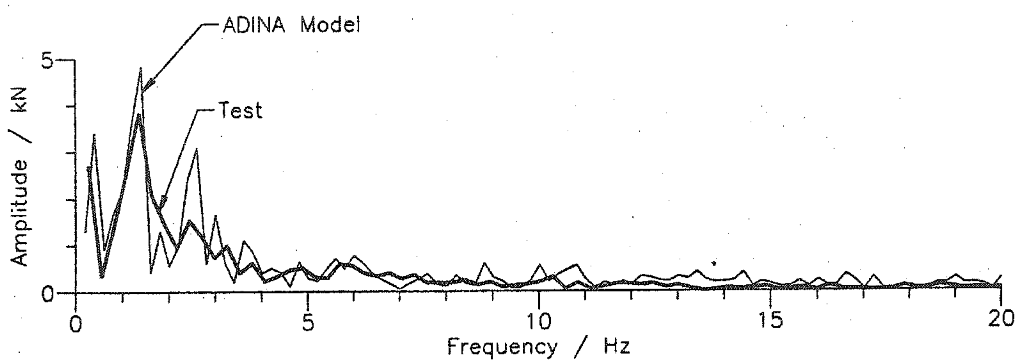

Figure 4-14
Frequency Content of Test IIIL3 and ADINA Model

The test report indicates (page 5-1) that "...the basic concern for the instrumentation was within the low frequency to DC range for the basic vibrational characteristics." The fundamental frequency of the tower was expected to be in the neighborhood of 5 Hz. The load cell signals were conditioned before recording with an oscillographic recorder. No detail is given about the extent of the signal conditioning; however, it is likely that a low pass analog filter was used to eliminate 60 Hz noise. Note that, even though higher frequencies would be expected in model tests, Kempner (1997) used a low pass filter with a 50 Hz cutoff in his model tests. Note also that analog low pass filters partially attenuate some of the frequencies below the nominal cutoff frequency. It can be reasonably inferred that any higher frequencies as shown in Figure 4-15 would, if they occurred in the tests, have been filtered out or attenuated before recording the data.

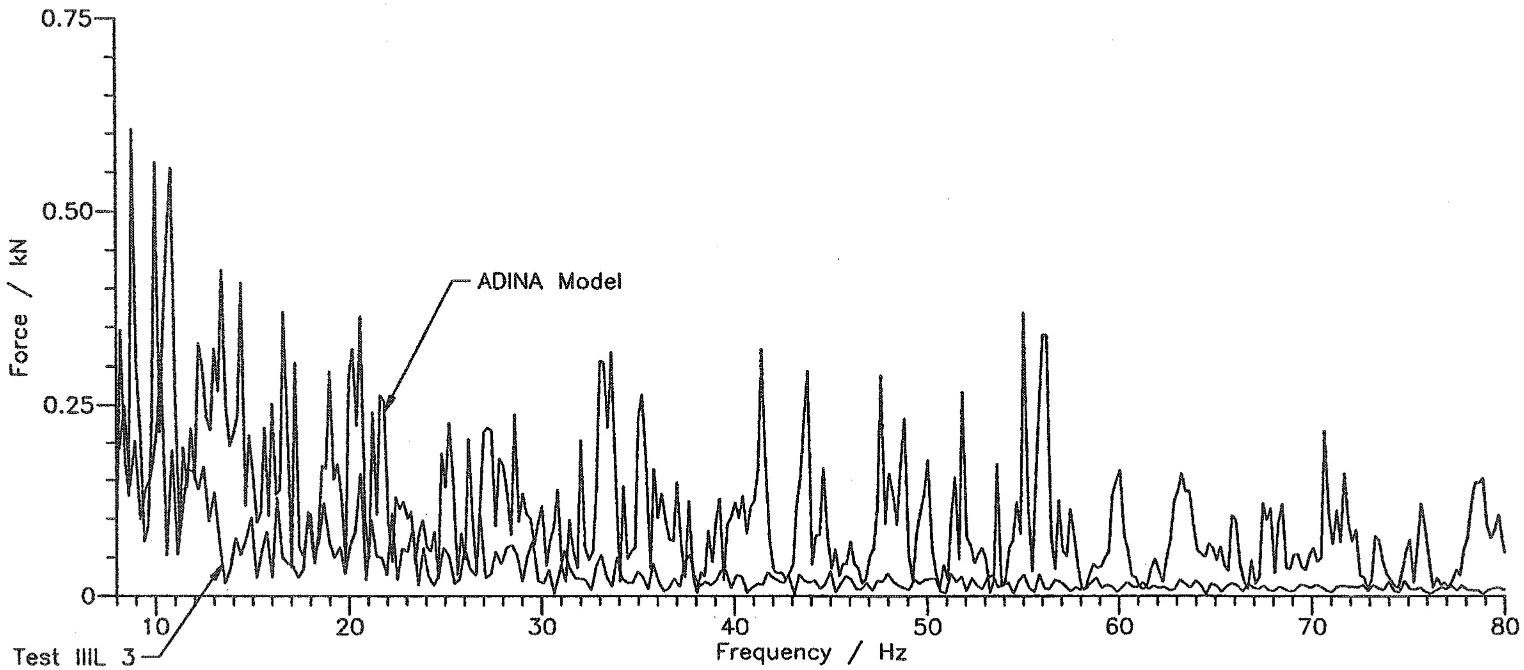

Figure 4-15 High Frequency Content of Test IIIL3 and ADINA Model

The ADINA time history analysis can itself be expected to introduce some higher frequencies in the response due to breaking up the continuous elements in the real structure into discrete pieces in the finite element model. In some past studies, damping has been increased to suppress these spurious frequencies in transmission line dynamic analysis (Roshan Fekr 1995). Holmes and Belytschko (1976) discuss the problem in reference to wave propagation problems and explore the use of digital filters to remove the spurious frequencies. Using unequal elements in the mesh will also introduce spurious frequencies due to reflections between elements (Bazant 1978). For this reason, using equal length elements to model the conductor is preferred. For convenience in calculation, lengths were made equal in the horizontal projection of the elements leading to small differences in the lengths within a span. Because spans must be divided up into an integral number of elements, there are also small differences in the length of elements used in the different spans. Some of the high frequency content shown in Figure 4-15 can reasonably be attributed to the modeling.

Digital filtering of the load cell tensions from the ADINA time history analysis is an effective way to remove the high frequency components for a better comparison with the full scale test data. Figure 4-16 shows the use of a 10 Hz low pass filter. A filter with a sharp cutoff was used because it is extremely easy to program once the Fourier coefficients have been determined. Figure 4-17 compares 10 and 15 Hz low pass filters. A 10 Hz low pass filter was used for subsequent time history analyses.

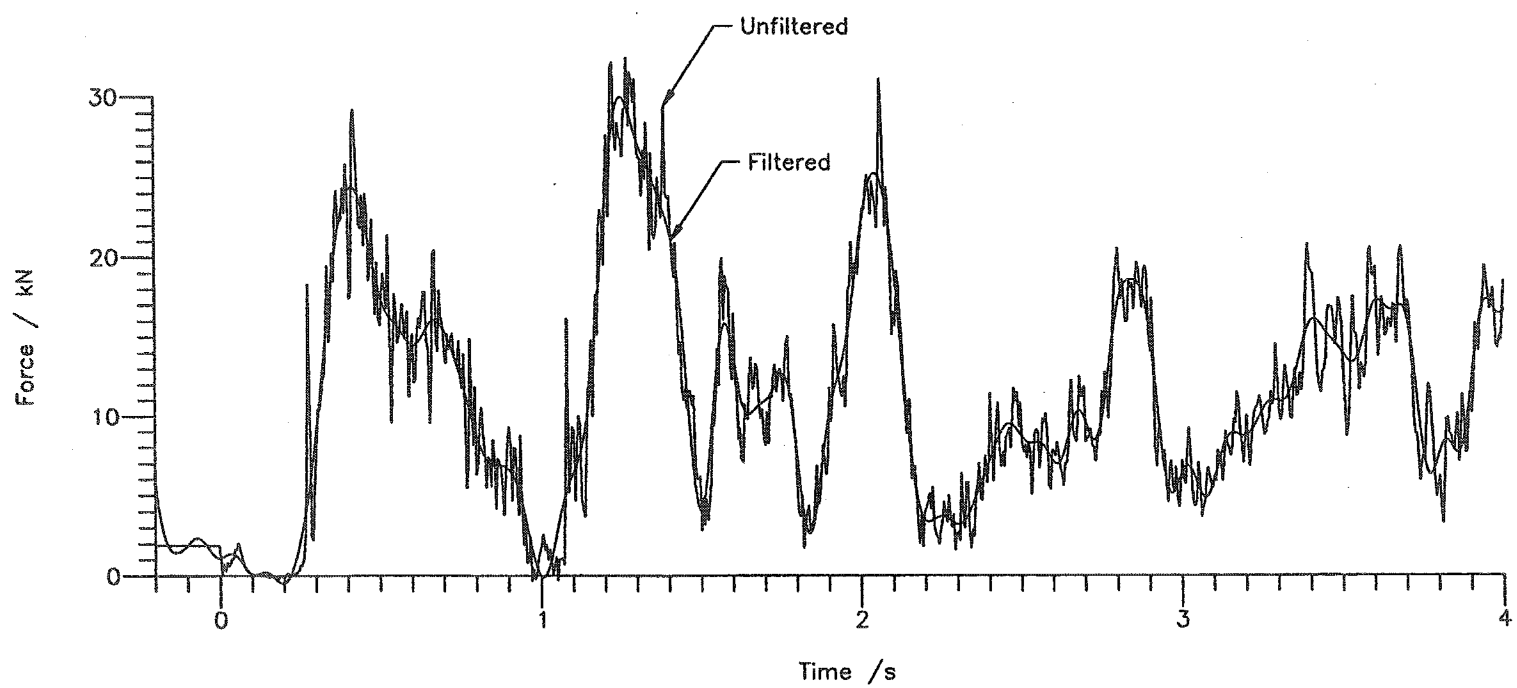

Figure 4-16 Insulator Tension at Tower T3, Test IIIL3
ADINA Model vs ADINA Model with 10 Hz Low Pass Filter

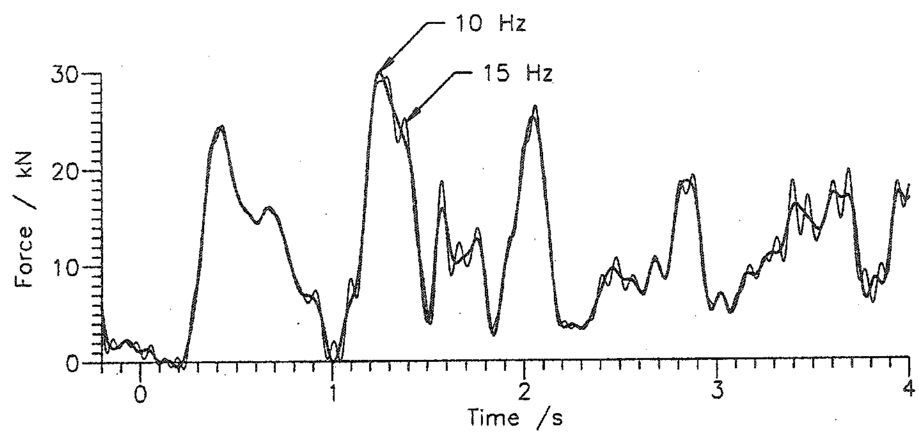

Figure 4-17
Insulator Tension at Tower T3, Test IIIL3
Comparison of 10 Hz and 15 Hz Low Pass Filters

Figures 4-18 to 4-20 compare the filtered results of the time history analyses for tests III L1, 2 and 3. In all three cases, there is a very good fit in the timing, the rise in tension and the peak tension of the first peak. The unloading part of the first peak does not have such a good fit. It appears to improve with the lower conductor tensions in tests IIIL2 and IIIL1. The small bumps on the rising part of the first peak may be explained by the bolted connections suddenly slipping during the loading cycle. Similarly the much faster reduction in tension during the fall of the first peak may be explained by permanent set in the tower caused by connections slipping. In a theoretical analysis of bolt slippage in the connections of lattice towers, Kitipornchai et al. (1994) report an increase in deflection of 20 percent due to slippage in the connections.

The timing of the second peak due to bottoming out of the fall of the first span of conductor is well predicted, but all three models substantially over-predict the magnitude of the peak. There is a small angle in line at tower T4 (1° 31') which was not included in the ADINA model. This may explain some of the difference. Increased movement of the tower under the impact due to slippage in the connections may also contribute to the difference.

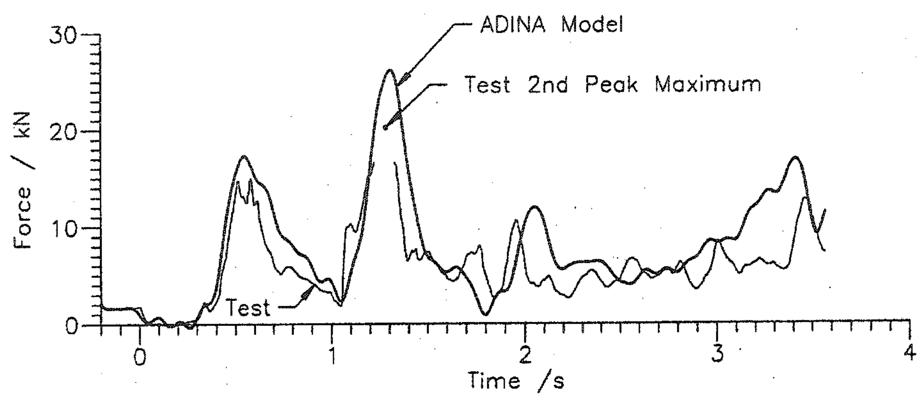

Figure 4-18
Insulator Tension at Tower T3
Test IIIL1 vs Filtered ADINA Model

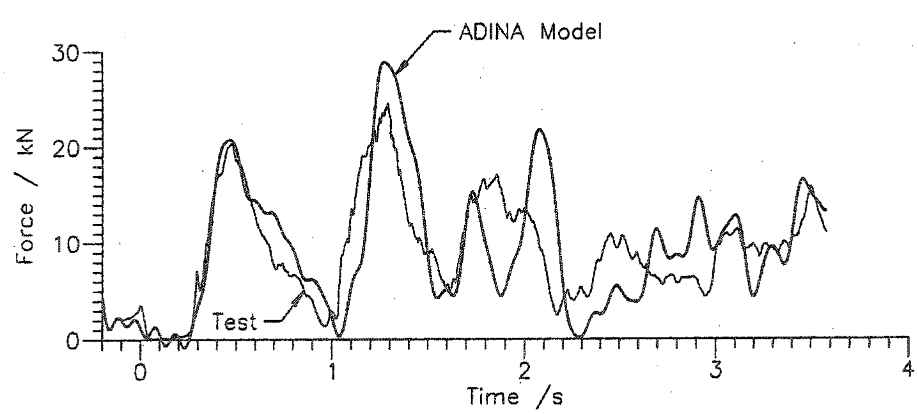

Figure 4-19
Insulator Tension at Tower T3
Test IIIL2 vs Filtered ADINA Model

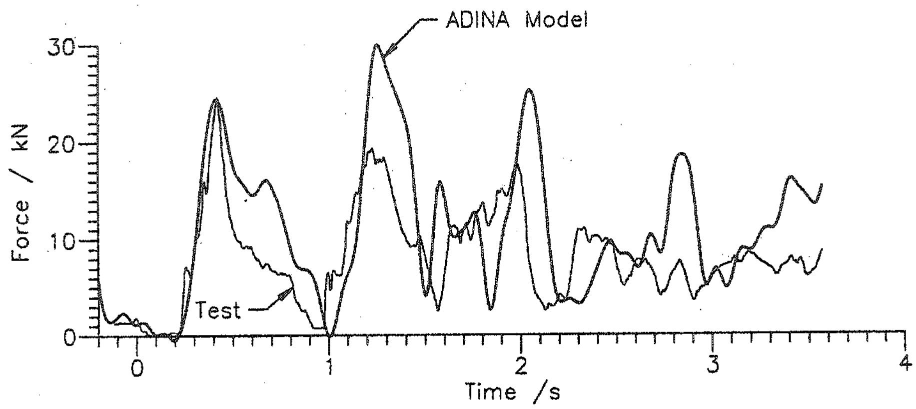

Figure 4-20
Insulator Tension at Tower T3
Test IIIL3 vs Filtered ADINA Model

Table 4-11 shows the magnitudes of the first and second peaks from the test. The magnitudes of the first peak follow in the order of the horizontal tension. The magnitudes of the 2nd peak in the tests are out of order with the test IIIL3 less than test IIIL2. As can be seen in Figure 4-21, the magnitudes of both peaks in the ADINA model are in order of horizontal tension. Unfortunately, there were no other successful tests with three tensions to indicate whether this is a problem with the tests or with the ADINA model.

Table 4-11
Peak Test Magnitudes

Test No.	Horizontal Tension (kN)	1st Peak (kN)	2nd Peak (kN)
IIIL1	12.43	14.96	20.27
IIIL2	17.77	20.27	24.61
IIIL3	21.32	24.61	21.72

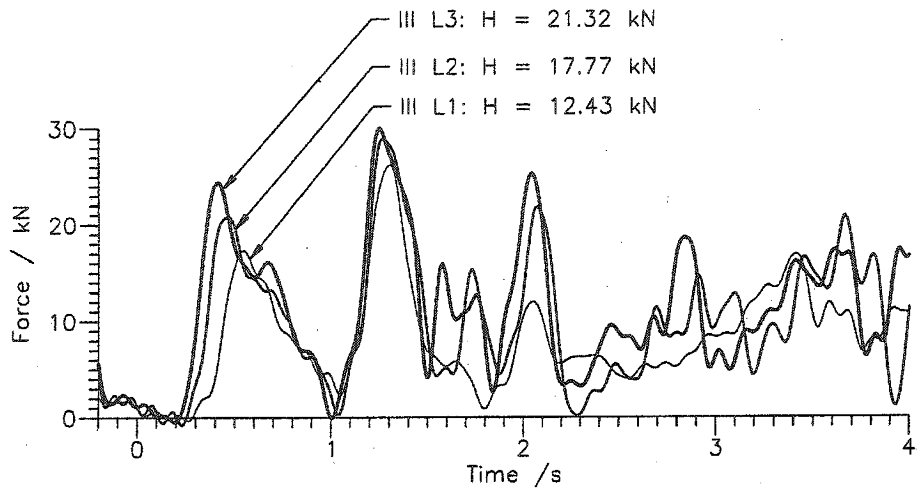

Figure 4-21
Insulator Tensions at Tower T3
ADINA Models of Tests IIIL1 to 3

4.7.1 Variations in the Model Parameters

Due to the discrepancy in the magnitudes of the second peaks from the tests, some variations in the model parameters were made to see the effects on the results.

Changing the modulus of elasticity of the wire rope in the insulator assemblies of towers T2 and T3 from 82.7 GPa to 41.35 GPa. (a 50% change) did not significantly affect the results.

The reduced tower model at tower T3 was replaced with the full tower model without any damping applied to the tower. There was no significant change in the results.

Changing the longitudinal and torsional natural frequencies of the towers from 4.6 to 4.0 and 7.2 to 6.6 Hz, respectively, by reducing the stiffness of the springs had only a minor effect on the results.

Changing the modulus of elasticity of the conductor from 74.2 GPa to 81.62 GPa had no significant effect on the magnitude and timing of the first two peaks; however, it made a noticeable difference after the second peak.

The effect of changing the insulator string lengths by changing only the length of the top element by 15 cm plus and minus (with no change in mass) is shown in Figure 4-22. The uncertainty in the insulator string length discussed above does not explain the difference between tests and ADINA models for the second peak

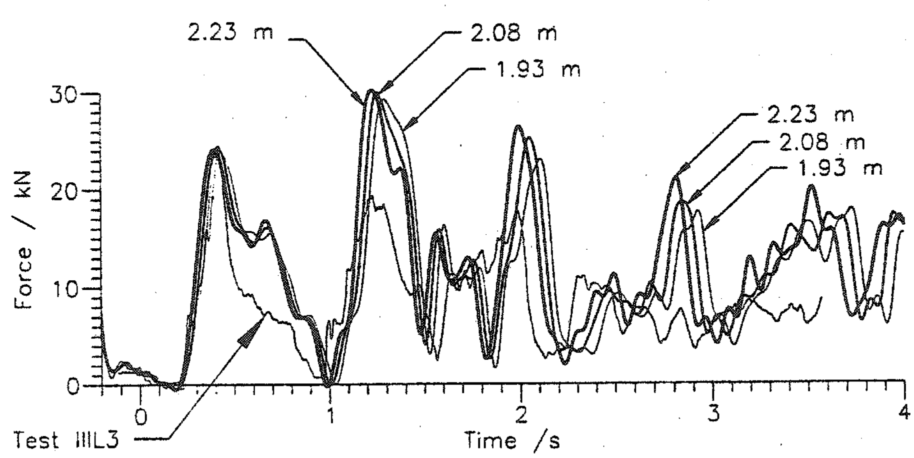

Figure 4-22
Test IIIL3, Effect of Changes in Insulator Length

Some model runs were made with the span between towers T3 and T4 changed to 279 m due to the discrepancy noted above. This did not improve the fit with the test data. Rayleigh damping was tried, also without significant improvement. However, one run made with the 279 m span is of interest. The axial and aerodynamic dampers were replaced with grounded vertical viscous dampers giving damping vertically of 3.2 kg/s-m. The longitudinal spring constant of the tower was reduced to 516 kN/m and the damping constant was increased to 2875 kg/s. This changed the longitudinal natural frequency of the tower from 4.6 Hz to 4.0 Hz and the damping ratio from 5 to 7 percent. The changes in the tower stiffness and damping were not significant, however, the change to the wire damping was. Figure 4-23 compares this damping with the original test data. The timing of the first peak is still good, but it is somewhat smaller in magnitude. The timing of the second peak is delayed, but the magnitude matches very well.

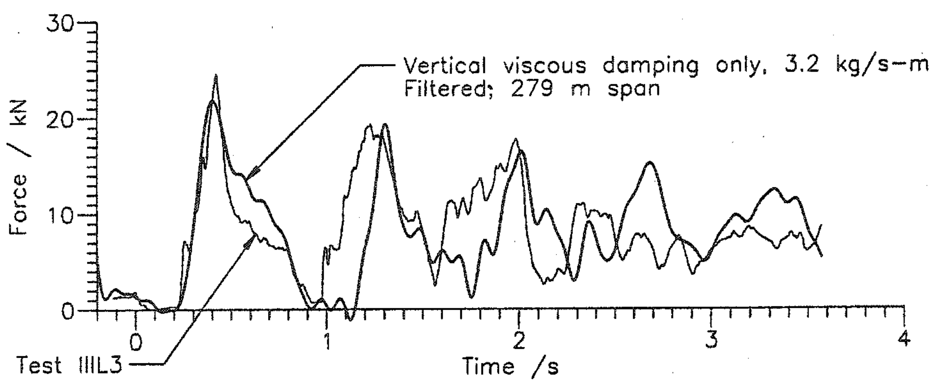

Figure 4-23
Insulator Tension at Tower T3
Test vs ADINA Model with Vertical Damping

4.8 Conclusions

Analog time histories from older tests can be digitized and analyzed for their frequency content. Digital filtering is an effective way to remove the high frequencies introduced by breaking continuous systems up into a finite element model.

The ADINA time history analysis does a good job of predicting the first peak due to loss of conductor tension but a relatively poor job of predicting the magnitude of the second peak due to the retensioning of the conductor at the bottom of its fall. For the purposes of the proposed research, the model is adequate. The first peak is well modeled. The second peak is on the conservative side for evaluating the effect of measures introduced into the tower and insulator system to control impact.

The poor fit between the analytic results and the tests after the first peak shows that there is still work to be done in modeling conductor. Questions that need to be answered include: whether the bending stiffness of the conductor needs to be taken into account, and the type of damping and its application that best represent the physics of the conductor and its motion in the transient phase of the response when the peaks that need mitigation occur.

4.9 Recommendations for Future Tests

While the documentation for these tests is the best that is currently available in the literature, there are a few things that were not done in these tests that would help in modeling future tests. When tests are made on double circuit towers or the outside phase of single circuit towers, in addition to the longitudinal natural frequency, the torsional natural frequency of the tower should be determined. Accurate measurements of the static deflections of the tower for both balanced and torsional longitudinal loads including any permanent set should be determined experimentally to give a measure of the effects of the foundation stiffness and bolt slippage. Permanent set of the tower after the application of each broken wire load should be determined. Accelerometers placed at the center of the tower and at the insulator attachment point would allow the actual tower movement to be compared directly to the tower model.

Experimental measurements are usually filtered in some fashion before being recorded. Finite element models also introduce noise because systems that are continuous in nature are broken up into discrete elements for analysis. As can be seen in Figure 4-16, the finite element results can also be filtered to remove some of the noise due to the model's discretization of a continuous structure. Knowing the filtering used in the physical measurements will allow similar filtering of the results from the finite element model, which should provide a better comparison between the measurements and the results of the finite element analysis.

The stress-strain relationship of new transmission conductor is highly nonlinear. The stress-strain characteristics of a conductor that has been in service are dependent on the installation technique and the in-service load history. If possible, the conductor properties, unit mass, area and modulus of elasticity, should be measured experimentally both before and after the tests.

The wire movement at the quarter points in the span should be recorded if possible. Analyzing the movement at these three points for both frequency and phase could allow separation of the effects of traveling waves and excitation of the span in its normal modes.

More testing is needed to determine the lateral damping properties of transmission conductors.

Chapter 5
Results and Discussion

In this chapter, the results of the time history analyses are presented for the following configurations:

- Bare shield wire deadended on the tower.
- Iced shield wire deadended on the tower.
- Bare shield wire attached to the tower with a post spring-damper system.
- Iced shield wire attached to the tower with a post spring-damper system.
- Bare conductor attached to the tower with a post spring-damper system.
- Iced conductor attached to the tower with a post spring-damper system.
- Bare conductor attached to a tower with a rotating crossarm spring-damper system.
- Iced conductor attached to a tower with a rotating crossarm spring-damper system.

After the results are presented, they are discussed in light of other methods that have been proposed for reducing the peak loads due to broken wires and other longitudinal disturbances to the wire tensioning system.

The time history analyses were performed for all the combinations of springs and dampers shown in Figure 3-17. The initial tensioning of the wire and application of the gravity load were done in one step. Using ADINA, this appears as one time step with a duration of one second. Thus the dynamic analyses begin at time t = 1 s. Referring to

Figure 3-11a, at t = 1.05 s element 7-1 dies, i.e. is removed from the model, which removes the tension holding the insulator string in place. This simulates the wire breaking at the point where the wire attaches to the insulator string (or for the deadended shield wire, to the tower). Each time history analysis extended for 10 s for a range of 1 to 11 s.

5.1 Post Spring-Damper Results

After the time history analysis was performed, the data for the elastic force in the spring representing the tower was examined to determine the peak forces predicted by the numerical model. The peak tower elastic forces for the shield wire and conductor post-spring damper systems are summarized in Figures 5-1 to 5-4. In all cases, the overall minimum peak tower elastic load was obtained using viscous dampers without springs.

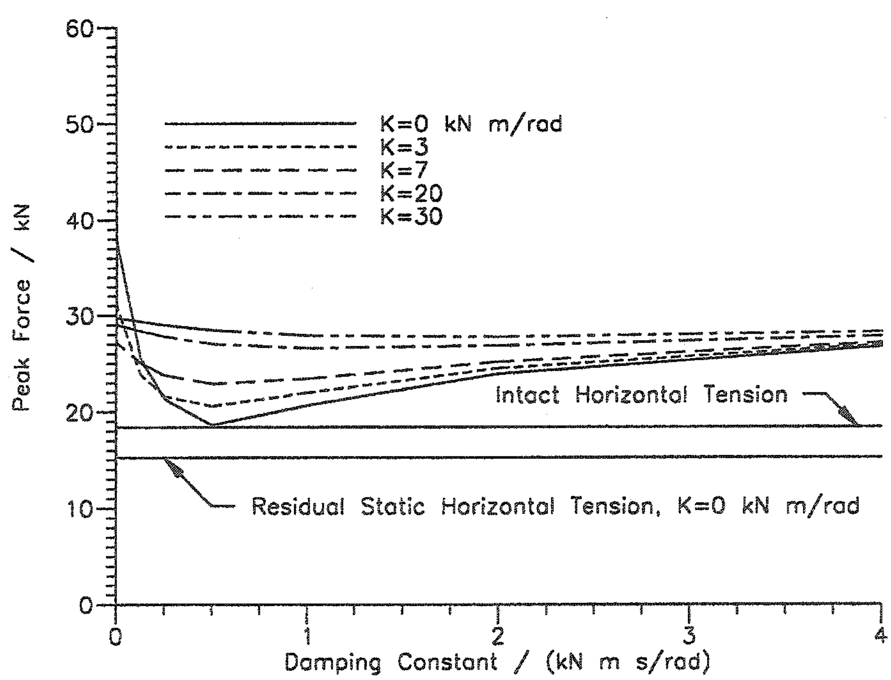

Figure 5-1
Post Spring-Damper, Tower Elastic Forces for Bare Shield Wire

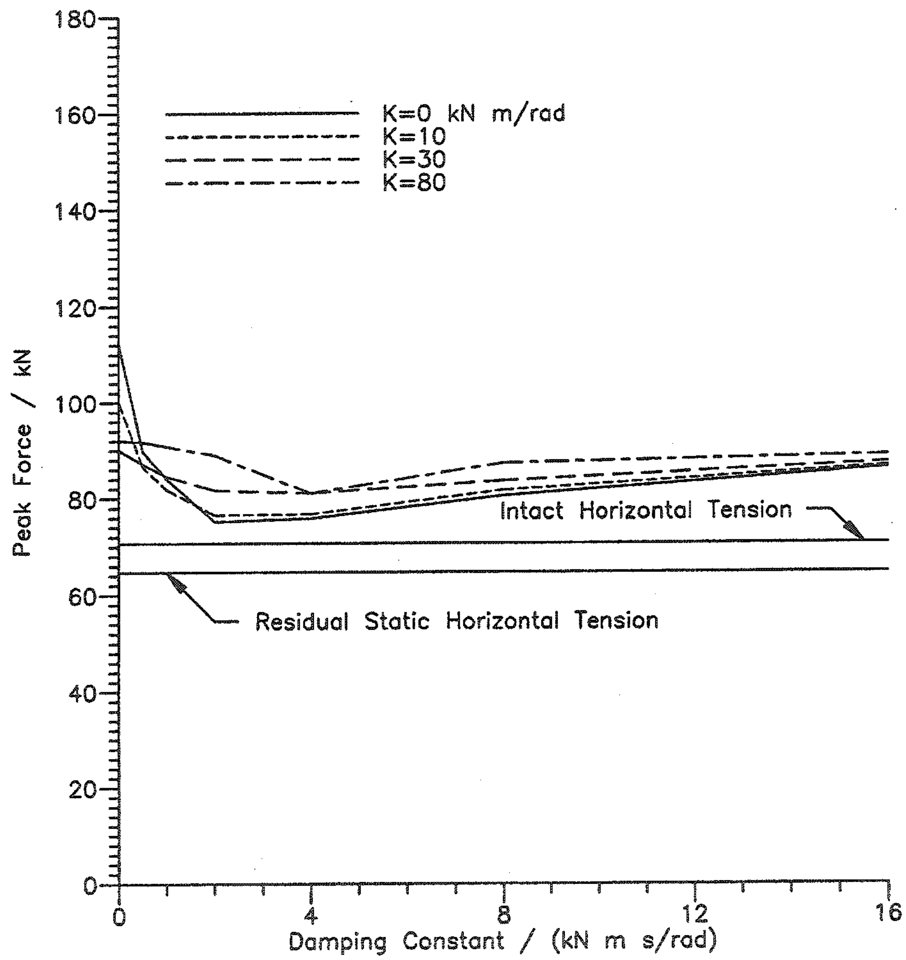

Figure 5-2
Post Spring-Damper
Tower Elastic Forces for Iced Shield Wire

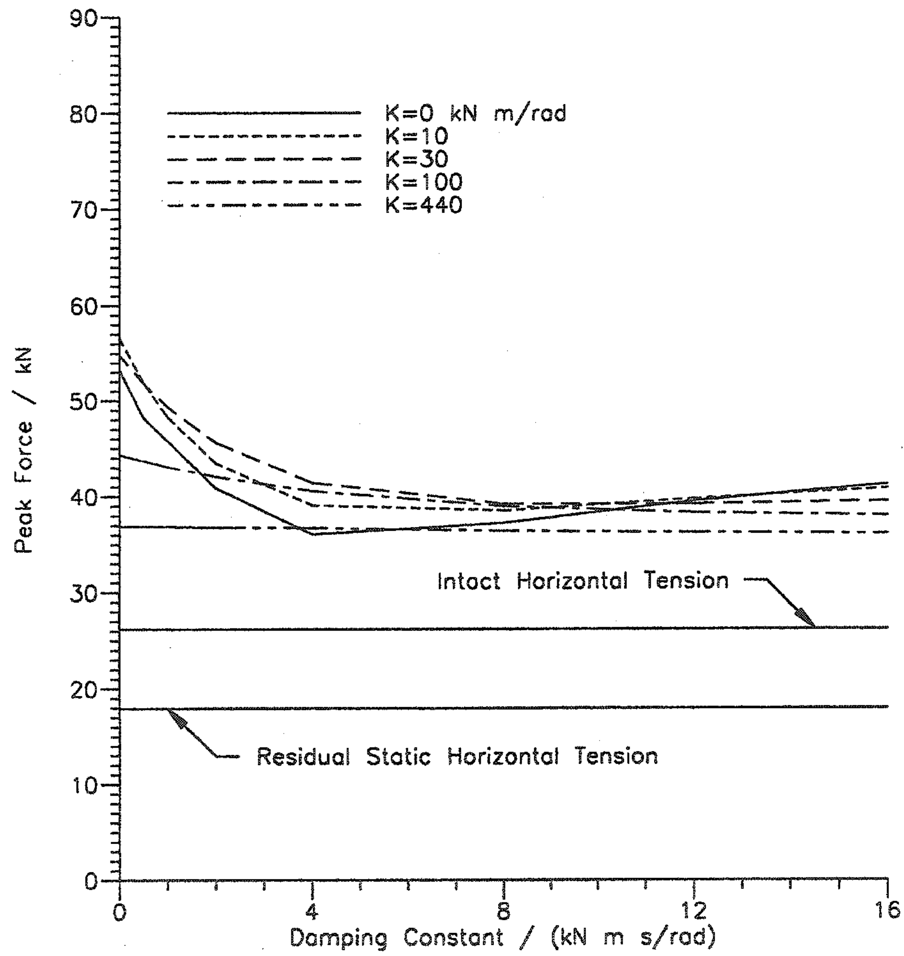

Figure 5-3
Post Spring-Damper
Tower Elastic Forces for Bare Conductor

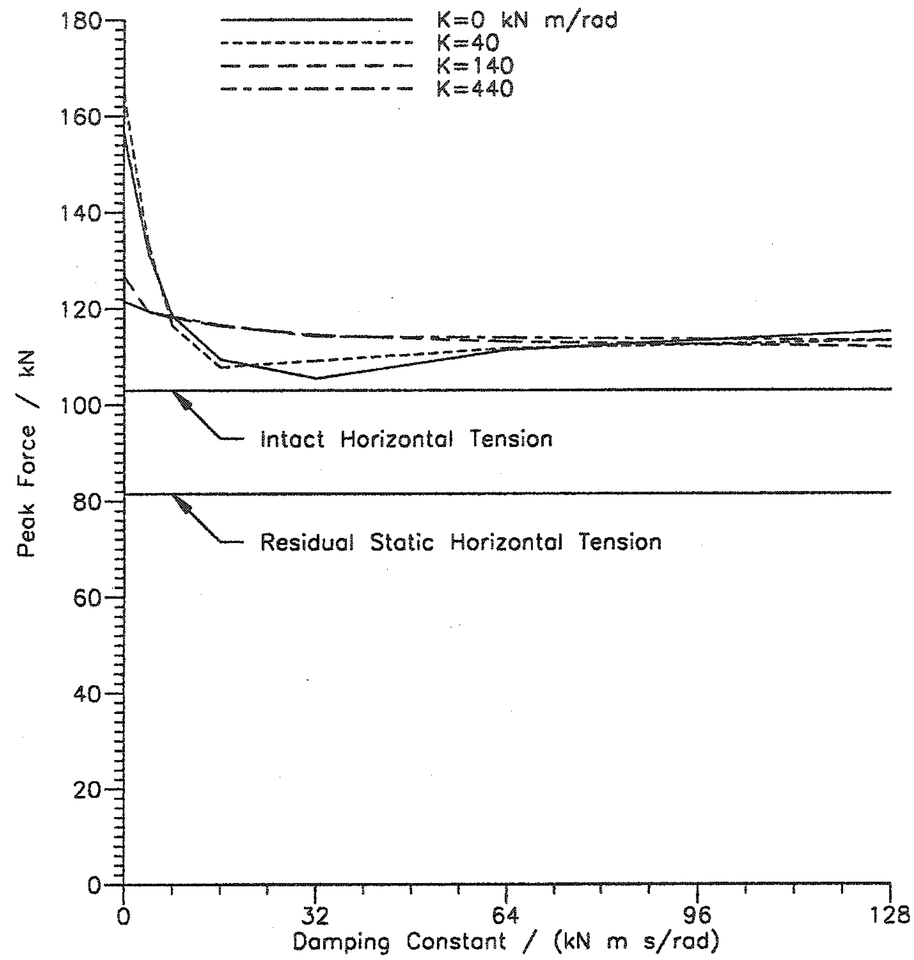

Figure 5-4
Post Spring-Damper
Tower Elastic Forces for Iced Conductor

Figure 5-5 shows the time histories for the bare shield wire deadended on the tower. Note that, while there is very little variation in the wire support tension, the tower responds with a peak elastic force well in excess of the intact wire tension.

Figure 5-6 shows the reference case time histories for the bare shield wire suspended from a post without any spring or damper. For ease of comparison, the time history of the elastic force for the deadended shield wire is included (Fig. 5-6d). The first two seconds of the time histories of the elastic force for both the tower with a post (Figure 5-6c) and with the shield wire deadended (Figure 5-6d) are very similar in appearance. The peak forces are practically of the same magnitude. The second and larger peak in the tower elastic force closely follows a peak in the support tension. It has a much larger magnitude with a shorter time interval.

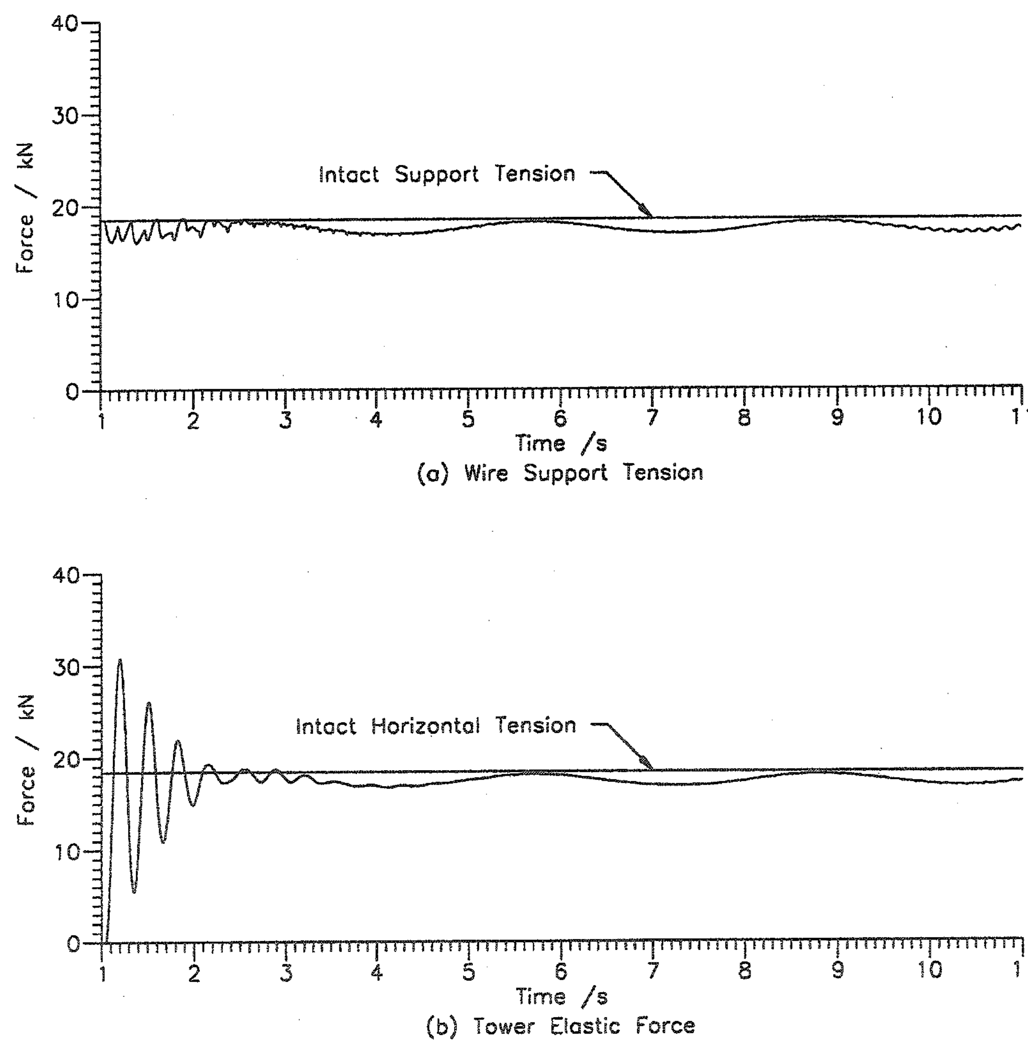

Figure 5-5
Time Histories for Deadended Bare Shield Wire

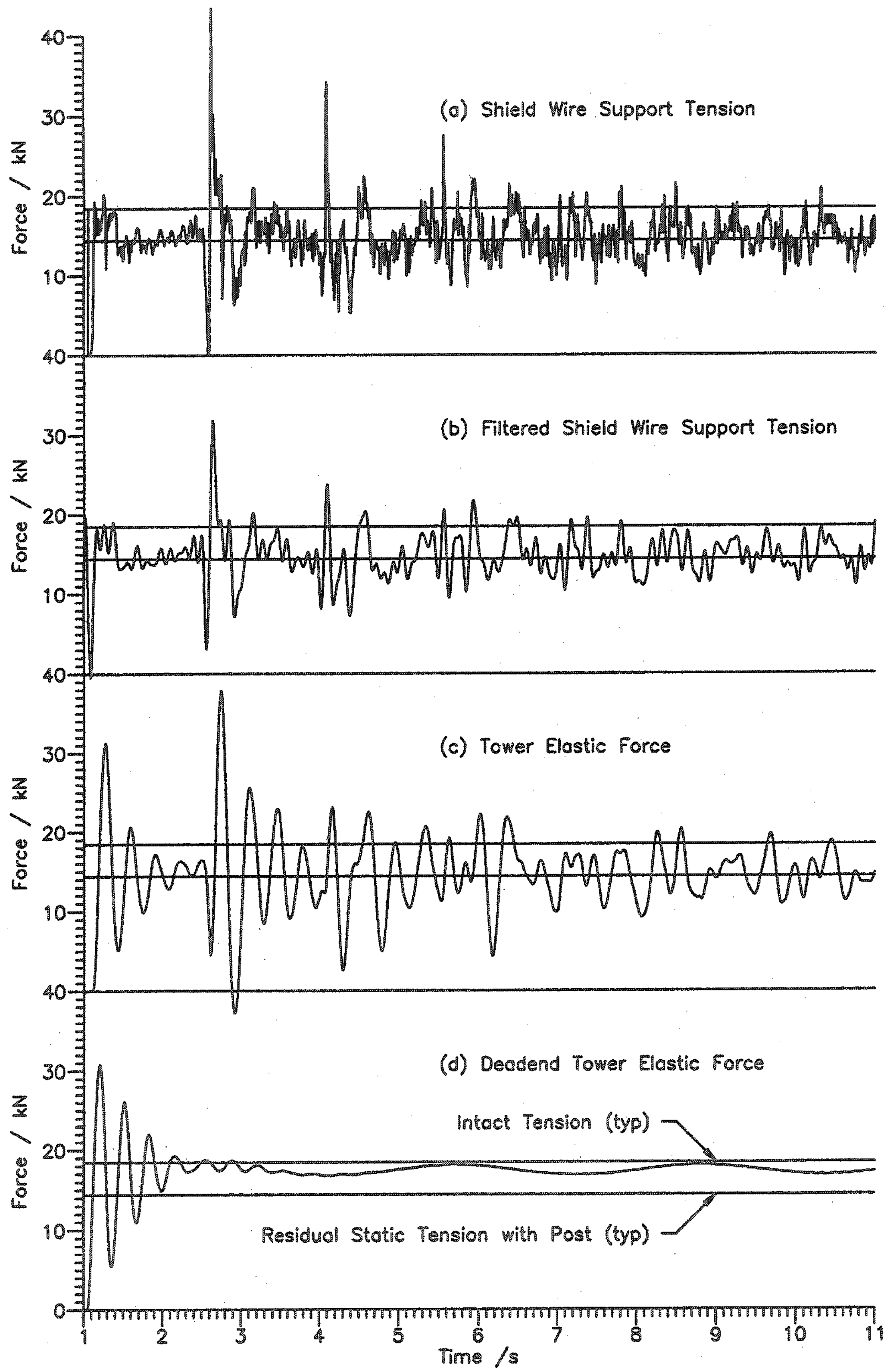

Figure 5-6
Bare Shield Wire Time Histories, K = 0, C = 0

Figure 5-7 shows the time histories of the bare shield wire suspended from a post with only a damper with C = 0.5 kN m s/rad and no spring, K=0 kN m/rad. Once again, the time history of the elastic force for the deadended shield wire is included for comparison (Figure 5-7d). Note that the shape of the first two seconds in Figure 5-7c is still similar to the deadended shield wire in Figure 5-7d, but heavily attenuated. The second peak in Figure 5-6c at around 2.7 s has been completely suppressed. The unfiltered support tension in Figure 5-7a has a short period saw tooth pattern superimposed on a longer-term variation. The distance between the gullets of the saw tooth is consistent with a period of 0.145 s (the time history data is saved every 0.005 s).

Figure 5-8 shows the time histories for the iced shield wire deadended on the tower. As with the deadended bare shield wire, the tower responds with a peak elastic force well in excess of the intact wire tension. Figures 5-9 and 5-10 show, respectively, the reference case without any spring-damper and the post with the optimum damper (C = 2 kN m s/rad) and no spring (K = 0 kN m/rad). A saw tooth pattern with a period of 0.53 s can be seen in the unfiltered conductor tension in both Figures 5-9a and 5-10a. In Figures 5-9c & d, the first peak in the tower elastic force, at approximately 1.2 s, is of practically the same magnitude for both the tower with an undamped post and the tower with the shield wire deadended. The highest peak for the undamped post occurs at about 7.5 s in Figure 5-9c. Figure 5-10c shows that this peak is completely suppressed by the dampers.

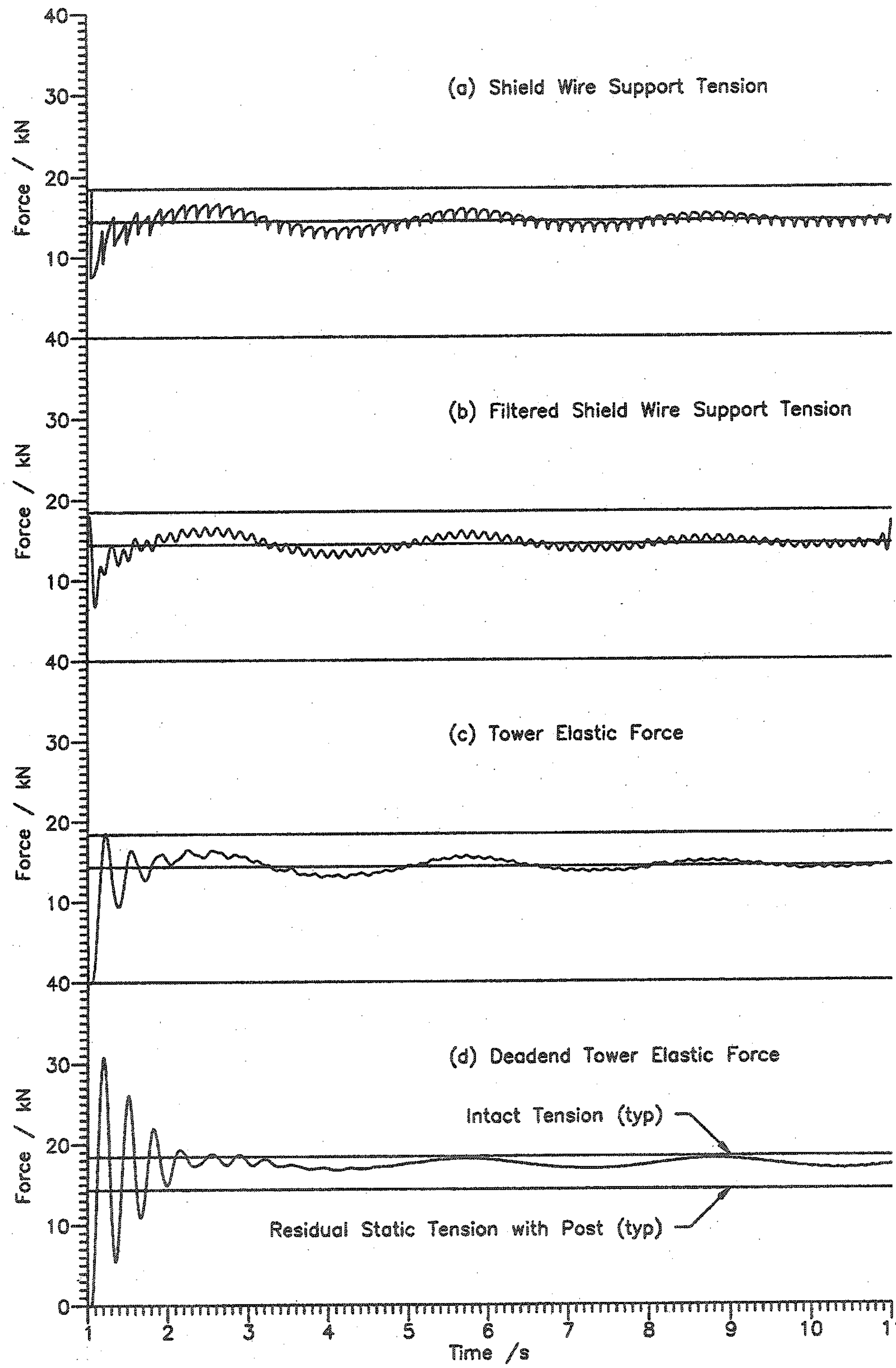

Figure 5-7
Bare Shield Wire Time Histories, K = 0, C = 0.5

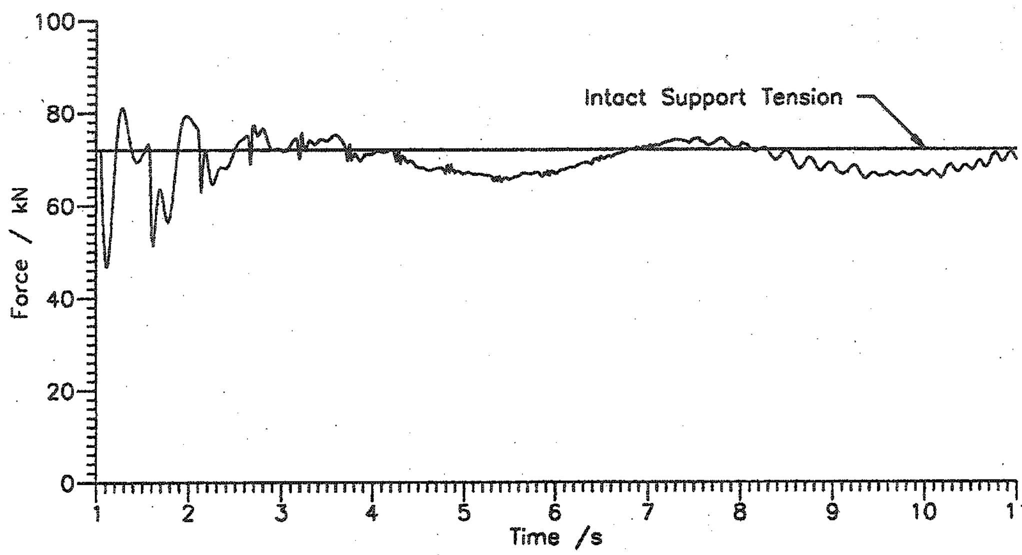

(a) Wire Support Tension

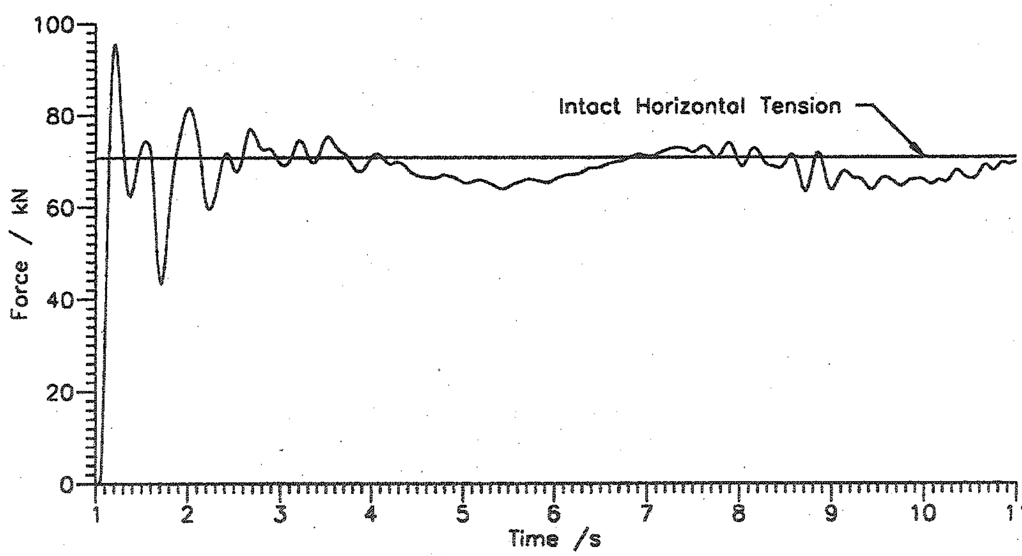

(b) Tower Elastic Force

Figure 5-8
Time Histories for
Deadended Iced Shield Wire

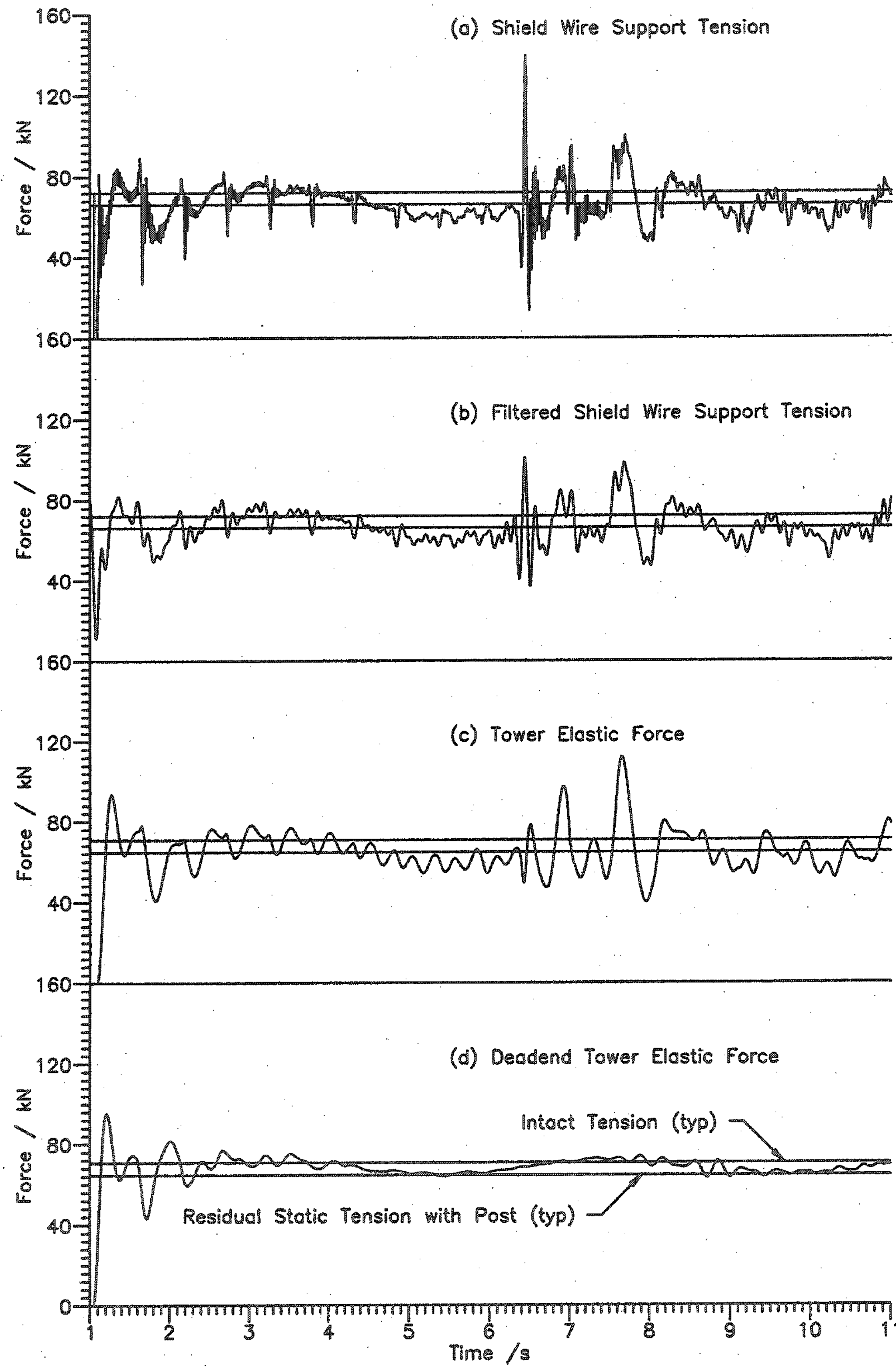

Figure 5-9
Iced Shield Wire Time Histories, K = 0, C = 0

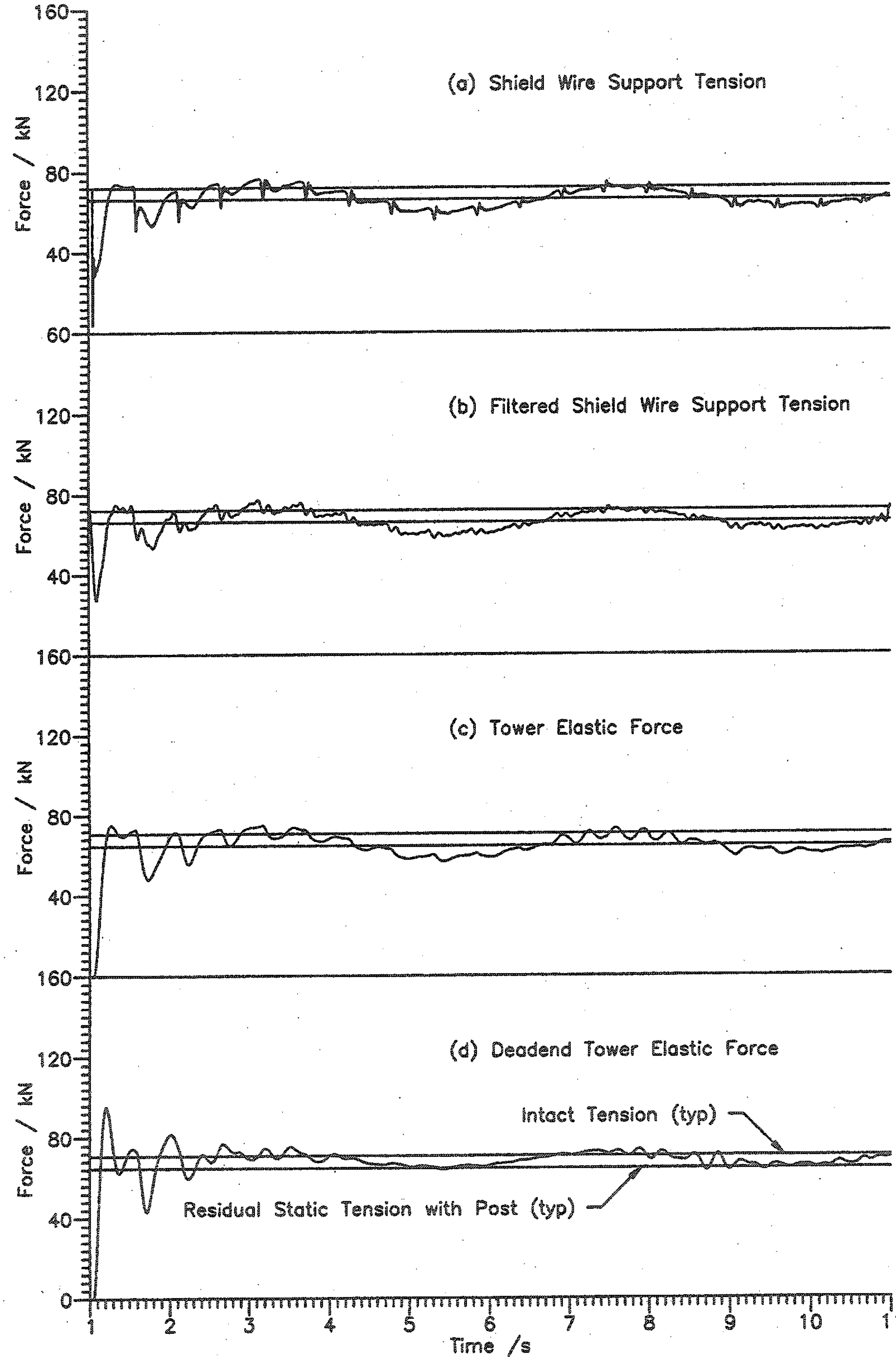

Figure 5-10
Iced Shield Wire Time Histories, K = 0, C = 2

Figure 5-11 shows broken wire time histories for a bare conductor with a freely swinging post. Figure 5-12 shows the comparable histories for a bare conductor with no spring (K = 0) and a damping constant C = 4 kN m s/rad. Figures 5-13 and 5-14 show the time histories for an iced conductor with a freely swinging post and with a spring constant of 0 and a damping constant C = 32 kN m s/rad, respectively. For both the bare and iced conductor, the addition of the damper substantially reduces the peak loads. The second and third peaks for the iced conductor in Figure 5-13 occur much later than the comparable peaks for the bare conductor shown in Figure 5-11. The saw tooth patterns noted above for the shield wire are also evident in Figures 5-12a and 5-14a and less prominently in Figure 5-11a and 5-13a.

Figures 5-15 to 5-18 show the time histories of the power being dissipated by the dampers for the bare shield wire, iced shield wire, bare conductor and iced conductor, respectively for each of the tend towers modeled. The total energy dissipated by the dampers over the 10 s period of the time histories is summarized in Table 5-1. The percentage of the total energy released is shown in Table 5-2.

Table 5-3 lists the intact, dynamic and residual static ground clearances assuming flat terrain.

Tables 5-4 to 5-7 compare the post rotation at each tower for a post free to swing (no spring-damper) and a post with the optimum damping.

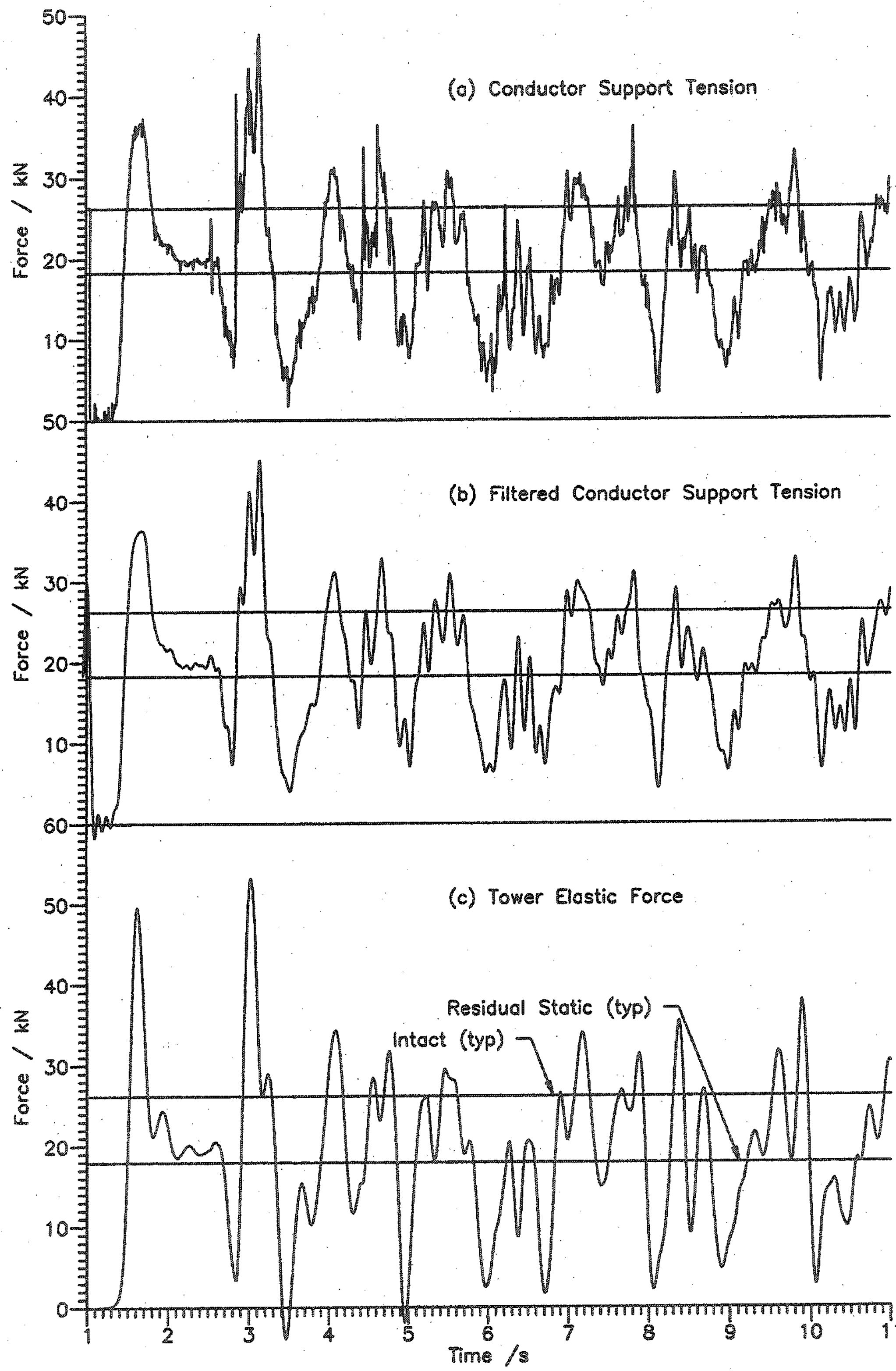

Figure 5-11
Bare Conductor Time Histories, K= 0, C = 0

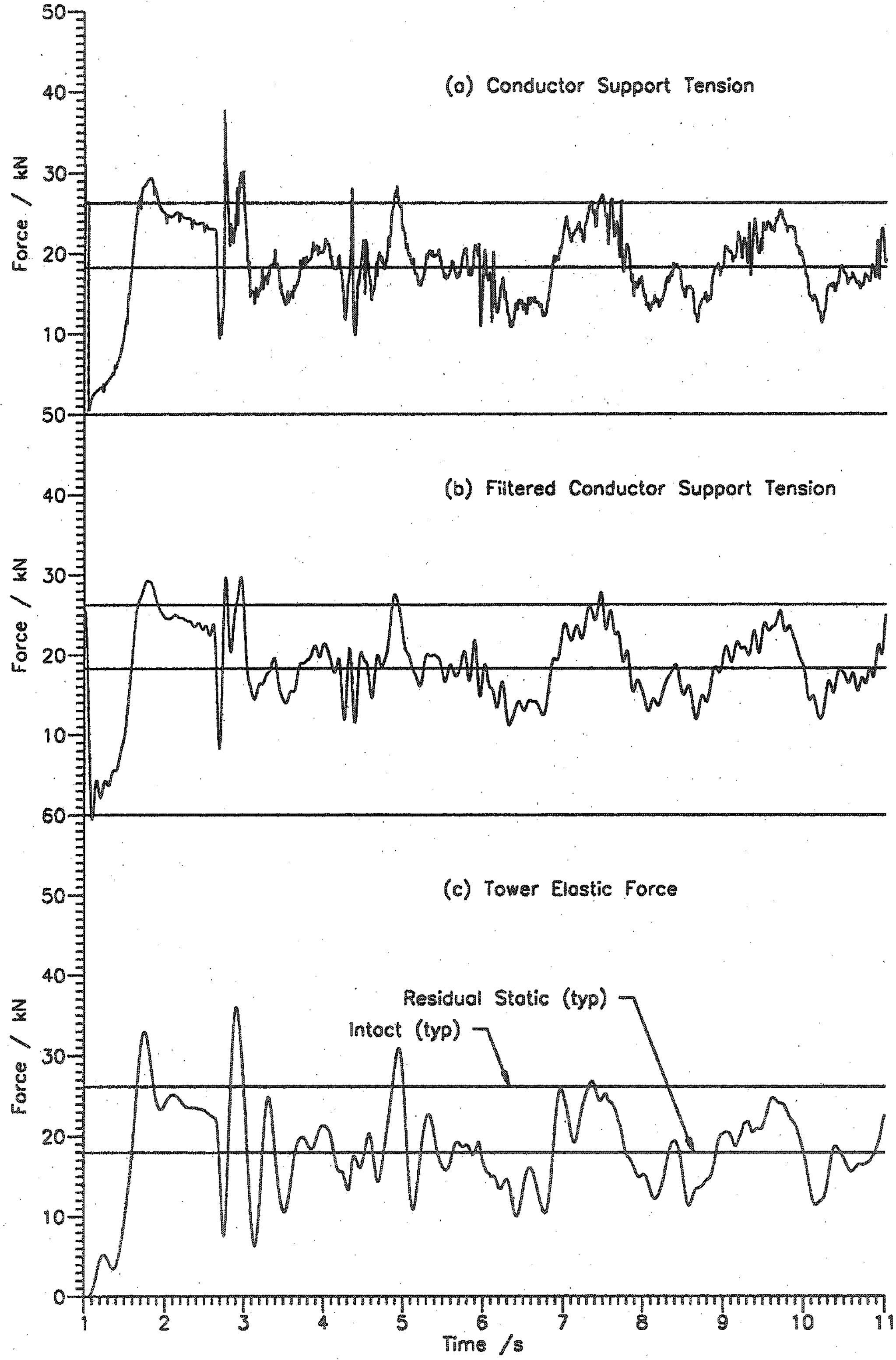

Figure 5-12
Bare Conductor Time Histories, K = 0, C = 4

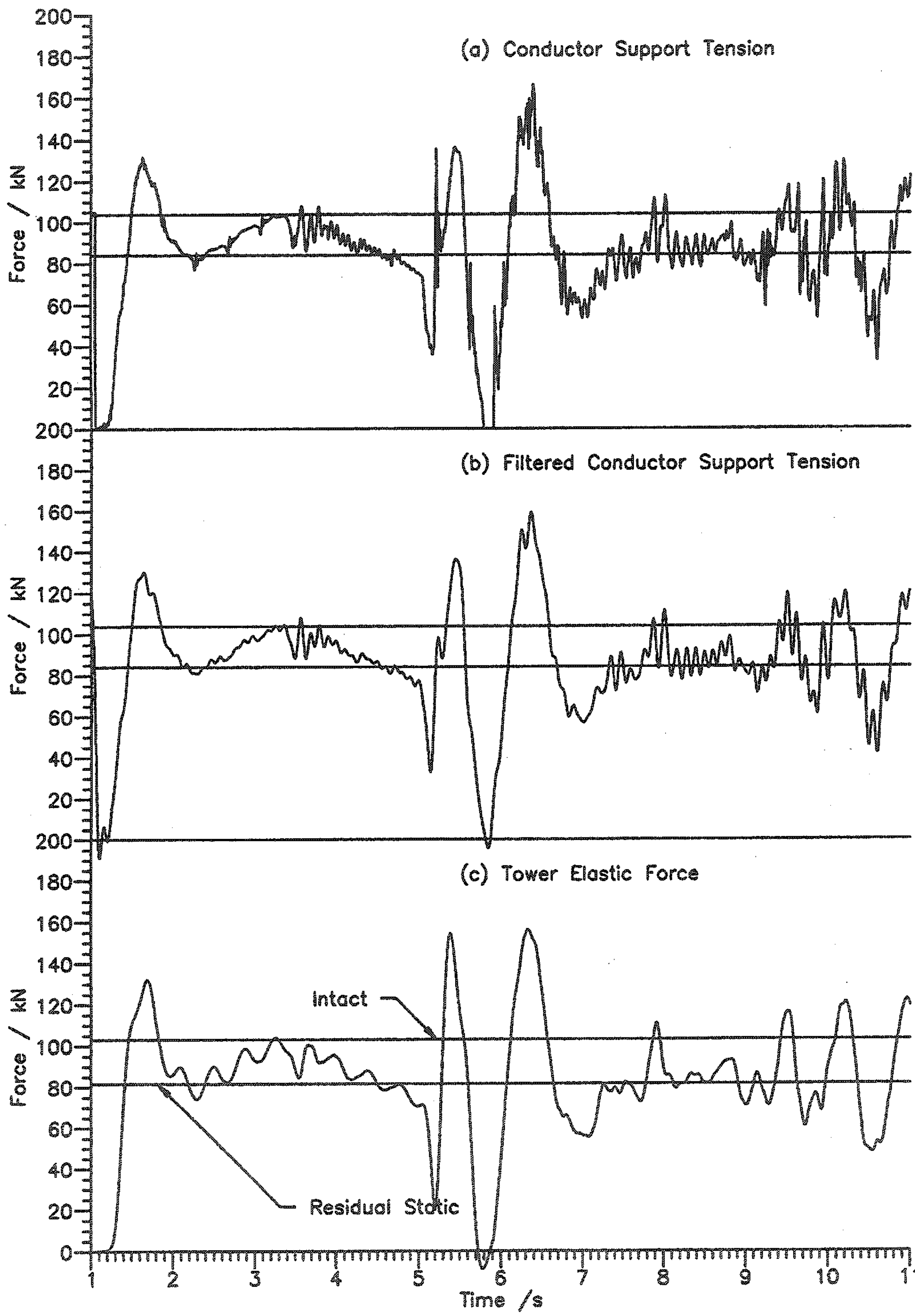

Figure 5-13
Iced Conductor Time Histories, K = 0, C = 0

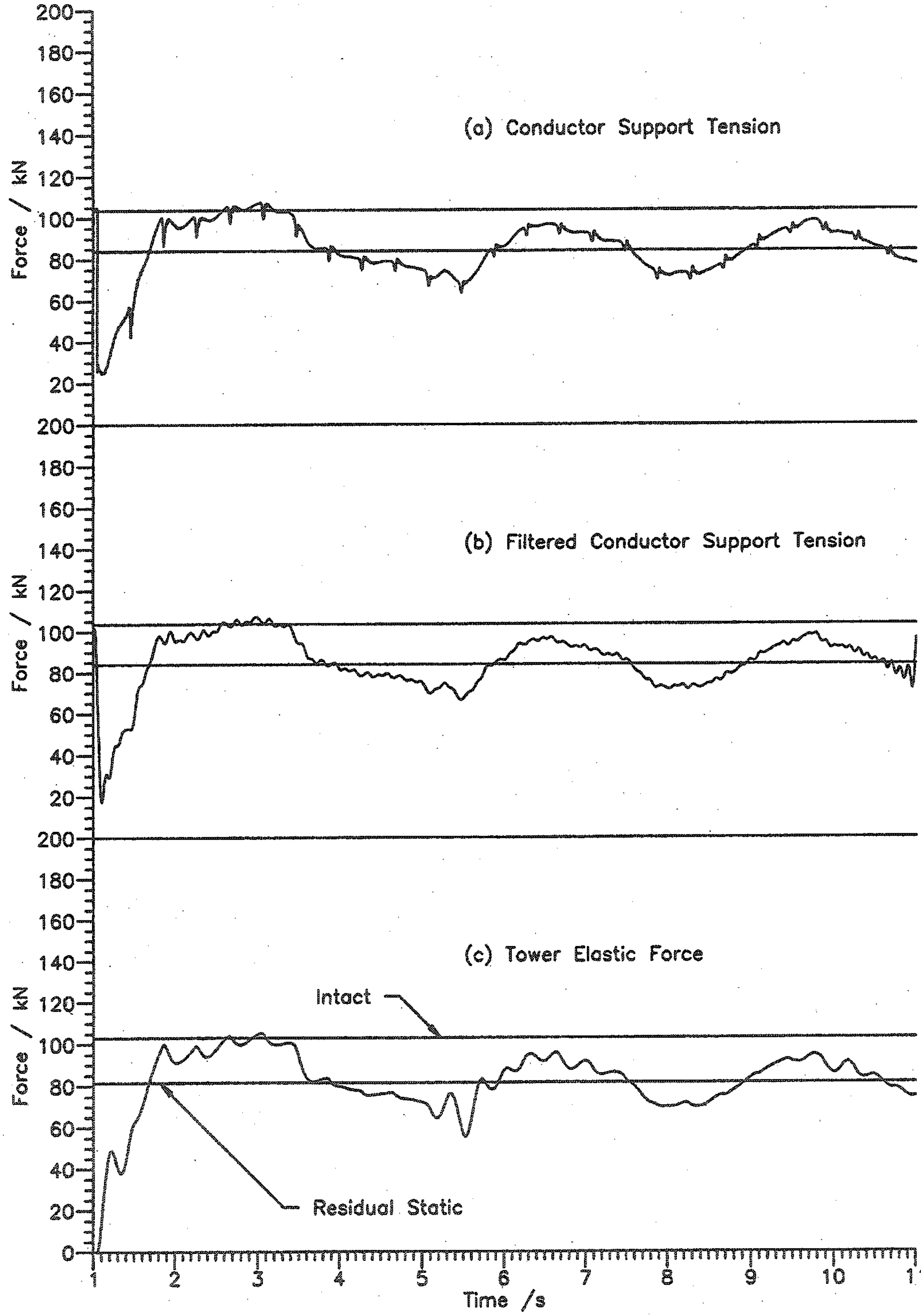

Figure 5-14
Iced Conductor Time Histories, K = 0, C = 32

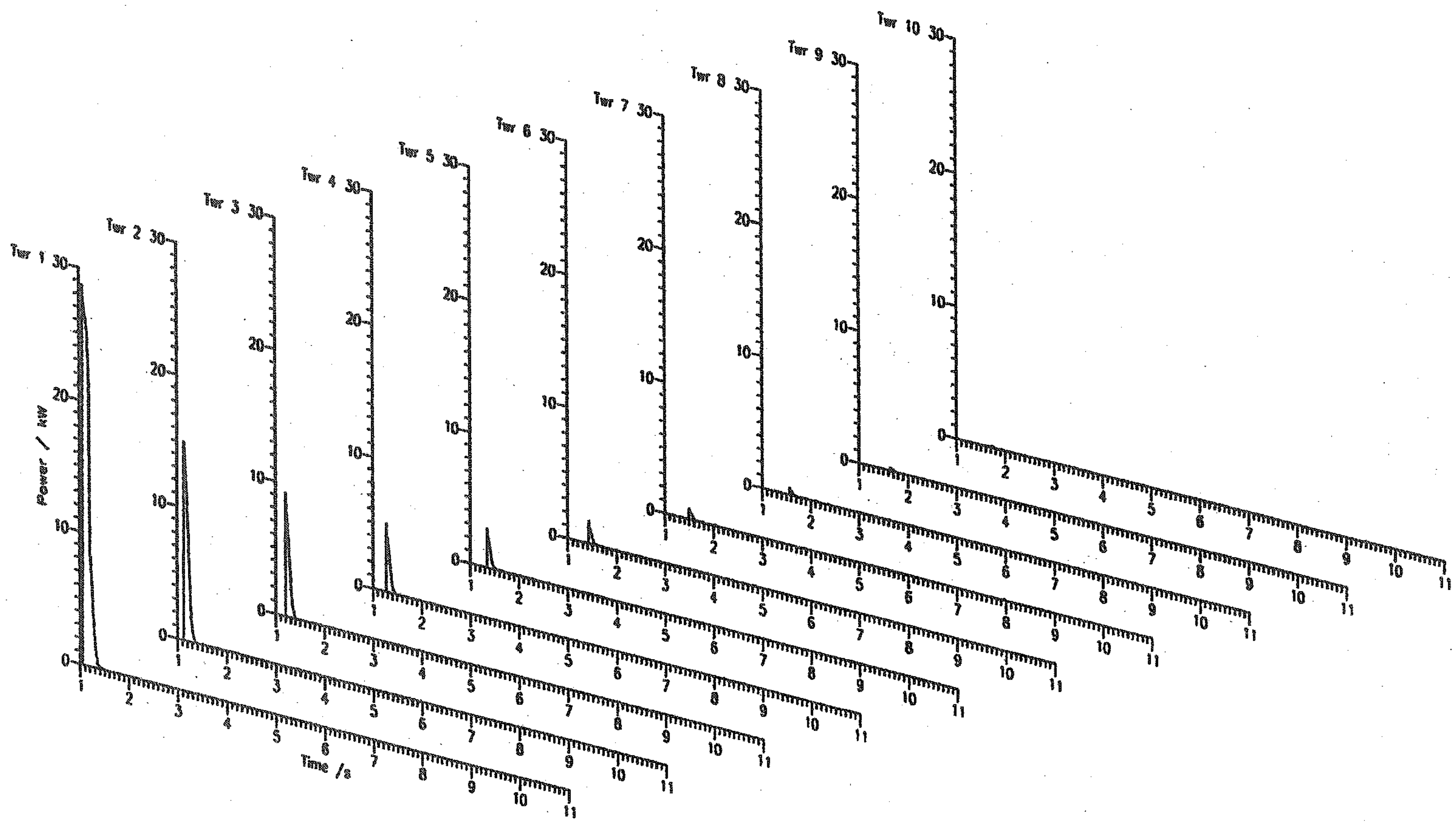

Figure 5-15 Power Dissipated by Dampers – Bare Shield Wire Post Spring-Damper

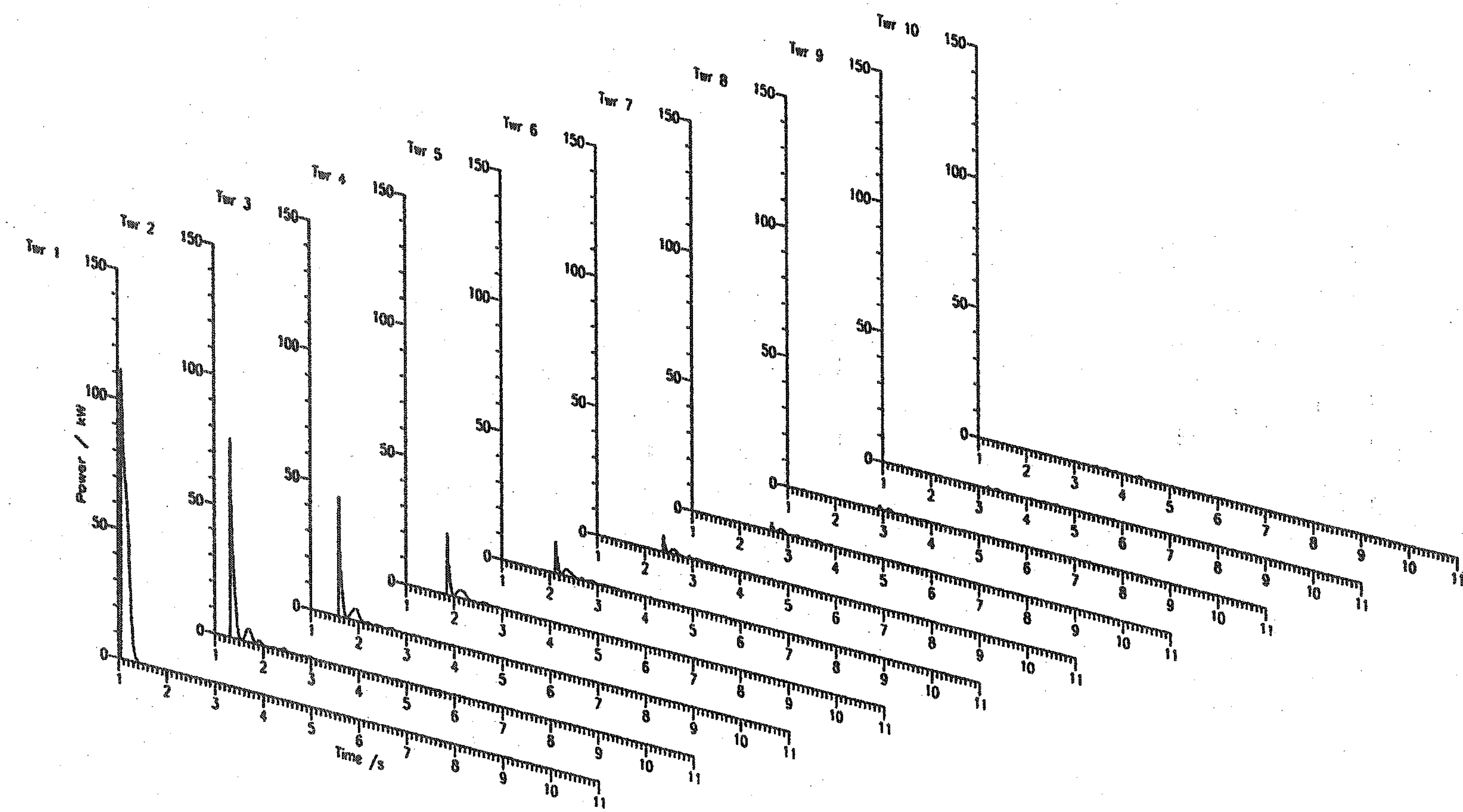

Figure 5-16 Power Dissipated by Dampers –Iced Shield Wire Post Spring-Damper

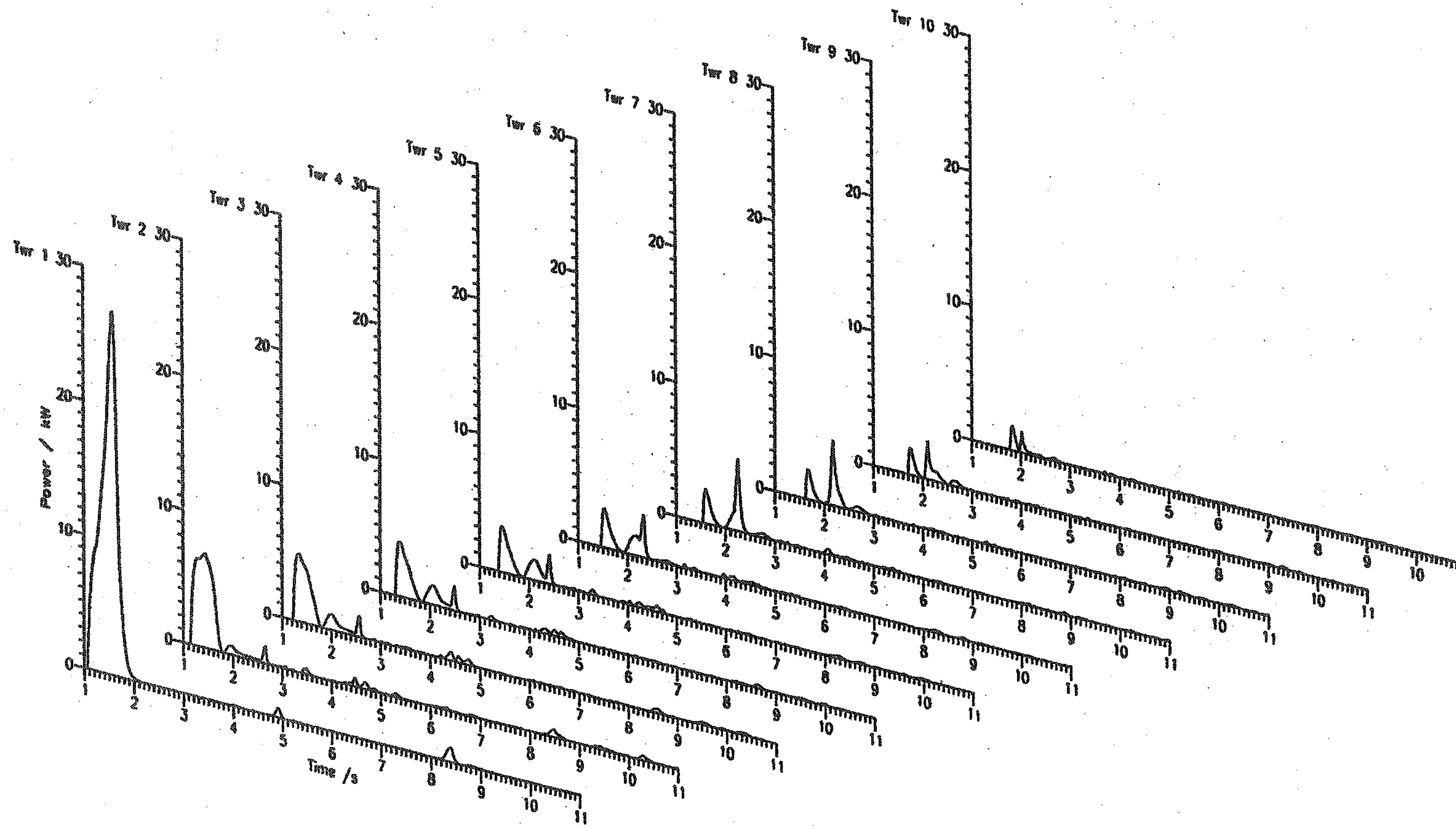

Figure 5-17 Power Dissipated by Dampers –Bare Conductor Post Spring-Damper

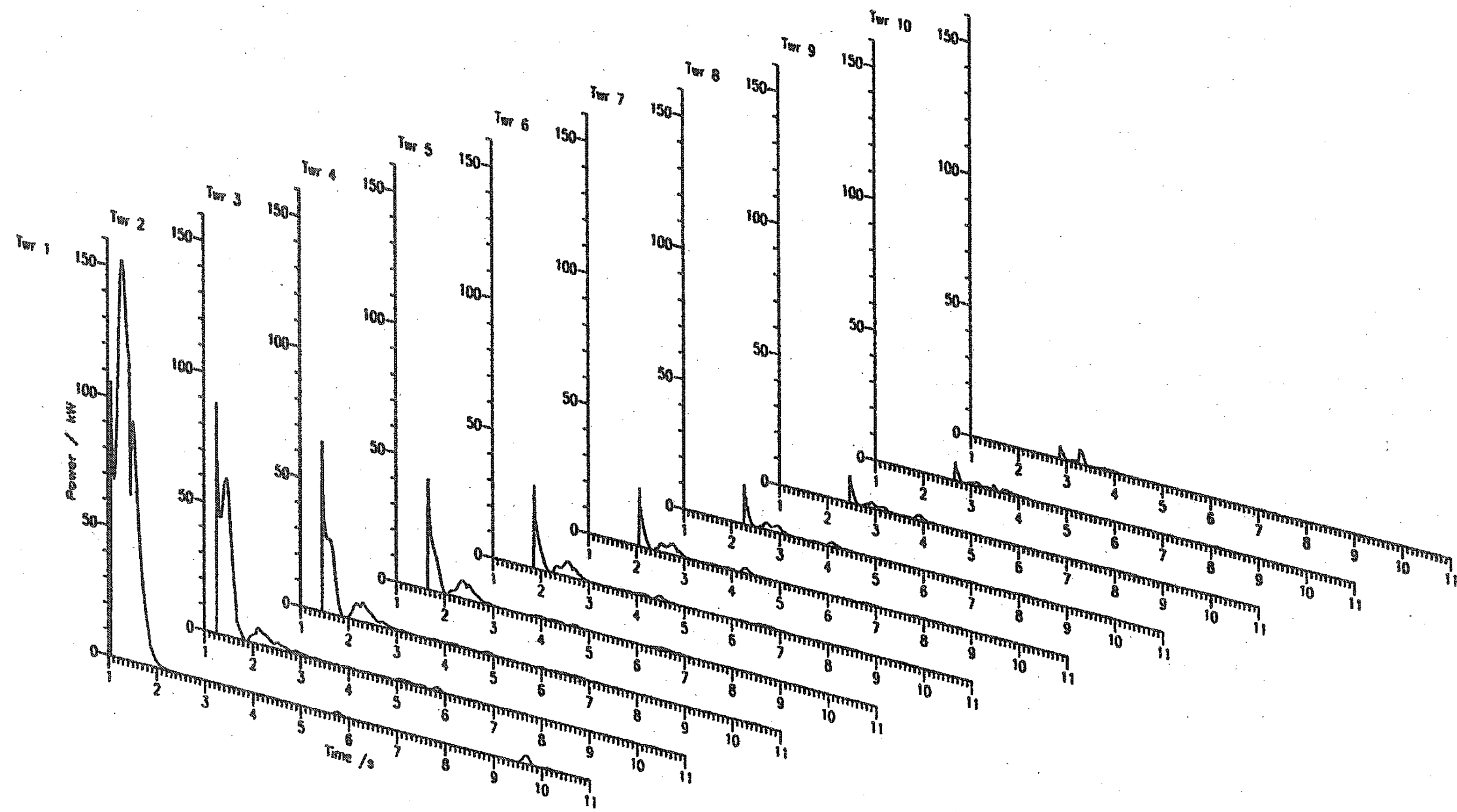

Figure 5-18 Power Dissipated by Dampers –Iced Conductor Post Spring-Damper

Table 5-1 Total Energy Dissipated (J)

Structure	Bare Shield Wire	Iced Shield Wire	Bare Conductor	Iced Conductor
Twr 1	4,260	14,150	10,490	67,670
Twr 2	1,530	5,520	3,960	23,180
Twr 3	750	2,970	2,670	13,680
Twr 4	400	1,760	2,100	8,970
Twr 5	220	1,100	1,750	6,240
Twr 6	120	730	1,570	4,480
Twr 7	70	510	1,480	3,210
Twr 8	40	380	1,240	2,300
Twr 9	20	290	880	1,760
Twr 10	20	230	470	1,200
Total Energy Dissipated	7,430	27,640	26,610	132,690
Total Energy Released	8,100	34,200	38,100	159,500

Table 5-2 Percentage of Total Energy Released Dissipated by Dampers

Structure	Bare Shield Wire	Iced Shield Wire	Bare Conductor	Iced Conductor
Twr 1	53	41	28	42
Twr 2	19	16	10	15
Twr 3	9	9	7	9
Twr 4	5	5	6	6
Twr 5	3	3	5	4
Twr 6	1	2	4	3
Twr 7	1	1	4	2
Twr 8	0	1	3	1
Twr 9	0	1	2	1
Twr10	0	1	1	1
Total Energy Dissipated	92	81	70	83

Table 5-3
Ground Clearance Comparison

Description	Radial Ice mm	Wire Attach Elev m	Intact Sag m	Intact Grnd Clr m	Resid-ual Static Grnd Clr m	Min Dynamic Ground Clr Un-damped m	Min Dynamic Ground Clr Damped m
Shield Wire	-	28.0	4.84	23.16	22.08	21.28	20.98
Shield Wire	45	28.0	16.68	11.32	10.01	8.68	8.57
Conductor	-	23.0	10.50	12.50	8.7	6.06	5.83
Conductor	45	23.0	16.90	6.08	2.57	contact	contact

Table 5-4
Post Spring-Damper
Bare Shield Wire Post Rotations (deg)

Twr	Free		Damped		Residual Static Position
	Min	Max	Min	Max	
1	78.4	95.9	84.5	86.2	85.8
2	10.6	72.1	32.1	43.4	38.9
3	-3.5	52.4	16.3	28.0	23.3
4	-12.6	48.0	8.5	19.0	14.6
5	-18.4	44.4	4.3	13.2	9.4
6	-23.3	41.4	1.9	9.2	6.0
7	-29.8	38.8	0.6	6.5	3.8
8	-31.9	36.6	0.1	4.7	2.4
9	-42.8	34.6	-0.1	3.3	1.4
10	-29.3	32.8	-0.2	2.2	0.6

Table 5-5
Post Spring-Damper
Iced Shield Wire Post Rotations (deg)

Twr	Free		Damped		Residual Static Position
	Min	Max	Min	Max	
1	67.0	89.1	75.4	78.8	78.1
2	-11.0	47.4	1.4	33.7	10.5
3	-22.2	38.1	-3.9	19.3	1.8
4	-21.6	32.3	-5.5	12.3	0.4
5	-17.9	28.1	-5.9	8.1	0.1
6	-16.3	24.7	-5.0	5.5	0.0
7	-15.3	21.8	-4.0	3.8	0.0
8	-14.9	19.4	-3.3	2.6	0.0
9	-29.2	17.7	-2.8	1.9	0.0
10	-27.7	17.5	-2.6	2.5	0.0

Table 5-6
Post Spring-Damper
Bare Conductor Post Rotations (deg)

Twr	Free		Damped		Residual Static Position
	Min	Max	Min	Max	
1	70.8	85.7	75.1	82.2	79.6
2	11.3	42.5	21.0	38.0	29.8
3	-3.8	32.7	6.9	26.6	16.3
4	-10.5	26.8	1.1	19.9	9.5
5	-13.2	22.5	-1.0	15.4	5.7
6	-13.4	19.2	-3.1	12.2	3.5
7	-12.1	16.5	-4.3	9.9	2.1
8	-12.1	14.3	-4.5	8.1	1.3
9	-10.7	12.5	-3.7	6.8	0.7
10	-6.1	9.8	-2.1	4.9	0.0

Table 5-7
Post Spring-Damper
Iced Conductor Post Rotations (deg)

Twr	Free		Damped		Residual Static Position
	Min	Max	Min	Max	
1	65.3	83.1	73.2	77.4	75.9
2	8.0	39.9	10.6	30.3	19.0
3	-4.1	29.4	-1.1	18.2	6.9
4	-10.6	23.8	-3.9	12.2	2.6
5	-14.4	20.0	-4.5	8.4	1.0
6	-14.0	17.1	-4.3	6.0	0.4
7	-13.9	15.7	-3.9	4.4	0.1
8	-14.2	16.8	-3.4	3.3	0.1
9	-18.6	17.4	-3.9	2.6	0.0
10	-20.9	11.9	-2.4	2.0	0.0

5.2 Discussion of the Post Spring-Damper Results

The post spring-dampers are very effective in reducing the peak dynamic loads on the towers. Without damaging the tower, the absolute minimum to which the peak load on the tower next to a broken wire can be reduced is the residual static load at that tower. One measure of the effectiveness of the post spring-damper is to compare the amount the peak load is reduced with this maximum possible reduction. Table 5-8 shows that the post spring-damper achieves 50 to 80% of this maximum possible reduction. It is more effective for the shield wire than for the conductor. The shield wire uses a 0.5 m post vs. the 2.0 m post of the conductor. The conductor is also heavier than the shield wire. From Table 5-1, 4.7 times the energy is released by a broken conductor than is released by a broken shield wire. The longer post means that substantially more gravitational potential energy is lost. Table 5-3 shows that the change from intact to residual static ground clearances for the conductor is much higher than for the shield wire (for the iced condition, 3.5 m for the conductor and 1.3 m for the shield wire).

Table 5-3 also shows that the minimum dynamic ground clearance is, in these cases, more for the freely swinging post than for the damped post. In both cases, the iced conductor passed through the theoretical ground plane (by 0.4 m undamped and 0.7 m damped) indicating that the conductor would touch the ground momentarily. In future research, a contact plane at the ground surface should be included to model this effect.

The comparison of the angles of swing of the posts in Tables 5-4 to 5-7 shows that the addition of dampers substantially reduces the range of angles through which the posts swing (note that the minimum angles listed are those experienced after the first positive peak angle has been reached). The much smaller variations in the swing angles around the residual static position for the damped posts compared with the undamped posts shows the effectiveness of the dampers in reducing the kinetic energy in the system.

Table 5-8
Percentage of Maximum Possible Force Reduction Obtained

Cable	Radial Ice mm	Peak Tower Elastic Force Undamped kN	Residual Static Horizontal Tension kN	Maximum Potential Reduction In Peak Force kN	Minimum Peak Tower Elastic Force Damped kN	Actual Reduction In Peak Force kN	Reduction Obtained % of Maximum Potential
7/16 EHS	-	37.9	14.4	23.5	18.6	19.3	82
7/16 EHS	45	112.1	64.7	47.4	75.2	36.9	79
Cardinal	-	53.2	18.0	35.2	36.0	17.2	49
Cardinal	45	156.3	81.5	74.8	105.4	50.9	68

In Figures 5-5 to 5-14, the tower elastic force is typically greater than the filtered wire support tension, particularly when there is no additional damping (Figures 5-6, 5-9, 5-11 and 5-13). This effect is most pronounced with the deadended shield wire in Figures 5-5 and 5-8. The wire break results in a step change in the longitudinal force on the tower. In the classic case, with a constant force after the step and no damping, the deflection and tower elastic force would be twice the static values (Chopra 1995, p 124). In this case, while the change in longitudinal force is not a perfectly constant step, and the tower has some damping, the step response is clearly evident. In the case of the conductor with a long post, the conductor support tension acts as a series of impulse loads on the tower. As can be seen in Figures 5-11b and c, the response of the tower to the impulse spans a shorter period of time with a higher peak force. Both the peak wire support tension and the peak tension in a suspension insulator may underestimate the static load for which a tower should be designed to resist the dynamic loads.

Figures 5-7 and 5-10 show that the post spring-damper for the shield wire is more effective in reducing the tower elastic load than using full deadends at every tower.

The dampers are very effective at dissipating the energy released by a broken wire, Table 5-2 shows that 70 to 90% of the energy released is dissipated by the dampers. In all cases, as anticipated, the damper at the tower next to the break dissipates the most energy. Figures 5-15 to 5-18 also show the highest rate of energy dissipation at the first tower. The conductor dampers dissipate energy both from an incident wave that propagates through the line section (seen in the delay from tower to tower) and from a reflected wave. Figures 5-15 and 5-16 show that the shield wire energy is practically all dissipated without any reflection.

In Figures 5-7, 5-9 and 5-10, saw tooth patterns were noted. In order to attempt to explain these phenomena, a Fourier analysis of the time history in Figure 5-7a was performed. Figure 5-19 shows this Fourier transform of the unfiltered wire tension for the damped bare shield wire. There are distinct peaks at frequencies of approximately 0.3 Hz and 6.9 Hz. The peak at 0.3 Hz appears to correspond to the first symmetric vibration mode of the span. The other higher frequency peaks, which can be clearly seen in Figure 5-19, are harmonics of 6.9 Hz. The longitudinal wave velocity in the shield wire from Equation 4-12 is 4809 m/s. The time for a longitudinal wave to travel from the insulator at Tower 1 to the insulator at Tower 2 and back, a distance of approximately 700 m, is 0.1456 s, and to travel from the left side to the end of the span and back to the right side (2.5 m less) is 0.1451 s. Since the saw tooth patterns are spaced at about 0.145 s they appear to be caused by longitudinal stress release waves and their reflections.

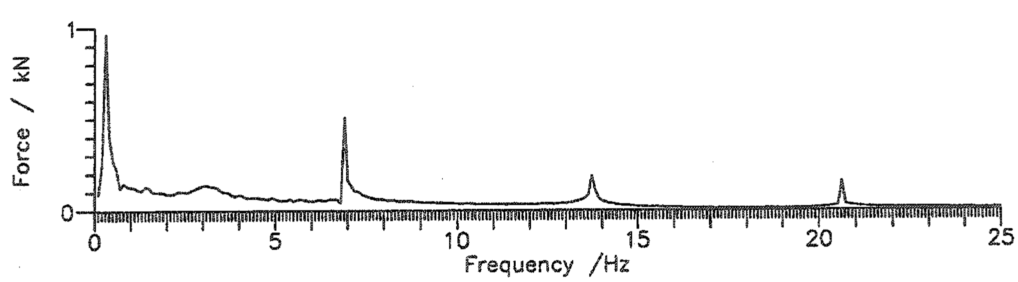

Figure 5-19
Fourier Transform of Damped Bare Shield Wire
Time History

5.3 Rotating Crossarm Spring-Damper Results

The peak tower elastic force for the rotating crossarm spring-dampers are summarized in Figures 5-20 and 5-21. For bare conductor, the minimum peak tower elastic load was found with a spring constant of 40 kN m/rad and a damping constant of 8 kN m s/rad. For the iced conductor a spring constant of 180 kN m/rad and a damping constant of 32 kN m s/rad gave the minimum peak tower elastic load.

The time histories for a rotating crossarm with bare conductor are shown in Figures 5-22 to 5-24. Figures 5-22 and 5-23 are for rotating crossarms with inclined and vertical axes, respectively, without any spring-damper. The time histories in Figure 5-24 include both a spring and a damper with optimal properties. Figures 5-25 to 5-27 are the comparable time histories for an iced conductor. The power dissipated by the dampers is shown in Figures 5-28 and 5-29 for bare and iced conductor, respectively.

Table 5-9 shows the energy dissipated by the dampers at each tower, the total energy dissipated and the percentage of the total energy dissipated. For comparison, the total energy released when rotating crossarms do not have a spring-damper is also shown. Results for rotating crossarms with both vertical axis and inclined axis are included.

Tables 5-10 and 5-11 show the range of motion of the crossarms and their residual static position (RSL) for bare and iced conditions, respectively. The minimum ground clearances recorded in the 10 s time histories are shown in Table 5-12. Table 5-13 shows the residual static ground clearances at the center point of each span.

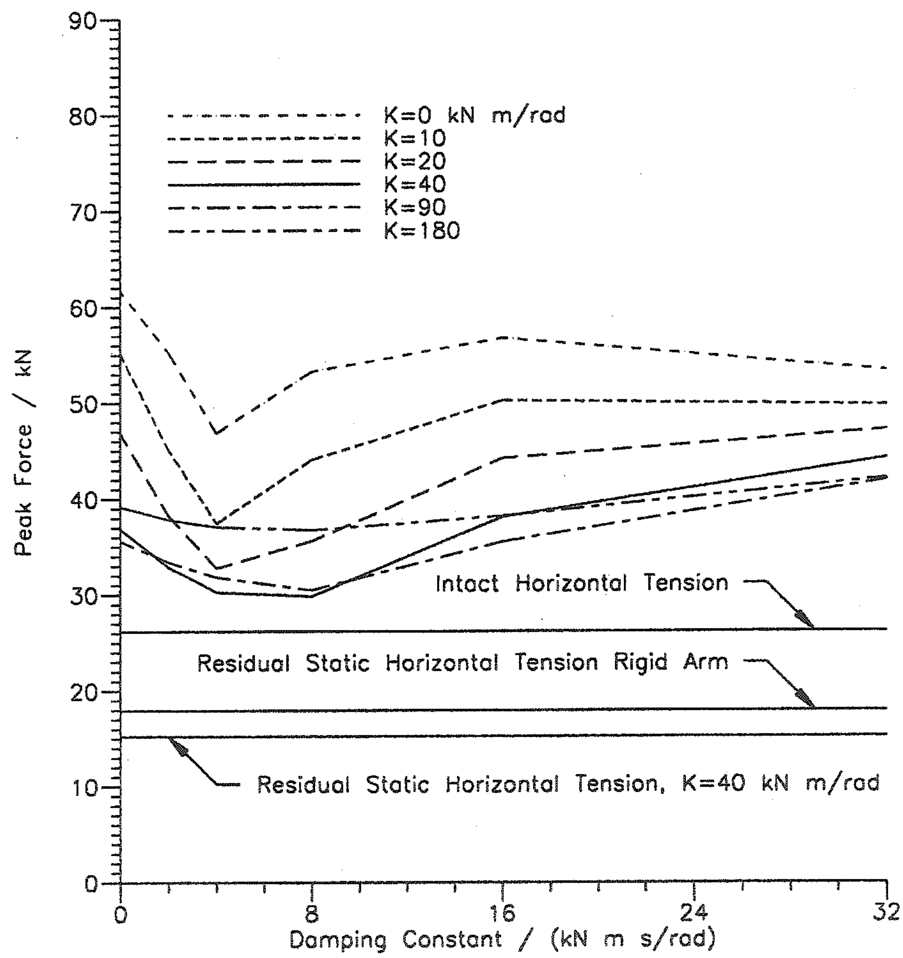

Figure 5-20
Rotating Crossarm Spring-Damper
Tower Elastic Forces for Bare Conductor

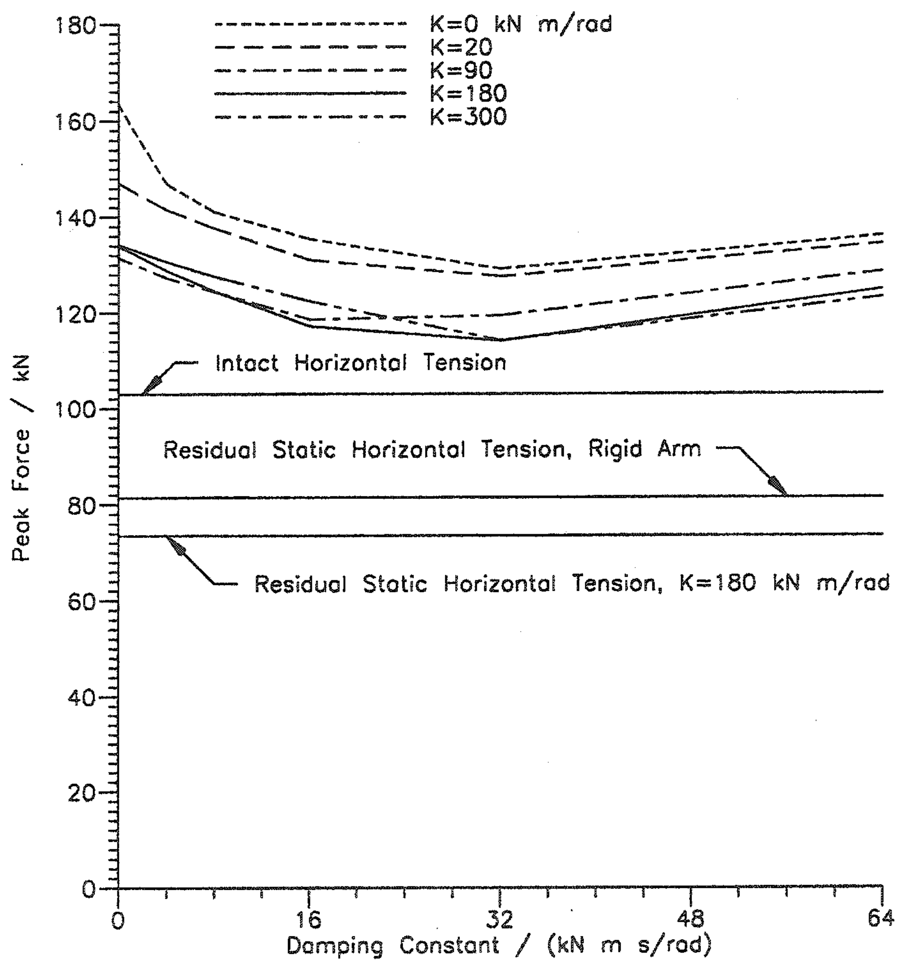

Figure 5-21
Rotating Crossarm Spring-Damper
Tower Elastic Forces for Iced Conductor

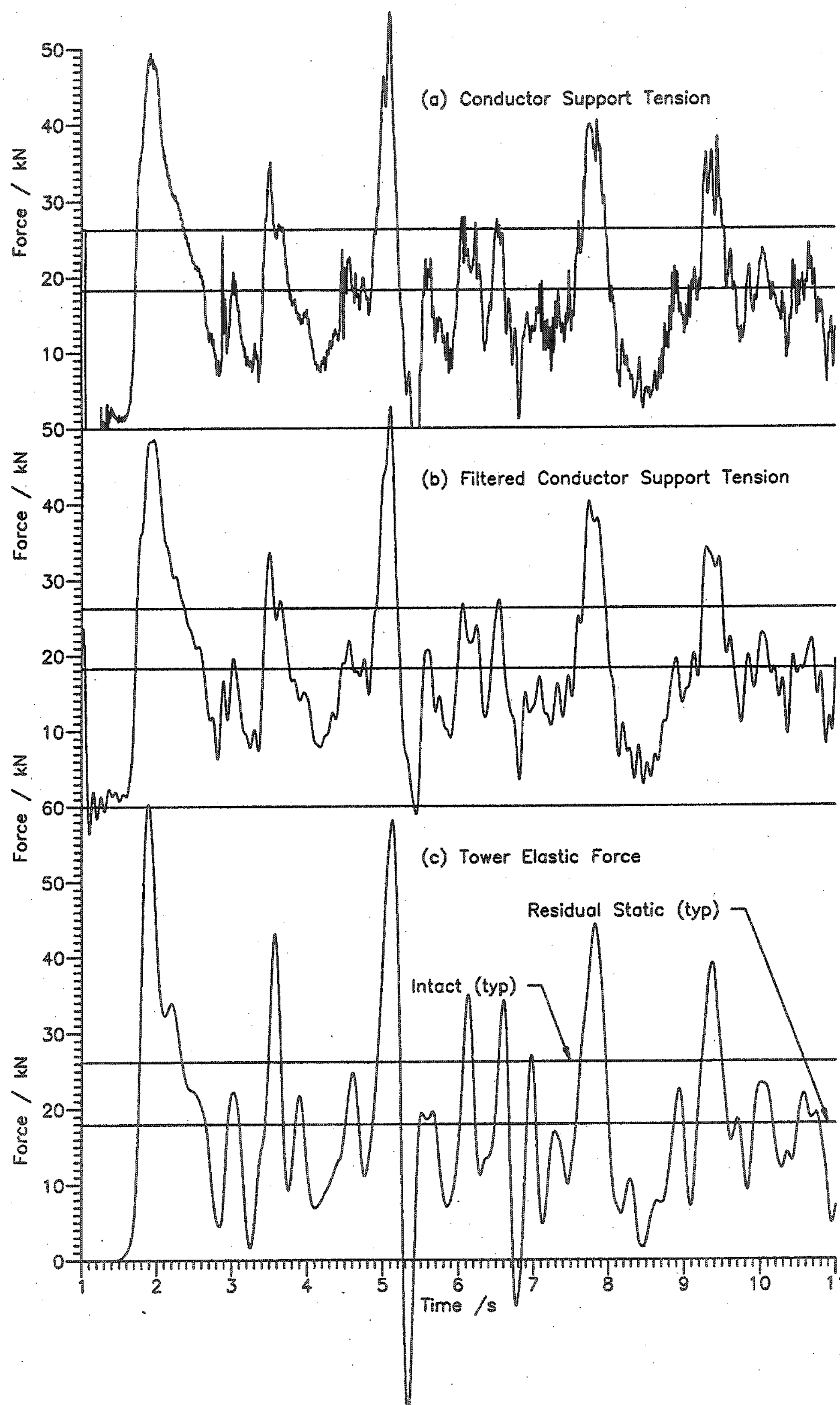

Figure 5-22 Rotating Crossarm with Inclined Axis Time Histories Bare Conductor, No Spring Damper

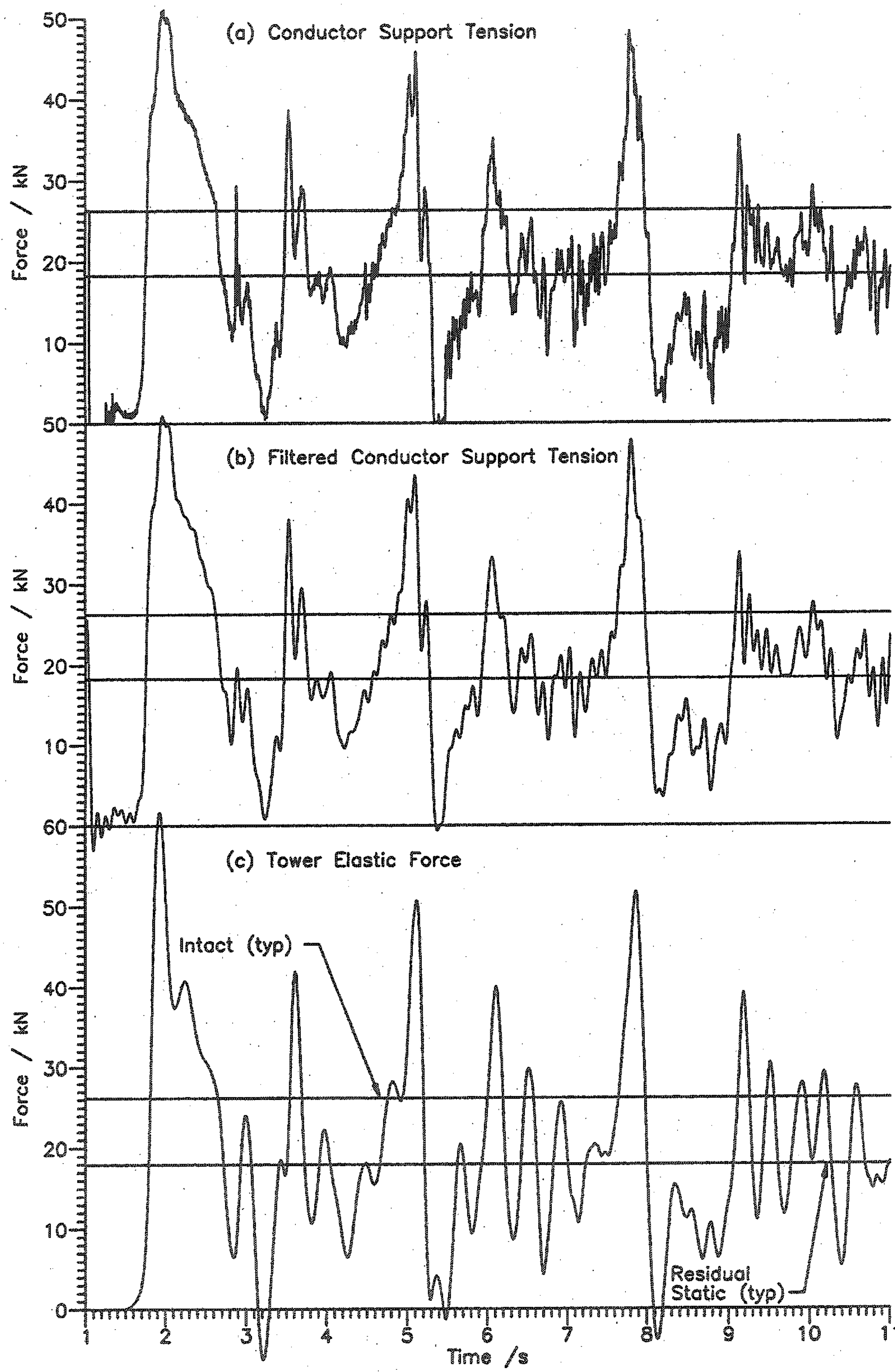

Figure 5-23
Rotating Crossarm with Vertical Axis, Time Histories Bare Conductor No Spring Damper

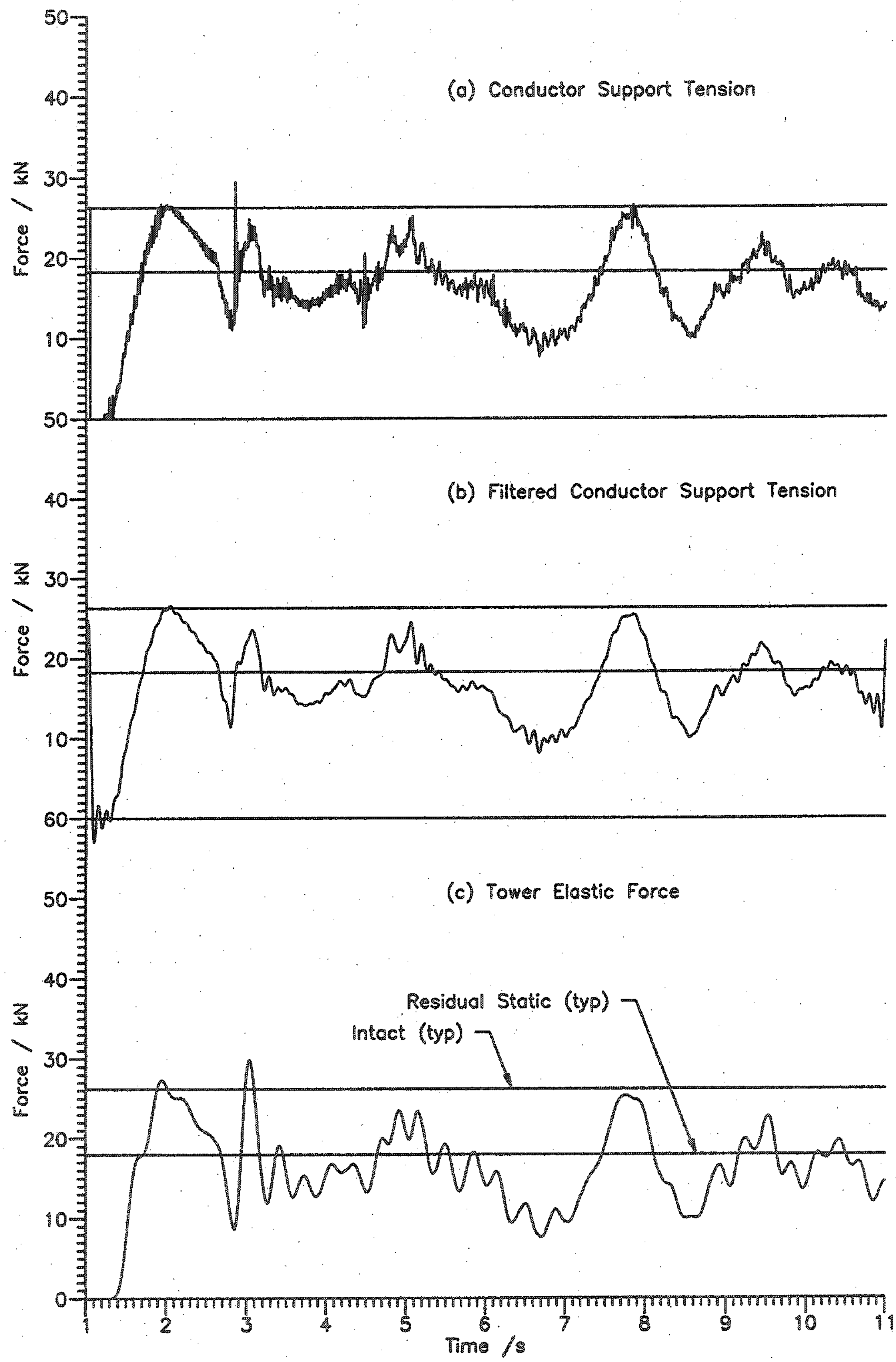

Figure 5-24
Rotating Crossarm with Spring-Damper, K = 40, C = 8
Time Histories Bare Conductor

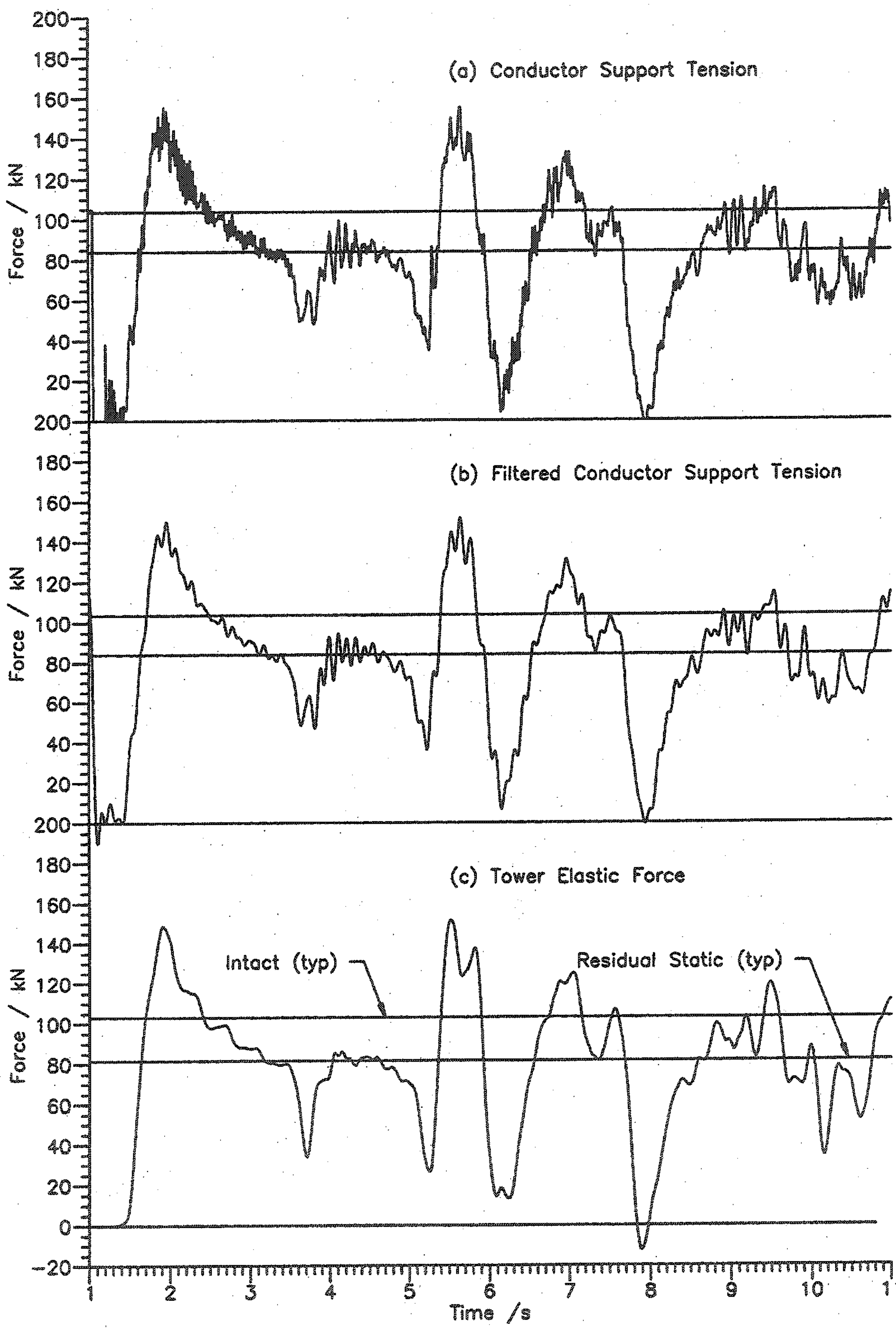

Figure 5-25
Rotating Crossarm with Inclined Axis, Time Histories
Bare Conductor, No Spring-Damper

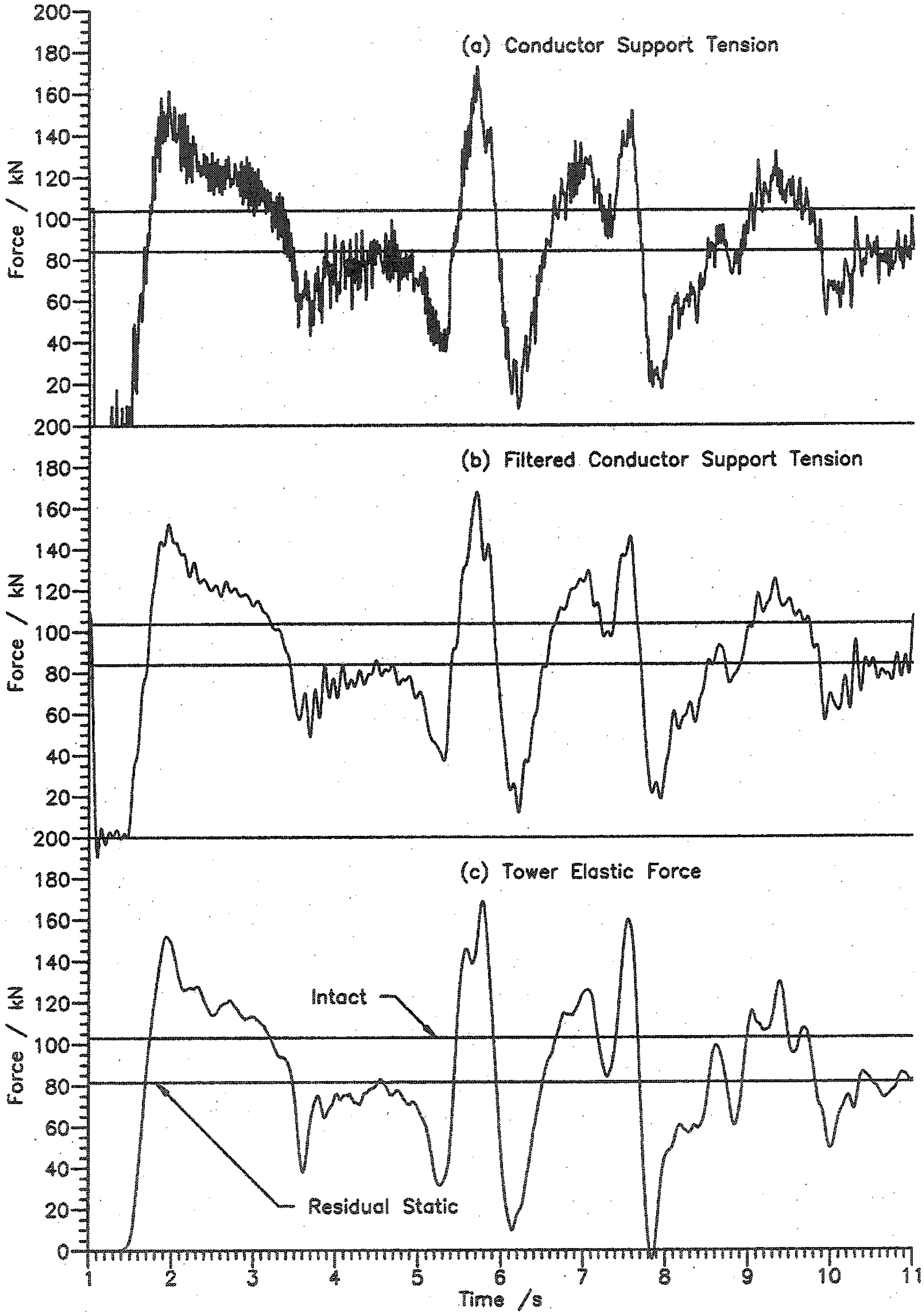

Figure 5-26
Rotating Crossarm with Vertical Axis
Time Histories Bare Conductor, No Spring-Damper

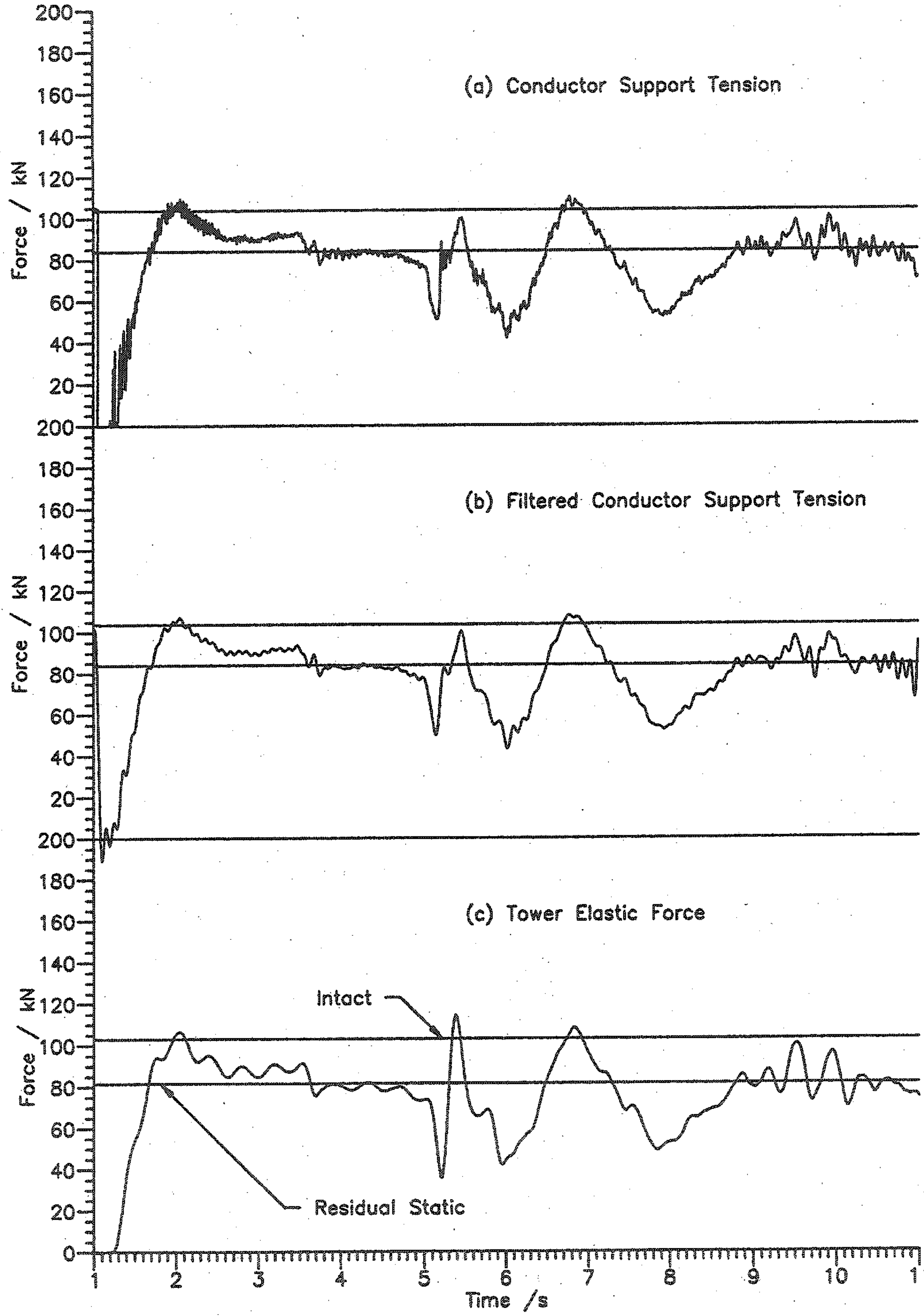

Figure 5-27
Rotating Crossarm with Spring-Damper
Time Histories Iced Conductor, K = 180, C = 32

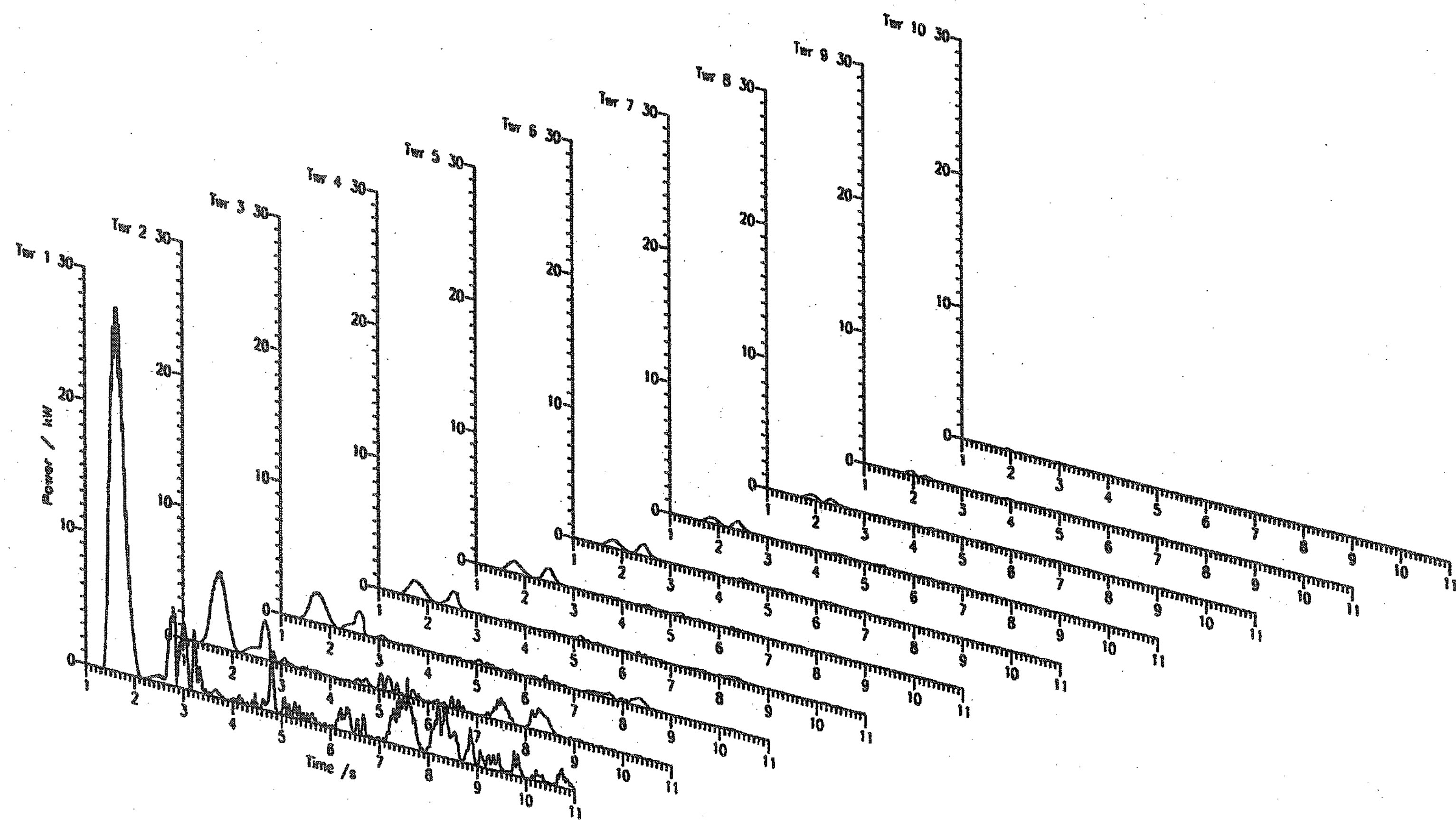

Figure 5-28 Power Dissipated by Dampers – Bare Conductor Rotating Crossarm Spring-Damper

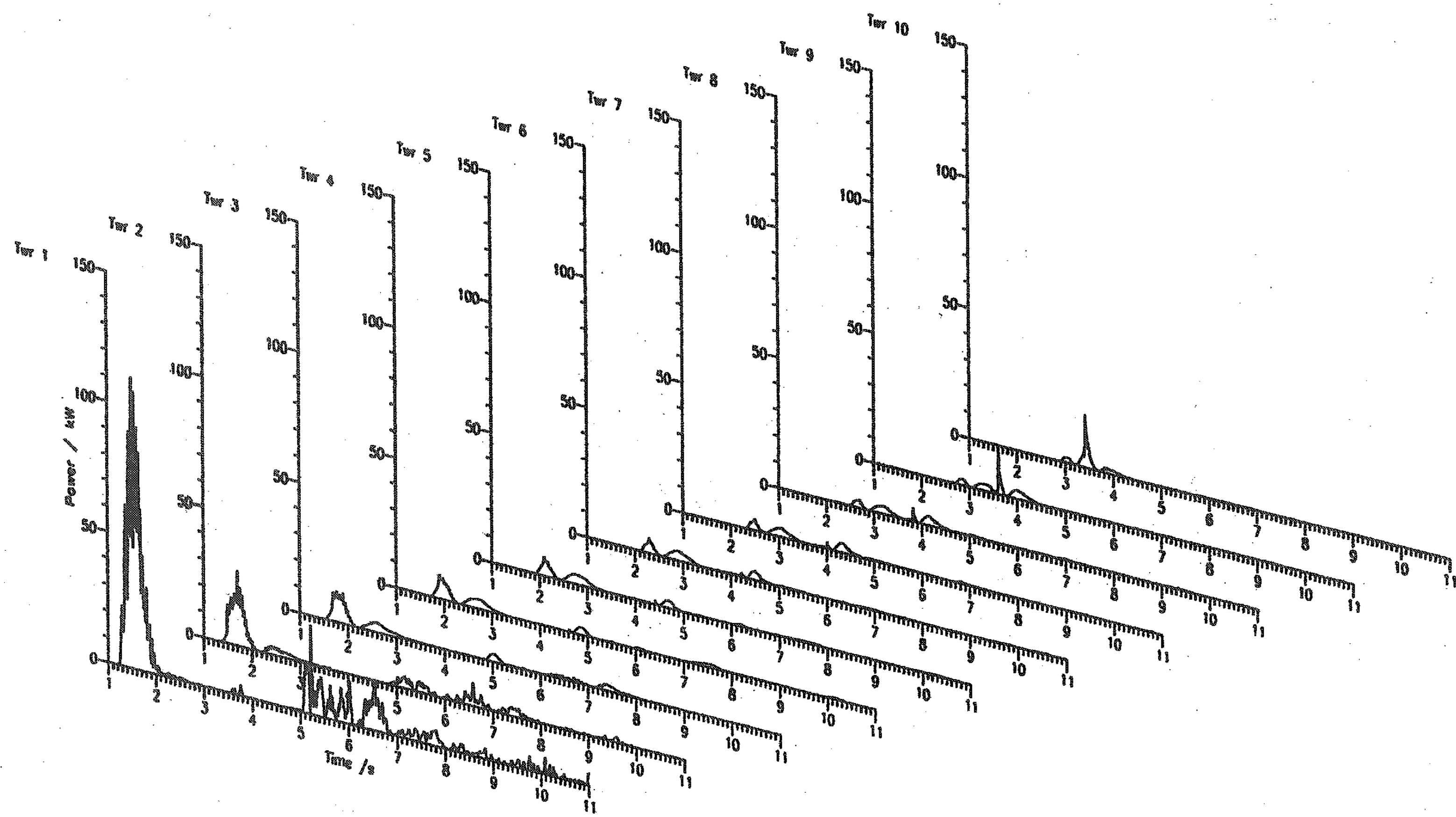

Figure 5-29 Power Dissipated by Dampers – Iced Conductor with Rotating Crossarm Spring-Damper

Table 5-9
Rotating Crossarm Spring-Dampers
Energy and Fraction of Total Energy Dissipated

Structure	Bare Conductor		Iced Conductor	
	Energy J	%Total Energy	Energy J	%Total Energy
Twr 1	17,179	33.6	48,083	22.1
Twr 2	4,580	8.9	14,335	6.6
Twr 3	1,993	3.9	7,704	3.5
Twr 4	1,191	2.3	5,684	2.6
Twr 5	832	1.6	4,488	2.1
Twr 6	620	1.2	3,845	1.8
Twr 7	460	0.9	3,618	1.7
Twr 8	314	0.6	3,445	1.6
Twr 9	174	0.3	3,527	1.6
Twr 10	46	0.1	2,936	1.3
Total Energy Dissipated Spring-Damper	27,389	53.5	97,665	44.9
Total Energy Released Spring-Damper	51,187	100.0	217,653	100.0
Total Energy Released Inclined Axis	73,565	-	307,803	-
Total Energy Released Vertical Axis	86,500	-	358,500	-

Table 5-10
Crossarm Rotations (deg) for Bare Conductor

Twr	Vertical Axis Freely Rotating			Inclined Axis Freely Rotating			Spring-Damper		
	Min	Max	RSL	Min	Max	RSL	Min	Max	RSL
1	79.8	100.7	90.0	71.1	88.2	80.3	24.8	48.1	36.1
2	59.5	136.6	90.0	33.1	88.7	51.5	6.7	23.1	12.2
3	45.5	138.2	89.6	8.5	57.7	36.0	1.1	15.2	6.6
4	49.8	132.8	85.0	3.4	41.4	25.9	-1.2	10.8	4.0
5	30.9	138.5	65.3	-0.9	36.0	18.9	-2.0	8.1	2.5
6	15.9	163.7	49.2	-4.8	30.5	13.8	-2.2	6.3	1.6
7	3.7	162.1	37.2	-10.1	26.6	9.9	-2.3	5.0	1.0
8	-3.5	68.9	26.8	-11.0	25.3	6.8	-2.0	3.9	0.6
9	-5.5	44.8	17.6	-12.1	22.3	4.3	-1.6	2.6	0.4
10	-7.7	32.3	8.7	-12.7	17.7	2.1	-.09	1.1	0.2

Table 5-11
Crossarm Rotations (deg) for Iced Conductor

Twr	Vertical Axis Freely Rotating			Inclined Axis Freely Rotating			Spring-Damper		
	Min	Max	RSL	Min	Max	RSL	Min	Max	RSL
1	84.6	95.3	90.0	70.7	83.6	79.4	28.5	45.3	37.5
2	63.1	122.3	89.9	24.3	75.7	41.2	5.3	21.0	10.4
3	56.0	133.5	88.1	1.7	44.0	22.6	-1.0	13.6	4.2
4	35.6	145.6	73.3	-5.0	37.1	12.9	-3.1	9.8	1.8
5	23.4	143.2	55.8	-13.1	31.7	7.6	-3.9	7.5	0.8
6	14.1	85.4	43.6	-11.1	27.2	4.4	-4.2	6.0	0.4
7	-1.6	64.9	33.5	-19.0	23.4	2.6	-4.3	4.9	0.2
8	-13.9	51.4	24.4	-20.2	21.2	1.5	-4.8	4.1	0.1
9	-21.1	32.2	16.0	-27.2	19.5	0.8	-6.2	3.5	0.0
10	-20.5	29.8	7.9	-19.5	18.0	0.4	-4.9	3.0	0.0

Table 5-12
Rotating Crossarm
Ground Clearance Comparison

	Vertical Axis, Freely Rotating	Inclined Axis, Freely Rotating	With Spring-Damper	Vertical Axis, Freely Rotating	Inclined Axis, Freely Rotating	With Spring-Damper
Radial Ice (mm)	-	-	-	45.0	45.0	45.0
Wire Attachment Elevation (m)	23.0	23.0	23.0	23.0	23.0	23.0
Intact Sag (m)	10.5	10.5	10.5	16.9	16.9	16.9
Intact Clearance (m)	12.5	12.5	12.5	6.1	6.1	6.1
Dynamic Clearance 1st Span (m)	6.2	4.9	3.1	contact	contact	contact
Residual Static Clearance (m)	8.5	7.5	6.5	2.5	1.3	contact

Table 5-13
Rotating Crossarm
Residual Static Ground Clearance (m)

		Bare Conductor			Iced Conductor		
Span	Node	Vertical Axis, Freely Rotating	Inclined Axis, Freely Rotating	With Spring-Damper	Vertical Axis, Freely Rotating	Inclined Axis, Freely Rotating	With Spring-Damper
1	171	8.47	7.52	6.47	2.47	1.35	contact
2	311	10.09	9.27	9.51	4.64	3.60	4.08
3	451	10.79	10.26	10.76	5.24	4.71	5.23
4	591	10.96	10.86	11.43	5.25	5.29	5.71
5	731	10.94	11.26	11.81	5.23	5.61	5.91
6	871	10.94	11.53	12.05	5.22	5.80	6.00
7	1011	10.93	11.72	12.20	5.22	5.91	6.04
8	1151	10.93	11.84	12.29	5.22	5.97	6.06
9	1291	10.93	11.92	12.34	5.22	6.01	6.07
10	1431	10.93	11.96	12.36	5.23	6.02	6.08

5.4 Discussion of Rotating Crossarm Spring-Damper Results

Adding a spring and a damper to the rotating crossarm is very effective in reducing the peak dynamic loads. As can be seen in Table 5-9, the dampers dissipate approximately one-half the energy released by a broken wire.

Using a freely rotating crossarm does not reduce the peak longitudinal dynamic load on the tower. This is true whether the axis of rotation is vertical or inclined. This conclusion can clearly be seen by comparing Figures 5-11, 5-22 and 5-23 for bare conductor and 5-13, 5-25 and 5-26 for iced conductor. If anything, the peak impact loads are actually higher for the freely swinging rotating crossarms than they are for a suspension insulator on a rigid crossarm. One advantage that the rotating crossarms do have, however, is that when used for double circuit towers and the outside phases of single circuit towers, they move the load closer to the tower body. This reduces the torsional moment on the tower leading to reduction in the forces in the X-bracing.

If a freely swinging crossarm is used, the axis should be inclined. Tables 5-10 and 5-11 show that with a vertical axis, the crossarm will rotate as much as 160 degrees. This would require bump stops to be built into the towers to avoid damage to the tower and crossarm. With the axis inclined 20° from vertical, the maximum rotation is always less than 90° requiring no bump stops.

Table 5-12 shows that, during a broken wire event, the iced conductor would hit the ground for all three types of rotating crossarm. Paradoxically, when the spring-damper is used on the rotating crossarm, the first span of wire falls farther below the theoretical ground level than when either of the freely swinging crossarms is used, 3.4 m vs. 0.8 m for a freely swinging vertical axis and 1.9 m for an inclined axis. This can be explained by looking at the residual static ground clearances in Table 5-12. With a freely swinging vertical axis, the movement of the crossarm tends to equalize the sags and ground clearances over the whole line section. When the axis is inclined, the conductor attachment point rises as the crossarm rotates providing some rotational stiffness. As a result, the tensions and sags are less well distributed among the successive spans. This reduces the ground clearance in the first span and increases it in the later spans. This effect is even more pronounced when the spring-damper is used. Under residual static conditions, the iced conductor's position is 0.7 m below the theoretical ground surface.

In future work, a contact plane at the ground surface should be used to model the effect of the conductor hitting the ground. This is expected to reduce the load slightly on the first tower and increase the load on the second tower.

The lack of reduction in the peak dynamic loads with freely rotating crossarms implies that fuses incorporating tethers to the tower will also not reduce the peak dynamic loads unless the tether includes an energy absorbing mechanism.

In Figures 3-15 and 3-16, the residual static force is minimized when the spring stiffness for bare conductor is 20 kN m/rad and for iced conductor 90 kN m/rad. The residual static swing angles are both between 50 and 55°. The dynamic force is minimized, however, when the spring stiffnesses are 40 and 180 kN m/rad for bare and iced conductor respectively (see Figures 5-20 and 5-21). The residual static swing angles from Figures 3-15 and 3-16 are both between 35 and 40°. A higher spring stiffness is needed to minimize the peak dynamic load (Figures 5-20 and 5-21) than is needed to minimize the residual static load (Figures 3-15 and 3-16).

5.5 Comparison of Methods

Comparing figures 5-12 and 5-24 for bare conductor and 5-14 and 5-27 for iced conductor, the rotating crossarm spring-damper is slightly more effective than the post spring-damper for the bare conductor and slightly less effective for iced conductor. For the parameters used in this study, they are considered equally effective.

Both the post spring-damper and the rotating crossarm spring-damper are new methods for reducing the peak impact loads on towers and thus the potential of lines to cascade. Methods that have been shown to be effective by full scale tests include deformable crossarms (Chappée and Mauzin 1948; Cook 1959), sliding clamps (Healy and Wright 1926; Moreau et al. 1978) and energy absorbing extension devices (ANCO 1989; Ibanez and Merz 1988). Ostendorp (1999) also invented an extension device; however, test reports are not available in the open literature.

The consistency of operation of deformable crossarms is dependent on the consistency of the properties of the structural steel used in their construction. To the author's knowledge, none of the common structural steels have properties that are controlled closely enough to assure reliable operation. The recent introduction of ASTM A921, which has an upper bound on yield strength, is, however, a step in the right direction. Use of a spring-damper to control a rotating crossarm allows manufacture of a consistent product that will have consistent results. This also applies to the post spring-damper system.

Sliding clamps have been used at different times since as early as 1926; however, they are in common use mainly in France. They have limited utility in areas with glaze ice because the ice prevents their proper operation. Calibration is also a problem because the frictional force is dependent on the aging of the components, the weight span and the preload on the clamp's keeper. The operation of both the post spring-damper and rotating crossarm spring-damper are independent of the weight span. It may be necessary in areas with glaze icing to provide shrouds to keep ice away from the rotating parts.

The tests of the ANCO device showed it could be very effective. To the author's knowledge, this device has never been installed on an operating line. The principal objection to its use is that it operates on the resultant of the vertical, transverse and longitudinal loads, whereas it is preferable to have a protective device sensitive only to the longitudinal load. It also uses structural steel plate, implying that the device must be designed not only for the intended transmission line but also for the yield strength of each plate used in production. Both the post spring-damper and the rotating crossarm spring-damper operate only under longitudinal loads, use elements commonly manufactured with consistent properties and do not need to be replaced after they operate.

Chapter 6
Conclusions

This research had two objectives:

- To determine the technical feasibility of incorporating longitudinal shock damping in high voltage transmission line towers.
- To demonstrate the application of longitudinal shock damping to a typical high voltage transmission line.

Both objectives have been met. Two new methods of incorporating dampers into electric transmission line structures were developed, the post spring-damper and the rotating crossarm spring-damper. Both methods were analyzed using the properties of a prototype 230 kV lattice tower transmission line. The analyses showed that both methods are very effective in reducing the peak dynamic loads due to broken wires.

A 69 kV line has an insulator length of 0.75 m and a 230 kV line has an insulator length of approximately 2 m. The post-spring-damper was modeled using a small diameter shield wire with a post length of 0.5 m and a mid range conductor with a post length of 2 m. Both bare wires and wires with 45 mm of radial ice were modeled. It appears that the good results, a reduction in peak load of 50 to 80% of the possible reduction, can be expected to apply over a broad range of voltages and wire sizes.

When rotating crossarms are used, if no spring is included, an inclined axis should be used to prevent excessive rotation of the arms.

6.1 Research Limitations

This research used a case study to test the feasibility of adding dampers to the structure-insulator system that supports the wires. Only one line section consisting of ten 350 m spans was used. Based on the patterns of power expended in the dampers and total energy dissipated in the dampers, it appears that the results apply to line sections with more spans; however, the applicability of the method to sections with one or two spans to the dead-end has not been demonstrated. For the post spring-damper, it is possible that a spring would be needed in these cases.

While ruling spans of 350 m spans are very common, many lines have much shorter spans and some longer spans. For spans much shorter or longer additional verification is needed.

The prototype tower is a four legged lattice steel tower. This type of tower is much stiffer than the also common planar H-frames. The increased flexibility of H-frames may require guys to stiffen them to allow the dampers to work properly.

6.2 Implications for Transmission Line Design Practice

This research has implications for design practice in two areas. First, it shows that the towers can themselves be designed in new ways that will reduce their potential for longitudinal cascades. Secondly, the analytical tools now available allow a wide range of difficult problems in transmission line dynamics to be analyzed. This must be qualified by saying that although the analytic tools are impressive, their user interface is not yet sufficiently friendly to use for everyday design. In the next five to ten years, these tools will move from being used mainly in academic research to being everyday design tools. As the tools become familiar to designers, new ways of preventing cascades will be developed and put into practice.

6.3 Recommendations for Future Research

With any new system, the best evidence that it works is experimental, with experiments performed at as close to full scale as possible. Both the post spring-damper and rotating crossarm spring-damper need to be tested to determine whether the modeling accurately represents the real world. This is also where the practical issues of ensuring operation over the full range of temperatures and icing conditions are best addressed.

Further analytic studies are needed to determine the full range of voltages practical for each system. For example, with currently available composite post insulators, the author suspects that the current practical upper limit for the post spring-damper is 345 kV. The rotating crossarm spring-damper should be usable at any voltage; however, at voltages above the prototype 230 kV, the influence of the conductor dragging on the ground will be of great importance. Modeling of the higher voltages with a ground contact surface would allow the method to be extended to the highest current North American operating voltage of 765 kV.

References

ADINA (Automatic Dynamic Incremental Nonlinear Analysis). (2001). Version 7.5. ADINA R&D, Inc., Watertown, MA.

ADINA (Automatic Dynamic Incremental Nonlinear Analysis). (2003). Version 8.0. ADINA R&D, Inc., Watertown, MA.

ADINA: A Finite Element Program for Automatic Dynamic Incremental Non Linear Analysis, Report No. AE-84-1, (1984). ADINA Engineering, Watertown, MA.

Alcoa. (1974). *Product Data; Aluminum Electrical Conductors: Stranded-Bare, Covered Line Wire and Multiplex Cables; General Index*, Alcoa Conductor Products Company, Pittsburgh, PA.

Alt, K., Bauer, K. H., Boos, K. V., Jurdens, C., and Paschen, R. (1984) "Dynamic Effects on Transmission Lines." *International Conference on Large High Voltage Electric Systems (CIGRE)*, Paris, Paper 22-08.

ANCO. (1984). *Conceptual Design of an Electric Power Transmission Line Conductor Break Load-Limiting Element*. Report No. 1354.7, ANCO Engineers, Inc., Culver City, CA.

ANCO. (1989). *Test Verification of a Device for Reduction of Severe Dynamic Loads in Electric Transmission Towers*. Report No. 1354.14, ANCO Engineers, Inc., Culver City, CA.

Anjam, R. (1991). *Galloping and Broken Conductor Analysis of Transmission Lines*, M.S. Thesis, Civil and Construction Engineering, Iowa State University, Ames, Iowa.

ASCE. (1991). *Guidelines for Electrical Transmission Line Structural Loading, ASCE 74*, ASCE Manuals and Reports on Engineering Practice, American Society of Civil Engineers, New York.

ASCE. (2001). *Guidelines for Electrical Transmission Line Structural Loading, ASCE 74, June 2001 Draft Revision*, ASCE Manuals and Reports on Engineering Practice, American Society of Civil Engineers, Reston, VA.

ASCE. (2002). *Minimum Design Loads for Buildings and Other Structures, ASCE 7-02*, American Society of Civil Engineers, Reston, VA.

Bachmann, H., Amman, W. J., Deischl, F., Eisenmann, J., Floegl, I., HIrsch, G. H., Klein, G. K., Lande, G. J., Mahrenholtz, O., Natke, H. G., Nussbaumer, H., Pretlove, A. J., Rainer, J. H., Saemann, E. U., and Steinbeisser, L. (1995). *Vibration Problems in Structures: Practical Guidelines*, Birkhauser Verlag, Basel and Boston.

Bastow, D., and Howard, G. (1993). *Car Suspension and Handling*, Society of Automotive Engineers, Warrendale, PA.

Bazant, Z. P. (1978). "Spurious Reflection of Elastic Waves in Nonuniform Element Grids." *Computer Methods in Applied Mechanics and Engineering*, 16(1), 91-100.

Binder, R. C. (1973). *Fluid Mechanics, Fifth Edition*, Prentice-Hall, Inc., Englwood Cliffs, NJ.

Bissiri, A., and Landau, M. (1947). "Broken Conductor Effect on Sags in Suspension Spans." *AIEE Transactions*, 66, 1181-1188.

Blevins, R. D. (1979). *Formulas for Natural Frequency and Mode Shape*, Van Nostrand Reinhold Co., New York.

Bonar, P. P. (1968) "Dynamic Testing of Lattice Steel Masts." *International Conference on Large High Tension Electric Systems (CIGRE)*, Paris, Paper 22-04.

Borges, J. F., Rochas, M., and Morechos, J. (1968). *Experimental Study of the Stresses Created by the Breakage of Conductors in High Voltage Lines, File 37/1/2245.* Dept. of Public Works, National Civil Engineering Laboratory, Lisbon, Portugal.

Brown, R. S. (1913). "Stresses Produced in a Transmission Line by Breaking of a Conductor." *Electrical World*, March 29, 1913, 673-676.

Broyden, C. G. (1970). "The Convergence of a Class of Double-rank Minimization Algorithms, 1. General Considerations." *Journal of the Institute of Mathematics and Its Applications*, 6(1), 76-90.

Buchanan, W. B. (1934). "Vibration Analysis-Transmission Line Conductors." *Transactions of the AIEE*, 53, 1478-1485.

Campbell, D. B. (1970). "Unbalanced Tensions in Transmission Lines." *Journal of the Structural Division, ASCE*, 96(ST 10), 2189-2207.

Carne, T. G. (1980). *Guy Cable Design and Damping for Vertical Axis Wind Turbines.* SAND80-2669, Sandia National Laboratories, Albuquerque, NM.

Chappée, and Mauzin. (1948) "The Protection of Pylons Against Accidental Longitudinal Stresses Phenomena Arising from Conductor Breakage." *International Conference on Large Electric Systems (CIGRE)*, Paris, Paper 213.

Chopra, A. K. (1995). *Dynamics of Structures: Theory and Applications to Earthquake Engineering*, Prentice-Hall International Series in Civil Engineering and Engineering Mechanics, Prentice Hall, Upper Saddle River, NJ.

CIGRE Working Group 22.06. (2000). *Load Control Devices on Overhead Transmission Lines*. Report No. 174, International Conference on Large High Voltage Electric Systems (CIGRE), Paris.

Clarke, G. M., and Kempson, R. E. (1997). *Introduction to the Design and Analysis of Experiments*, John Wiley & Sons, Inc., New York.

Comellini, E., and Manuzio, C. (1968) "Rational Determination of Design Loadings for Overhead Line Line Towers." *International Conference on Large Electric Systems (CIGRE)*, Paris, Paper 23-08.

Commission - 1998 Ice Storm. (1999a). *Facing the Unforeseeable, Lessons from the Ice Storm of '98*, Les Publications du Québec, Québec.

Commission - 1998 Ice Storm. (1999b). *La Sécurité Civile (Public Safety): Rapport de la Commision Scientifique et Technique Chargée D'analyser les Événements Relatifs à la Tempête de Verglas Survenue du 5 au 9 Janvier 1998 (Report of the Scientific and Technical Commission Charged with Analyzing the Events Relative to the Glaze Ice Storm of January 5 to 9, 1998)*, Les Publications du Québec, Québec.

Commission - 1998 Ice Storm. (1999c). *Le Cadre Juridique de la Gestion des Sinistres au Québec (The Legal Context for Disaster Management in Quebec): Rapport de la Commision Scientifique et Technique Chargée D'analyser les Événements Relatifs à la Tempête de Verglas Survenue du 5 au 9 Janvier 1998 (Report of the Scientific and Technical Commission Charged with Analyzing the Events Relative to the Glaze Ice Storm of January 5 to 9, 1998)*, Les Publications du Québec, Québec.

Commission - 1998 Ice Storm. (1999d). *Les Conditions Climatiques et L'Approvisionnement en Énergie (The Climatic Conditions and Energy Supply): Rapport de la Commision Scientifique et Technique Chargée D'analyser les Événements Relatifs à la Tempête de Verglas Survenue du 5 au 9 Janvier 1998 (Report of the Scientific and Technical Commission Charged with Analyzing the Events Relative to the Glaze Ice Storm of January 5 to 9, 1998)*, Les Publications du Québec, Québec.

Commission - 1998 Ice Storm. (1999e). *Les Impacts Sociaux, Économiques et Environnementaux (The Social, Economic and Environmental Impacts): Rapport de la Commision Scientifique et Technique Chargée D'analyser les Événements Relatifs à la Tempête de Verglas Survenue du 5 au 9 Janvier 1998 (Report of the Scientific and Technical Commission Charged with Analyzing the Events Relative to the Glaze Ice Storm of January 5 to 9, 1998)*, Les Publications du Québec, Québec.

Cook, L. H. J. (1959). "The British Columbia Electric Company's 360-kV and 230-kV Transmission Line Designs." *Transactions of the AIEE*, 78(Aug. 1959), 537-545.

Coombs, R. D. (1916). *Pole and Tower Lines for Electric Power Transmission*, McGraw-Hill Book Company, Inc., New York.

Cross, H. (1932). "Analysis of Continuous Frames by Distributing Fixed-End Moments." *Transactions of the ASCE*, 96, 1-10.

CSA. (1997). *CAN/CSA-C22.3 No. 1 -M87 (Reaffirmed 1997), Overhead Systems, Canadian Electrical Code, Part III- Outside Wiring*, Canadian Standards Association, Rexdale, Ontario.

Den Hartog, J. P. (1928). "Calculation of Sags in a Transmission Line with a Broken Conductor." *The Electric Journal*, XXV(1), 24-26.

Diana, G., Falco, M., Cigada, A., and Manenti, A. (2000). "On the Measurement of Over Head Transmission Lines Conductor Self-Damping." *IEEE Transactions on Power Delivery*, 15(1), 285-292.

Dillon. (1998). *Dillon Strain Gauge Loadcells, Bulletin #500.7*, Dillon Force Measurement Products and Systems Division of Weigh-Tronix, Inc., Fairmont, MN.

Dixon, J. C. (1996). *Tires, Suspension, and Handling*, Society of Automotive Engineers, Warrendale, PA.

Dixon, J. C. (1999). *The Shock Absorber Handbook*, Society of Automotive Engineers, Warrendale, Pa.

Dumora, D., Feldmann, D., and Gaudry, M. (1990). "Mechanical Behavior of Flexurally Stressed Composite Insulators." *IEEE Transactions on Power Delivery*, 5(2), 1066-1073.

Dyrbye, C., and Hansen, S. O. (1996). *Wind Loads on Structures*, John Wiley & Sons, Ltd, Chichester, GB.

Edwards, A. T., Chadha, J., and Hogg, A. D. (1972). *Experience with the End-Point Damping System for the Control of Galloping*. Ontario Hydro, Toronto.

EEI. (2000). *Statistical Yearbook of the Electric Utility Industry, 2000 Edition*, Edison Electric Institute, Washington, DC.

Efdyn. (1993). *Kinetrol Dashpots (Catalog DP-1198)*. Efdyn, Tulsa, OK.

Ehrenburg, D. O. (1935). "Transmission Line Catenary Calculations." *Transactions of the AIEE*, 54(7), 719-728.

Eisner, F. (1931). Das Widerstandsproblem. In *Proceedings of the 3rd International Congress for Applied Mechanics, Stockholm 24-29 August 1930*, edited by C. W. Oseen and W. Weibull. AB. Sveriges Litografiska Tryckerier. Stockholm.

Electrical Week. (1975). "In 345-kV Line Collapse Probe, Staff Questions Design, Urges Code Revamp." *Electrical Week*, July 14, 1975, 1-2.

Electrical World. (1969). "Towers Collapse being Studied by Management." *Electrical World*, Dec. 8, 1969, 34.

Elgerd, O. I. (1963). "Transient Suspension Forces Caused by Broken Transmission Line Conductors." *Journal of the Franklin Institute*, 275(3), 227-245.

Els, P. S., and Holman, T. J. (1999). "Semi-active Rotary Damper for a Heavy Off-Road Wheeled Vehicle." *Journal of Terramechanics*, 36, 51-60.

ENR. (1928). "Transmission Tower with Rotating Crossarm Developed." *Engineering News Record*, May 24, 1928, 814.

EPRI. (1978). "Film of Longitudinal Loading Test on a Transmission Line, Madison Wisconsin, December 1977. EPRI Project 1096-1." Electric Power Research Institute.

EPRI. (1990). *Electric Power Research Institute's TL Workstation Software, Module ETADS*, Electric Power Research Institute, Palo Alto, CA.

Farr, H. H. (1980). *Transmission Line Design Manual*, United States Government Printing Office, Denver, CO.

Fleming, J. F., Atkins, S. R., and Mozer, J. D. (1978). "A Program for Longitudinal Load Analysis of Electric Transmission Lines." *Computers and Structures*, Sept. 1978, 237-253.

Fletcher, R. (1970). "A New Approach to Variable Metric Algorithms." *The Computer Journal*, 13(3), 317-322.

Frandsen, A. G., and Juul, P. H. (1976) "Cascade of Tower Collapses. Design Criteria." *International Conference on High Voltage Electric Systems (CIGRE)*, Paris, Paper 22-10.

Ghannoum, E. (2002) "Evolution of IEC 60826 'Loading and Strength of Overhead Lines'." *Electrical Transmission in a New Age*, Omaha, NB, 59-73.

Gilbert/Commonwealth. (1979). *Transmission Line Reference Book: Wind-Induced Conductor Motion*, Electric Power Research Institute, Palo Alto, Calif.

Goldfarb, D. (1970). "A Family of Variable-Metric Methods Derived by Variational Means." *Mathematics of Computation*, 24(109), 23-26.

Govers, A. (1969). "Main Results of Tests Regarding the Longitudinal Forces on High Tension Towers After Conductor Breakage." Unpublished Manuscript.

Govers, A. (1970) "On the Impact of Uni-Directional Forces on High-Voltage Towers Following Conductor-Breakage." *International Conference on Large Electric Systems at High Tension (CIGRE)*, Paris.

Grand Forks Herald. (1983). March 10.

Gupta, S. (1991). *Nonlinear Analysis of Transmission Line Structures Subjected to Ice Loads*, M.S. Thesis, Civil and Construction Engineering, Iowa State University, Ames, Iowa.

Gupta, S., Wipf, T. J., Fanous, F., Baenziger, M., and Hahm, Y. H. (1993) "Structural Failure Analysis of 345 KV Transmission." IEEE PES Summer Meeting, Vancouver, BC, Paper No. 93 SM 441-6 PWRD.

Haro, L., Magnusson, B., and Ponni, K. (1956) "Investigations on forces Acting on a Support after Conductor Breakage." *International Conference on Large Electric Systems (CIGRE)*, Paris, Report 210.

Healy, E. S., and Wright, A. J. (1926). "Unbalanced Conductor Tensions: Tests to Show their Effects in a Long-Span Transmission Line." *Transactions of the AIEE*, XLV, 1064-1070.

Holmes, N., and Belytschko, T. (1976). "Postprocessing of Finite Element Transient Response Calculations by Digital Filters." *Computers and Structures*, 6, 211-216.

Houdaille, M. (1909). "Shock-Absorbing Apparatus." US Patent No. 933,076. Sept. 7, 1909.

Hydro-Québec. (2003). *Our Transmission System*. Hydro-Québec, July 2002 [cited Feb. 17, 2003]. Available from www.hydroquebec.com/transenergie/transmission.

Ibanez, P., and Merz, K. L. (1988). "Compact Device for Long Stroke Energy Absorption." U.S. Patent No. 4,791,243. Dec. 13, 1988.

Ibanez, P., and Stoessel, J. (1996). Transmission Tower Load Limiter. In *Longitudinal Loading and Cascading Failure Risk Assessment Workshop March 18-19, 1996*, edited by M. Ostendorp and L. Marr. Electric Power Research Institute. Palo Alto, CA.

Irvine, M. (1992). *Cable Structures*, Dover Publications, Inc., Mineola, New York.

Jamaleddine, A., McClure, G., Rousselet, J., and Beauchemin, R. (1993). "Simulation of Ice-Shedding on Electrical Transmission Lines Using ADINA." *Computers and Structures*, 47(4/5), 523-536.

Jones, K. F. (2003). *Ice Storms in the St. Lawrence Valley Region*. Cold Regions Research and Engineering Laboratory, Hanover, NH.

Jones, K. F., and Mulherin, N. D. (1998). *An Evaluation of the Severity of the January 1998 Ice Storm in Northern New England, Report for FEMA Region 1*. Cold Regions Research and Engineering Laboratory, Hanover, NH.

Kansog, J. O. C. (1973). "Sags and Tensions by Computer." *Transmission and Distribution*, Oct. 1973, 92, 94, 96 & 97.

Kaup, N., Davidson, G. A., and Walsh, A. J. (1990). *Review and Analysis of the Storm Damage on the Lehigh-Sycamore 345 kV Transmission Line*. Stone & Webster Engineering Corporation, Denver, CO.

Kempner, L. J. (1997). *Longitudinal Impact Loading on Electrical Transmission Line Towers: A Scale Model Study*, Ph.D. Thesis, Systems Science : Civil Engineering, Portland State University, Portland, Oregon.

Kinetrol. (1996). "Kinetrol Rotary Dashpots." Kinetrol Limited, Farnham, England, 12p.

Kitipornchai, S., Al-Bermani, F. G. A., and Peyrot, A. H. (1994). "Effect of Bolt Slippage on Ultimate Behavior of Lattice Structures." *Journal of Stuctural Engineering*, 120(8), 2281-2287.

Kluge, R. O. (2002). Comments on EPRI Wisconsin Tests (Private correspondence), June.

LaForest, J. J. E. (1982). *Transmission Line Reference Book, 345 kV and Above*, Electric Power Research Institute, Palo Alto, CA.

Lapointe, M. (2003). *Dynamic Analysis of a Power Line Subjected to Longitudinal Loads*, Master of Engineering Thesis, Dept. of Civil Engineering and Applied Mechanics, McGill University, Montreal, Quebec.

Lilien, J. L., and Dal Maso, F. (1990) "Contribution to Line Design by Accurate Predetermination of Severe but Occasional Stresses." *International Conference on Large High Voltage Electric Systems (CIGRE)*, Paris.

Lindsey, K. E. (1978a). "Mathematical Theory of Longitudinally Loaded Elastic-Plastic Transmission Lines - Statics." *IEEE Transactions on Power Apparatus and Systems*, PAS-97(2), 574-582.

Lindsey, K. E. (1978b). "Post-insulator Bases Prevent Cascading Failures." *Electrical World*, January 1, 1978.

Lindsey, L. E. (1970). "High Tension Insulator Mounting Bracket Assembly with Detachable Appearance Cover." U.S. Patent No. 3,522,363. 1970.

Lindsey, L. E., and Sammons, H. F. (1967). "Insulator Mounting Bracket." U.S. Patent No. 3,329,767. July 4, 1967.

Lummis, J., and Pohlman, J. C. (1974) "Flexible Transmission Structures Operate to Suppress Cascading Failures." IEEE PES Winter Meeting, New York, NY, Paper No. C 74 055-0.

Lye, L. M. (2002) "Design of Experiments in Civil Engineering: Are We Still in the 1920's." *Annual Conference of the Canadian Society of Civil Engineers*, Montreal, Quebec, Canada, Paper GE-069.

Mahmoodi, P., Robertson, L. E., Yontar, M., Moy, C., and Feld, L. (1987) "Performance of Viscoelastic Dampers in World Trade Center Towers." *Structure's Congress '87*, Orlando, FL, 632-644.

Main, I. G. (1978). *Vibrations and Waves in Physics*, Cambridge University Press, Cambridge.

McClure, G. (1986). *Analyse Dynamique des Structures Avec Câbles: Revue Bibliographique (Dynamic Analysis of Structures with Cables: Bibliographic Review), In French*. EPM/RT-86-12, Ecole Polytechnique de Montréal, Montreal.

McClure, G. (1989). *Interactions Dynamiques dans les Lignes Aériennes de Transport d'Électricité Soumises aux Bris de Câbles (Dynamic Interactions in Overhead Electrical Lines from Broken Wires, in French)*, Ph.D. Thesis, Départment de Génie Civil (Department of Civil Engineering), Ecole Polytechnique de Montréal, Montreal.

McClure, G., and Lapointe, M. (2003). "Modeling the Structural Dynamic Response of Overhead Transmission Lines." *Computers and Structures*, 81, 825-834.

McClure, G., and Tinawi, R. (1987). "Mathematical Modeling of the Transient Response of Electric Transmission Lines Due to Conductor Breakage." *Computers and Structures*, 26(12), 41-56.

McClure, G., and Tinawi, R. (1989a). "Comportement dynamique des lignes aériennes de transport d'électricité dû aux bris de câbles. I. Modélisation mathématique. (Dynamic Behavior of Overhead Electric Transmission Lines Due to Broken Cables. I Mathematical Modeling)." *Canadian Journal of Civil Engineering*, 16(3), 335-353.

McClure, G., and Tinawi, R. (1989b). "Comportement dynamique des lignes aériennes de transport d'électricité dû aux bris de câbles. II. Problèmes numériques associés à la modélisation mathématique. (Dynamic Behavior of Overhead Electric Transmission Lines Due to Broken Cables. II Numerical Problems Associated with the Mathematical Modeling)." *Canadian Journal of Civil Engineering*, 16(3), 354-374.

Mecano Cable (2003). Samtech [cited July 31, 2003]. Available from www.samcef.com.

Moreau, M., Rigoet, P., and Dalle, B. (1978) "Designing of Overhead Lines in View of Avoiding Cascades, Use of Controlled Sliding Suspension Clamps." *International Conference on Large High Voltage Electric Systems (CIGRE)*, Paris, Paper 22-08.

Morris, R., and Dowling, S. (1987). "Hydraulic Damper." U.S. Patent No. 4,674,608. June 23, 1987.

Mozer, J. D. (1978). *Longitudinal Unbalanced Loads on Transmission Line Structures*, Electric Power Research Institute, Palo Alto, CA.

Mozer, J. D. (1983). *Longitudinal Unbalanced Loads on Transmission Line Structures, Documentation of Computer Programs BRODI2 and BROFLX*, Electric Power Research Institute, Palo Alto, CA.

Mozer, J. D. (2003). Personal Correspondence. Monroeville, PA, July-Sept.

Nafie, A. M. A. E. (1997). *Development of Computer Software for Simulation of Transmission Line Dynamic Behavior (Stiffness, Cable, Truss)*, Ph.D. Thesis, Civil Engineering, Iowa State University, Ames, Iowa.

Nash, R. C. (1995). "Dashpots." US Patent No. 5,450,932. Sep. 19, 1995.

Newmark, N. M. (1959). "A Method of Computation for Structural Dynamics." *Journal of theEngineering Mechanics Division, Proceedings of the American Society of Civil Engineers*, 85(EM 3), 67-95.

Oliver, C. R. (1925). "Sleet and Ice Troubles on Transmission Lines in New England." *AIEE Transactions*, XLIV, 574-580.

Ostendorp, M. (1997a). *Longitudinal Load and Cascading Failure Risk Assessment (CASE) Volume 1: Simplified Approach*. TR-107087-V1, Electric Power Research Institute, Palo Alto, CA.

Ostendorp, M. (1997b). *Longitudinal Load and Cascading Failure Risk Assessment (CASE) Volume 2: Advanced Methods*. TR-107087-V2, Electric Power Research Institute, Palo Alto, CA.

Ostendorp, M. (1997c). *Longitudinal Load and Cascading Failure Risk Assessment (CASE) Volume 3: Wood H-Frame Tests*. TR-107087-V3, Electric Power Research Institute, Palo Alto, CA.

Ostendorp, M. (1997d). *Longitudinal Load and Cascading Failure Risk Assessment (CASE) Volume 4: Steel Pole Tests*. TR-107087-V4, Electric Power Research Institute, Palo Alto, CA.

Ostendorp, M. (1998a). *Longitudinal Load and Cascading Failure Risk Assessment (CASE): Central Louisiana Electric Cooperative's 500-kV Toledo-Coushatta Transmission Line*. TR-108192, Electric Power Research Institute, Palo Alto, CA.

Ostendorp, M. (1998b). "Transmission Line Loading Research." Overheads of Presentation to the Commission to Investigate the 1998 Ice Storm.

Ostendorp, M. (1999). "Protective Overload Device." U. S. Patent No. 5,898,558. Apr. 27, 1999.

Pall, A. S. (1979). *Limited Slip Bolted Joints - A Device to Control the Seismic Response of Large Panel Structures*, Ph.D. Thesis, Centre for Building Studies, Concordia University, Montreal, Quebec.

Pall, A. S., and Marsh, C. (1982). "Response of Friction Damped Braced Frames." *Journal of the Structural Division, ASCE*, 108(ST6), 1313-1323.

Pall, A. S., Verganelakis, V., and Marsh, C. (1987) "Friction Dampers for Seismic Control of Concordia University Library Building." *Proceedings of the Fifth Canadian Conference on Earthquake Engineering*, Ottawa, Ontario, 191-200.

Paris, L. (1960) "Contribution to the Study of Reduced Scale Models in the Field of High Voltage Transmission Lines." *International Conference on Large Electric Systems (CIGRE)*, Paris, Paper 222.

Peabody, A. B. (2001). *Transmission Line Longitudinal Loads, A Review of Design Philosophy*, Structural Engineering Series No. 2001-02, Department of Civil Engineering and Applied Mechanics, McGill University, Montreal.

Peabody, A. B., and McClure, G. (2002a) "Linking Line Security with Atmospheric Icing Levels." *The Tenth International Workshop on Atmospheric Icing of Structures*, Brno, Czech Republic, Paper 7-02.

Peabody, A. B., and McClure, G. (2002b) "Load Limiters for Overhead Lines." *4th Structural Specialty Conference of the Canadian Society of Civil Engineers*, Montreal, Quebec, ST-141.

Peyrot, A. H. (1999). Commentary on the Report Prepared by the Structures Group. In *Les Conditions Climatiques et L'Approvisionnement en Énergie (The Climatic Conditions and Energy Supply).* Les Publications du Québec. Québec.

Peyrot, A. H., and Goulois, A., M. (1978). "Analysis of Flexible Transmission Lines." *Journal of the Structural Division, ASCE*, 104(ST5), 763-779.

Peyrot, A. H., Kluge, R. O., and Lee, J. W. (1978). *Longitudinal Loading Tests on a Transmission Line*. EPRI EL-905, Electric Power Research Institute, Palo Alto, CA.

Pohlman, J. C., and Kaup, N. (1991). *Notes of Field Inspection, Ice Storm Damage, Iowa Power, Raun-Lehigh & Lehigh-Sycamore 345 KV Lines*. J.O. No. 18825.50, Stone & Webster Engineering, Denver.

Poskitt, T. J. (1964). "Some Problems in the Structural Analysis of Overhead Electric Lines." *Proceedings, Institution of Civil Engineers*, 28, 397-405.

Pultruded Composites Properties (2001). Glasforms, Inc., June 14 [cited March 17, 2003]. Available from www.glassforms.com/material_properties.htm.

Ralston, P. (1979) "Discussion of Paper A79 106-6, Some Destructive Mechanisms Activated by Galloping Conductors." *IEEE Power Engineering Society Winter Meeting*, New York, NY.

Rawlins, C. B. (1981). "Analysis of Conductor Galloping Field Observations - Single Conductor." *IEEE Transactions on Power Apparutus and Systems*, PAS-100(8), 3744-3753.

REA. (1992). *REA Bulletin 1724E-200, Design Manual for High Voltage Transmission Lines*, U.S. Government Printing Office, Washington.

Richardson, A. S. (1976). *Dynamic Load Model Study for Overhead Transmission Lines, Final Report for the Period Nov. 1975 to Sep. 1976*. Energy Research and Development Admin CONS/2063-1, Research Consulting Associates, Lexington, MA.

Richardson, A. S. (1977). *Dynamic Load Model Study for Overhead Transmission Lines, Final Report for the Period Jan. 1977 - Sep. 1977*. HCP/T-2063/2, Research Consulting Associates, Lexington, MA.

Richardson, A. S. (1987). "Longitudinal Dynamic Loading of a Steel Pole Transmission Line." *IEEE Transactions on Power Delivery*, PWRD-2(2), 425-436.

Richardson, A. S., Martuccelli, J. R., and Price, W. S. (1965) "Research Study on Galloping of Electric Power Transmission Lines." *Wind Effects on Buildings and Structures*, London, 612-686.

Roshan Fekr, M. (1995). *Dynamic Response of Overhead Transmission Lines to Ice Shedding*, M.Eng. Thesis, Civil Engineering and Applied Mechanics, McGill University, Montreal, Quebec.

RUS. (1998). *Bulletin 1726C-115, Checking Sag in a Conductor by the Return Wave Method*, USDA Rural Utilities Service, Washington, D.C.

SAGSEC. (1998). Version 1. Power Line Systems, Inc., Madison, WI.

Shanno, D. F. (1970). "Conditioning of Quasi-Newton Methods for Function Minimization." *Mathematics of Computation*, 24(111), 647-656.

Shears, M. (1968). *Static and Dynamic Behaviour of Guyed Masts*. Report No. 68-6, Structural Engineering Laboratory, University of California Berkeley, California, Berkeley, CA.

Siddiqui, F. M. A. (1981). *Dynamic Analysis and Behavior of Electric Transmission Line Systems Subjected to Broken Wires*, Ph.D. Thesis, University of Pittsburgh, Pittsburgh, Pennsylvania.

Soong, T. T., and Dargush, G. F. (1997). *Passive Energy Dissipation Systems in Structural Engineering*, John Wiley & Sons, Chichester.

Stefoff, J. W., Swart, R. L., and Zobel, E. S. (1961) "Field Testing of Tower for Broken Conductor Impact Load." AIEE Fall General Meeting, Detroit, MI, Paper No. CP 61-1189.

Sverdrup, and EPRI. (1986). *Broken Conductor Tests of ANCO/DOE Load Limiters*. RP 1717-89, TLMRC Test No. 41, Sverdrup Technology, Inc. and Electric Power Research Institute, Haslet, TX.

Taylor, D. P. (2003). *History, Design and Applications of Fluid Dampers in Structural Engineering*. Taylor Devices, Inc. [cited July 18, 2003]. Available from www.taylordevices.com/papers/history/design.htm.

Thomas, M. B. (1981). *Broken Conductor Loads on Transmission Line Structures*, Ph.D. Thesis, Civil and Environmental Engineering, The University of Wisconsin - Madison, Madison, Wisconsin.

Thrash, R., Hudson, G., Cooper, D., and Sanders, G., eds. (1994). *Overhead Conductor Manual*. Carrollton, Georgia: Southwire Company.

Transmission Line Design Data for the Reid-to-Wilson-to-Coleman 345-kV Transmission Lines, (1982). Burns & McDonnell Engineering Company, Kansas City, MO.

Wen, Y. K. (1968). *Dynamic Response of Transmission Line System to Turbulent Wind Load*, Masters Thesis, Faculty of Engineering Science, Faculty of Graduate Studies University of Western Ontario, London, Ontario.

Wilkinson, C. T. (1910). "Supports for Transmission Lines, Some Mechanical Aspects of Flexible Tower Construction." *Electrical World*, May 19, 1910, 1290-1293.

Wilson, E. L., Farhoomand, I., and Bathe, K.-J. (1973). "Nonlinear Dynamic Analysis of Complex Structrures." *Earthquake Engineering and Structural Dynamics*, 1, 241-252.

Wire Rope Technical Board. (1993). *Wire Rope Users Manual*, Wire Rope Technical Board, Woodstock, MD.

Wisconsin PSC. (1975). *Report on the January 11, 1975 Failure of the North Madsion - South Fond du Lac 345-kV Electric Transmission Line of the Madison Gas and Electric Company*. Public Service Commission of Wisconsin, Engineering Division, Madison.

Wisconsin PSC. (1976). *Report on the January 11, 1975 Failure of the South Fond du Lac - Fitzgerald 345-kV Electric Transmission Line of the Wisconsin Power & Light Company*. Public Service Commission of Wisconsin, Engineering Division, Madison.

Young, H. D., and Freedman, R. A. (2000). *Sears and Zemansky's University Physics*, Addison-Wesley series in physics, Addison-Wesley, San Francisco.

Yu, A. T. (1952). "Vibration Damping of Stranded Cable." *Experimental Stress Analysis*, 9(2), 141-158.

Appendix A
Conductor Natural Frequencies and Mode Shapes

A.1 Introduction

Calculation of the natural frequencies of suspended cables is described in Irvine (1992). This method is based on a parabolic approximation to the catenary shape of a suspended wire. The following equations have been adapted from Irvine's description of the natural frequencies of inclined spans using the simplifications of Blevins (1979) and adopting the notation for describing the cable used by Ehrenburg (1935). Ehrenburg's is among the best presentations of methods for calculating the properties of a catenary cable, including formulas for calculating the position of the low point of sag in inclined spans, the effective tension, the stressed and unstressed lengths and other useful information.

The natural frequencies and mode shapes can be divided into three categories. The in-plane symmetric modes, the in-plane antisymmetric modes, and the out-of-plane modes. The in-plane modes occur in the plane defined by the sag of the cable. The first out of plane mode can be described as a pendulum mode in which the cable swings back and forth about its supports perpendicular to the plane of the cable at rest. The in-plane symmetric modes have an odd number of loops in a span while the in-plane antisymmetric modes have an even number of loops.

A.2 In-Plane Antisymmetric Modes

Equation A-1 gives the natural frequencies of the in-plane anti-symmetric modes where a is the span, c is the chord length (the straight line distance between supports) in an inclined span, m is the unit mass per length of the cable and H is the horizontal component of the tension.

$$\omega_n = \frac{n\pi}{\sqrt{ac}}\sqrt{\frac{H}{m}} \qquad n = 2, 4, 6... \qquad \text{Equation A-1}$$

A.3 In-Plane Symmetric Modes

For both inclined and flat spans, Equation A-2 gives the sag d based on the parabolic approximation to the catenary where w is the weight per unit length or mg. In the parabolic approximation, the unit weight of the cable is assumed to be uniform along the horizontal projection of the curve rather than along the arc length.

$$d = \frac{wa^2}{8H} \qquad \text{Equation A-2}$$

Equation A-3 gives a parameter described by Blevins as the "virtual cable length."

$$L_e = c\left[1 + 8\left(\frac{d}{c}\right)^2\right] \qquad \text{Equation A-3}$$

The natural frequencies of the symmetric modes are calculated using the non-zero roots in λ of the transcendental equation shown in Equation A-4.

$$Tan\frac{\lambda\pi}{2} - \frac{\lambda\pi}{2} + \frac{4}{\alpha^2}\left(\frac{\lambda\pi}{2}\right)^3 = 0 \qquad \text{Equation A-4}$$

Where α is given by equation A-5, E is the modulus of elasticity and A is the cross-sectional area.

$$\alpha = \frac{8d}{c}\sqrt{\frac{EAc}{HL_e}} \qquad \text{Equation A-5}$$

The in-plane symmetric natural frequencies ω_n are given by Equation A-6. Note the similarity to equation A-1 where n is replaced by λ.

$$\omega_n = \frac{\lambda\pi}{\sqrt{ac}}\sqrt{\frac{H}{m}} \qquad \text{Equation A-6}$$

A second method for calculating the in-plane symmetric natural frequencies was developed by Shears (1968). This method is also described in Peyrot et al. (1978) where it is used (in the fortran program CABLE5) to calculate the first symmetric in-plane natural frequency of the first span of the copper conductor used in one of the EPRI Wisconsin tests. In this method, the symmetric natural frequencies are given by the solution of the eigenproblem in Equation A-7.

$$|K - \Omega I| = 0 \qquad \text{Equation A-7}$$

Ω is the matrix of eigenvalues of K. K is given by Equation A-8 where ω_n is given by Equation A-1 with n = 1, 3, 5, ... and ζ is given by Equation A-9.

$$K = \begin{bmatrix} \omega_1^2(1+\zeta) & \frac{\omega_1^2\zeta}{1^3\cdot 3} & \frac{\omega_1^2\zeta}{1^3\cdot 5} & \frac{\omega_1^2\zeta}{1^3\cdot 7} & \frac{\omega_1^2\zeta}{1^3\cdot 9} \\ \frac{\omega_1^2\zeta}{3^3\cdot 1} & \omega_3^2\left(1+\frac{\zeta}{3^4}\right) & \frac{\omega_1^2\zeta}{3^3\cdot 5} & \frac{\omega_1^2\zeta}{3^3\cdot 7} & \frac{\omega_1^2\zeta}{3^3\cdot 9} \\ \frac{\omega_1^2\zeta}{5^3\cdot 1} & \frac{\omega_1^2\zeta}{5^3\cdot 3} & \omega_5^2\left(1+\frac{\zeta}{5^4}\right) & \frac{\omega_1^2\zeta}{5^3\cdot 7} & \frac{\omega_1^2\zeta}{5^3\cdot 9} \\ \frac{\omega_1^2\zeta}{7^3\cdot 1} & \frac{\omega_1^2\zeta}{7^3\cdot 3} & \frac{\omega_1^2\zeta}{7^3\cdot 5} & \omega_7^2\left(1+\frac{\zeta}{7^4}\right) & \frac{\omega_1^2\zeta}{7^3\cdot 9} \\ \frac{\omega_1^2\zeta}{9^3\cdot 1} & \frac{\omega_1^2\zeta}{9^3\cdot 3} & \frac{\omega_1^2\zeta}{9^3\cdot 5} & \frac{\omega_1^2\zeta}{9^3\cdot 7} & \omega_9^2\left(1+\frac{\zeta}{9^4}\right) \end{bmatrix} \qquad \text{Equation A-8}$$

$$\zeta = \frac{8AEw^2a^5}{\pi^4H^3c^3} \qquad \text{Equation A-9}$$

Then the in-plane symmetric natural frequencies are given by Equation A-10.

$$\omega_n = \sqrt{\Omega_n} \qquad \text{Equation A-10}$$

A.4 Out-of-Plane Modes

Equation A-11 gives the out-of-plane natural frequencies based on Irvine and Blevins.

$$\omega_n = \frac{n\pi}{\sqrt{ac}}\sqrt{\frac{H}{m}} \quad n = 1, 2, 3... \qquad \text{Equation A-11}$$

It is interesting to compare the first natural frequency given by Equation A-11 with that of a physical pendulum (Young and Freedman 2000, Section 13-7, p409) in the form of a parabolic cable as given in Equation A-12.

$$\omega = \frac{\sqrt{10}}{a}\sqrt{\frac{H}{m}} \qquad \text{Equation A-12}$$

For a level span where $a = c$, the ratio of the two natural frequencies is 0.993, very good agreement for the first pendulum mode derived in two different ways.

A.5 Natural Frequencies and Mode Shapes using ADINA

ADINA has the capability of calculating natural frequencies and mode shapes of a suspended cable modeled as prestressed truss elements. A mass proportional load is defined to provide starting vectors for the frequency analysis. Table A-1 compares the natural frequencies calculated using ADINA with those calculated in accordance with the theory described above (a visual basic computer program was written to solve Equation A-4). Table 4-2 contains the conductor properties used for the IBIS conductor.

Calculations were based on a 300 m span and horizontal component of tension of 14.4 kN.

Figure A-1
Comparison of Frequencies (in Hz)
Ibis: 300 m Span, H = 14.4 kN

Mode	Blevins & Irvine	Shears & Peyrot	ADINA Frequency Analysis Elements in 300 m Span				
			300	120	60	30	15
Symmetric Modes							
1	0.4186	0.4192	0.4183	0.4184	0.4189	0.4179	0.4172
3	0.6814	0.6815	0.6798	0.6791	0.6787	0.6765	0.6794
5	1.1116	1.1115	1.1093	1.1078	1.1054	1.0959	1.0584
7	1.5532	1.5532	1.5501	1.5470	1.5405	1.5147	1.4140
Antisymmetric Modes							
2	0.4435	0.4435	0.4420	0.4416	0.4414	0.4408	0.4384
4	0.8870	0.8870	0.8851	0.8840	0.8828	0.8780	0.8588
6	1.3305	1.3305	1.3278	1.3256	1.3215	1.3052	1.2414
8	1.7741	1.7740	1.7703	1.7662	1.7565	1.7181	1.5697

Appendix B
ADINA Model Parameters for EPRI-Wisconsin Power & Light Tests

Table B-1
Test Catenary Constants

Test	Horizontal Tension - H (kN)	Unit Weight - w (N/m)	H/w (m)
IIIL1	12.43	7.977	1558
IIIL2	17.77	7.977	2228
IIIL3	21.32	7.977	2673

Table B-2
Tower and Insulator Model Parameters

Description	**Value**
Longitudinal Effective Mass	817 kg
Longitudinal Spring Constant	682 kN/m
Longitudinal Damping Constant	2360 kg/s
Longitudinal Damping Coefficient	5%
Longitudinal Frequency	4.60Hz
Torsional Effective Mass	4255 kg-m^2
Torsional Spring Constant	8708 kN-m/rad
Torsional Damping Constant	19000 kg-m^2/s
Torsional Damping Coefficient	5%
Torsional Frequency	7.2 Hz
Vertical Effective Mass	21100 kg-m^2
Vertical Spring Constant	17620 kN-m/rad
Vertical Damping Constant	61000 kg-m^2/s
Vertical Damping Coefficient	5%
Vertical Frequency	4.6 Hz
Insulator Length	2.08 m

Table B-3
Conductor Parameters

Description	Value
Length of Span T3 to T4	297 m
Finite Element Length	2.5 m ±
Area	234 mm^2
Density	3476 kg/m^3
Modulus of Elasticity	74.2 GPa
Horizontal Tension	See Table B-1
Axial Viscous Damping Constant	37.58 kg/s
Axial Viscous Damping Coefficient	0.5%
Aerodynamic Drag Coefficient	1.25
Aerodynamic Damping Constant	0.381/m

Table B-4
Analysis Parameters

Description	Value
Time Integration Method	Wilson-Theta (1.4)
Displacements	Large
Strains	Small
Equilibrium Iteration Method	BFGS
Calculation Time Step	0.1 ms
Time Interval for Saved Data	5.0 ms
Convergence Criteria	Energy & Displacement
Relative Energy Tolerance (ETOL)	0.10 E-06
Relative Displacement Tolerance (DTOL)	0.10 E-04
Line Convergence Tolerance (STOL)	0.10
Stiffness Matrix Update Frequency	Every Equilibrium Step

Appendix C
Transmission Line Characteristics

The main structural components of a line are the conductors which carry the electric current, the shield wires which are used in areas with frequent thunderstorms to shield the conductors from lightning, the towers and foundations and the insulators, hardware and fittings which splice the conductors and shield wires and connect them to the towers.

Electric transmission lines can be classified by voltage, by tower material, tower construction, by conductor type and by insulator type. Operating transmission line voltages in North America vary from 69 kV to 765 kV. Sub-transmission and distribution lines connect the transmission system to the homes and businesses that use electricity. Transmission towers are constructed of steel, aluminum, wood and concrete. Towers are constructed as lattice space trusses, as space frames, planar frames and monopoles. Conductors are made in many configurations using copper, aluminum, galvanized steel, and steel coated with aluminum or copper (alumoweld and copperweld).

The important transmission line variables from the point of the broken wire loads include:

- Voltage (which affects nearly all the rest of the properties)
- Tower dynamic characteristics (stiffness and natural frequencies)
- Conductor (area, diameter, modulus of elasticity)
- Span and number of spans to the nearest dead-end

- Insulator assembly length
- Insulator Properties (diameter, modulus of elasticity, strength)
- Ground clearance
- Ice loads

Following is a discussion of these variables.

C.1 Voltage

Table C-1 shows the total installed length of transmission circuits by voltage in Quebec (Hydro-Québec 2003) and the United States (EEI 2000). A voltage of 230 kV was chosen for the prototype line.

Table C-1
Circuit Kilometers of Transmission Line in Quebec and the United States

Voltage Range	Typical Voltages Quebec and U.S. (kV)	Quebec (km)	United States (km)
41 to 70 kV	69	3,337	256,554
71 to 131	115 & 120	6,546	156,147
132 to 143	138	0	114,096
144 to 188	161	1,869	40,929
189 to 253	230	3,081	114,545
254 to 400	315 & 345	4,942	75,422
401 to 600	500	1,218*	45,763
601 to 800	735 & 765	11,280	4,406

* ± 450 kV Direct Current

C.2 Tower Dynamic Characteristics

Stiff towers can be represented by a reduced spring-mass-damper model (Thomas 1981). The important parameters are the stiffness and natural frequency (or the mass associated with the stiffness) as the suspension insulator and hardware assemblies decouple the conductors from the towers. Although utilities have extensive internal reports about tower design and testing, there are very few published references which provide sufficient information to accurately model typical lattice transmission towers. ASCE (1991, p 91) indicates that lattice towers have frequencies in the range of 2 to 4 Hz and H-frames in the range 1 to 2 Hz.

C.3 Conductor

C.3.1 Size

Conductor size is based first on the voltage and then on the amount of current that will be carried. For each voltage, there is a minimum diameter required to limit the gradient in the electric field to a level that does not exceed the insulating capacity of the air around the conductor. At higher voltages, this is achieved by using two to four cables spaced to keep the electric field gradient below the needed level. The diameter of each of these subconductors also has a minimum diameter based on the arrangement of the subconductors. Table C-2 shows recommended minimum conductor sizes for single conductor. Sizes through 230 kV are taken from the U.S. Rural Utilities Service guidelines (REA 1992) with the diameters based on the smallest diameter standard ACSR conductor. While most 345 kV lines use a two-conductor bundle, there have been several 345 kV lines constructed with single conductors (LaForest 1982), which typically used conductors with a diameter of 45 mm (1.762 in). Most 345 kV lines use either one large conductor (Bluebird or equivalent) or use two two-conductor bundles. 500 kV lines use two-, three- or four-conductor bundles and 735-765 kV lines use four-conductor bundles. In Laforest (1982), the smallest 345-kV subconductor listed is Tern with a diameter of 27 mm (1.063 in) and for 500 and 765 kV lines, the smallest conductor listed is Rail with a diameter of 29.6 mm (1.165 in).

Once the minimum diameter has been satisfied, then the area of the conductor needed to carry the required current and the strength needed to resist the ice and wind loads can be determined. Today, most conductors use aluminum as the current carrying element with a steel core added when additional strength is needed.

Table C-2
Recommended Minimum Single Conductor Sizes

Nominal Line-to-Line Voltage (kV)	Conductor Name	Stranding Alum/Stl	Aluminum Area (kcmil or AWG)	Minimum Diameter (mm)	Minimum Diameter (in)
69	Pigeon	6/1	3/0	12.8	.502
115	Waxwing	18/1	266.8	15.5	.609
138	Merlin	18/1	336.4	17.4	.684
161	Chickadee	18/1	397.5	18.9	.743
230	Coot	36/1	795.0	26.4	1.040
345	Bluebird	84/19	2156.0	44.8	1.762

A 954 kcmil conductor was chosen for the prototype line. Table C-3 shows the moduli of elasticity for different strandings of 954 kcmil conductor.

Table C-3
Conductor Moduli of Elasticity for Typical 954 kcmil Conductors

Name	Stranding Alum/Stl	% Steel by Weight	Modulus of Elasticity (GPa)
Magnolia	37/0	0	57.92
Goldenrod	61/0	0	59.29
Catbird	36/1	7.30	62.74
Rail	45/7	16.30	64.19
Cardinal	54/7	26.75	65.84
Canvasback	30/19	39.20	74.74

Based on the ice loads discussed later, Cardinal was chosen for the prototype line. The shield wire was chosen to have sags compatible with the conductor.

C.3.2 Conductor Tension

Tables D-1, D-2 and D-3 in Appendix D show the sag and tension limits used for the sag-tensions calculations for the prototype line. The sag-tension data is also included in Appendix D.

C.4 Span and Number of Spans

The span length of 350 m was chosen based on the author's experience as being typical of lattice steel tower lines in this voltage range. Ten spans were modeled as being a reasonable number of spans between stop structures in an area of heavy icing (Peabody and McClure 2002a)

C.5 Insulator Assembly Length

Table C-4 shows the length of typical insulator assemblies using porcelain or toughened glass insulators. The 69 kV assembly length is based on a suspension hook between the top insulator and the structure. The rest of the single conductor strings are based on a shackle and oval eye ball being used (see Figure 3-1). A 2.0 m insulator length was chosen for the 230 kV prototype line.

Table C-4
Typical I-String Insulator Assembly Lengths
(To Center of Conductor or Bundle)

Nominal Line-to-Line Voltage (kV)	No. Standard Bells	Single Conductor (m)	Two Conductor Bundle (m)	Four Conductor Bundle (m)
69	4	0.75		
115	7	1.28		
138	8	1.42		
161	10	1.71		
230	12	2.01		
345	18	2.88	3.08	
500	24		3.96	4.33
735	28*			5.45
765	34			5.79

* Non-standard 165 mm (6½ in) Bells.

C.6 Composite Insulator Properties

Composite insulators have a central high quality fiberglass rod that provides the insulator's strength and internal electrical resistance. The rod is covered and protected by molded rubber that is shaped into sheds that provide the electrical insulating properties that are needed. Today, the rubber is typically either an EPDM (Ethylene Propylene Diene Monomer) or silicone based compound. Most manufacturers injection mold the rubber onto the rod; however one manufacturer uses individual sheds or sections of sheds that are slid onto the rod, with an insulating silicone grease used between the sheds and the rod to keep moisture from penetrating the joints. Composite insulators are manufactured for use as both suspension insulators and line and station post insulators. Suspension insulators are intended to carry only tensile forces. Post insulators are designed for use as cantilever bending members. The end fittings which are used to connect the fiberglass strength member to the structure are, today, typically swaged onto the rod. End fittings are available in many different configurations. In large quantities, it may be possible to use custom end fittings if the purchaser is willing to bear the cost of design and tooling. Posts are available with nominal solid rod sizes of approximately 45, 63, 76, and 88 mm (1.75, 2.5, 3, 3.5 in) with the exact diameter depending on the manufacturer. Lengths for use with voltages up to 345-kV are catalogued by the major manufacturers. Dumora et al. (1990) give an excellent description of the factors important in the design of the rod. Most important for this research is the distinction between the short term and long term strength of the rod. Fiberglass rod subjected to a long term continuous load creeps and will fail at a lower stress than when loaded instantaneously. The instantaneous failure strength is reported to be approximately 800 Mpa. The damage limit, which is defined as the stress level below which no permanent damage to the rod occurs is reported to be approximately 500 Mpa. They report the modulus of elasticity (considering the composite insulator to be uniform cylinder) to be 37 GPa with Poisson's ratio of 0.28. The end fittings, usually of aluminum, are of much larger diameter than the rod. Dumora et. al. report that failures typically occurred at the interface with the base end fitting; beginning with failure of the surface fibers on the tension side, progressing to a crushing failure on the compression side opposite to the tension failure and then delamination all along the rod on the neutral axis, which is probably a shear failure. The shear strength of the epoxy matrix is not given. Table C-5 compares these properties with typical pultruded fiberglass rod properties from Glasforms, Inc. (*Pultruded* 2001).

Table C-5
Fiberglass Composite Rod Properties

Property	Dumora et. al.	Glasform, Inc.
Density (kg/m^3)	-	2020
Modulus of Elasticity (GPa)	37.0	41.4
Tensile Strength (MPa)	-	827
Bending Strength (Mpa)	800	827
Compressive Strength (Mpa)	-	483
Poisson's Ratio	0.28	-

While the end fittings could be modeled as rigid ends, at least for the first runs, the properties will be assumed to be those of the fiberglass rod for the full length of the member.

C.7 Ground Clearance

Ground clearance is important because in some cases the conductor in the intact spans may hit the ground during a broken wire event. Part of the span may lie on the ground at the residual static tension.

Ground clearances are based on the height of an assumed object under the line, the voltage between the line and ground during an assumed switching surge, which may be over three times the normal operating voltage, and the clearance required between the object and the wire to have a low probability of flashover with the assumed switching surge. For the higher voltage lines (typically 345 kV and above) clearance must also be high enough to limit the short circuit current between an insulated object (typically a tractor trailer truck) and ground induced by the electric field surrounding the line. Codes typically require the ground clearance to be maintained at final sag with the maximum operating temperature and at a specified temperature and ice load. Table C-6 shows typical ground clearances for cropland that is accessible to highway trucks (reference height: CA 4.15 m, US 4.27 m) for different voltage lines. The clearance for 345 kV is based on calculations of the induced currents in a highway tractor trailer (*Transmission* 1982) and those for 500 kV are based on typical values in LaForest (1982), while 735 and 765 kV values are based on the Canadian Electrical Code (CSA 1997).

Table C-6
Minimum Ground Clearances

Nominal Line-to-Line Voltage (kV)	Max Operating Voltage Line-to-Ground (kV)	Canadian Electrical Code (m)	NESC 2002 (m)
69	39.8	5.2	5.8
115	69.7	5.5	6.1
138	83.7	5.5	6.2
161	97.6	5.8	6.4
230	139.4	6.1	6.8
345	209.1	6.7	7.5
500	303.1	9.2	8.4
735	445.6	12.7	9.8
765	463.8	13.2	10.0

While code ground clearances are generally specified for radial ice thicknesses of around 12.7 mm, the prototype tower was based on a ground clearance of approximately 6.1 m with the design ice load.

C.8 Ice Loads

Fifty year mean return period ice loads in the United States vary from no ice in Southern Florida to 31.8 mm in parts of New England, the west end of Lake Superior and parts of the State of Washington (ASCE 2002). In January 1998 there was massive freezing rain storm which encompassed parts of Ontario, Quebec, New York and New England. While there is still great controversy among experts in the field concerning the ice thicknesses that accreted during the storm and their return period, Jones (2003), author of the map in ASCE 7, reports a fifty year return period radial ice thickness of 33 mm for this region with a maximum in this storm of 55 mm with a return period of 250 years.

Ghannoum (2002) reports that the latest version of the IEC Standard 60826 "Loading and Strength of Overhead Lines" recommends that transmission lines that are critical for the functioning of the transmission grid may be designed for loads with return periods of 150 to 500 years. A return period of 150 years is recommended for 230 kV lines. Using the multipliers on the 50-year mean recurrence interval ice thickness from ASCE 7-02 (ASCE 2002), the range of possible design radial ice thicknesses in Quebec and the U.S. is from no ice to approximately 66 mm (for a 500 year return period). A 150-year return period ice thickness for the St. Lawrence region of 45 mm was chosen for the prototype line

Appendix D
Prototype Line Data

Table D-1
Conductor Tension Limits

	Temp (°C)	Wind Pressure (Pa)	Radial Ice (mm)	Ice Density (kg/m^3)	"k" N/m	Initial or Final	Tension Limit %RTS	Design Tension after Load %RTS	Design Tension after Creep %RTS	Source
Vibration Control										
	5.0	-	-		-	I	25.0	16.5	16.5	CSA
	5.0	-	-		-	F	20.0	13.3	15.5	CSA
	15.0	-	-		-	I	35.0	16.0	16.0	NESC
	15.0	-	-		-	F	25.0	13.2	15.1	NESC
	-17.8	-	-		-	I	33.3	17.6	17.6	REA
	-17.8	-	-		-	F	25.0	13.8	16.6	REA
	-15.0	-	-		-	F	23.0	13.7	16.5	Alcan
Load Limits										
CSA Heavy	-17.8	383.0	12.7	913		I	60.0	33.1	-	CSA
NESC Heavy	-17.8	191.5	12.7	913	4.4	I	60.0	33.0	-	NESC
NESC Heavy	-17.8	191.5	12.7	913	4.4	I	50.0	33.0	-	REA
Heavy Ice	0.0	0.0	45.0	913	0.0	I	70.0	68.3	-	REA
Heavy Ice & Wind	-15.0	196.0	45.0	913	0.0	I	70.0	70.0	-	Author
High Wind	5.0	1000.0	0.0	-	0.0	I	70.0	28.9	-	NESC

Notes: Annual mean temperature at Montreal McGill is 7.4 C, used 5.0 C

Average minimum temperature of the coldest month at Montreal McGill is –12.4 C, used –15 C for Alcan vibration control

Table D-2
Shield Wire Tension Limits

	Temp (°C)	Wind Pressure (Pa)	Radial Ice (mm)	Ice Density (kg/m^3)	"k" N/m	Initial or Final	Tension Limit %RTS	Design Tension after Load %RTS	Design Tension after Creep %RTS	Source
Vibration Control										
	5.0	-	-		-	I	25.0	18.1	18.1	CSA
	5.0	-	-		-	F	20.0	10.2	18.1	CSA
	15.0	-	-		-	I	35.0	17.3	17.3	NESC
	15.0	-	-		-	F	25.0	9.9	17.3	NESC
	-17.8	-	-		-	I	25.0	20.2	20.2	REA
	-17.8	-	-		-	F	25.0	10.8	20.2	REA
	-15.0	-	-		-	F	?	10.7	19.9	Alcan
Load Limits										
CSA Heavy	-17.8	383.0	12.7	913		I	60.0	37.6	-	CSA
NESC Heavy	-17.8	191.5	12.7	913	4.4	I	60.0	37.9	-	NESC
NESC Heavy	-17.8	191.5	12.7	913	4.4	I	50.0	37.9	-	REA
Heavy Ice	0.0	0.0	45.0	913	0.0	I	80.0	76.7	-	REA
Heavy Ice & Wind	-15.0	196.0	45.0	913	0.0	I	80.0	77.9	-	Author
High Wind	5.0	1000.0	0.0	-	0.0	I	?	27.3	-	NESC

Table D-3
Shield Wire Sag Limits

	Temp (°C)	Wind Pressure (Pa)	Radial Ice (mm)	Ice Density (kg/m^3)	"k" N/m	Initial or Final With Creep	Sag Limit % Conductor Sag	Initial Sag % Conductor Sag	Final Sag After Load % Conductor Sag	Final Sag After Creep % Conductor Sag
Lightning Shielding	15.0	-	-	-	-	F	80.0	48.5	69.7	45.9
Heavy Ice & Wind	-15.0	196.0	45.0	913	0.0	I	100.0	100	100.0	-

Sag-Tension Data

Apr 11, 2003 SagtenM Version 1, 3/25/2003

Conductor = 7/16" EHS Chart No. 1-1246
Area = 74.6 mm^2 Diameter = 11.05 mm Unit weight = 05.823 N/m
Ruling Span = 350 m Rated Tensile Strength = 92.52 kN

				Final					Initial						
Temp °C	Ice mm	Wind Pa	Const N/m	Sag m	Avrg Tension kN	Final % RTS	Horz Tension kN	Supp Tension kN	Sag m	Avrg Tension kN	Init % RTS	Horz Tension kN	Supp Tension kN	Load N/m	Ice Density kg/m^3
-35.0	0.00	0.0	0.00	8.53	10.48	11.3	10.46	10.51	4.39	20.31	21.9	20.29	20.32	5.823	913
-17.8	0.00	0.0	0.00	8.95	9.99	10.8	9.96	10.02	4.78	18.67	20.2	18.66	18.69	5.823	913
-17.8	12.70	0.0	0.00	10.74	20.49	22.1	20.41	20.57	7.59	28.92	31.3	28.87	28.98	14.308	913
-17.8	12.70	191.5	4.38	11.68	26.76	28.9	26.64	26.87	8.88	35.10	37.9	35.00	35.19	20.297	913
-17.8	12.70	383.0	0.00	11.63	26.45	28.6	26.34	26.57	8.82	34.80	37.6	34.71	34.89	19.991	913
-15.0	0.00	0.0	0.00	9.02	9.92	10.7	9.89	9.94	4.84	18.43	19.9	18.42	18.44	5.823	913
-15.0	0.00	143.6	0.00	9.08	10.21	11.0	10.19	10.24	4.94	18.71	20.2	18.70	18.73	6.036	913
-15.0	25.40	0.0	0.00	13.17	37.32	40.3	37.11	37.53	10.84	45.23	48.9	45.05	45.40	31.866	913
-15.0	31.75	0.0	0.00	14.38	47.29	51.1	46.97	47.61	12.48	54.37	58.8	54.09	54.64	44.047	913
-15.0	39.62	0.0	0.00	15.89	60.85	65.8	60.35	61.34	14.77	65.37	70.7	64.91	65.83	62.497	913
-15.0	44.96	0.0	0.00	16.88	70.48	76.2	69.83	71.13	16.68	71.32	77.1	70.68	71.96	76.797	913
-15.0	25.40	191.5	0.00	13.40	39.14	42.3	38.91	39.36	11.14	46.95	50.7	46.75	47.13	33.996	913
-15.0	31.75	191.5	0.00	14.59	49.03	53.0	48.69	49.37	12.77	55.90	60.4	55.60	56.19	46.304	913
-15.0	39.62	191.5	0.00	16.07	62.48	67.5	61.95	63.00	15.07	66.52	71.9	66.04	67.02	64.854	913
-15.0	44.96	191.5	0.00	17.04	72.04	77.9	71.36	72.71	17.04*	72.04	77.9	71.36	72.71	79.198	913
0.0	0.00	0.0	0.00	9.38	9.53	10.3	9.51	9.56	5.20	17.17	18.6	17.15	17.18	5.823	913
0.0	12.70	0.0	0.00	11.08	19.87	21.5	19.79	19.95	7.93	27.69	29.9	27.64	27.75	14.308	913
0.0	25.40	0.0	0.00	13.39	36.71	39.7	36.49	36.92	11.05	44.37	48.0	44.20	44.55	31.866	913
0.0	31.75	0.0	0.00	14.58	46.65	50.4	46.33	46.97	12.66	53.61	57.9	53.34	53.89	44.047	913
0.0	39.62	0.0	0.00	16.07	60.18	65.0	59.68	60.68	14.90	64.81	70.0	64.34	65.27	62.497	913
0.0	44.96	0.0	0.00	17.05	69.80	75.4	69.15	70.46	16.76	70.97	76.7	70.33	71.61	76.797	913
5.0	0.00	0.0	0.00	9.50	9.42	10.2	9.39	9.44	5.32	16.77	18.1	16.75	16.78	5.823	913
5.0	0.00	1000.7	0.00	10.87	17.69	19.1	17.62	17.76	7.58	25.30	27.3	25.26	25.35	12.497	913
15.0	0.00	0.0	0.00	9.74	9.19	9.9	9.16	9.22	5.57	16.03	17.3	16.01	16.04	5.823	913
37.8	0.00	0.0	0.00	10.27	8.72	9.4	8.69	8.75	6.15	14.52	15.7	14.50	14.54	5.823	913
48.9	0.00	0.0	0.00	10.52	8.51	9.2	8.49	8.55	6.43	13.88	15.0	13.86	13.89	5.823	913
75.0	0.00	0.0	0.00	11.09	8.08	8.7	8.05	8.11	7.11	12.56	13.6	12.54	12.59	5.823	913

Apr 11, 2003 SagtenM Version 1, 3/25/2003

Conductor = 7/16" EHS Chart No. 1-1246
Area = 74.6 mm^2 Diameter = 11.05 mm Unit weight = 05.823 N/m
Ruling Span = 350 m Rated Tensile Strength = 92.52 kN

				Final					Initial						
Temp °C	Ice mm	Wind Pa	Const N/m	Sag m	Avrg Tension kN	Final % RTS	Horz Tension kN	Supp Tension kN	Sag m	Avrg Tension kN	Init % RTS	Horz Tension kN	Supp Tension kN	Load N/m	Ice Density kg/m^3
-35.0	0.00	0.0	0.00	4.39	20.31	22.0	20.29	20.32	4.39	20.31	22.0	20.29	20.32	5.823	913
-17.8	0.00	0.0	0.00	4.78	18.66	20.2	18.64	18.67	4.78	18.68	20.2	18.66	18.69	5.823	913
-15.0	0.00	0.0	0.00	4.85	18.41	19.9	18.39	18.42	4.84	18.43	19.9	18.42	18.44	5.823	913
0.0	0.00	0.0	0.00	5.21	17.13	18.5	17.11	17.14	5.20	17.17	18.6	17.15	17.18	5.823	913
5.0	0.00	0.0	0.00	5.33	16.73	18.1	16.71	16.74	5.32	16.77	18.1	16.76	16.79	5.823	913
15.0	0.00	0.0	0.00	5.59	15.97	17.3	15.96	15.99	5.57	16.03*	17.3	16.01	16.04	5.823	913
37.8	0.00	0.0	0.00	6.18	14.45	15.6	14.43	14.47	6.15	14.52	15.7	14.50	14.54	5.823	913
48.9	0.00	0.0	0.00	6.47	13.79	14.9	13.78	13.82	6.43	13.88	15.0	13.86	13.89	5.823	913
75.0	0.00	0.0	0.00	7.16	12.47	13.5	12.45	12.49	7.11	12.57	13.6	12.54	12.59	5.823	913

Apr 11, 2003 SagtenM Version 1, 3/25/2003

Conductor = Cardinal Chart No. 1-838
Area = 545.9 mm^2 Diameter = 30.38 mm Unit weight = 17.936 N/m
Ruling Span = 350 m Rated Tensile Strength = 150.35 kN

				Final					Initial						
Temp °C	Ice mm	Wind Pa	Const N/m	Sag m	Avrg Tension kN	Final % RTS	Horz Tension kN	Supp Tension kN	Sag m	Avrg Tension kN	Init % RTS	Horz Tension kN	Supp Tension kN	Load N/m	Ice Density kg/m^3
-35.0	0.00	0.0	0.00	12.84	21.53	14.3	21.42	21.65	9.82	28.06	18.7	27.97	28.15	17.936	913
-17.8	0.00	0.0	0.00	13.38	20.68	13.8	20.55	20.79	10.40	26.51	17.6	26.42	26.60	17.936	913
-17.8	12.70	0.0	0.00	14.12	36.44	24.2	36.20	36.67	11.77	43.59	29.0	43.39	43.79	33.325	913
-17.8	12.70	191.5	4.38	14.38	42.28	28.1	42.00	42.57	12.24	49.55	33.0	49.31	49.79	39.374	913
-17.8	12.70	383.0	0.00	14.39	42.48	28.3	42.20	42.77	12.26	49.76	33.1	49.51	50.00	39.586	913
-15.0	0.00	0.0	0.00	13.47	20.55	13.7	20.42	20.67	10.50	26.28	17.5	26.18	26.37	17.936	913
-15.0	0.00	143.6	0.00	13.49	21.10	14.0	20.98	21.23	10.55	26.91	17.9	26.81	27.01	18.458	913
-15.0	25.40	0.0	0.00	15.19	58.83	39.1	58.39	59.27	13.59	65.62	43.6	65.22	66.01	57.789	913
-15.0	31.75	0.0	0.00	15.74	72.17	48.0	71.58	72.74	14.57	77.84	51.8	77.31	78.38	73.423	913
-15.0	39.62	0.0	0.00	16.47	90.45	60.2	89.66	91.25	15.92	93.52	62.2	92.75	94.28	96.197	913
-15.0	44.96	0.0	0.00	16.97	103.52	68.9	102.57	104.49	16.90	103.92	69.1	102.97	104.89	113.383	913
-15.0	25.40	191.5	0.00	15.26	60.63	40.3	60.18	61.09	13.72	67.30	44.8	66.90	67.72	59.844	913
-15.0	31.75	191.5	0.00	15.81	73.97	49.2	73.36	74.56	14.70	79.44	52.8	78.88	80.00	75.593	913
-15.0	39.62	191.5	0.00	16.54	92.21	61.3	91.39	93.02	16.05	94.96	63.2	94.17	95.75	98.468	913
-15.0	44.96	191.5	0.00	17.04	105.24	70.0	104.26	106.23	17.04	105.24	70.0	104.26	106.23	115.703	913
0.0	0.00	0.0	0.00	13.73	20.15	13.4	20.03	20.27	10.99	25.10	16.7	25.01	25.20	17.936	913
0.0	12.70	0.0	0.00	14.61	35.23	23.4	34.99	35.47	12.25	41.90	27.9	41.70	42.11	33.325	913
0.0	25.40	0.0	0.00	15.56	57.44	38.2	56.99	57.89	13.91	64.13	42.7	63.73	64.53	57.789	913
0.0	31.75	0.0	0.00	16.09	70.61	47.0	70.02	71.20	14.85	76.38	50.8	75.84	76.93	73.423	913
0.0	39.62	0.0	0.00	16.80	88.70	59.0	87.88	89.50	16.15	92.17	61.3	91.39	92.95	96.197	913
0.0	44.96	0.0	0.00	17.29	101.66	67.6	100.68	102.64	17.11	102.68	68.3	101.71	103.65	113.383	913
5.0	0.00	0.0	0.00	13.82	20.03	13.3	19.91	20.16	11.16	24.74	16.5	24.64	24.84	17.936	913
5.0	0.00	1000.7	0.00	14.83	36.77	24.5	36.51	37.03	12.53	43.41	28.9	43.20	43.64	35.297	913
15.0	0.00	0.0	0.00	13.98	19.81	13.2	19.68	19.93	11.48	24.05*	16.0	23.95	24.15	17.936	913
37.8	0.00	0.0	0.00	14.33	19.32	12.8	19.19	19.45	12.20	22.65	15.1	22.54	22.76	17.936	913
48.9	0.00	0.0	0.00	14.51	19.09	12.7	18.96	19.22	12.54	22.04	14.7	21.92	22.15	17.936	913
75.0	0.00	0.0	0.00	14.91	18.58	12.4	18.45	18.72	13.33	20.76	13.8	20.64	20.88	17.936	913

Mar 28, 2003 SagtenM Version 1, 3/25/2003

Conductor = Cardinal Chart No. 1-838
Area = 545.9 mm^2 Diameter = 30.38 mm Unit weight = 17.936 N/m
Ruling Span = 350 m Rated Tensile Strength = 150.35 kN
Creep is a factor

				Final					Initial						
Temp °C	Ice mm	Wind Pa	Const N/m	Sag m	Avrg Tension kN	Final % RTS	Horz Tension kN	Supp Tension kN	Sag m	Avrg Tension kN	Init % RTS	Horz Tension kN	Supp Tension kN	Load N/m	Ice Density kg/m^3
-35.0	0.00	0.0	0.00	10.42	26.48	17.6	26.39	26.57	9.82	28.06	18.7	27.97	28.15	17.936	913
-17.8	0.00	0.0	0.00	11.04	25.00	16.6	24.90	25.10	10.40	26.51	17.6	26.42	26.60	17.936	913
-17.8	12.70	0.0	0.00	12.02	42.69	28.4	42.49	42.89	11.77	43.59	29.0	43.39	43.79	33.325	913
-17.8	12.70	191.5	4.38	12.36	49.09	32.6	48.84	49.32	12.24	49.55	33.0	49.31	49.79	39.374	913
-17.8	12.70	383.0	0.00	12.37	49.30	32.8	49.06	49.55	12.26	49.76	33.1	49.51	50.00	39.586	913
-15.0	0.00	0.0	0.00	11.14	24.78	16.5	24.68	24.88	10.50	26.28	17.5	26.18	26.37	17.936	913
0.0	0.00	0.0	0.00	11.66	23.69	15.8	23.58	23.79	10.99	25.11	16.7	25.01	25.20	17.936	913
0.0	12.70	0.0	0.00	12.57	40.86	27.2	40.65	41.07	12.25	41.90	27.9	41.70	42.11	33.325	913
5.0	0.00	0.0	0.00	11.83	23.35	15.5	23.24	23.45	11.16	24.74	16.5	24.64	24.84	17.936	913
15.0	0.00	0.0	0.00	12.16	22.71	15.1	22.60	22.82	11.48	24.05*	16.0	23.95	24.15	17.936	913
37.8	0.00	0.0	0.00	12.91	21.43	14.3	21.31	21.54	12.20	22.65	15.1	22.54	22.76	17.936	913
48.9	0.00	0.0	0.00	13.26	20.87	13.9	20.75	20.99	12.54	22.04	14.7	21.92	22.15	17.936	913
75.0	0.00	0.0	0.00	14.05	19.71	13.1	19.58	19.83	13.33	20.76	13.8	20.64	20.88	17.936	913

Apr 11, 2003 SagtenM Version 1, 3/25/2003

Conductor = 7/16" EHS Chart No. 1-1246
Area = 0.1156 in^2 Diameter = 0.4350 in Unit weight = 0.3990 lb/ft
Ruling Span = 1,148 ft Rated Tensile Strength = 20,800 lb

				Final					Initial						
Temp °F	Ice in	Wind psf	Const lbf/ft	Sag ft	Avrg Tension lbf	Final % RTS	Horz Tension lbf	Supp Tension lbf	Sag ft	Avrg Tension lbf	Init % RTS	Horz Tension lbf	Supp Tension lbf	Load lbf/ft	Ice Density pcf
-31.0	0.00	0.0	0.00	27.97	2357	11.3	2352	2363	14.41	4565	21.9	4562	4568	0.3990	57.00
0.0	0.00	0.0	0.00	29.37	2246	10.8	2240	2252	15.67	4198	20.2	4196	4202	0.3990	57.00
0.0	0.50	0.0	0.00	35.24	4606	22.1	4589	4623	24.90	6501	31.3	6490	6515	0.9804	57.00
0.0	0.50	4.0	0.30	38.32	6015	28.9	5988	6041	29.14	7890	37.9	7869	7910	1.3908	57.00
0.0	0.50	8.0	0.00	38.17	5946	28.6	5921	5973	28.94	7823	37.6	7804	7844	1.3698	57.00
5.0	0.00	0.0	0.00	29.60	2229	10.7	2223	2234	15.88	4143	19.9	4140	4147	0.3990	57.00
5.0	0.00	3.0	0.00	29.78	2296	11.0	2290	2302	16.21	4207	20.2	4204	4211	0.4136	57.00
5.0	1.00	0.0	0.00	43.20	8390	40.3	8342	8437	35.56	10168	48.9	10128	10206	2.1835	57.00
5.0	1.25	0.0	0.00	47.19	10631	51.1	10560	10702	40.96	12223	58.8	12160	12283	3.0182	57.00
5.0	1.56	0.0	0.00	52.14	13679	65.8	13567	13791	48.46	14696	70.7	14592	14800	4.2824	57.00
5.0	1.77	0.0	0.00	55.39	15845	76.2	15699	15991	54.72	16033	77.1	15890	16178	5.2623	57.00
5.0	1.00	4.0	0.00	43.96	8799	42.3	8747	8849	36.56	10554	50.7	10511	10596	2.3295	57.00
5.0	1.25	4.0	0.00	47.86	11023	53.0	10946	11098	41.89	12566	60.4	12500	12632	3.1728	57.00
5.0	1.56	4.0	0.00	52.71	14046	67.5	13928	14162	49.43	14955	71.9	14847	15067	4.4439	57.00
5.0	1.77	4.0	0.00	55.90	16195	77.9	16043	16347	55.90*	16195	77.9	16043	16347	5.4268	57.00
32.0	0.00	0.0	0.00	30.79	2143	10.3	2137	2149	17.05	3859	18.6	3856	3863	0.3990	57.00
32.0	0.50	0.0	0.00	36.35	4467	21.5	4449	4485	26.01	6226	29.9	6214	6239	0.9804	57.00
32.0	1.00	0.0	0.00	43.93	8252	39.7	8204	8300	36.25	9975	48.0	9936	10015	2.1835	57.00
32.0	1.25	0.0	0.00	47.85	10487	50.4	10415	10559	41.54	12052	57.9	11990	12116	3.0182	57.00
32.0	1.56	0.0	0.00	52.73	13529	65.0	13416	13642	48.89	14569	70.0	14465	14674	4.2824	57.00
32.0	1.77	0.0	0.00	55.94	15692	75.4	15546	15840	55.00	15954	76.7	15810	16099	5.2623	57.00
41.0	0.00	0.0	0.00	31.18	2117	10.2	2110	2123	17.46	3770	18.1	3766	3773	0.3990	57.00
41.0	0.00	20.9	0.00	35.65	3977	19.1	3962	3993	24.86	5688	27.3	5678	5699	0.8563	57.00
59.0	0.00	0.0	0.00	31.95	2066	9.9	2059	2072	18.27	3603	17.3	3599	3606	0.3990	57.00
100.0	0.00	0.0	0.00	33.68	1961	9.4	1954	1967	20.17	3264	15.7	3260	3268	0.3990	57.00
120.0	0.00	0.0	0.00	34.50	1914	9.2	1908	1921	21.11	3120	15.0	3115	3124	0.3990	57.00
167.0	0.00	0.0	0.00	36.38	1816	8.7	1809	1824	23.32	2824	13.6	2820	2829	0.3990	57.00

Apr 11, 2003 SagtenM Version 1, 3/25/2003

Conductor = 7/16" EHS Chart No. 1-1246
Area = 0.1156 in^2 Diameter = 0.4350 in Unit weight = 0.3990 lb/ft
Ruling Span = 1,148 ft Rated Tensile Strength = 20,800 lb

				Final					Initial						
Temp °F	Ice in	Wind psf	Const lbf/ft	Sag ft	Avrg Tension lbf	Final % RTS	Horz Tension lbf	Supp Tension lbf	Sag ft	Avrg Tension lbf	Init % RTS	Horz Tension lbf	Supp Tension lbf	Load lbf/ft	Ice Density pcf
-31.0	0.00	0.0	0.00	14.41	4566	22.0	4562	4568	14.41	4566	22.0	4562	4568	0.3990	57.00
0.0	0.00	0.0	0.00	15.69	4194	20.2	4190	4197	15.67	4199	20.2	4196	4202	0.3990	57.00
5.0	0.00	0.0	0.00	15.90	4138	19.9	4135	4141	15.88	4143	19.9	4140	4147	0.3990	57.00
32.0	0.00	0.0	0.00	17.09	3850	18.5	3847	3854	17.05	3859	18.6	3856	3863	0.3990	57.00
41.0	0.00	0.0	0.00	17.50	3760	18.1	3757	3764	17.45	3771	18.1	3768	3775	0.3990	57.00
59.0	0.00	0.0	0.00	18.33	3590	17.3	3587	3594	18.27	3603*	17.3	3599	3606	0.3990	57.00
100.0	0.00	0.0	0.00	20.27	3248	15.6	3244	3252	20.17	3265	15.7	3260	3268	0.3990	57.00
120.0	0.00	0.0	0.00	21.23	3101	14.9	3098	3106	21.11	3120	15.0	3115	3124	0.3990	57.00
167.0	0.00	0.0	0.00	23.50	2804	13.5	2799	2808	23.32	2825	13.6	2820	2829	0.3990	57.00

Apr 11, 2003 SagtenM Version 1, 3/25/2003

Conductor = Cardinal Chart No. 1-838
Area = 0.8462 in^2 Diameter = 1.1960 in Unit weight = 1.2290 lb/ft
Ruling Span = 1,148 ft Rated Tensile Strength = 33,800 lb

				Final					Initial						
Temp °F	Ice in	Wind psf	Const lbf/ft	Sag ft	Avrg Tension lbf	Final % RTS	Horz Tension lbf	Supp Tension lbf	Sag ft	Avrg Tension lbf	Init % RTS	Horz Tension lbf	Supp Tension lbf	Load lbf/ft	Ice Density pcf
-31.0	0.00	0.0	0.00	42.12	4841	14.3	4815	4867	32.23	6308	18.7	6288	6328	1.2290	57.00
0.0	0.00	0.0	0.00	43.90	4648	13.8	4621	4675	34.13	5959	17.6	5939	5981	1.2290	57.00
0.0	0.50	0.0	0.00	46.32	8193	24.2	8139	8245	38.62	9799	29.0	9755	9843	2.2835	57.00
0.0	0.50	4.0	0.30	47.18	9505	28.1	9442	9569	40.16	11140	33.0	11085	11194	2.6980	57.00
0.0	0.50	8.0	0.00	47.21	9551	28.3	9486	9615	40.21	11186	33.1	11131	11240	2.7125	57.00
5.0	0.00	0.0	0.00	44.18	4619	13.7	4592	4646	34.44	5907	17.5	5886	5928	1.2290	57.00
5.0	0.00	3.0	0.00	44.27	4744	14.0	4716	4772	34.61	6050	17.9	6028	6071	1.2648	57.00
5.0	1.00	0.0	0.00	49.82	13226	39.1	13126	13324	44.58	14752	43.6	14662	14839	3.9598	57.00
5.0	1.25	0.0	0.00	51.64	16224	48.0	16093	16353	47.80	17499	51.8	17379	17620	5.0311	57.00
5.0	1.56	0.0	0.00	54.03	20334	60.2	20157	20513	52.22	21024	62.2	20852	21196	6.5916	57.00
5.0	1.77	0.0	0.00	55.68	23272	68.9	23058	23491	55.46	23363	69.1	23149	23580	7.7692	57.00
5.0	1.00	4.0	0.00	50.06	13630	40.3	13528	13734	45.01	15130	44.8	15039	15224	4.1006	57.00
5.0	1.25	4.0	0.00	51.88	16628	49.2	16492	16761	48.23	17858	52.8	17734	17984	5.1798	57.00
5.0	1.56	4.0	0.00	54.26	20729	61.3	20546	20912	52.65	21348	63.2	21170	21526	6.7472	57.00
5.0	1.77	4.0	0.00	55.90	23660	70.0	23438	23881	55.90	23660	70.0	23438	23881	7.9282	57.00
32.0	0.00	0.0	0.00	45.06	4530	13.4	4502	4558	36.06	5643	16.7	5622	5666	1.2290	57.00
32.0	0.50	0.0	0.00	47.94	7920	23.4	7865	7975	40.19	9420	27.9	9375	9467	2.2835	57.00
32.0	1.00	0.0	0.00	51.05	12913	38.2	12812	13014	45.63	14418	42.7	14326	14507	3.9598	57.00
32.0	1.25	0.0	0.00	52.80	15873	47.0	15741	16007	48.73	17172	50.8	17049	17294	5.0311	57.00
32.0	1.56	0.0	0.00	55.13	19940	59.0	19757	20121	53.00	20720	61.3	20546	20896	6.5916	57.00
32.0	1.77	0.0	0.00	56.73	22853	67.6	22634	23075	56.15	23084	68.3	22866	23303	7.7692	57.00
41.0	0.00	0.0	0.00	45.33	4504	13.3	4476	4531	36.60	5562	16.5	5539	5584	1.2290	57.00
41.0	0.00	20.9	0.00	48.66	8267	24.5	8208	8325	41.10	9760	28.9	9711	9810	2.4186	57.00
59.0	0.00	0.0	0.00	45.85	4453	13.2	4425	4481	37.66	5407*	16.0	5384	5430	1.2290	57.00
100.0	0.00	0.0	0.00	47.03	4343	12.8	4315	4372	40.02	5092	15.1	5067	5116	1.2290	57.00
120.0	0.00	0.0	0.00	47.61	4292	12.7	4262	4321	41.15	4954	14.7	4929	4979	1.2290	57.00
167.0	0.00	0.0	0.00	48.93	4178	12.4	4148	4208	43.72	4667	13.8	4640	4694	1.2290	57.00

Mar 28, 2003 SagtenM Version 1, 3/25/2003

Conductor = Cardinal Chart No. 1-838
Area = 0.8462 in^2 Diameter = 1.1960 in Unit weight = 1.2290 lb/ft
Ruling Span = 1,148 ft Rated Tensile Strength = 33,800 lb
Creep is a factor

				Final					Initial						
Temp °F	Ice in	Wind psf	Const lbf/ft	Sag ft	Avrg Tension lbf	Final % RTS	Horz Tension lbf	Supp Tension lbf	Sag ft	Avrg Tension lbf	Init % RTS	Horz Tension lbf	Supp Tension lbf	Load lbf/ft	Ice Density pcf
-31.0	0.00	0.0	0.00	34.17	5953	17.6	5932	5974	32.23	6308	18.7	6288	6328	1.2290	57.00
0.0	0.00	0.0	0.00	36.21	5620	16.6	5599	5643	34.13	5959	17.6	5939	5981	1.2290	57.00
0.0	0.50	0.0	0.00	39.44	9598	28.4	9553	9643	38.62	9799	29.0	9755	9843	2.2835	57.00
0.0	0.50	4.0	0.30	40.55	11035	32.6	10979	11088	40.16	11140	33.0	11085	11194	2.6980	57.00
0.0	0.50	8.0	0.00	40.58	11084	32.8	11030	11140	40.21	11186	33.1	11131	11240	2.7125	57.00
5.0	0.00	0.0	0.00	36.54	5571	16.5	5548	5593	34.44	5907	17.5	5886	5928	1.2290	57.00
32.0	0.00	0.0	0.00	38.25	5325	15.8	5301	5348	36.06	5644	16.7	5622	5666	1.2290	57.00
32.0	0.50	0.0	0.00	41.23	9186	27.2	9140	9234	40.19	9420	27.9	9375	9467	2.2835	57.00
41.0	0.00	0.0	0.00	38.81	5249	15.5	5225	5272	36.60	5562	16.5	5539	5584	1.2290	57.00
59.0	0.00	0.0	0.00	39.91	5106	15.1	5081	5130	37.66	5407*	16.0	5384	5430	1.2290	57.00
100.0	0.00	0.0	0.00	42.34	4817	14.3	4790	4843	40.02	5092	15.1	5067	5116	1.2290	57.00
120.0	0.00	0.0	0.00	43.49	4691	13.9	4664	4718	41.15	4954	14.7	4929	4979	1.2290	57.00
167.0	0.00	0.0	0.00	46.10	4430	13.1	4401	4458	43.72	4667	13.8	4640	4694	1.2290	57.00

Table D-4
230 kV Single Circuit Tower Loads

	Weight Span m	Temp °C	Radial Ice mm	Wind Pa	V_S kN	T_S kN	L_S kN	V_P kN	T_P kN	L_P kN	W Pa	θ deg	k
NESC Heavy	420	-17.8	12.7	191.5	9.15	6.11	0.00	22.46	9.48	0.00	1532	0	1.5
Heavy Ice	420	-15.0	45.0	191.5	32.42	6.77	0.00	49.56	8.12	0.00	868	0	1.0
High Wind	420	5.0	0.0	1000.0	2.53	3.87	0.00	8.51	10.91	10.00	4400	0	1.0
NESC Heavy	280	-17.8	12.7	191.5	6.14	6.11	0.00	15.16	9.48	0.00	1532	0	1.5
Heavy Ice	280	-15.0	45.0	191.5	21.58	6.77	0.00	32.72	8.12	0.00	868	0	1.0
High Wind	280	5.0	0.0	1000.0	1.72	3.87	0.00	6.00	10.91	0.00	4400	0	1.0
Long Wind Twr	420	5.0	0.0	1000.0	2.53	0.00	0.00	8.51	0.00	0.00	4400	90	1.0
RSL Shield	280 420	-15.0	0.0	0.0	1.72 2.53	0.00	18.40 0.00	8.51	0.00	0.00	0	0	1.0
RSL Phase	280 420	-15.0	0.0	0.0	2.53	0.00	0.00	6.00 8.51	0.00	17.00 0.00	0	0	1.0

Notes:

1. V_S, T_S, L_S and V_P, T_P, L_P are the vertical, transverse and longitudinal loads at the shield wire and phase conductor attachment points, weights of insulators and attachment hardware are included.
2. θ is the angle between the transverse centerline of the tower and the wind direction, W is the wind pressure to be applied to the projected area of one face of the tower and k is the overload capacity factor by which the dead load of the tower shall be multiplied.
3. For the RSL load cases, the load in the numerator shall be applied at any one shield or phase attachment with the load in the denominator applied at the remaining attachment points.

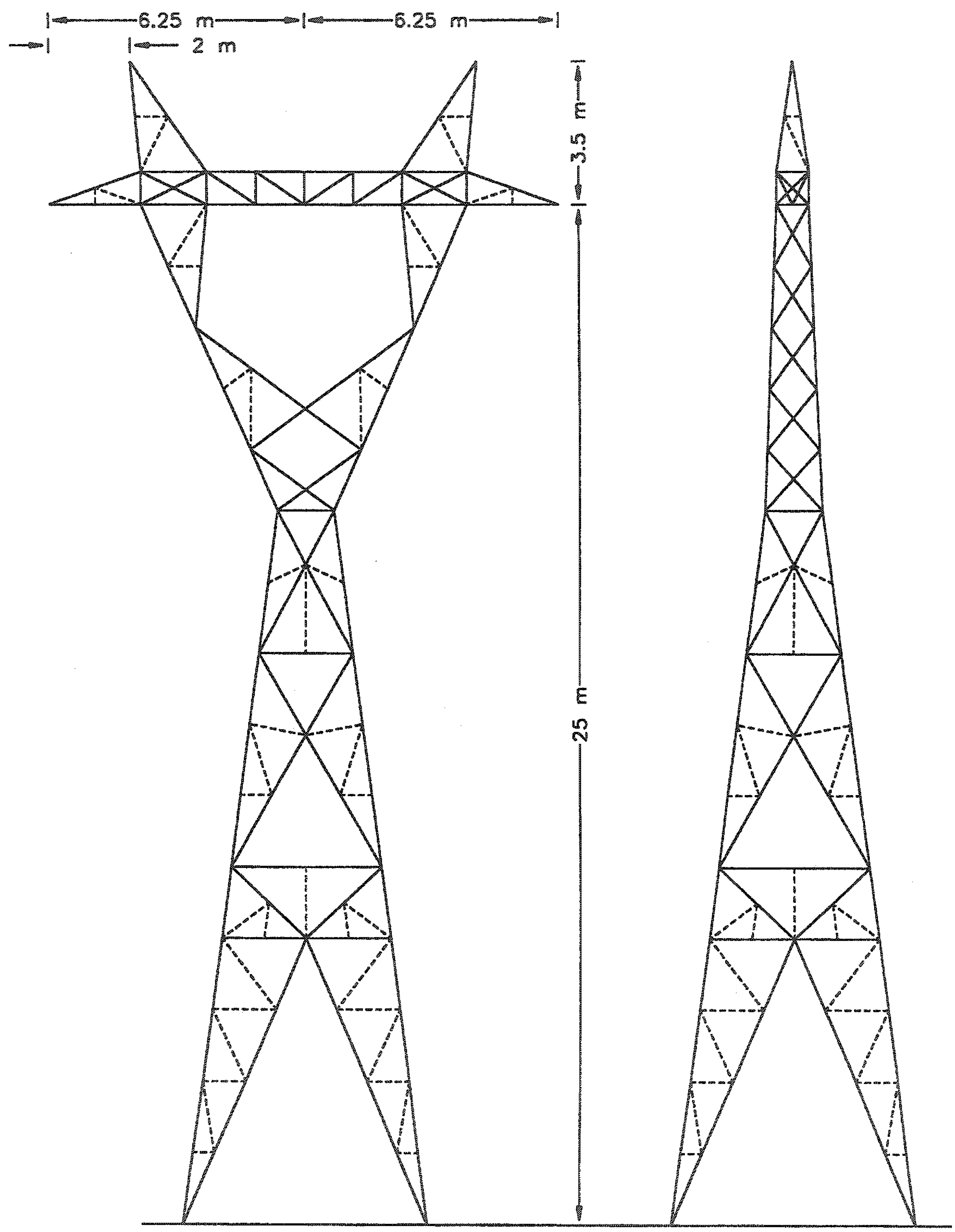

Figure D-1
Prototype Tower